TAMPEREEN TEKNILLINEN YLIOPISTO
TAMPERE UNIVERSITY OF TECHNOLOGY

Aki Hakkarainen

I/Q Imbalance in Multiantenna Systems: Modeling, Analysis and RF-Aware Digital Beamforming

Julkaisu 1447 • Publication 1447

Tampere 2017

Tampereen teknillinen yliopisto. Julkaisu 1447
Tampere University of Technology. Publication 1447

Aki Hakkarainen

I/Q Imbalance in Multiantenna Systems: Modeling, Analysis and RF-Aware Digital Beamforming

Thesis for the degree of Doctor of Science in Technology to be presented with due permission for public examination and criticism in Tietotalo Building, Auditorium TB109, at Tampere University of Technology, on the 13th of January 2017, at 12 noon.

Tampereen teknillinen yliopisto - Tampere University of Technology
Tampere 2017

Supervisor

Mikko Valkama, Professor
Department of Electronics and Communications Engineering
Tampere University of Technology
Tampere, Finland

Pre-examiners

Pascal Chevalier, Professor
Département Électronique, Automatisme, Systèmes
Conservatoire National des Arts et Métiers
Paris, France

Thomas Eriksson, Professor
Department of Signals and Systems
Chalmers University of Technology
Gothenburg, Sweden

Opponent

Elisabeth de Carvalho, Associate Professor
Department of Electronic Systems
Aalborg University
Aalborg, Denmark

ISBN 978-952-15-3871-1 (printed)
ISBN 978-952-15-3877-3 (PDF)
ISSN 1459-2045

Abstract

Wireless communications has experienced an unprecedented increase in data rates, numbers of active devices and selection of applications during recent years. However, this is expected to be just a start for future developments where a wireless connection is seen as a fundamental resource for almost any electrical device, no matter where and when it is operating. Since current radio technologies cannot provide such services with reasonable costs or even at all, a multitude of technological developments will be needed. One of the most important subjects, in addition to higher bandwidths and flexible network functionalities, is the exploitation of multiple antennas in base stations (BSs) as well as in user equipment (UEs). That kind of multiantenna communications can boost the capacity of an individual UE-BS link through spatial antenna multiplexing and increase the quality as well as robustness of the link via antenna diversity. Multiantenna technologies provide improvements also on the network level through spatial UE multiplexing and sophisticated interference management. Additionally, multiple antennas can provide savings in terms of the dissipated power since transmission and reception can be steered more efficiently in space, and thus power leakage to other directions is decreased. However, several issues need to be considered in order to get multiantenna technologies widely spread. First, antennas and the associated transceiver chains are required to be simple and implementable with low costs. Second, size of the antennas and transceivers need to be minimized. Finally, power consumption of the system must be kept under control. The importance of these requirements is even emphasized when considering massive multiple-input multiple-output (MIMO) systems consisting of devices equipped with tens or even hundreds of antennas.

In this thesis, we consider multiantenna devices where the associated transceiver chains are implemented in such a way that the requirements above can be met. In particular, we focus on the direct-conversion transceiver principle which is seen as a promising radio architecture for multiantenna systems due to its low costs, small size, low power consumption and good flexibility. Whereas these aspects are very promising, direct-conversion transceivers have also some disadvantages and are vulnerable to certain imperfections in the analog radio frequency (RF) electronics in particular. Since the effects of these imperfections usually get even worse when optimizing costs of the devices,

the scope of the thesis is on the effects and mitigation of one of the most severe RF imperfection, namely in-phase/quadrature (I/Q) imbalance.

Contributions of the thesis can be split into two main themes. First of them is multiantenna narrowband beamforming under transmitter (TX) and receiver (RX) I/Q imbalances. We start by creating a model for the signals at the TX and RX, both under I/Q imbalances. Based on these models we derive analytical expressions for the antenna array radiation patterns and notice that I/Q imbalance distorts not only the signals but also the radiation characteristics of the array. After that, stemming from the nature of the distortion, we utilize widely-linear (WL) processing, where the signals and their complex conjugates are processed jointly, for the beamforming task under I/Q imbalance. Such WL processing with different kind of statistical and adaptive beamforming algorithms is finally shown to provide a flexible operation as well as distortion-free signals and radiation patterns when being under various I/Q imbalance schemes.

The second theme extends the work to wideband systems utilizing orthogonal frequency-division multiplexing (OFDM)-based waveforms. The focus is on uplink communications and BS RX processing in a multiuser MIMO (MU-MIMO) scheme where spatial UE multiplexing is applied and further UE multiplexing takes place in frequency domain through the orthogonal frequency-division multiple access (OFDMA) principle. Moreover, we include the effects of external co-channel interference into our analysis in order to model the challenges in heterogeneous networks. We formulate a flexible signal model for a generic uplink scheme where I/Q imbalance occurs on both TX and RX sides. Based on the model, we analyze the signal distortion in frequency domain and develop augmented RX processing methods which process signals at mirror subcarrier pairs jointly. Additionally, the proposed augmented methods are numerically shown to outperform corresponding per-subcarrier method in terms of the instantaneous signal-to-interference-and-noise ratio (SINR). Finally, we address some practical aspects and conclude that the augmented processing principle is a promising tool for RX processing in multiantenna wideband systems under I/Q imbalance.

The thesis provides important insight for development of future radio networks. In particular, the results can be used as such for implementing digital signal processing (DSP)-based RF impairment mitigation in real world transceivers. Moreover, the results can be used as a starting point for future research concerning, e.g., joint effects of multiple RF impairments and their mitigation in multiantenna systems. Overall, this thesis and the associated publications can help the communications society to reach the ambitious aim of flexible, low-cost and high performance radio networks in the future.

Preface

This thesis is based on the research work carried out during the years 2012–2016 at the Department of Electronics and Communications Engineering, Tampere University of Technology, Tampere, Finland.

First and foremost, I would like to express my deepest gratitude to Prof. Mikko Valkama for offering me the opportunity to work at the department under his supervision and guidance. It has been a pleasure to work with him and to follow his vision of the research in the field of wireless communications. His dedication to work and willingness to help people have motivated me to work also during the hard times. I would like to thank also Prof. Markku Renfors for all his efforts for our department and research group as well as for creating such a good and inspiring atmosphere over the years. I also wish to thank Toni Levanen and Jarno Niemelä for helping me to get the position in our department, without you guys I would not have been working here.

I am grateful to the thesis pre-examiners, Prof. Pascal Chevalier and Prof. Thomas Eriksson for their valuable time and careful reviews. I also wish to thank Prof. Elisabeth de Carvalho for agreeing to act as the opponent at my defense.

I am grateful to acknowledge the financial support of the following organizations and funds: Finnish Funding Agency for Technology and Innovation (Tekes; under the projects "Reconfigurable Antenna-based Enhancement of Dynamic Spectrum Access Algorithms" and "Future Small-Cell Networks using Reconfigurable Antennas"), the Academy of Finland (under the projects 251138 "Digitally-Enhanced RF for Cognitive Radio Devices", 284694 "Fundamentals of Ultra Dense 5G Networks with Application to Machine Type Communication" and 288670 "Massive MIMO: Advanced Antennas, Systems and Signal Processing at mm-Waves"), the Industrial Research Fund of Tampere University of Technology (Tuula and Yrjö Neuvo Fund), and the Foundation of Nokia Corporation.

I wish to dedicate special thanks to my friendly ex-roommate and co-author Janis Werner who has put lots of effort to go through my work over and over again. His constructive and encouraging feedback has been truly invaluable. The office wouldn't have been the same without my other roommates Sener Dikmese, Simran Singh, Mike

Koivisto and Jukka Talvitie with whom I have had a pleasure to discuss work and life in general. I wish to thank also Ahmet Gökceoglu, Dani Korpi, Ville Syrjälä and Yaning Zou for the nice moments when traveling worldwide. I would like to thank Markus Allén, Jaakko Marttila and Timo Huusari for the discussion regarding LaTeX templates, layouts and tricks. The work in the department would have been too exhausting without relaxing breaks and events with the aforementioned people as well as with Mahmoud Abdelaziz, Lauri Anttila, Ondrej Daniel, Tero Isotalo, Vesa Lehtinen, Pedro Silva, Paschalis Sofotasios, Joonas Säe, Matias Turunen and Kui Wang who have always been there when it comes to coffee, lunch, sports or sauna. I am grateful also to our helpful secretaries Heli Ahlfors, Tarja Erälaukko, Tuija Grek, Daria Ilina, Sari Kinnari, Soile Lönnqvist and Kirsi Viitanen who have taken care of all the daily practicalities at work. In addition, I want to thank Karoliina Jolkkonen and Daniel Pitt for proofreading the language of the thesis.

For pleasant and fruitful co-operation during our common research projects, I wish to thank Prof. Kapil Dandekar, Nikhil Gulati, Damiano Patron and Doug Pfeil from the Drexel University; and Mário Costa, Petteri Kela and Kari Leppänen from Huawei Technologies, Finland R&D Center.

I would like to thank my parents Maria Liisa and Teuvo, as well as my sister Nina and her family for encouraging me to push forward and for supporting me throughout my studies and life in every way. Most of all, I want to thank my beloved fiancée Mari for all the love, patience and care over the years, and my lovely son Luukas for bringing random processes to my life and for teaching me every day some new and extraordinary ways of thinking. Finally, I want to thank Mari's parents Tuula and Juha as well as Mari's siblings Anna and Kalle, including their families, for welcoming me to join their family and for supporting us in the uphills. Thank you all.

Tampere, November 2016
Aki Hakkarainen

Table of Contents

List of Publications

This thesis is a compound thesis based on the following eight publications.

[P1] A. Hakkarainen, J. Werner, and M. Valkama, "RF Imperfections in Antenna Arrays: Response Analysis and Widely-Linear Digital Beamforming," in *Proceedings of IEEE Radio and Wireless Symposium (RWS)*, Austin, TX, USA, January 2013.

[P2] A. Hakkarainen, J. Werner, K. R. Dandekar, and M. Valkama, "RF-Aware Widely-Linear Beamforming and Null-Steering in Cognitive Radio Transmitters," in *Proceedings of the 8th International Conference on Cognitive Radio Oriented Wireless Networks (CROWNCOM)*, Washington, DC, USA, July 2013.

[P3] A. Hakkarainen, J. Werner, M. Renfors, K. Dandekar, and M. Valkama, "RF-Aware Widely-Linear MMSE Beamforming," in *Proceedings of the 10th International Symposium on Wireless Communication Systems (ISWCS)*, Ilmenau, Germany, August 2013.

[P4] A. Hakkarainen, J. Werner, K. R. Dandekar, and M. Valkama, "Widely-Linear Beamforming and RF Impairment Suppression in Massive Antenna Arrays," in *Journal of Communications and Networks*, volume 15, number 4, pages 383–397, August 2013.

[P5] A. Hakkarainen, J. Werner, K. Dandekar, and M. Valkama, "Interference Suppression with Antenna Arrays in OFDM Systems under Transceiver I/Q Imbalance," in *Proceedings of the 9th International Conference on Cognitive Radio Oriented Wireless Networks (CROWNCOM)*, Oulu, Finland, June 2014.

[P6] A. Hakkarainen, J. Werner, K. R. Dandekar, and M. Valkama, "Precoded Massive MU-MIMO Uplink Transmission under Transceiver I/Q Imbalance," in *Proceedings of IEEE Global Communications Conference (GLOBECOM) Workshops*, Austin, TX, USA, December 2014.

[P7] A. Hakkarainen, J. Werner, M. Renfors, K. R. Dandekar, and M. Valkama, "Transceiver I/Q Imbalance and Widely-Linear Spatial Processing in Large Antenna Systems," in *Proceedings of the 12th International Symposium on Wireless Communication Systems (ISWCS)*, Brussels, Belgium, August 2015.

[P8] A. Hakkarainen, J. Werner, K. R. Dandekar, and M. Valkama, "Analysis and Augmented Spatial Processing for Uplink OFDMA MU-MIMO Receiver with Transceiver I/Q Imbalance and External Interference," in *IEEE Transactions on Wireless Communications*, volume 15, number 5, pages 3422–3439, May 2016.

Abbreviations

2D	Two dimensional
3D	Three dimensional
3G	Third generation
3GPP	3rd Generation Partnership Project
4G	Fourth generation
5G	Fifth generation
ADC	Analog-to-digital converter
AGC	Automatic gain control
BPF	Bandpass filter
BS	Base station
CFO	Carrier frequency offset
CP	Cyclic prefix
CR	Cognitive radio
CSI	Channel state information
DAC	Digital-to-analog converter
DC	Direct current
DCR	Direct-conversion receiver
DCT	Direct-conversion transmitter
DL	Downlink
DoA	Direction of arrival
DSP	Digital signal processing
EGC	Equal-gain combining
FFT	Fast Fourier transform
FIR	Finite impulse response
I/Q	In-phase/quadrature
IC	Integrated circuit
ICI	Inter-carrier interference
IEEE	Institute of Electrical and Electronics Engineers
IF	Intermediate frequency

IFFT	Inverse fast Fourier transform
IIR	Infinite impulse response
IoT	Internet of things
IRR	Image rejection ratio
LCMV	Linearly constrained minimum variance
LMMSE	Linear minimum mean-square error
LMS	Least mean square
LNA	Low noise amplifier
LO	Local oscillator
LoS	Line of sight
LPF	Lowpass filter
LTE	Long term evolution
LTE-A	Long term evolution advanced
MIMO	Multiple-input multiple-output
MISO	Multiple-input single-output
MMSE	Minimum mean square error
mmWave	Millimeter wave
MRC	Maximal-ratio combining
MRT	Maximal-ratio transmission
MSE	Mean square error
MU-MIMO	Multiuser MIMO
MU-MISO	Multiuser MISO
MU-SIMO	Multiuser SIMO
MVDR	Minimum variance distortionless response
NLMS	Normalized LMS
OFDM	Orthogonal frequency-division multiplexing
OFDMA	Orthogonal frequency-division multiple access
PA	Power amplifier
PCB	Printed circuit board
QAM	Quadrature amplitude modulation
QoS	Quality of service
RF	Radio frequency
RLS	Recursive least squares
RX	Receiver
SC-FDMA	Single-carrier frequency-division multiple access
SIMO	Single-input multiple-output
SINR	Signal-to-interference-and-noise ratio
SIR	Signal-to-interference ratio
SISO	Single-input single-output
SMF	Spatial matched filter
SNR	Signal-to-noise ratio
SOI	Signal of interest
SU-MIMO	Single user MIMO
SU-MISO	Single user MISO
SU-SIMO	Single user SIMO
SU-SISO	Single user SISO

SVD	Singular value decomposition
TX	Transmitter
UE	User equipment
UL	Uplink
ULA	Uniform linear array
WiMAX	Worldwide Interoperability for Microwave Access
WL	Widely-linear
WLAN	Wireless local area network
ZF	Zero forcing

Symbols

$\widetilde{\mathbf{A}}_{\mathrm{Txi}}$	WL null-steering matrix under TX I/Q imbalance
$\widetilde{\mathbf{A}}_{\mathrm{Rxi}}(\theta_{\mathrm{d}})$	WL steering matrix to desired direction θ_{d} under RX I/Q imbalance
$\widetilde{\mathbf{A}}_{\mathrm{Txi}}(\theta_{\mathrm{un},i})$	WL steering matrix corresponding to $\theta_{\mathrm{un},i}$ under TX I/Q imbalance
$\mathbf{a}(\theta)$	Antenna array steering vector
$\widetilde{\mathbf{a}}_{\mathrm{Txi}}(\theta_{\mathrm{d}})$	RF-aware WL steering vector to θ_{d} under TX I/Q imbalance
$\widetilde{\mathbf{a}}_{\mathrm{Txi,SI}}(\theta_{\mathrm{d}})$	WL steering vector corresponding to self interference
$\mathbf{a}(\theta_{\mathrm{int},l})$	Steering vector of external interferer in direction $\theta_{\mathrm{int},l}$
c	Subcarrier index
C	Size of FFT
C_{a}	Number of active subcarriers
c'	Mirror subcarrier of subcarrier c
$D(\theta)$	Radiation pattern with linear processing
$D_{\mathrm{Rxi}}(\theta)$	Radiation pattern with RX I/Q imbalance and linear processing
$\widetilde{D}_{\mathrm{Rxi}}(\theta)$	Radiation pattern with RX I/Q imbalance and WL processing
$D_{\mathrm{Txi}}(\theta)$	Radiation pattern with TX I/Q imbalance and linear processing
$\widetilde{D}_{\mathrm{Txi}}(\theta)$	Radiation pattern with TX I/Q imbalance and WL processing
d	Antenna spacing
$\mathbf{e}_i$	Natural basis vector, the i^{th} entry equals one and the rest are zeros
f	Frequency variable
f_{LO}	Local oscillator frequency
$\mathbf{G}$	Precoder matrix
$\mathbf{G}_{u,c}$	Precoder matrix of UE u at subcarrier c
$\mathbf{G}_{v,c'}$	Precoder matrix of UE v at subcarrier c'
g_{Rx}	Frequency-independent RX gain imbalance coefficient
$g_{\mathrm{Rx},c}$	RX gain imbalance coefficient at subcarrier c
$g_{\mathrm{Rx1}}(t)$	RX I/Q imbalance coefficient
$g_{\mathrm{Rx2}}(t)$	RX I/Q imbalance coefficient
g_{Tx}	Frequency-independent TX gain imbalance coefficient

$g_{\mathrm{Tx},c}$	TX gain imbalance coefficient at subcarrier c
$g_{\mathrm{Tx1}}(t)$	TX I/Q imbalance coefficient
$g_{\mathrm{Tx2}}(t)$	TX I/Q imbalance coefficient
$\mathbf{h}$	Channel vector
$\mathbf{H}_{\mathrm{int},l,c}$	Channel matrix of external interferer l at subcarrier c
$\mathbf{H}_{u,c}$	Channel matrix of UE u at subcarrier c
$\mathbf{H}$	Channel matrix
$\mathbf{H}_{v,c}$	Channel matrix of UE v at subcarrier c
$h_{\mathrm{L}}(t)$	Baseband equivalent of $h_{\mathrm{RF}}(t)$
$h_{\mathrm{RF}}(t)$	Impulse response of wireless channel
$h_{\mathrm{Rx}}(t)$	Frequency-dependent RX impulse response imbalance
$h_{\mathrm{Tx}}(t)$	Frequency-dependent TX impulse response imbalance
i	OFDM symbol index
J_l	Number of TX antennas in the l^{th} external interferer
$\mathbf{K}_{\mathrm{Rx1}}$	Diagonal RX I/Q imbalance matrix
$\mathbf{K}_{\mathrm{Rx1},c}$	Diagonal BS RX I/Q imbalance matrix at subcarrier c
$\mathbf{K}_{\mathrm{Rx2}}$	Diagonal RX I/Q imbalance matrix
$\mathbf{K}_{\mathrm{Rx2},c}$	Diagonal BS RX I/Q imbalance matrix at subcarrier c
$\mathbf{K}_{\mathrm{RxA},c}$	Augmented BS RX I/Q imbalance matrix at subcarrier c
$\mathbf{K}_{\mathrm{RxB},c}$	Augmented BS RX I/Q imbalance matrix at subcarrier c
$\mathbf{K}_{\mathrm{Tx1}}$	Diagonal TX I/Q imbalance matrix
$\mathbf{K}_{\mathrm{Tx1},u,c}$	Diagonal TX I/Q imbalance matrix of UE u at subcarrier c
$\mathbf{K}_{\mathrm{Tx2}}$	Diagonal TX I/Q imbalance matrix
$\mathbf{K}_{\mathrm{Tx2},u,c}$	Diagonal TX I/Q imbalance matrix of UE u at subcarrier c
$K_{\mathrm{Rx1},c}$	RX I/Q imbalance coefficient at subcarrier c
$K_{\mathrm{Rx2},c}$	RX I/Q imbalance coefficient at subcarrier c
$K_{\mathrm{Tx1},c}$	TX I/Q imbalance coefficient at subcarrier c
$K_{\mathrm{Tx2},c}$	TX I/Q imbalance coefficient at subcarrier c
k	Sample index
L	Number of external interferers
l	Index of external interferers
M_u	Number of TX antennas in UE u
M_v	Number of TX antennas in UE v
$\mathbf{n}$	Additive white Gaussian noise vector
$\mathbf{n}_c$	Additive white Gaussian noise vector at subcarrier c
N	Number of RX antennas
N_{in}	Number of parallel input samples of digital combiner
n	Additive white Gaussian noise
$n_{\mathrm{L}}(t)$	Baseband equivalent of $n_{\mathrm{RF}}(t)$
$n_{\mathrm{RF}}(t)$	Radio frequency additive white Gaussian noise in RX
$\mathbf{P}_{\widetilde{\mathbf{A}}_{\mathrm{Txi}}}$	Orthogonal projection matrix of $\widetilde{\mathbf{A}}_{\mathrm{Txi}}$
$\widetilde{P}_{\mathrm{ISI},q,u,c}$	Output power of inter-stream interference from subcarrier c
$\widetilde{P}_{\mathrm{IUI},u,c}$	Output power of inter-user interference from subcarrier c
$\widetilde{P}_{\mathrm{IUI},u,c'}$	Output power of inter-user interference from mirror subcarrier c'
$\widetilde{P}_{q,u,c}$	Total output power of data stream q of UE u at subcarrier c

$\widetilde{P}_{x,q,u,c}$	Output power of desired data stream q of UE u at subcarrier c
$\widetilde{P}_{z,c}$	Output power of external interference and noise from subcarrier c
$\widetilde{P}_{z,c'}$	Output power of ext. interference and noise from mirror subcarrier c'
Q	Number of data streams
$Q_{\mathrm{u},c}$	Number of data streams of UE u at subcarrier c
$Q_{\mathrm{v},c'}$	Number of data streams of UE v at subcarrier c'
q	Data stream index
$\mathbf{r}$	Received signal vector
$\widetilde{\mathbf{R}}_{\mathrm{Rxi}}$	Augmented covariance matrix under RX I/Q imbalance
$\widetilde{\mathbf{R}}_{\mathrm{TxRxi},c}$	Aug. covariance matrix at subcarrier c under TX+RX I/Q imb.
$\mathbf{R}_{\mathrm{z},c}$	Covariance matrix of external interference and noise at subcarrier c
$\mathbf{r}_c$	Received signal vector at subcarrier c under ideal I/Q balance
$\mathbf{r}_{\mathrm{TxRxi},c}$	RX signal vector at subcarrier c and under TX+RX I/Q imbalance
$\widetilde{\mathbf{r}}_{\mathrm{TxRxi},c}$	Aug. RX signal vector at subcarrier c and under TX+RX I/Q imb.
$\mathbf{r}(\theta)$	RX signal vector when DoA is equal to θ
$\widetilde{\mathbf{r}}(\theta)$	WL RX signal vector when DoA is equal to θ
$\mathbf{r}_{\mathrm{Rxi}}(\theta)$	RX signal vector under I/Q imbalance when DoA is equal to θ
$\widetilde{\mathbf{r}}_{\mathrm{Rxi}}(\theta)$	WL RX signal vector under I/Q imbalance when DoA is equal to θ
$r_{\mathrm{int},l}$	Received signal from the l^{th} external interference
$r_c(i)$	Received data at subcarrier c
$r_{\mathrm{Rxi},c}(i)$	Received data under RX I/Q imbalance at subcarrier c
$r(k)$	Digital baseband RX signal
$r_{\mathrm{Rxi}}(k)$	Received data under RX I/Q imbalance
$r(t)$	Analog baseband RX signal
$r_I(t)$	Analog in-phase baseband RX signal
$r_{\mathrm{L}}(t)$	Baseband equivalent of $r_{\mathrm{RF}}(t)$
$r_Q(t)$	Analog quadrature-phase baseband RX signal
$r_{\mathrm{RF}}(t)$	Analog radio frequency RX signal
$r_{\mathrm{Rxi}}(t)$	Baseband equivalent of RX signal under RX I/Q imbalance
$\mathbf{s}$	Digital signal vector in TX beamformer or after TX precoding
$\widetilde{\mathbf{s}}$	Digital signal vector in WL TX beamformer
$\mathbf{s}_{\mathrm{int},l,c}$	Effective received signal of external interferer l at subcarrier c
$\mathbf{s}_{\mathrm{Txi}}$	Digital signal vector in TX beamformer under TX I/Q imbalance
$\widetilde{\mathbf{s}}_{\mathrm{Txi}}$	Digital signal vector in WL TX beamformer under TX I/Q imb.
$\mathbf{s}_{\mathrm{Txi},u,c}$	Precoded TX signal vector of UE u at subc. c under TX I/Q imb.
$\mathbf{s}_{\mathrm{Txi},v,c}$	Precoded TX signal vector of UE v at subc. c under TX I/Q imb.
$\mathbf{s}_{u,c}$	Precoded TX signal vector of UE u at subcarrier c
$\mathbf{s}_{v,c'}$	Precoded TX signal vector of UE v at subcarrier c'
S	Total number of transmitted data streams
$s_{\mathrm{TX}}(\theta)$	Baseband equivalent of TX beamformer output to direction θ
$\widetilde{s}_{\mathrm{TX}}(\theta)$	Baseband equiv. of WL TX beamformer output to direction θ
$s_{\mathrm{Txi}}(\theta)$	Baseband equiv. of TX beamformer output to θ under TX I/Q imb.
$\widetilde{s}_{\mathrm{Txi}}(\theta)$	Baseband equiv. of WL TX beamformer output to θ under TX IQI
t	Time variable
U	Number of UEs at subcarrier c

u	Index of UEs at subcarrier c
$u(f)$	Unit step function
$\widetilde{\mathbf{V}}_{\mathrm{TxRxi},c}$	Aug. cross-correlation matrix at subcarrier c under TX+RX I/Q imb.
V	Number of UEs at mirror subcarrier c'
v	Index of UEs at mirror subcarrier c'
$\mathbf{W}$	Combiner weight matrix
$\mathbf{W}_c$	Combiner weight matrix at subcarrier c
$\widetilde{\mathbf{W}}_c$	Augmented combiner weight matrix at subcarrier c
$\widetilde{\mathbf{W}}^{\mathrm{LMMSE}}_{\mathrm{TxRxi},c}$	Aug. Wiener weight matrix at subcarrier c under TX+RX I/Q imb.
$\mathbf{W}^{\mathrm{MRC}}_{\mathrm{TxRxi},c}$	MRC weight matrix at subcarrier c under TX+RX I/Q imbalance
$\mathbf{w}$	Weight vector for antenna array
$\mathbf{w}_{q,u,c}$	Weight vector for data stream q of UE u at subcarrier c
$\widetilde{\mathbf{w}}_{q,u,c}$	Augmented weight vector for data stream q of UE u at subcarrier c
$\mathbf{w}(\theta_{\mathrm{d}})$	Beamforming weight vector for direction θ_{d}
$\widetilde{\mathbf{w}}(\theta_{\mathrm{d}})$	WL beamforming weight vector for direction θ_{d}
$\widetilde{\mathbf{w}}^{\mathrm{MVDR}}_{\mathrm{Rxi}}(\theta_{\mathrm{d}})$	WL-MVDR beamforming weight vector for θ_{d} under RX I/Q imb.
$\widetilde{\mathbf{w}}^{\mathrm{NS}}_{\mathrm{Txi}}(\theta_{\mathrm{d}})$	WL null-steering beamforming weights for θ_{d} under TX I/Q imb.
w_1	Processing weight for original signal
w_2	Processing weight for complex conjugate of original signal
$\mathbf{x}$	Digital signal vector in multiantenna TX
$\mathbf{x}_{u,c}$	Parallel TX data streams of UE u at subcarrier c
$\mathbf{x}_{v,c'}$	Parallel TX data streams of UE v at subcarrier c'
$x_{q,u,c}$	Transmitted data stream q of UE u at subcarrier c
$x_c(i)$	Transmitted data at subcarrier c
$x_{\mathrm{Txi},c}(i)$	Transmitted data under TX I/Q imbalance at subcarrier c
$x(k)$	Digital baseband TX signal
$x_I(k)$	Digital in-phase baseband TX signal
$x_Q(k)$	Digital quadrature-phase baseband TX signal
$x(t)$	Analog baseband TX signal
$x_I(t)$	Analog in-phase baseband TX signal
$x_{\mathrm{L}}(t)$	Analog baseband equivalent of $x_{\mathrm{RF}}(t)$
$x_Q(t)$	Analog quadrature-phase baseband TX signal
$x_{\mathrm{RF}}(t)$	Analog radio frequency TX signal
$x_{\mathrm{RF}+}(t)$	Analytical signal consisting of positive frequency terms of $x_{\mathrm{RF}}(t)$
$x_{\mathrm{Txi}}(t)$	Baseband equivalent of the TX signal under TX I/Q imbalance
$\mathbf{y}_c$	RX combiner output at subcarrier c and under ideal I/Q balance
$\mathbf{y}_{\mathrm{RX}}$	RX combiner output signal vector
$\mathbf{y}_{\mathrm{TxRxi},c}$	RX combiner output at subcarrier c and under TX+RX I/Q imb.
$\widetilde{\mathbf{y}}_{\mathrm{TxRxi},c}$	Aug. RX combiner output at subc. c and under TX+RX I/Q imb.
y_{RX}	RX combiner output signal
$\widetilde{y}_{\mathrm{Rxi},c}$	Aug. RX combiner output at subcarrier c and under RX I/Q imb.
$y_{\mathrm{RX}}(\theta)$	RX beamformer output when DoA is equal to θ
$\widetilde{y}_{\mathrm{RX}}(\theta)$	WL RX beamformer output when DoA is equal to θ
$y_{\mathrm{Rxi}}(\theta)$	RX beamformer output under I/Q imb. when DoA is equal to θ
$\widetilde{y}_{\mathrm{Rxi}}(\theta)$	WL RX beamformer output under RX IQI when DoA is equal to θ

$\mathbf{z}$	External interference plus noise vector in BS RX
$\mathbf{z}_c$	External interference plus noise vector at subcarrier c in BS RX
$\widetilde{\alpha}$	Power scaling factor of null-steering beamformer
α_{Rx}	I/Q imbalance coefficient for symmetrical RX I/Q imbalance model
α_{Tx}	I/Q imbalance coefficient for symmetrical TX I/Q imbalance model
β_{Rx}	I/Q imbalance coefficient for symmetrical RX I/Q imbalance model
β_{Tx}	I/Q imbalance coefficient for symmetrical TX I/Q imbalance model
$\mathbf{\Gamma}_{q,u,c}$	Stream selection matrix referring to desired data stream q of UE u
$\mathbf{\Delta}_{q,u,c}$	Stream selection matrix referring to interfering data streams of UE u
$\delta(t)$	Dirac delta function
ϵ_{Rx}	Gain imbalance coefficient for symmetrical RX I/Q imbalance model
ϵ_{Tx}	Gain imbalance coefficient for symmetrical TX I/Q imbalance model
$\Theta_{\mathrm{combining},c}$	Computational complexity of digital combining
Θ_{FFT}	Computational complexity of FFT
$\Theta_{\mathrm{tot},c}$	Total computational complexity of digital combiner
$\Theta^{\mathrm{LMS}}_{\mathrm{weights},c}$	Computational complexity of LMS implementation
$\Theta^{\mathrm{RLS}}_{\mathrm{weights},c}$	Computational complexity of RLS implementation
θ_{d}	Desired spatial direction
$\theta_{\mathrm{un},i}$	Undesired spatial direction
κ	Wavenumber
λ	Wavelength
$\widetilde{\mathbf{\Xi}}_{u,c}$	Aug. matrix of UE u at subc. c inc. channel and TX+RX I/Q imb.
$\sigma^2_{\mathrm{int},l,c}$	Power of l^{th} external interferer at subcarrier c
$\sigma^2_{\mathrm{n},c}$	Power of additional RX noise at subcarrier c
$\sigma^2_{x,u,c}$	TX power of single data stream of UE u at subcarrier c
$\widetilde{\mathbf{\Phi}}_{v,c}$	Aug. matrix of UE v at subc. c inc. channel and TX+RX I/Q imb.
ϕ_{Rx}	Frequency-independent RX phase imbalance coefficient
$\phi_{\mathrm{Rx},c}$	RX phase imbalance coefficient at subcarrier c
ϕ_{Tx}	Frequency-independent TX phase imbalance coefficient
$\phi_{\mathrm{Tx},c}$	TX phase imbalance coefficient at subcarrier c
$\widetilde{\mathbf{\Psi}}_{u,c}$	Matrix of UE u at subc. c including channel and TX+RX I/Q imb.
$\widetilde{\mathbf{\Omega}}_{v,c}$	Matrix of UE v at subc. c including channel and TX+RX I/Q imb.

CHAPTER 1

Introduction

1.1 Background and Motivation

Connecting people. That used to be the slogan of the Finnish telecommunications company called Nokia. They were pioneers in communications engineering and have made a successful business out of connecting people via mobile phones and wireless networks. Whereas mobile phone calls and text messages were a "dream-come-true" a few decades ago, the development in the modern lifestyle has resulted in much higher communications rates. On the one hand, people want nowadays to keep in touch with their friends, families and workmates everywhere and all the time. Emerging social media applications have resulted in an unforeseen increase in data rates when people share their thoughts, pictures and videos, and when other people download this content to be enjoyed in their mobile devices. Email and messaging services, in turn, can include huge amounts of data to be distributed to the recipients who can be on the road anywhere in the world. On the other hand, companies constantly push digital advertisements to attract people to buy their services and products. In addition, media distributors provide a vast selection of audio and video content to be bought by customers day and night. However, all this is not enough, not even close.

It is foreseen that the concept of so-called internet of things (IoT) [82], where billions of things communicate with each other, will expand the usage of wireless communications to a completely different scale. Various kinds of sensors will observe and measure the surrounding world and communicate the data forward to be processed by other devices and services. The processed data can be used to control devices such as switches, actuators and robots, which are able to automatically operate in the desired tasks. The data can also be used for predicting future events in the observed systems via sophisticated big data processing and machine learning algorithms. However, the rise of IoT is not the whole story. The communications needs between people or between people and machines are also constantly increasing. As an example, people develop and utilize better quality services, such as 4K resolution for entertainment systems, video conferences and remote controlled medical operations. Furthermore, due to higher computational processing capabilities and cheaper monitoring provided by new technologies, augmented

reality, self-driving cars and three dimensional (3D) video applications are going to be of special interest in the future. All this will involve huge amounts of data to be communicated via existing and forthcoming communication networks, preferably without impractical and costly cables and wires in each of the devices.

Obtaining the unprecedented increase in wireless data transfer is a big challenge and requires developments towards fifth generation (5G) technologies. First of all, considerably higher bandwidths are needed. Some new frequencies can be obtained, e.g., by utilizing carrier aggregation of multiple contiguous or non-contiguous carriers [30, 94] as well as by opportunistic and dynamic spectrum access schemes in the cognitive radio (CR) framework [120]. However, the most promising prospects are seen in the so-called millimeter wave (mmWave) frequencies, i.e. 30 GHz–300 GHz, where significantly higher bandwidths are available for communications [8, 29, 50, 62, 81, 147, 148, 152]. Second, in order to support stringent requirements of heterogeneous groups of devices and various use cases in 5G networks, network functionalities must be more flexible than today. In particular, this means support for higher mobility, higher data rates, very low latencies, ultra-high reliability and communications in extremely crowded areas, depending on the use case at hand [29, 50, 76, 81, 133, 134]. These aims create a demand for optimized signal waveforms with scalable numerology [76, 93, 102, 133], flexible multiple access schemes [76] as well as for improved backhaul communications [50, 133]. Furthermore, the spatial dimension needs better exploitation. It is expected that, especially in densely populated areas, the network densification will happen, i.e., the distance between neighboring base stations (BSs) in cellular networks will be decreased resulting in smaller cells [8,19,21,29,62,76,133,134]. This, in turn, means smaller amount of user equipment (UEs) per cell and thus provides more capacity and consequently better quality of service (QoS) for a single UE. The spatial component can be boosted also by multiantenna solutions [50] where one or both sides of a communication link are equipped with multiple antennas [61]. On the transmitter (TX) side, the data to be transmitted can be flexibly precoded to TX antennas, resulting in spatial TX multiplexing [121, p. 465] and TX antenna diversity [121, p. 273]. On the receiver (RX) side, the received signals from all RX antennas are combined and jointly processed in order to provide the desired performance. Note that when the BS is equipped with multiple antennas, also spatial UE multiplexing is possible, which can, in turn, be highly beneficial in terms of capacity improvements [61]. Third and finally, due to the vast number of communicating devices, the costs, size and power consumption of a single device must be low. Since each device contains, among other things, a radio frequency (RF) front-end, which carries out the conversion between the baseband data signal and RF antenna signal, the aforementioned requirements are valid also for RF electronics inside the devices. This is even more so at the advent of a massive multiple-input multiple-output (MIMO) [8, 29, 74, 75, 99, 110, 116, 153, 189] where at least one of the devices is expected to have a massive amount of antennas and the associated RF electronics. One very prominent option to meet these hardware requirements is the direct-conversion radio architecture or “homodyne” radio architecture as it was called in the original publication [41] according to the information given in [178]. In direct-conversion transmitters (DCTs) the baseband data signal is converted directly to a high frequency antenna signal without intermediate stages, whereas in direct-conversion receivers (DCRs) the conversion is done vice versa [3, 68, 119]. Consequently, this kind

of approach needs less bulky, costly and power hungry components than traditional superheterodyne transceivers [17], and most of the operations can be integrated on a single chip [3, 119, 149].

Whereas the direct-conversion radio architecture is advantageous in terms of costs, size, power consumption and flexibility [115], it has also some disadvantages. In particular, it is more vulnerable to certain imperfections in the RF electronics, namely in-phase/quadrature (I/Q) imbalance, local oscillator (LO) leakage and even-order nonlinearities, than the superheterodyne transceiver [119, 149]. In general, RF imperfections cause signal distortion, and therefore can result in significant performance degradations. If the occurrence of imperfections was prevented by improving the quality of analog RF electronics, the total costs of the components would easily climb to an intolerable level. Instead of doing these costly changes, the overall performance can fortunately be improved also by exploiting the "dirty RF" principle [54] where the imperfections of analog electronics are mitigated by digital signal processing (DSP) algorithms. Note that the exploitation of DSP provides not only better performance with the current analog components, but it can also relax the quality requirements of the components, and thus provide lower costs, smaller size and better energy efficiency even all at once. Naturally, as being such a promising approach, "dirty RF" has resulted in lots of research regarding different aspects on various imperfections in modern RF front-ends. However, so far, the combination of inevitable RF imperfections and increasingly popular multiantenna systems has not been studied comprehensively, and therefore the focus of the thesis is on that particular issue.

1.2 Objectives and Scope of the Thesis

The main objective of the thesis is to facilitate the implementation of a cost/size/power efficient RF front-end in modern multiantenna communications systems. Towards this end, the focus is on modeling, analyzing and digital mitigation of one of the most severe RF imperfections, namely I/Q imbalance, in multiple direct-conversion radios operating in parallel. At the modeling stage, the physical phenomena in the analog electronics are described by mathematical models. These models are then analyzed comprehensively to get an overall understanding of the physical imperfections. The DSP developments naturally follow the obtained models and analysis resulting in algorithms which can effectively mitigate the RF imperfections in practical conditions. Finally, the performance of the developed algorithms is evaluated by extensive computer simulations where different real-world use cases are imitated. Note that including the other RF imperfections of DCTs/DCRs would have resulted in a too wide topic to be covered in a single thesis, and consequently they are not in the scope of this thesis although being very important aspects as well.

1.3 Thesis Contributions and Structure

The main contributions of the thesis are the following

- recognition and analysis of radiation pattern distortion caused by transceiver I/Q imbalances in TX and RX antenna arrays [P1–P4]

- proposal of widely-linear (WL) RX beamforming methods [P1, P3–P4] and a TX beamforming method [P2] for error free beamforming under transceiver I/Q imbalances
- uplink signal model and frequency domain analysis for a flexible multiuser MIMO (MU-MIMO) orthogonal frequency-division multiple access (OFDMA) setup under TX+RX I/Q imbalances where also the effects of external co-channel interferers are taken into account [P6–P8]
- augmented subcarrier processing principle applied to multiantenna BS RX operating in the MU-MIMO OFDMA scheme [P6–P8]
- derivation and analysis of the instantaneous per-data-stream signal-to-interference-and-noise ratio (SINR) after RX processing [P8]
- numerical illustrations of the aspects listed above as a function of several system and transceiver parameters [P1–P8]

The publications [P1–P8] provide more details and numerical performance illustrations compared to what is given in this thesis summary. In order to provide consistent and fluent reading experience, the notation of the thesis differs at some parts slightly from the associated publications.

The thesis is organized as follows. Chapter 2 introduces the essential background theory, whereas Chapters 3 and 4 present the contributions of the thesis. In detail, Chapter 2 focuses on complex I/Q signals and systems, direct-conversion radio architectures and the associated RF imperfections as well as on multiantenna communications principles. In Chapter 3, a basic understanding to the effects and WL mitigation of I/Q imbalance is provided in a case of the classical narrowband antenna array based RX beamforming published in [P1, P3–P4] and corresponding TX beamforming based on the study in [P2]. Subsequently, based on the results from [P5–P8], the studies are extended in Chapter 4 to cover wideband orthogonal frequency-division multiplexing (OFDM)/OFDMA waveforms with the augmented subcarrier processing principle and full MIMO communications incorporating also external interference in the heterogeneous network framework. Chapter 4 addresses also some practical aspects of the proposed solutions, such as adaptive optimization, computational complexity and robustness to time and frequency synchronization errors. Finally, the conclusions of the thesis are drawn in Chapter 5.

1.4 Author's Contributions to the Publications

The research topic regarding analysis and digital mitigation of RF imperfections in multiantenna systems was proposed by Prof. Mikko Valkama. The results of the research were reported in publications [P1–P8] on which this thesis is also based. The author of this thesis is the main contributor for derivations, simulations and composing the publications. Prof. Valkama and D.Sc. Janis Werner have been co-authors in all of the publications and contributed to them by sharing their ideas, solving problems and preparing the publications. The author presented the results of the conference papers

[P2, P5–P7] whereas Prof. Valkama presented the work of [P1] in Austin, TX, USA in 2013 and Prof. Markku Renfors gave the presentation of [P3] in Ilmenau, Germany in 2013. Prof. Kapil R. Dandekar has supported the work by sharing his ideas and observations on RF imperfections in practical radio testbeds.

1.5 Basic Mathematical Notations and Definitions

Throughout the thesis vectors are written in bold lower case ($\mathbf{x}$) and the i^{th} entry of $\mathbf{x}$ is denoted by x_i. Matrices are written in bold upper case ($\mathbf{X}$) and the (ij) entry of $\mathbf{X}$ is given by x_{ij}. The superscripts $(\cdot)^{\mathrm{T}}$, $(\cdot)^{\mathrm{H}}$, $(\cdot)^*$ and $(\cdot)^{-1}$ represent transpose, Hermitian (conjugate) transpose, complex conjugate and matrix inverse, respectively. The tilde sign ($\widetilde{\cdot}$) is used to present a WL and augmented quantities as well as the results obtained by WL and augmented processing. We write $\mathrm{diag}\,(x_{11}, x_{22}, \cdots, x_{ii}, \cdots)$ to denote a diagonal matrix $\mathbf{X}$ that is composed of the entries x_{ii} on the main diagonal. The natural basis vector, where the i^{th} entry is equal to one and the rest are zeros, is denoted as $\mathbf{e}_i$. The absolute value and the argument of a complex variable x are denoted with $|x|$ and $\arg\{x\}$, respectively. The real and imaginary parts of a complex-valued variable x are given by $\Re\{x\}$ and $\Im\{x\}$, respectively. The statistical expectation is denoted with $\mathbb{E}[\cdot]$. Unless otherwise stated, we assume that all signals are zero-mean. A complex random variable x is called circular or proper if $\mathbb{E}[x] = \mathbb{E}[x^2] = 0$.

The Dirac function $\delta(t)$ has the following properties [86, p. 414]

$$\begin{aligned} \delta(t) &= 0 && (t \neq 0) \\ \int_{-\infty}^{\infty} \delta(t)\mathrm{d}t &= \int_{a}^{b} \delta(t)\mathrm{d}t = 1 && \text{where } a < 0,\, b > 0. \end{aligned} \tag{1.1}$$

The Fourier transform of a continuous-time signal $x(t)$ is defined by [86, p. 644]

$$\mathscr{F}\{x(t)\} = X(f) = \int_{-\infty}^{\infty} x(t) e^{-j2\pi f t}\mathrm{d}t \tag{1.2}$$

whereas the corresponding inverse Fourier transform is defined by [86, p. 644]

$$\mathscr{F}^{-1}\{X(f)\} = x(t) = \int_{-\infty}^{\infty} X(f) e^{j2\pi f t}\mathrm{d}f. \tag{1.3}$$

Furthermore, the Fourier transform of a discrete-time signal $x(k)$ is given by [86, p. 676]

$$\mathscr{F}\{x(k)\} = X(e^{j\omega}) = \sum_{k=-\infty}^{\infty} x(k) e^{-j\omega k} \tag{1.4}$$

where $\omega = 2\pi f T$ and T is the time between signal samples. The corresponding inverse Fourier transform is equal to [86, p. 677]

$$\mathscr{F}^{-1}\{X(e^{j\omega})\} = x(k) = \frac{1}{2\pi} \int_{-\pi}^{\pi} X(e^{j\omega}) e^{j\omega k}\mathrm{d}\omega. \tag{1.5}$$

The convolution of two piecewise-continuous functions $x(t)$ and $y(t)$ is equal to [86, p. 443]

$$x(t) \star y(t) = \int_{-\infty}^{\infty} x(\tau) y(t-\tau) \mathrm{d}\tau. \tag{1.6}$$

Finally, the convolution of two discrete-time functions $x(k)$ and $y(k)$ is given by [101, p. 13]

$$x(k) \star y(k) = \sum_{l=-\infty}^{\infty} x(l) y(k-l). \tag{1.7}$$

Let $\mathbf{x} \in \mathbb{C}^{N\times 1}$ be a vector with zero mean. Then, the correlation matrix $\mathbf{R} \in \mathbb{C}^{N\times N}$ of $\mathbf{x}$ is defined by [73, p. 39]

$$\mathbf{R} = \mathbb{E}[\mathbf{x}\mathbf{x}^{\mathrm{H}}]. \tag{1.8}$$

Stemming from the fact that $\mathbf{x}$ has a zero mean, correlation and covariance of $\mathbf{x}$ are equal [66, p. 581], and consequently $\mathbf{R}$ can also be referred to as covariance matrix.

CHAPTER 2

Essential Signal Models and Basic Concepts

This chapter introduces shortly the essential signal and system models as well as the basic concepts related to the topics of the thesis. First, the focus is on the basics of I/Q signal processing in direct-conversion radio architectures, and on fundamental properties of the signals in different processing stages. We continue to essential RF imperfections occurring in direct-conversion transceivers, focusing on I/Q imbalance whereas the other RF imperfections are also shortly discussed. Finally, we introduce multiantenna communications through several basic concepts, namely beamforming, antenna diversity, spatial multiplexing and massive MIMO.

2.1 Complex I/Q Signals and Systems

Complex-valued I/Q signals are a common and convenient mathematical representation for a pair of real-valued signals in communications systems [101, p. 12]. When considering transmission of a signal, the data to be transmitted is first pre-processed by DSP algorithms, as depicted in Fig. 2.1. The digital signal is then fed to a TX RF front-end for sending the data to the recipients in a wireless manner. In general, the digital complex-valued input signal of a TX RF front-end can be denoted by $x(k) = x_I(k) + jx_Q(k)$ where k denotes the sample index. The real part $x_I(k) = \Re\{x(k)\}$ and the imaginary part $x_Q(k) = \Im\{x(k)\}$ are called in-phase (I) and quadrature (Q) signals, respectively. Since these signals are independent of each other, they can be processed separately in most of the processing blocks of the TX RF front-end. The real-valued input signals are first converted to continuous analog signals by digital-to-analog converters (DACs). The resulting analog signals are then filtered by lowpass filters (LPFs) to remove harmful harmonics generated in the conversion. We denote the filtered signals by $x_I(t)$ and $x_Q(t)$, yielding a complex-valued signal equal to $x(t)= x_I(t) + jx_Q(t)$. The steps described above are typical to all TX RF front-ends operating with complex-valued signals. The next step, however, is a specialty of the direct-conversion architecture. There $x_I(t)$ is multiplied with a real-valued high frequency LO signal $\cos(2\pi f_{\mathrm{LO}} t)$, which locates

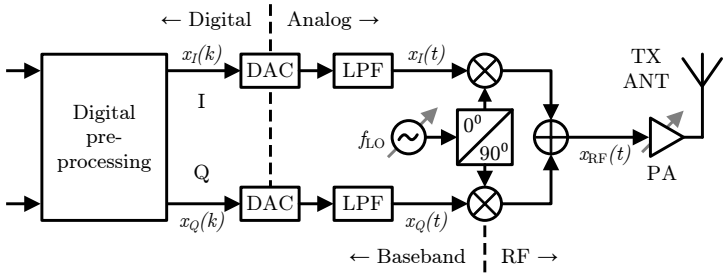

Figure 2.1: Conceptual direct-conversion transmitter block diagram with the used notation.

in the desired RF band. Here f_{LO} denotes the LO frequency. Furthermore, $x_Q(t)$ is multiplied with $-\sin(2\pi f_{\mathrm{LO}}t)$, which has 90° phase difference compared to $\cos(2\pi f_{\mathrm{LO}}t)$ used in the I branch [157]. The process can be interpreted also as taking the real part of the product of complex-valued $x(t)$ and a complex-valued high frequency LO signal $e^{j2\pi f_{\mathrm{LO}}t} = \cos(2\pi f_{\mathrm{LO}}t) + j\sin(2\pi f_{\mathrm{LO}}t)$. Mathematically expressed the resulting RF signal is thus given by [66, 157]

$$\begin{aligned} x_{\mathrm{RF}}(t) &= \Re\left\{x(t)e^{j2\pi f_{\mathrm{LO}}t}\right\} \\ &= \frac{1}{2}\left(x(t)e^{j2\pi f_{\mathrm{LO}}t} + x^*(t)e^{-j2\pi f_{\mathrm{LO}}t}\right) \\ &= x_I(t)\cos(2\pi f_{\mathrm{LO}}t) - x_Q(t)\sin(2\pi f_{\mathrm{LO}}t). \end{aligned} \tag{2.1}$$

Note that this step, known as quadrature or I/Q mixing, is indeed a clear difference compared to the commonly used superheterodyne architecture where the mixing is implemented in two (or more) consecutive mixing stages through intermediate frequency (IF) [68, p. 115]. After I/Q mixing, the RF signal is amplified with a power amplifier (PA) and finally converted from an altering current distribution to electromagnetic radiation by a TX antenna. In practice, the RF signal experiences additional filtering between the PA and antenna, but this filtering stage is not illustrated here for simplicity.

To form a solid basis for the rest of the thesis, it is useful to notice a couple of things from the frequency contents of the signals in different processing stages. In general, $x(k)$ and $x(t)$ are considered as baseband (low-pass) signals, which have content only close to zero frequency. As an example, Fig. 2.2a illustrates the amplitude spectrum $|X(f)| = |\mathscr{F}\{x(t)\}|$. Furthermore, as visible in Fig. 2.2b depicting the amplitude spectra $|X_{\mathrm{RF}}(f)| = |\mathscr{F}\{x_{\mathrm{RF}}(t)\}|$, the quadrature mixing in DCTs converts the baseband signal $x(t)$ directly to RF frequencies. Consequently, the mixing process in TXs is referred to as up-conversion [174, p. 22]. Note also that the resulting RF signal is real-valued, and thus has a symmetric spectrum around the zero frequency, although the original complex-valued input signal $x(t)$ does not, in general, fulfill such a rule. Finally, since most of the signal processing in transceivers is done at the baseband, a definition for the baseband equivalent of real-valued bandpass signal $x_{\mathrm{RF}}(t)$ is needed [174, p. 22]. However, as an intermediate step, we need an analytical signal which contains the contents of $X_{\mathrm{RF}}(f)$ only above the zero frequency [144, p. 21]. Mathematically, such a signal is given by $x_{\mathrm{RF}+}(t) = \mathscr{F}^{-1}\{X_{\mathrm{RF}+}(f)\} = \mathscr{F}^{-1}\{u(f)X_{\mathrm{RF}}(f)\} = \frac{1}{2}x(t)e^{j2\pi f_{\mathrm{LO}}t}$ where $u(f)$ is the unit step function. The amplitude spectrum of $x_{\mathrm{RF}+}(t)$ is depicted in Fig. 2.2c. The

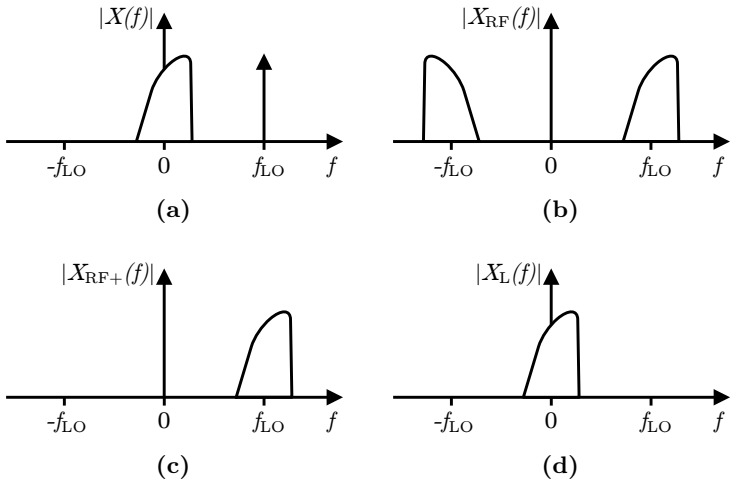

Figure 2.2: Spectrum illustration of (a) complex-valued baseband signal $x(t)$ and LO signal $e^{j2\pi f_{\mathrm{LO}}t}$, (b) real-valued RF signal $x_{\mathrm{RF}}(t)$, (c) complex-valued analytical signal $x_{\mathrm{RF}+}(t)$, and (d) complex-valued baseband equivalent signal $x_{\mathrm{L}}(t)$.

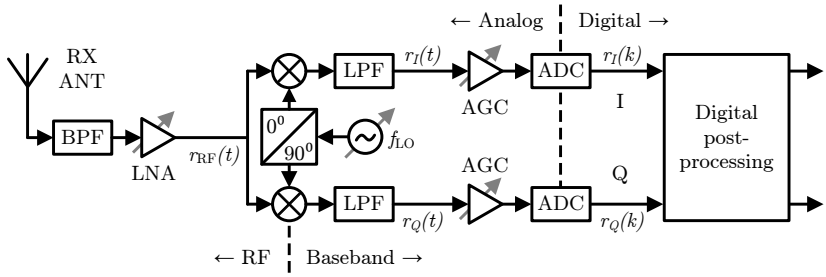

Figure 2.3: Conceptual direct-conversion receiver block diagram with the used notation.

baseband equivalent of $x_{\mathrm{RF}}(t)$ is then given by $x_{\mathrm{L}}(t)= 2x_{\mathrm{RF}+}(t)e^{-j2\pi f_{\mathrm{LO}}t}$ [144, p. 22], being eventually a down-converted version of $x_{\mathrm{RF}+}(t)$. The amplitude spectrum of $x_{\mathrm{L}}(t)$ is depicted in Fig. 2.2d showing that the baseband equivalent signal $x_{\mathrm{L}}(t)$ matches perfectly with the original baseband signal $x(t)$. This is indeed the case when assuming perfect frequency conversions and ideal RF front-ends.

In a DCR, depicted in Fig. 2.3, the signal flow follows similar principles but naturally the order is reversed when compared to a DCT. Now, an antenna converts the received electromagnetic radiation to a signal in the device. The obtained signal goes first through a bandpass filter (BPF), which mitigates the unwanted frequency components, i.e. out-of-band interference, while passing through the desired frequencies. The filtered signal, which can be very weak in power, is next amplified by a low noise amplifier (LNA) resulting in a signal denoted here by $r_{\mathrm{RF}}(t)$. Subsequently, the amplified RF signal is down-converted to the baseband. This is carried out by a LO signal which has the same frequency as the LO signal in the TX but now the sign is the opposite, i.e. the RX LO

signal has a form of $e^{-j2\pi f_{\mathrm{LO}}t}$. After removing higher order down-conversion products by LPFs, the resulting baseband signal is equal to [157, p. 143]

$$r(t) = \mathrm{LPF}\left\{r_{\mathrm{RF}}(t)e^{-j2\pi f_{\mathrm{LO}}t}\right\}. \tag{2.2}$$

The I and Q components of $r(t)$ are given straightforwardly by $r_I(t)= \Re\{r(t)\}$ and $r_Q(t)= \Im\{r(t)\}$, respectively. These two real-valued signals are further amplified in automatic gain control (AGC) stages and then converted to digital signals $r_{\mathrm{I}}(k)$ and $r_{\mathrm{Q}}(k)$ by analog-to-digital converters (ADCs). The obtained digital signals are finally forwarded for further digital post-processing stages, such as channel equalization and detection.

The frequency contents of the received signals are similar to the ones in the TX. That is, the received signal $r_{\mathrm{RF}}(t)$ locates on RF frequencies, and $r(t)$ and $r(k)$ are baseband signals. However, it should be noted that the received signals include also the effects of the wireless propagation channel between the TX and RX. In addition, the RX electronics and especially the LNA generate some additive noise to the received signal. Consequently, following the used notation, the received signal is given by $r_{\mathrm{RF}}(t) = h_{\mathrm{RF}}(t) \star\ x_{\mathrm{RF}}(t) + n_{\mathrm{RF}}(t)$ where $h_{\mathrm{RF}}(t)$ denotes the impulse response of the wireless propagation channel and $n_{\mathrm{RF}}(t)$ is the additive white Gaussian noise occurring in the RX electronics [144, p. 11]. Moreover, the baseband equivalent of the received continuous-time RF signal $r_{\mathrm{RF}}(t)$ is equal to $r_{\mathrm{L}}(t) = h_{\mathrm{L}}(t) \star\ x_{\mathrm{L}}(t) + n_{\mathrm{L}}(t)$ where all variables refer to their corresponding baseband equivalents [143, p. 154]. Since the linear convolution in time-domain is transformed into a product in frequency-domain [86, p. 673], the Fourier transform of the baseband equivalent received signal is given by $\mathscr{F}\{r_{\mathrm{L}}(t)\} = R_{\mathrm{L}}(f) = H_{\mathrm{L}}(f)X_{\mathrm{L}}(f) + N_{\mathrm{L}}(f)$.

2.2 RF Imperfections in Direct-Conversion Transceivers

2.2.1 I/Q Imbalance

As discussed in Section 2.1 and depicted in Fig. 2.1, I and Q branches in direct-conversion TXs carry independent real-valued signals. The impulse responses of different branches are ideally equal but this is not the case in practice since RF components have some variations due to manufacturing tolerances [157]. On the one hand, the amplitude responses of the filtering, amplification, DAC/ADC and mixing stages are not exactly the same in both branches. That causes *gain imbalance* between the signals in the I and Q branches [119, 149]. On the other hand, the concept of quadrature mixing is based on 90° phase difference between the LO signals for I and Q signals. However, such an exact value is challenging to obtain in real world implementations. Practically, errors in the nominal 90° phase shift violate the quadrature mixing principle and cause *phase imbalance* between the branches [119,149]. Moreover, the phase imbalance is affected also by the unequal phase responses between the I and Q branches. Together, gain and phase imbalances result in a signal distortion called *I/Q imbalance*. It is noteworthy that the gain and phase imbalances can be frequency-dependent already within practical signal bandwidths, and thus also the I/Q imbalance becomes highly dependent on frequency.

In general, I/Q imbalance can be modeled either symmetrical or asymmetrical [157, p. 143]. In the symmetrical model, the effects of I/Q imbalance are divided equally for both branches, see e.g. [106, 130, 151, 162, 169, 173, 195], whereas in the asymmetrical model the effects of I/Q imbalance are distributed unequally between the branches, see e.g. [13, 119, 149, 157, 185, 204]. These models are equivalent from the I/Q imbalance perspective, as shown in Appendix A, and throughout this thesis the asymmetrical model is preferred. Note that the I/Q imbalance models provided in this section are commonly used in the literature and have been verified with extensive RF measurements, e.g., in [11, 12, 95, 183, 204].

Considering a bandpass signal suffering from TX I/Q imbalance, the corresponding baseband equivalent signal can be expressed as [13, 204]

$$x_{\mathrm{Txi}}(t) = g_{\mathrm{Tx1}}(t) \star x_{\mathrm{L}}(t) + g_{\mathrm{Tx2}}(t) \star x_{\mathrm{L}}^{*}(t) \tag{2.3}$$

where the TX I/Q imbalance coefficients are equal to

$$g_{\mathrm{Tx1}}(t) = \frac{\delta(t) + h_{\mathrm{Tx}}(t) g_{\mathrm{Tx}} e^{j\phi_{\mathrm{Tx}}}}{2}, \qquad g_{\mathrm{Tx2}}(t) = \frac{\delta(t) - h_{\mathrm{Tx}}(t) g_{\mathrm{Tx}} e^{j\phi_{\mathrm{Tx}}}}{2}. \tag{2.4}$$

Here, $\delta(t)$ denotes the Dirac delta function, $h_{\mathrm{Tx}}(t)$ is the frequency-dependent impulse response imbalance between the I and Q branches, g_{Tx} denotes the relative frequency-independent TX gain imbalance of the mixing stage and ϕ_{Tx} is the frequency-independent TX phase imbalance parameter. Note that these models include only the effects of the gain and phase imbalances whereas the impulse response common for the I and Q branches has been neglected since it does not change the relative strengths of the signal components [13, 204]. Ideally, i.e. without TX I/Q imbalance, $h_{\mathrm{Tx}}(t) = \delta(t)$, $g_{\mathrm{Tx}} = 1$ and $\phi_{\mathrm{Tx}} = 0$ resulting in $g_{\mathrm{Tx1}}(t) = \delta(t)$ and $g_{\mathrm{Tx2}}(t) = 0$ as expected.

The effects of RX I/Q imbalance can be presented similarly to the TX side. The baseband equivalent of a signal under RX I/Q imbalance is given by [13, 204]

$$r_{\mathrm{Rxi}}(t) = g_{\mathrm{Rx1}}(t) \star r_{\mathrm{L}}(t) + g_{\mathrm{Rx2}}(t) \star r_{\mathrm{L}}^{*}(t) \tag{2.5}$$

where the RX I/Q imbalance coefficients are equal to

$$g_{\mathrm{Rx1}}(t) = \frac{\delta(t) + h_{\mathrm{Rx}}(t) g_{\mathrm{Rx}} e^{-j\phi_{\mathrm{Rx}}}}{2}, \qquad g_{\mathrm{Rx2}}(t) = \frac{\delta(t) - h_{\mathrm{Rx}}(t) g_{\mathrm{Rx}} e^{j\phi_{\mathrm{Rx}}}}{2}. \tag{2.6}$$

The notation here follows similar principles to the TX I/Q imbalance given in (2.3) and (2.4). Also now the ideal case, i.e. no RX I/Q imbalance, is obtained by substituting $h_{\mathrm{Rx}}(t) = \delta(t)$, $g_{\mathrm{Rx}} = 1$ and $\phi_{\mathrm{Rx}} = 0$. As visible in (2.3) and (2.5), the resulting imbalanced signals $x_{\mathrm{Txi}}(t)$ and $r_{\mathrm{Rxi}}(t)$ consist of both the original signal ($x_{\mathrm{L}}(t)$ or $r_{\mathrm{L}}(t)$) and its complex conjugate. Thus, I/Q imbalance can be considered as a *WL transformation* and consequently the imbalanced signals are non-circular or non-proper, even if the original signals were circular [13, 161].

The effects of I/Q imbalance in frequency domain can be clarified through the Fourier transforms of (2.3) and (2.5). They are given by [13, 204]

$$X_{\mathrm{Txi}}(f) = G_{\mathrm{Tx1}}(f) X_{\mathrm{L}}(f) + G_{\mathrm{Tx2}}(f) X_{\mathrm{L}}^{*}(-f), \tag{2.7}$$

$$R_{\mathrm{Rxi}}(f) = G_{\mathrm{Rx1}}(f) R_{\mathrm{L}}(f) + G_{\mathrm{Rx2}}(f) R_{\mathrm{L}}^{*}(-f). \tag{2.8}$$

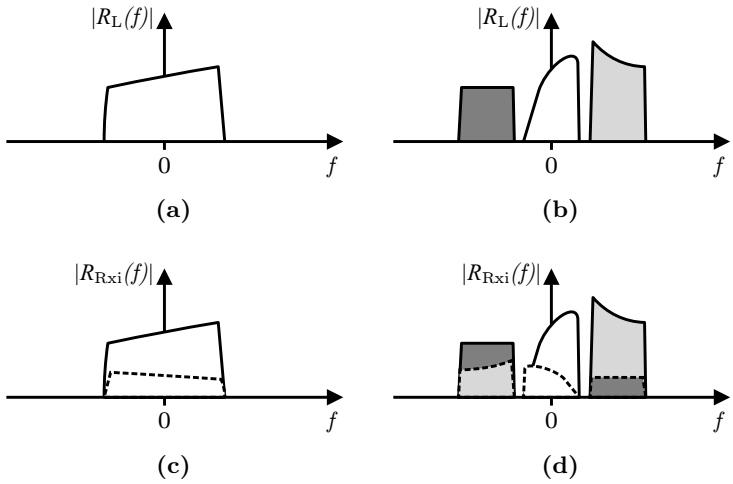

Figure 2.4: Spectrum of the baseband equivalent of (a) single-channel signal with ideal RX I/Q balance, (b) multi-channel signal with ideal RX I/Q balance, (c) single-channel signal with RX I/Q imbalance, and (d) multi-channel signal with RX I/Q imbalance. Dashed lines present the spectra of the mirror frequency interference components.

where

$$G_{\mathrm{Tx1}}(f) = \frac{1 + H_{\mathrm{Tx}}(f) g_{\mathrm{Tx}} e^{j\phi_{\mathrm{Tx}}}}{2}, \qquad G_{\mathrm{Tx2}}(f) = \frac{1 - H_{\mathrm{Tx}}(f) g_{\mathrm{Tx}} e^{j\phi_{\mathrm{Tx}}}}{2}, \tag{2.9}$$

$$G_{\mathrm{Rx1}}(f) = \frac{1 + H_{\mathrm{Rx}}(f) g_{\mathrm{Rx}} e^{-j\phi_{\mathrm{Rx}}}}{2}, \qquad G_{\mathrm{Rx2}}(f) = \frac{1 - H_{\mathrm{Rx}}(f) g_{\mathrm{Rx}} e^{j\phi_{\mathrm{Rx}}}}{2}. \tag{2.10}$$

Based on (2.7) and (2.8), it is evident that TX and RX I/Q imbalances create the mirror-frequency interference through the image signals $X^*_{\mathrm{L}}(-f)$ and $R^*_{\mathrm{L}}(-f)$, which are weighted with the transfer functions $G_{\mathrm{Tx2}}(f)$ and $G_{\mathrm{Rx2}}(f)$ determined by TX and RX I/Q imbalances, respectively [191]. In general, the mirror-frequency interference is visible as overlapping spectral components illustrated for a DCR in Fig. 2.4. The spectra of the baseband equivalents of single- and multi-channel signals with ideal I/Q balance are given in Figs. 2.4a and 2.4b, respectively. Furthermore, the spectrum of the single-channel case under RX I/Q imbalance is depicted in Fig. 2.4c. As visible there, the spectrum of the mirror-frequency component overlaps with the spectrum of the signal of interest (SOI) and thus causes self-interference. Similar effect is seen for the middle channel signal in Fig. 2.4d depicting the spectrum for the multi-channel case under RX I/Q imbalance. The figure shows also that the signals on the outermost channels suffer from the alternate channel interference [13]. Consequently, the severity of the mirroring effect is evidently dependent on the relative power levels of the signals on different channels. Moreover, the transfer functions given in (2.9) and (2.10) and especially the ratios $G_{\mathrm{Tx1}}(f)/G_{\mathrm{Tx2}}(f)$ and $G_{\mathrm{Rx1}}(f)/G_{\mathrm{Rx2}}(f)$ affect the influence of I/Q imbalance as will be discussed in more detail on page 14. Finally, it should be noted that, since the baseband equivalent of the received signal is equal to $r_{\mathrm{L}}(t) = h_{\mathrm{L}}(t) \star x_{\mathrm{L}}(t) + n_{\mathrm{L}}(t)$ having the Fourier transform $R_{\mathrm{L}}(f) = H_{\mathrm{L}}(f)X_{\mathrm{L}}(f) + N_{\mathrm{L}}(f)$, the Fourier transform of

the received signal in (2.8) can be expressed also as

$$\begin{aligned} R_{\mathrm{Rxi}}(f) = {} & G_{\mathrm{Rx1}}(f)H_{\mathrm{L}}(f)X_{\mathrm{L}}(f) + G_{\mathrm{Rx2}}(f)H_{\mathrm{L}}^{*}(-f)X_{\mathrm{L}}^{*}(-f) \\ & + G_{\mathrm{Rx1}}(f)N_{\mathrm{L}}(f) + G_{\mathrm{Rx2}}(f)N_{\mathrm{L}}^{*}(-f). \end{aligned} \tag{2.11}$$

The last term in (2.11) shows that also the noise is affected by the mirroring in the RX. With reasonable I/Q imbalance values, $|G_{\mathrm{Rx2}}(f)| \ll |G_{\mathrm{Rx1}}(f)|$ and the mirrored noise is not very strong but it still makes the aggregated noise non-circular [13]. Furthermore, if $n_{\mathrm{L}}(t)$ is considered to include also the effects of any interference, having possible very high power levels, the mirroring of the noise and interference might cause significant distortion to the signal at frequency f [P5–P8].

Since many modern communications systems utilize OFDM-based waveforms [66, p. 374], which are considered also in [P5–P8], it is useful at this point to pay more attention for I/Q imbalances in OFDM-based systems. In such systems, the overall frequency band, having a bandwidth of tens or even hundreds of megahertz, is utilized by multiple orthogonal narrowband subcarrier signals. The number of subcarriers is selected in such a way that the resulting subcarrier bandwidth is less than the expected channel coherence bandwidth. Consequently, the wireless propagation channel within a single subcarrier band can be considered to be flat [66, p. 374]. Furthermore, due to the narrow subcarrier bandwidth, also the effects of I/Q imbalance within a single subcarrier can be modeled frequency-independent. The actual digital OFDM signal processing flow is, in turn, introduced below, following the description in [66, p. 386]. In the TX side, the digital frequency-domain data stream is first converted to C_{a} parallel data streams where C_{a} is the number of active subcarriers. The parallel streams are then used to modulate orthogonal subcarrier signals. This is done by converting the parallel frequency-domain data streams into a time-domain signal sequence, also known as an OFDM symbol, through the inverse fast Fourier transform (IFFT) with the size of $C \geq C_{\mathrm{a}}$. The cyclic prefix (CP) is then added to the symbol and the resulting time samples are ordered by the parallel-to-serial converter. Finally the resulting signal is forwarded to a RF front-end. In the RX side, the process is reversed, i.e. the RF front-end is followed by the CP removal, serial-to-parallel converter and fast Fourier transform (FFT). The essential data exist thus at subcarrier level, and consequently it is sensible to investigate the effects of I/Q imbalances from a viewpoint of a single frequency-domain subcarrier signal. We index the subcarriers by $c \in \{-C/2, \ldots, -1, 1, \ldots, C/2\}$ and denote the mirror subcarrier of subcarrier c by $c' = -c$. That is, c and c' have an equal distance to the carrier frequency at RF and to the zero frequency at the baseband, hence locating at mirrored positions in terms of the carrier/zero frequency. With these definitions, the frequency-domain data at subcarrier c under TX/RX I/Q imbalance is equal to [98, 137, 156, 157, 191]

$$x_{\mathrm{Txi},c}(i) = K_{\mathrm{Tx1},c}x_c(i) + K_{\mathrm{Tx2},c}x_{c'}^{*}(i) \tag{2.12}$$

$$r_{\mathrm{Rxi},c}(i) = K_{\mathrm{Rx1},c}r_c(i) + K_{\mathrm{Rx2},c}r_{c'}^{*}(i) \tag{2.13}$$

where a perfect frequency and timing synchronization is assumed between the TX and RX. Here $x_c(i)$ and $r_c(i)$ denote the digital frequency-domain TX and RX data at subcarrier c within OFDM symbol i. Note that the data variables are written in lower case letters for consistency with publications [P5–P8]. The I/Q imbalance parameters at

subcarrier c are given by

$$K_{\mathrm{Tx1},c} = \frac{1 + g_{\mathrm{Tx},c} e^{j\phi_{\mathrm{Tx},c}}}{2}, \qquad K_{\mathrm{Tx2},c} = \frac{1 - g_{\mathrm{Tx},c} e^{j\phi_{\mathrm{Tx},c}}}{2}, \tag{2.14}$$

$$K_{\mathrm{Rx1},c} = \frac{1 + g_{\mathrm{Rx},c} e^{-j\phi_{\mathrm{Rx},c}}}{2}, \qquad K_{\mathrm{Rx2},c} = \frac{1 - g_{\mathrm{Rx},c} e^{j\phi_{\mathrm{Rx},c}}}{2}. \tag{2.15}$$

As visible in (2.12) and (2.13), OFDM systems under I/Q imbalances suffer from *inter-carrier interference (ICI)* where the signal from the mirror subcarrier c' leaks to subcarrier c. Clearly, this is a special case of the mirror-frequency interference shown already in Fig. 2.4. The I/Q imbalance expressions in (2.12)–(2.15) are used in publications [P5–P8] and also in Chapter 4 in this thesis.

The expressions in (2.3) and (2.5) provide generic models for frequency-selective and time-variant TX and RX I/Q imbalances whereas (2.12) and (2.13) describe I/Q imbalances with OFDM-based signals. However, when considering only narrowband signals, the provided models are simplified. In particular, the frequency-independent, instantaneous time-domain models for TX and RX I/Q imbalances are given by [13]

$$x_{\mathrm{Txi}}(t) = K_{\mathrm{Tx1}} x_{\mathrm{L}}(t) + K_{\mathrm{Tx2}} x_{\mathrm{L}}^{*}(t), \tag{2.16}$$

$$r_{\mathrm{Rxi}}(t) = K_{\mathrm{Rx1}} r_{\mathrm{L}}(t) + K_{\mathrm{Rx2}} r_{\mathrm{L}}^{*}(t) \tag{2.17}$$

where the I/Q imbalance coefficients are similar to (2.14) and (2.15) but now just without the subcarrier indices. Moreover, the I/Q imbalance coefficients are equal to

$$K_{\mathrm{Tx1}} = \frac{1 + g_{\mathrm{Tx}} e^{j\phi_{\mathrm{Tx}}}}{2}, \qquad K_{\mathrm{Tx2}} = \frac{1 - g_{\mathrm{Tx}} e^{j\phi_{\mathrm{Tx}}}}{2}, \tag{2.18}$$

$$K_{\mathrm{Rx1}} = \frac{1 + g_{\mathrm{Rx}} e^{-j\phi_{\mathrm{Rx}}}}{2}, \qquad K_{\mathrm{Rx2}} = \frac{1 - g_{\mathrm{Rx}} e^{j\phi_{\mathrm{Rx}}}}{2}. \tag{2.19}$$

The models given in (2.16)–(2.19) are used in [P1–P4] and also in Chapter 3 in this thesis for analyzing beamforming properties of narrowband signals under TX and RX I/Q imbalances.

A common measure to quantify the quality of a single analog TX/RX radio front-end in terms of I/Q imbalance is the image rejection ratio (IRR). Depending on the used signal model, the IRRs for a TX and RX are given by

$$\mathrm{IRR}_{\mathrm{Tx}}(f) = \frac{|G_{\mathrm{Tx1}}(f)|^2}{|G_{\mathrm{Tx2}}(f)|^2}, \quad \mathrm{IRR}_{\mathrm{Tx},c} = \frac{|K_{\mathrm{Tx1},c}|^2}{|K_{\mathrm{Tx2},c}|^2}, \quad \mathrm{IRR}_{\mathrm{Tx}} = \frac{|K_{\mathrm{Tx1}}|^2}{|K_{\mathrm{Tx2}}|^2}, \tag{2.20}$$

$$\mathrm{IRR}_{\mathrm{Rx}}(f) = \frac{|G_{\mathrm{Rx1}}(f)|^2}{|G_{\mathrm{Rx2}}(f)|^2}, \quad \mathrm{IRR}_{\mathrm{Rx},c} = \frac{|K_{\mathrm{Rx1},c}|^2}{|K_{\mathrm{Rx2},c}|^2}, \quad \mathrm{IRR}_{\mathrm{Rx}} = \frac{|K_{\mathrm{Rx1}}|^2}{|K_{\mathrm{Rx2}}|^2}. \tag{2.21}$$

Here the leftmost expressions are for the frequency-dependent signal models in (2.3) and (2.5), the expressions in the middle are for the OFDM signal models given in (2.12)–(2.13), and the rightmost are for the narrowband models in (2.16)–(2.17). As an illustrative example, the dependency of the IRR on the actual gain and phase imbalances is depicted in Fig. 2.5. Individual processing stages, such as mixers and I/Q demodulators, in real-world RF front-end implementations are reported to have the IRR in a range of

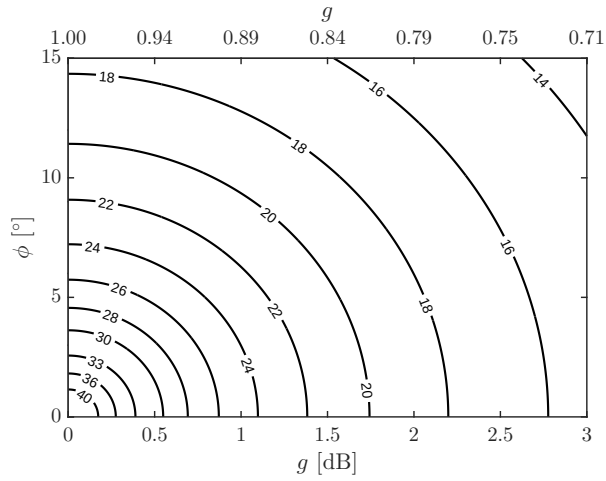

Figure 2.5: Contour lines of the IRR as a function of the gain imbalance g and the phase imbalance ϕ. The IRR values are given in decibels.

15 dB–55 dB [7, 104] depending on the used bandwidth, power consumption etc. whereas typical IRR values of the whole transceiver, without additional I/Q calibration, are around 25 dB–40 dB [12, 191]. Note also that stemming from the frequency-selective terms in (2.9)–(2.10) and (2.14)–(2.15), the resulting IRR may have a variation of several decibels already within a few megahertz [11, 95, 111, 204].

The severity of the signal distortion caused by I/Q imbalances is clearly application-specific. It is well known that I/Q imbalance becomes a bigger problem with larger signal constellations since the probability for erroneous detection increases due to more dense constellation points. That does not bode well for the future, since the development of communications systems has been pushing towards larger and larger constellations due to the demand of higher data rates. Moreover, new technologies such as exploitation of mmWaves in 5G systems might not be able to reach the same level of RF front-end performance as the well-established implementations in the third generation (3G) and fourth generation (4G) systems. As an example, mixers and RF front-ends at mmWave frequencies are reported to have the IRR equal to 12 dB–30 dB [33, 59, 60]. When comparing these values, e.g. with the minimum requirement of 25 dB IRR in the 3rd Generation Partnership Project (3GPP) long term evolution (LTE)/long term evolution advanced (LTE-A) specification [1], it becomes obvious that the poor IRR performance of mmWave implementations may not be sufficient as such for all purposes. When further assuming that the increasingly popular concepts of the IoT and massive MIMO are based on low-cost and low-power implementations, being consequently vulnerable for performance degradations, there will be a big demand for effective I/Q imbalance mitigation solutions in the future.

According to the dirty RF paradigm, the signal distortions due to imperfections in the analog electronics are mitigated by DSP algorithms [54]. Fortunately, that is a valid approach also for I/Q imbalance and the actual processing can be implemented either on the TX side by signal pre-distortion, or on the RX side by signal post-processing.

Naturally, the pre-distortion technique fits better for TX I/Q imbalance whereas the RX compensation can handle RX or TX+RX I/Q imbalances. The mitigation methods can, in general, be divided into blind and data-aided techniques [13]. The data-aided methods utilize known training signals whereas the blind methods are based on the statistical properties of the signals. When first concentrating on the RX side, the data-aided methods compare the received signal with a known pilot or beacon signal for estimating the I/Q imbalance parameters along with the propagation channel. The obtained estimates are then used for I/Q imbalance cancellation together with the channel equalization, see e.g. [48, 109, 162, 171, 173, 176]. In the TX side, the data-aided principle is similar but there the comparison is made between the known transmit signal and an internal feedback signal including the effects of TX I/Q imbalance [12, 46]. In contrast to the data-aided approach, the blind methods exploit, e.g., the fact that I/Q imbalance performs a WL transformation to the original signal and thus creates correlation between the I and Q signals. This makes the complex-valued signal non-circular, and thus the distortion can be mitigated by the so-called recircularization. This removes the correlation by restoring the circularity property of the received signal, and thus mitigates the harmful I/Q imbalance effects [72, 145, 182]. In addition to circularity and second-order statistics, blind compensation can be based also on higher order statistics or adaptive interference cancellation methods [180, 181]. Whereas the discussion above is about the basic principles of I/Q imbalance mitigation, more detailed discussion of studies related to the work in this thesis are given in Sections 3.1 and 4.1.

2.2.2 Other Essential RF Imperfections

In addition to I/Q imbalance, direct-conversion architectures suffer also from other RF imperfections. One of these is *the direct current (DC) offset* which occurs in DCRs. It arises due to imperfect isolation between the signal and LO paths [3, 68, 119]. Practically, LO signal, which locates on the same frequencies as the SOI, is coupled to the RF signal coming from the antenna. Consequently, the existence of the LO signal in both the RF and LO inputs of a mixer results in a DC component at the mixer output. In addition, the phenomenon can happen in the other direction. That is, a strong in-band interference signal coming from the RX antenna might be coupled to the LO port of the mixer resulting in a time-variant DC component in the mixer output due to self-mixing. Removal of the DC components is essential since a strong DC component can distort the signal and even saturate the following processing stages [149]. However, the removal might be challenging to be implemented purely in analog electronics since also the SOI, possibly having components locating close to the zero frequency, is easily affected. Therefore, the cancellation might also be implemented jointly by analog and digital parts [68].

The imperfect isolation of the LO and signal paths might also cause another problem. If the LO signal finds its way to the antenna, it can cause unwanted radiation on the signal band [3, 68, 71, 119, 149, 175]. This *LO leakage* might interfere with other receiving devices nearby. Consequently, in order to meet the strict requirements of spurious transmission, the isolation between the LO and RX antenna needs to be designed carefully, meaning practically a proper design of RF shielding, RF integrated circuits (ICs) and printed circuit board (PCB) layouts.

Direct-conversion transceivers are known to suffer also from amplifier nonlinearities. In addition to the common odd-order nonlinearities occurring in TX PAs and RX LNAs, *even-order nonlinearities* might become an issue in DCRs [68, 119, 149]. This happens especially when there are two strong interferers with frequencies of f_1 and f_2 so that the second-order intermodulation products, with frequencies of $f_1 - f_2$ and $f_2 - f_1$, are located at the baseband after the LNA. Due to finite isolation of mixers, some parts of the intermodulation products in the RF input leak to the output of the mixer and result in an interference at the band of the SOI [149, 183]. Another drawback of even-order nonlinearities is that the second harmonic of the SOI might be mixed with the second harmonic of the LO signal. Also that results in baseband interference signal which, in fact, has twice the bandwidth of the SOI [68]. In general, amplifier nonlinearities can be mitigated by exploiting specific hardware structures [150] and DSP methods, see e.g. [5, 51, 163] and references therein.

Due to the fact that the down-converted signal in DCRs locates around zero frequency, also *the flicker noise* with a $1/f$ power spectral density can cause problems. The received signal is usually low in power, even after being amplified by the LNA, and thus the flicker noise might have some severe effects in the following processing stages [68, 128, 149]. In particular, the signal-to-noise ratio (SNR) is lower than in superheterodyne RXs where only thermal noise is present [3]. However, the harmful effects can be mitigated in different ways, such as by incorporating large baseband components minimizing the flicker noise [149] or by utilizing special mixer structures in the DCRs [140, 201].

In addition to the RF imperfections listed above, direct-conversion transceivers are vulnerable to certain other RF imperfections which are typical in modern wireless communications systems, especially in OFDM-based systems, independent of the RF front-end architecture. In particular, *the carrier frequency offset (CFO)* and *phase noise* distort the signals and can cause problems if not taken properly into account [16, 45, 122, 132, 142, 157]. The CFO is caused by the frequency difference of the LO signals in the TX and RX, and by Doppler shifts due to moving transceivers. This results in a rotation and attenuation of the received signal, and generates ICI between OFDM subcarriers [157, p. 42]. The frequency synchronization is a common task for all RXs and commonly implemented by DSP algorithms, see e.g. [159, 179, 186]. The phase noise, in turn, describes small, random, time-variant frequency fluctuations of the LO signal, modeled as a random excess phase [157, p. 83]. Its effects to the received signal are a common phase error for all OFDM subcarriers and the ICI due to the loss of mutual orthogonality among the subcarriers [16, 126]. Also the effects of the phase noise can be mitigated by DSP, see e.g. [168] and references therein.

All imperfections described above exist to some extent in direct-conversion RF front-ends. Naturally, this results in a question what their joint effects are on a single or multiple parallel direct-conversion transceivers. This undoubtedly interesting and important question would, however, be a too vast research topic to be covered in a single thesis, and consequently the focus of this thesis is purely on I/Q imbalance in multiantenna systems. Further information regarding the joint effects and mitigation of I/Q imbalance with amplifier nonlinearities can be found from [9, 14, 77, 146], with CFO from [20, 40, 43, 96, 129, 169, 170], with phase noise from [65, 70, 87, 177, 202, 203], and finally with two or more RF imperfections from [23–26, 52, 123, 170].

2.3 Multiantenna Communications

A wireless communications link is, in its simplest form, established by two single-antenna devices. Whereas such a single-input single-output (SISO) connection, depicted in Fig. 2.6a, is very straightforward and intuitive, it has also many drawbacks. In particular, it is highly dependent on the propagation environment between the TX and RX antennas. In addition, the SISO approach has very limited number of degrees of freedom in terms of signal processing in the TX and RX. Consequently, the connection can suffer heavily of obstacles between the antennas, interfering signal sources in the surroundings or movement of the TX and RX devices, to name a few. Fortunately, wireless connections can be improved by adding antennas to the associated devices, resulting in multiantenna communications. By definition, multiantenna connections are categorized as follows: a multiple-input single-output (MISO) connection (in Fig. 2.6b) consists of a multiantenna TX and a single-antenna RX, a single-input multiple-output (SIMO) connection (in Fig. 2.6c) comprises a single-antenna TX and a multiantenna RX [174, p. 73] and finally, a MIMO connection (in Fig. 2.6d) consists of multiple antennas in both TX and RX sides [22, p. 1]. In general, exploitation of multiple antennas provide more flexibility than the point-to-point approach with a SISO connection, and hence enables higher capacities as well as better robustness against wireless propagation environment. Regarding the common multiantenna related terminology, *array gain* comes from a coherent combining of the signals at a RX and thus increases the received signal strength and the SNR, *diversity gain* improves the quality and reliability of reception by receiving multiple copies of the transmitted signals experiencing uncorrelated or partly correlated fading, and *spatial multiplexing gain* provides data rate improvement by transmitting multiple data streams over a single frequency-time resource, but with spatial separation [22, p. 2-3]. In the following subsections, the focus is on the most essential principles and features of multiantenna communications concerning the work in this thesis.

2.3.1 Classical Beamforming

In point-to-point communications, it is beneficial to exploit directional antennas, which have an ability to focus the transmission or reception to a certain direction. In this context, the gain of an antenna, defined as 4π times the ratio of the radiation intensity in a certain direction to the net input power of the antenna [167, p. 41], becomes an essential concept. The higher is the gain of a TX/RX antenna, the larger portion of the total power is transmitted/received to/from a certain direction. Conventionally, antennas with high gain suffer, e.g., from high costs, large size and poor flexibility. However, multiantenna systems provide an alternative solution for directional communications via the concept of beamforming. This is essentially an ability to focus transmission/reception of a group of antennas, called an antenna array, along a specific spatial direction even when the individual antenna elements are not directional as such. In fact, the antenna elements are usually considered to be omnidirectional, defined as antennas whose radiation patterns are circles in one plane [167, p. 36]. Instead of highly directive antenna elements, the directional characteristics of an antenna array are obtained by adjusting the amplitude and phase of each antenna signal separately. Due to the superposition principle, the signal adjustment results in direction-dependent constructive/destructive signal summation,

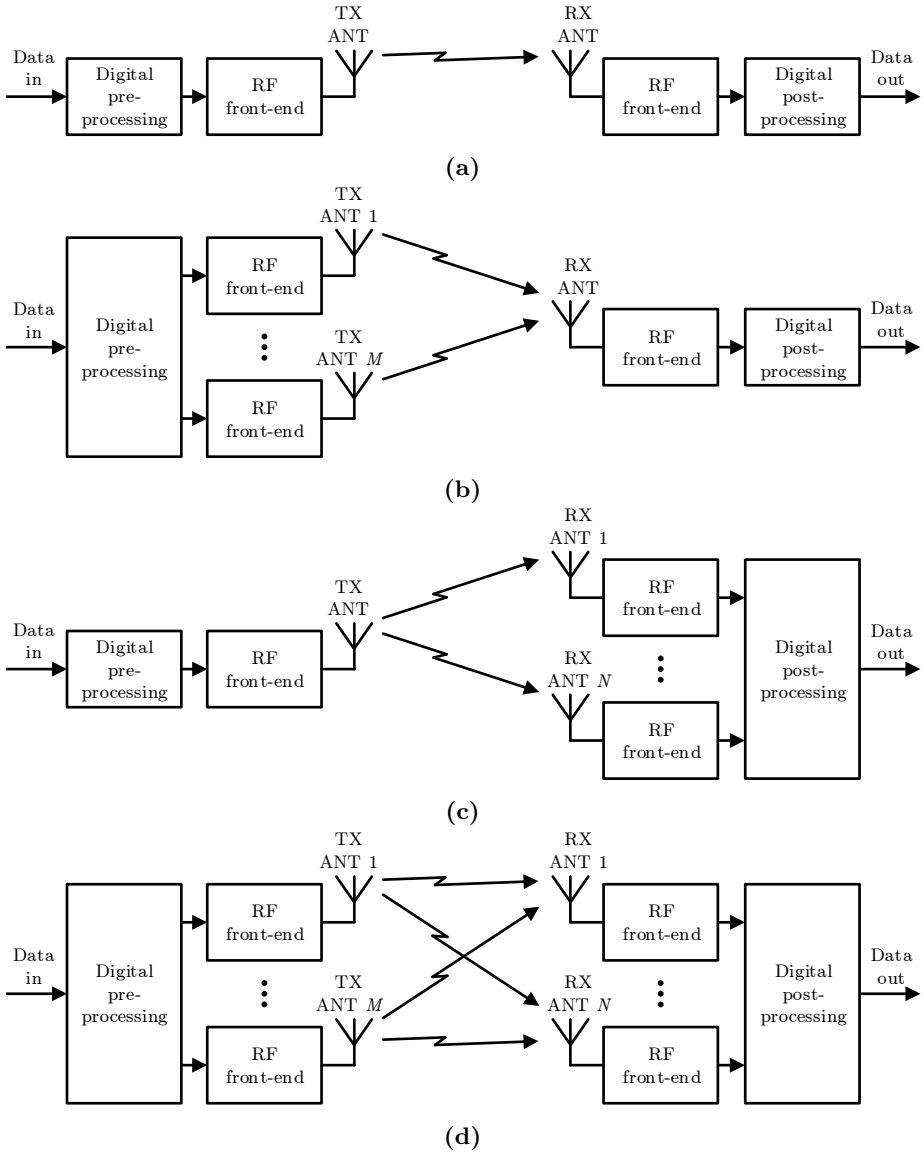

Figure 2.6: Conceptual (a) SISO, (b) MISO, (c) SIMO, and (d) MIMO connection between two devices.

and thus forms beams (high gain) and nulls (high attenuation) to the radiation pattern of the array [105, p. 29]. It is important to note that these beams and nulls can be steered purely electrically so that neither the array nor the antenna elements need to be moved or rotated. Spatial beams and nulls make sense mostly in line of sight (LoS) environments where physical directions map directly to points in the spatial response, and consequently classical beamforming and radiation pattern analysis is usually applied to LoS schemes

with flat fading channels. Note also that the classical beamforming methods described in this thesis are applicable best for narrowband signals whereas wideband signals would require more complicated beamforming structures such as tapped delay-lines or finite impulse response (FIR)/infinite impulse response (IIR) filters [108, p. 8].

Classical beamforming can be implemented either in the analog parts of transceivers, by DSP algorithms or with hybrid beamforming being essentially a combination of the analog and digital methods. Whereas beamforming methods including analog processing need arrays of phase shifters and one or multiple signal combiners, digital beamforming needs separate RF front-ends for each of the antenna signals. However, due to the great flexibility and configurability as well as high computational power, digital beamforming is considered to outperform analog beamforming [105, p. 9]. In particular, digital beamforming enables easy spatial scanning, very fast processing and generation of multiple different radiation patterns at once, each just utilizing a different set of the amplitude and phase adjustment coefficients referred to as beamforming weights. A set of simultaneous radiation patterns, in turn, makes spatial UE multiplexing possible by serving each UE under an individual beam and thus distinguishing the UEs in the angular domain. This improvement can be even boosted when, instead of two dimensional (2D) beamforming, exploiting 3D beamforming enabled by planar array structures.

In the following, we formulate basic signal models and radiation patterns for systems utilizing digital TX and RX beamforming. In order to provide basic understanding and an intuitive starting point for the beamforming principles, the models are given for a simple uniform linear array (ULA) where the antenna elements are all located along a line and the distance between two consecutive antenna elements is equal to d. However, the models for more complicated structures, i.e. planar and 3D arrays, can be obtained by straightforward extensions of the provided ULA model. Starting from the RX beamformer depicted in Fig. 2.7a, RF signal $r_{\mathrm{RF}}(t)$ arrives as a plane wave from direction θ, i.e., direction of arrival (DoA) is equal to θ. Since we consider LoS propagation and assume the antenna spacing to be around one half of the carrier wavelength, the fast and slow fading conditions are the same for all N antennas. Consequently, the main difference in the received antenna signals comes from different lengths of the propagation paths which, in turn, cause unequal propagation delays and thereon unequal phases [187]. After RF front-ends the digital baseband equivalent signal vector $\mathbf{r}(\theta) \in \mathbb{C}^{N\times 1}$ is given by

$$\mathbf{r}(\theta) = \mathbf{a}(\theta)r + \mathbf{n} \tag{2.22}$$

where we omit the sample index k for notational convenience and consistency. Here, $\mathbf{a}(\theta) = \left[1, e^{jd\kappa\cos\theta}, e^{j2d\kappa\cos\theta}, \ldots, e^{j(N-1)d\kappa\cos\theta}\right]^{\mathrm{T}} \in \mathbb{C}^{N\times 1}$ is the steering vector based on the array geometry, $\mathbf{n} \in \mathbb{C}^{N\times 1}$ represents additive white Gaussian noise generated in the RX electronics, $\kappa = 2\pi/\lambda$ denotes the wavenumber, and λ denotes the carrier wavelength [92, p. 322]. The output signal of the digital RX beamformer is then equal to [64, 105]

$$y_{\mathrm{RX}}(\theta) = \sum_{i=1}^{N} w_i^*(\theta_{\mathrm{d}})r_i(\theta) = \mathbf{w}^{\mathrm{H}}(\theta_{\mathrm{d}})\mathbf{r}(\theta) = \mathbf{w}^{\mathrm{H}}(\theta_{\mathrm{d}})\mathbf{a}(\theta)r + \mathbf{w}^{\mathrm{H}}(\theta_{\mathrm{d}})\mathbf{n} \tag{2.23}$$

where $\mathbf{w}(\theta_{\mathrm{d}}) \in \mathbb{C}^{N\times 1}$ refers to the RX beamforming weight vector under a given optimization criteria towards the desired direction θ_{d}.

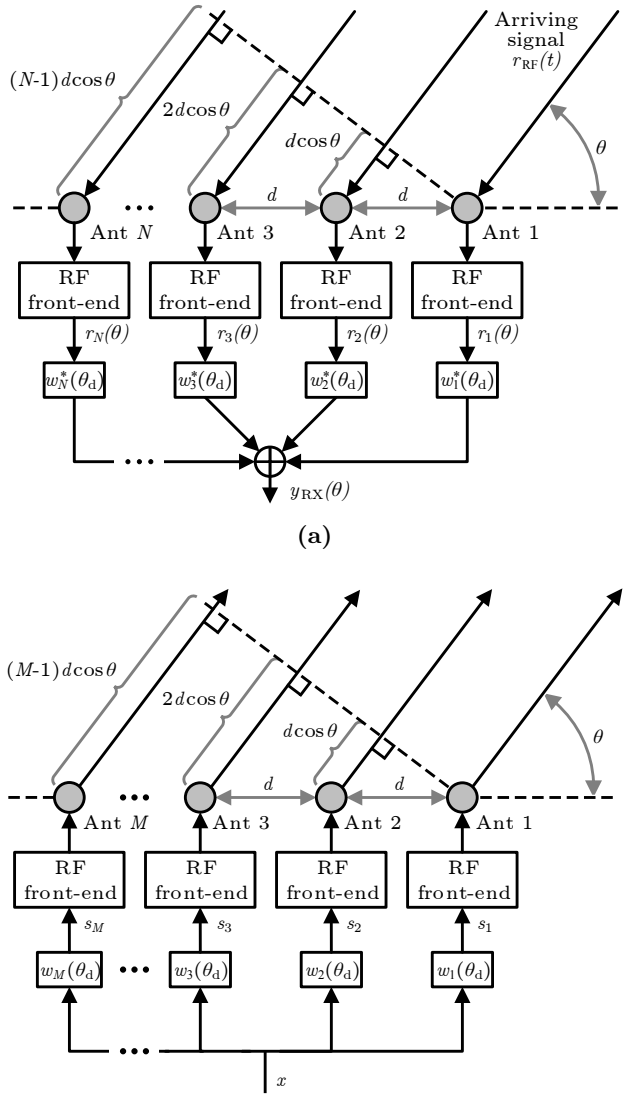

Figure 2.7: Illustration of conceptual ULA (a) RX beamformer and (b) TX beamformer.

TX beamforming is in many sense a reversed version of RX beamforming as visible in Fig. 2.7b. Now, the digital signal to be transmitted is denoted by x and the number of TX antennas is equal to M. The baseband signal $\mathbf{s} \in \mathbb{C}^{M\times 1}$ after the weighting is then given by $\mathbf{s} = \mathbf{w}(\theta_\mathrm{d})x$ where $\mathbf{w}(\theta_\mathrm{d}) \in \mathbb{C}^{M\times 1}$ denotes now the TX beamforming weight vector. Consequently, the analog continuous-time antenna signals consist all of x but just with separate weighting coefficients. Assuming that the individual antenna elements are omnidirectional, all antennas transmit their own signals to all directions with constant

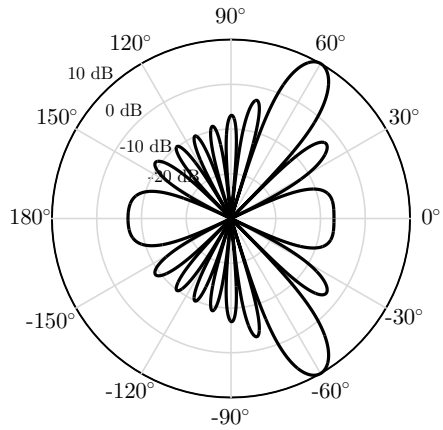

Figure 2.8: Example of the radiation pattern of a ULA with 10 antenna elements and SMF weights $\mathbf{w}(60^\circ) = \mathbf{a}(60^\circ)/\sqrt{N}$.

powers but the aggregated signal in the associated RX is heavily dependent on the angle between the TX array and the RX due to the superposition principle. That is, the effective transmitted baseband equivalent signal towards direction θ can be expressed as

$$s_{\mathrm{TX}}(\theta) = \mathbf{a}^{\mathrm{H}}(\theta)\mathbf{s} = \mathbf{a}^{\mathrm{H}}(\theta)\mathbf{w}(\theta_{\mathrm{d}})x. \tag{2.24}$$

Based on the formulations in (2.23) and (2.24), it is evident that the spatial characteristics of antenna array reception/transmission are purely determined through the products $\mathbf{w}^{\mathrm{H}}(\theta_{\mathrm{d}})\mathbf{a}(\theta)$ and $\mathbf{a}^{\mathrm{H}}(\theta)\mathbf{w}(\theta_{\mathrm{d}})$. In fact, the radiation pattern of an antenna array can be given by

$$D(\theta) = \left|\mathbf{w}^{\mathrm{H}}(\theta_{\mathrm{d}})\mathbf{a}(\theta)\right|^2. \tag{2.25}$$

Practically speaking, this means that the beamforming weights need to be selected in such a way that response to the desired directions is maximized while the response to any possible undesired directions is minimized. An example of a radiation pattern for a RX antenna array with 10 elements is given in Fig. 2.8. There the ULA structure is oriented such that the antenna broadside is headed to $+90^\circ$ and the main beam points to $+60^\circ$. Furthermore, the weights are determined by the conventional spatial matched filter (SMF) so that $\mathbf{w}(\theta_{\mathrm{d}}) = \mathbf{a}(\theta_{\mathrm{d}})/\sqrt{N}$ [28, p. 302]. Note that the radiation pattern is symmetrical relative to 0° and 180° which stems from the fact that the steering vector of a ULA is symmetrical with respect to those points. The concepts of the radiation pattern and beamforming form the basis for publications [P1–P4]. In addition, the RX array response given in (2.23) is exploited in [P1, P3–P4] through various different weighting approaches whereas the corresponding TX response given in (2.24) is used in [P2] with the null-steering principle.

In general, beamforming is a concept of a great flexibility allowing better resource reuse with lower costs than in single-antenna systems. The flexibility of beamforming is seen not only in the spatial multiplexing through multiple simultaneous beams, but

also in the enhanced interference mitigation capabilities via null steering [63]. Moreover, beamforming can be implemented purely electrically with a static antenna array whereas a conventional non-reconfigurable high-gain antenna needs physical orientation adjustment every time when the main beam direction is wanted to be changed. Beamforming provides also better robustness against hardware failures than single antenna systems due to being able to operate even when an individual transceiver chain is malfunctioning. Finally, an antenna array might also have significantly lower costs than a high-gain antenna due to the simple and low-cost antenna elements.

2.3.2 Antenna Diversity

In contrast to classical beamforming which assumes a strong dominance of LoS propagation, antenna diversity becomes sensible in multipath scenarios where constructive/destructive signal summation causes location dependent fading at the spatial scale of the order of the carrier wavelength [174, p. 10]. Whereas a single TX–RX antenna link can hence be strongly faded, at a given time, exploiting multiple antennas at least in one side of the communications link provides higher probability for favorable propagation with less attenuation [66, p. 204]. Consequently, the connection becomes more robust against the wireless propagation and yields better quality of the received signal through the diversity gain [22, p. 3].

Let us first consider RX antenna diversity where the transmitted signal is received by N antennas which are assumed to have sufficient spatial separation resulting in independent multipath channels between the TX and each RX antenna. Denoting the TX–RX channel vector, including the amplitude and phase coefficients representing the aggregated effects of multipath propagation, by $\mathbf{h} = [h_1, \ldots, h_N] \in \mathbb{C}^{N\times 1}$, the received baseband equivalent signal vector $\mathbf{r} \in \mathbb{C}^{N\times 1}$ can be expressed by

$$\mathbf{r} = \mathbf{h}x + \mathbf{n}. \tag{2.26}$$

Consequently, by combining the signals from the separate antenna branches with a proper weighting, we get the combiner output y_{RX} being equal to

$$y_{\mathrm{RX}} = \sum_{i=1}^{N} w_i^* r_i = \mathbf{w}^{\mathrm{H}}\mathbf{r} = \mathbf{w}^{\mathrm{H}}\mathbf{h}x + \mathbf{w}^{\mathrm{H}}\mathbf{n}. \tag{2.27}$$

Here $\mathbf{w} \in \mathbb{C}^{N\times 1}$ denotes the weighting vector of the combiner. Obviously, (2.26) and (2.27) have many similarities with the corresponding formulations in (2.22) and (2.23) regarding RX beamforming. However, it is important to note that now the steering vector is replaced with a more generic channel response including arbitrary amplitude and phase response for each antenna branch. Consequently, the combiner weights do not anymore match with any particular physical direction but need to be adjusted according to the generic channel response and this kind of multiantenna-based signal combining is hereafter referred to as *spatial RX processing*. The actual weight selection and optimization, in turn, can be implemented by many methods, which differ especially in complexity and performance. The simplest method is selection combining [66, p. 208] where only the signal with the highest instantaneous SNR is used for detection. However, if the channel state information (CSI) is available, considerably better performance

can be obtained by more advanced methods such as conventional equal-gain combining (EGC) [66, p. 216] and maximal-ratio combining (MRC) [66, p. 214]. Diversity combining can be implemented in RXs also by exploiting knowledge of the channel statistics. An example of a statistical RX diversity method is the linear minimum mean-square error (LMMSE) approach [73, p. 102] which can take into account also possible spatial correlation of the noise and interference. However, accurate statistical information is often difficult to obtain in practice, but fortunately the statistical approaches can be approximated effectively by adaptive methods such as least mean square (LMS) [73, p. 231] and recursive least squares (RLS) [73, p. 436] assuming that some kind of known training signals are utilized. Regarding the work in this thesis, the MRC scheme is used in [P7], while the adaptive LMS method is utilized in [P5] and the statistical LMMSE approach is used in [P5–P8].

Antenna diversity can be exploited also in the TX side. In such a case, a single data stream is transmitted from M spatially separated TX antennas either with or without exploiting the CSI in the TX, and processing prior the transmission is, in general, called *TX precoding*. When the CSI is available, the process is pretty similar to RX diversity [66, p. 217]. That is, the transmitted antenna signals are phase shifted so that they experience coherent summation in the desired RX. Additionally, the total TX power is divided for different TX antenna branches relative to the channel gains. The precoded signal vector is, in general, given by $\mathbf{s} = \mathbf{w}x \in \mathbb{C}^{M\times 1}$ and results in the received signal equal to

$$r = \mathbf{h}\mathbf{s} + n = \mathbf{h}\mathbf{w}x + n \tag{2.28}$$

where the propagation channel is denoted by $\mathbf{h} \in \mathbb{C}^{1\times M}$, the processing weight vector is $\mathbf{w} \in \mathbb{C}^{M\times 1}$ and n denotes the additive noise. Similarly to the RX case, (2.28) has obvious similarities with the beamforming formulation in (2.24) but also now the main difference lies in the used generic channel model and the corresponding weighting. When the CSI is not available in the TX, the case is more complicated since phase adjustment and power division cannot be matched with the wireless channel. Instead, the so-called space-time coding principle can be utilized in order to benefit from the TX array. Possibly the best known space-time coding method is the Alamouti scheme [6] with two antennas, which is an elegant example of a case where transmission of two separate data symbols is divided over spatial and temporal dimensions so that the TX antenna diversity is exploited in an optimal way [66, p. 220].

The benefits of RX and TX diversity schemes are basically the same, i.e., the received signal strength and in particular the instantaneous SNR distribution are improved due to the enhanced connection providing array and diversity gains as well as better propagation robustness than in single-antenna connections. In practice, the quality improvement due to RX as well as TX antenna diversity can be exploited, e.g., by decreasing TX powers and thus saving energy, or by using higher-order constellations providing higher data rates.

2.3.3 Spatial Multiplexing

While the utilization of conventional orthogonal resources, i.e., frequencies, time slots and codes, is often very limited, the capacity of a wireless communications system can

be improved by spatial multiplexing [22, p. 3]. Unlike antenna diversity where the same data is transmitted and/or received over multiple channels, spatial multiplexing is a method to transmit independent data streams from multiple TX antennas over a shared frequency-time-code resource, and thus to enhance the link capacity significantly. Since the mapping of data streams to TX antennas is done prior the transmission, also spatial multiplexing related TX processing is considered as *TX precoding*. The baseband equivalent of the precoded signal vector $\mathbf{s} \in \mathbb{C}^{M\times 1}$ can be expressed as

$$\mathbf{s} = \mathbf{G}\mathbf{x} \tag{2.29}$$

where $\mathbf{G} \in \mathbb{C}^{M\times Q}$ denotes the precoder matrix and $\mathbf{x} \in \mathbb{C}^{Q\times 1}$ is the original data stream vector to be transmitted where Q is the total number of parallel data streams. The received signal $\mathbf{r} \in \mathbb{C}^{N\times 1}$ is then equal to

$$\mathbf{r} = \mathbf{H}\mathbf{s} + \mathbf{n} = \mathbf{H}\mathbf{G}\mathbf{x} + \mathbf{n} \tag{2.30}$$

where $\mathbf{H} \in \mathbb{C}^{N\times M}$ denotes the wireless propagation channel matrix. The signals are eventually separated in the RX side by their spatial signatures stemming from different locations of TX antennas [22, p. 17]. Mathematically, that is expressed by

$$\mathbf{y}_{\mathrm{RX}} = \mathbf{W}^{\mathrm{H}}\mathbf{r} = \mathbf{W}^{\mathrm{H}}\mathbf{H}\mathbf{G}\mathbf{x} + \mathbf{W}^{\mathrm{H}}\mathbf{n} \tag{2.31}$$

where $\mathbf{y}_{\mathrm{RX}} \in \mathbb{C}^{Q\times 1}$ represents the separated data streams and $\mathbf{W} \in \mathbb{C}^{N\times Q}$ denotes the RX weight matrix. In order to ensure reliable communications by effective signal separation methods, $N \geq M$ RX antennas are needed [22, p. 13].

As in the case of antenna diversity, the processing coefficients of spatial multiplexing systems can be selected and optimized by several methods. In TXs, the precoding matrix $\mathbf{G}$ can be adjusted, e.g., according to the zero forcing (ZF) principle which maximizes the gain from the TX to RX and provides received signals that are free of interference [88], or by codebook oriented approaches where the precoding weights are selected, based on the channel conditions, from a predefined set of quantized weight vectors [121, p. 485]. Furthermore, the RX processing weight matrix $\mathbf{W}$ can be optimized with the same principles as in the RX diversity, e.g., by the simple MRC [66, p. 214], the statistical LMMSE [73, p. 102] or the adaptive LMS [73, p. 231] algorithm. An optimal way to distribute processing between the TX and RX is, in turn, the singular value decomposition (SVD)-based method where the channel matrix is decomposed into parallel and non-interfering SISO channels [22, 66].

In general, spatial multiplexing provides improved resource allocation, and thus enables up to $\min(M, N)$-fold increase in the overall capacity [22, p. 3]. In order to exemplify spatial multiplexing a bit, let us consider uplink transmission in a typical cellular network. In the coverage area of a single cell, U UEs, each equipped with M_{U} antennas, transmit parallel but independent signals towards the BS and thus the resulting MU-MIMO connection [121, p. 488] has a combined channel with the dimensions equal to $UM_{\mathrm{U}} \times N_{\mathrm{BS}}$. It is known that the sum rate capacity of such a scenario increases linearly with $\min(UM_{\mathrm{U}}, N_{\mathrm{BS}})$ [22, p. 50]. Consequently, since the number of UEs, U, can be increased easily and the number of BS antennas N_{BS} in 5G networks is expected to increase significantly compared to 4G deployments, it is easy to see that spatial

multiplexing can provide considerable improvements in future cellular networks. More detailed signal model regarding spatial UE multiplexing and the performance analysis of such a case in uplink MU-MIMO scheme under I/Q imbalance is given in [P6–P8].

2.3.4 Massive MIMO

Massive MIMO, first introduced in the seminal paper [116], is often considered to be a MIMO system having an order of magnitude more antennas in the BS (or, in general, in the access node) than active UEs [24–26, 75, 91, 99, 100, 110]. However, it is stated in [27] that such a strict rule is not required and massive MIMO can be defined simply as a system with unconventionally many active antenna elements that can serve an unconventionally large number of UEs. No matter what is the exact number of the BS antennas, massive MIMO is anyway extending the conventional sized MIMO systems to the next level. In fact, it is expected to provide substantial improvements in capacity, energy efficiency, robustness and resolution when compared to the existing systems where the BSs are usually equipped with less than ten antennas. As a result, the concept of massive MIMO is seen as a very promising technological candidate for the demanding future 5G systems [8, 25, 29, 57, 58, 91, 110, 134, 153, 188, 189].

As being mainly an extension to conventional MIMO setups, massive MIMO is in theory applicable with the same operation and processing principles as smaller MIMO systems. However, the very high number of antennas may become an issue if not taken properly into account. In particular, if the complexity of the system increases, e.g. quadratically or cubically in the number of antennas, massive MIMO system might end up to be very slow, expensive or power hungry. Therefore, massive MIMO systems require extreme simplicity not only in the hardware but also in the associated signal processing [99]. As a practical example of simple hardware, the radio front-ends can possibly be equipped with ADCs/DACs with a resolution of a few bits or even one bit due to the significant array processing gain provided by the vast number of antennas and parallel RF chains [39, 69, 85, 190]. In the signal processing developments, in turn, all signal processing phases must be implemented without excessive computational complexity. Practically, algorithms involving linear or nearly linear processing principles are of a special interest due to their straightforward implementations [99, 110]. Examples of such processing principles in downlink (DL) TX precoding are the ZF and maximal-ratio transmission (MRT) methods, whereas the ZF, LMMSE and MRC methods can be utilized in uplink (UL) RX processing [88]. Although some performance losses most probably occur in the individual RF chains due to more simple signal processing algorithms, the resulting overall performance is at a good level thanks to parallel processing. To summarize, due to the possibility of using simple processing principles and despite the high number of the antennas, massive MIMO systems are considered to have a complexity within a practical realm [27].

Massive MIMO needs a special attention also in terms of the array layout and the resulting physical dimensions. Whereas the traditional ULA structure might have an unpractical length for many use cases, other types of array structures are often envisioned for massive MIMO systems. In particular, planar and cylindrical arrays, which result in more compact antenna structures, are seen as promising solutions [56, 99]. Additionally, antenna elements can be distributed spatially, e.g., above roof tops. In such cases the

main parts of the processing are parallelized into the antenna branches and only some operations, such as the signal combining, are executed in a centralized computation center [27].

In addition to the implementation related issues, massive MIMO involves a big challenge regarding the network functionalities. This is pilot contamination, which arises from the fact that the amount of orthogonal pilots, used for uplink channel estimation, is limited, and therefore relatively tight pilot reuse is needed in massive MIMO systems [26, 75, 99, 116, 153]. When the same pilot is used in two or more closely located areas, channel estimates are contaminated in the RX due to the linear combination of all heard copies of the pilot signal. This, in turn, degrades the ability to mitigate inter-cell interference and thus causes performance losses. Fortunately, the effects of pilot contamination can be mitigated in several ways [49, 110]. One option is to use time-shifted pilot transmission where UEs using the same pilot sequence are not transmitting simultaneously [15, 53]. The solution in [166], in turn, is based on pilot sequence hopping providing conditions where the effects of non-orthogonal pilots are randomized in time, and thus the pilot contamination is mitigated when the channel estimation is done over multiple time slots. Another approach is to exploit the second-order statistics of the desired and interfering UEs in the pilot assignment [55, 193, 194]. Pilot contamination can be mitigated also by utilizing collaborative precoding schemes such as the ones provided in [18, 90, 103], or by utilizing a combination of downlink and uplink channel learning [199]. The mitigation can even be done blindly based either on the data covariance matrix and a short training sequence [131] or on reducing the dimensions of the problem by subspace analysis [42, 124, 125]. Unfortunately, these mitigation methods have also some downsides. Many of them increase the network controlling overhead significantly while others require statistical channel information, which might not be available, or are not widely applicable for different use cases. Therefore, despite these and many other mitigation proposals, mitigation of pilot contamination in massive MIMO is still an open issue in a great extent.

Massive MIMO and particularly the effects of RF imperfections in massive MIMO systems is a general theme in publications [P4, P6–P7] as well as considered in a smaller scale also in [P8]. Note that our work is not focused on the asymptotic number of BS antennas but instead we provide analysis and results for antenna arrays which have a practically feasible number of antenna elements.

CHAPTER 3

Classical Narrowband Beamforming and Antenna Arrays under I/Q Imbalance: Modeling, Analysis and Digital Mitigation

This chapter is based on the results provided in publications [P1–P4] and focuses on I/Q imbalance and its effects in classical narrowband beamforming systems. In particular, we model the harmful signal distortion in an antenna array and show how it affects the array radiation properties. We continue by developing WL processing principles for I/Q imbalance mitigation in BSs in terms of uplink and downlink directions. Finally, we demonstrate the performance of the provided processing methods by numerical examples whereas more examples can be found from [P1–P4]. Note that the discussion regarding I/Q imbalance in multiantenna systems utilizing OFDM-based wideband waveforms is left for Chapter 4. Unless otherwise stated, we consider digital baseband equivalent signals and omit the subindex L for notational convenience in the continuation.

3.1 Background and State of the Art

As discussed in Section 2.2.1 the harmful effects of TX and RX I/Q imbalances can be mitigated by several different approaches which are extensively studied in the conventional single user SISO (SU-SISO) transmission setup, e.g., in [13, 32, 119, 149, 151, 185] and references therein. Nonetheless, I/Q imbalance in multiantenna systems using narrowband type of signal models have gained considerably less attraction. This is because utilization of multiple antennas is often connected with wideband signal models. However, in order to obtain basic understanding of I/Q imbalance in multiantenna transmission, it is beneficial to first focus on some elementary narrowband models.

In order to introduce some fundamental I/Q imbalance mitigation principles, let us first consider a single-antenna RX suffering from I/Q imbalance. In such a case, the imbalanced analog signal is equal to $r_{\mathrm{Rxi}}(t) = K_{\mathrm{Rx1}} r(t) + K_{\mathrm{Rx2}} r^*(t)$ as given in (2.17)

and the corresponding digitized signal is given by $r_{\mathrm{Rxi}}(k) = K_{\mathrm{Rx1}} r(k) + K_{\mathrm{Rx2}} r^*(k)$. Obviously, this is a WL transformation of the ideal received signal $r(k)$. Therefore, in terms of I/Q imbalance mitigation, the signal distortion caused by I/Q imbalance guides us towards the so-called WL time-domain processing introduced originally in the seminal paper [31] and proposed for processing non-circular signals, e.g., in [4, 141, 160]. The method is based on joint processing of the original signal and its complex conjugate but both with separate weighting. In the context of I/Q imbalance, the RX signal after WL processing is then given by

$$\begin{aligned} \widetilde{y}(k) &= w_1 r_{\mathrm{Rxi}}(k) + w_2 r^*_{\mathrm{Rxi}}(k) \\ &= \left(w_1 K_{\mathrm{Rx1}} + w_2 K^*_{\mathrm{Rx2}}\right) r(k) + \left(w_1 K_{\mathrm{Rx2}} + w_2 K^*_{\mathrm{Rx1}}\right) r^*(k) \end{aligned} \tag{3.1}$$

where w_1 and w_2 denote the processing weights. Now, we should find such weights that $w_1 K_{\mathrm{Rx1}} + w_2 K^*_{\mathrm{Rx2}} = 1$ and $w_1 K_{\mathrm{Rx2}} + w_2 K^*_{\mathrm{Rx1}} = 0$. In fact, when substituting [10]

$$w_1 = \frac{K^*_{\mathrm{Rx1}}}{|K_{\mathrm{Rx1}}|^2 - |K_{\mathrm{Rx2}}|^2}, \qquad w_2 = \frac{-K_{\mathrm{Rx2}}}{|K_{\mathrm{Rx1}}|^2 - |K_{\mathrm{Rx2}}|^2} \tag{3.2}$$

we notice that the processed signal $\widetilde{y}(k) = r(k)$ and is thus perfectly recovered from RX I/Q imbalance. Another form of WL I/Q imbalance mitigation is the asymmetrical WL method where only the conjugate signal is processed [13]. This kind of solution can suppress the conjugate term completely but leaves a slight linear distortion in the compensated signal. In this thesis, we concentrate purely on the symmetrical processing described in (3.1). Based on the example above, WL processing can be considered as a powerful tool being able to mitigate all the harmful effects of I/Q imbalances with low computational complexity. Practically speaking, a perfect knowledge of the needed I/Q imbalance parameters in (3.2) might of course be hard to obtain but even high quality estimates provided by iterative or blind estimators yield good performance. More examples of WL time domain RX processing for I/Q imbalance mitigation purposes can be found, e.g., from [10, 11, 43, 97, 107, 182, 196–198]. Note that whereas the example above considered only RX I/Q imbalance mitigation in the RX, WL processing can be used also for TX I/Q imbalance mitigation in the TX, see e.g. [9, 12, 13, 200].

In general, many of the principles regarding I/Q imbalance in single-antenna devices can be extended straightforwardly to multiantenna scenarios. As useful examples of the basic effects and methods, fundamentals for space-time coded transmission under I/Q imbalance can be found for a single user MISO (SU-MISO) case in [184] and for a single user MIMO (SU-MIMO) in [204, 208]. Furthermore, extending the narrowband I/Q imbalance studies to a scenario where UEs are multiplexed spatially, the work in [197] is focused on multiuser MISO (MU-MISO) downlink precoding whereas [196,198] introduce multiuser SIMO (MU-SIMO) uplink transmission. When considering solely I/Q imbalance mitigation, it can be carried out as in single-antenna systems, i.e separately in each transceiver branch as done in [139]. Such a processing approach is thus simply an array of multiple replicated I/Q imbalance mitigation blocks, which can utilize any available I/Q imbalance mitigation method. However, when keeping in mind that multiantenna-based beamforming involves signal weighting and combining as introduced in Section 2.3.1, *why not to combine I/Q imbalance mitigation and beamforming weighting into a single processing block in each of the antenna branches?* In fact, that is the main

idea of the signal processing developments in this chapter and stemming from the promising WL processing, we focus on WL beamforming methods. It is noteworthy that the combination of I/Q imbalance mitigation and beamforming, referred to as RF-aware WL beamforming, removes the need for separate I/Q imbalance mitigation. Doubling the dimension of the input data, in turn, increases the computational complexity of the actual beamforming processing, but the *total* computational complexity depends highly on the actual I/Q imbalance mitigation and beamforming algorithms, as discussed later in Sections 3.5 and 4.6.3. Note, however, that our aim is also to show that the concept of RF-aware WL beamforming can provide the same performance as a system with ideal I/Q balance, and thus provides an alternative solution to beamforming under I/Q imbalance. This is a fact that can be possibly exploited, e.g., in future signal processing developments.

The idea of WL beamforming was originally introduced in [34] for processing non-stationary signals having time-dependent statistics and possibly second order non-circular complex envelope. The WL extension of the linearly constrained minimum variance (LCMV) beamformer was then developed in [38] for non-circular signals. Furthermore, a WL version of the conventional minimum variance distortionless response (MVDR) is given in [117] for processing signals whose complementary covariance matrix is not zero. Another WL variant of the MVDR method is developed in [35] for signals which include non-circular interference. The approach is extended in [36, 37] where not only the interference but also the SOI can be non-circular. WL-MVDR is considered also in [192] where frequency offset aspects are taken into account. The study in [47], in turn, focuses on developing WL version of the iterative RLS algorithm whereas the study in [164] does the same for the LMS algorithm. In addition, in [165] WL auxiliary vector filtering utilizing second-order statistics is developed for non-circular signals. Finally, WL extensions for the MRT/MRC algorithm are given in [44]. What is noteworthy, however, is that none of these studies consider I/Q imbalance and its mitigation in particular, and are signal processing developments for non-circular signals in general.

3.2 Signal and Radiation Distortion in Antenna Arrays

Considering RX beamforming with N antenna elements and ideal I/Q matching, the received signal vector is equal to $\mathbf{r}(\theta) = \mathbf{a}(\theta)r + \mathbf{n} \in \mathbb{C}^{N\times 1}$ as given in (2.22). Furthermore, based on (2.23), such an input results in the RX beamformer output signal equal to $y_{\mathrm{RX}}(\theta) = \mathbf{w}^{\mathrm{H}}(\theta_{\mathrm{d}})\mathbf{r}(\theta) = \mathbf{w}^{\mathrm{H}}(\theta_{\mathrm{d}})\mathbf{a}(\theta)r + \mathbf{w}^{\mathrm{H}}(\theta_{\mathrm{d}})\mathbf{n}$. The radiation pattern of such a setup was given in (2.25) as $D(\theta) = \left|\mathbf{w}^{\mathrm{H}}(\theta_{\mathrm{d}})\mathbf{a}(\theta)\right|^2$. However, when considering the fact that I/Q imbalance occurs in the RX electronics, the received signal is distorted and the formulas above are not valid anymore. In particular, the distorted signal in a single RX branch is of the form $r_{\mathrm{Rxi}} = K_{\mathrm{Rx1}}r + K_{\mathrm{Rx2}}r^*$. Note that the sample index k is omitted here for notational convenience. The received signal vector in an antenna array under RX I/Q imbalance can then be expressed as [P1, P3–P4]

$$\begin{aligned}\mathbf{r}_{\mathrm{Rxi}}(\theta) &= \mathbf{K}_{\mathrm{Rx1}}\mathbf{r}(\theta) + \mathbf{K}_{\mathrm{Rx2}}\mathbf{r}^*(\theta) \\ &= \mathbf{K}_{\mathrm{Rx1}}\mathbf{a}(\theta)r + \mathbf{K}_{\mathrm{Rx2}}\mathbf{a}^*(\theta)r^* + \mathbf{K}_{\mathrm{Rx1}}\mathbf{n} + \mathbf{K}_{\mathrm{Rx2}}\mathbf{n}^*\end{aligned} \tag{3.3}$$

where the I/Q imbalance matrices $\mathbf{K}_{\mathrm{Rx1}} = \mathrm{diag}\left(K_{\mathrm{Rx1},1}, K_{\mathrm{Rx1},2}, \ldots, K_{\mathrm{Rx1},N}\right) \in \mathbb{C}^{N\times N}$ and $\mathbf{K}_{\mathrm{Rx2}} = \mathrm{diag}\left(K_{\mathrm{Rx2},1}, K_{\mathrm{Rx2},2}, \ldots, K_{\mathrm{Rx2},N}\right) \in \mathbb{C}^{N\times N}$ refer to the I/Q imbalance parameters in N parallel RX branches. Based on (3.3), the signal vector is distorted through two different mechanisms. First of all, each of the elements of the desired signal component $\mathbf{a}(\theta)r$ are scaled with the corresponding I/Q imbalance coefficient in $\mathbf{K}_{\mathrm{Rx1}}$. Whereas this causes somewhat harmless multiplicative distortion, which can be handled jointly with the channel equalization/detector [13], the other distortion mechanism is much more harmful. That is, the presence of the conjugated term $\mathbf{a}^*(\theta)r^*$ causes non-linear self interference to the signal.

Processing the distorted signal by the conventional RX beamformer results in the output signal equal to [P1, P3–P4]

$$\begin{aligned} y_{\mathrm{Rxi}}(\theta) &= \mathbf{w}^{\mathrm{H}}(\theta_{\mathrm{d}})\mathbf{r}_{\mathrm{Rxi}}(\theta) \\ &= \mathbf{w}^{\mathrm{H}}(\theta_{\mathrm{d}})\mathbf{K}_{\mathrm{Rx1}}\mathbf{a}(\theta)r + \mathbf{w}^{\mathrm{H}}(\theta_{\mathrm{d}})\mathbf{K}_{\mathrm{Rx2}}\mathbf{a}^*(\theta)r^* \\ &\quad + \mathbf{w}^{\mathrm{H}}(\theta_{\mathrm{d}})\mathbf{K}_{\mathrm{Rx1}}\mathbf{n} + \mathbf{w}^{\mathrm{H}}(\theta_{\mathrm{d}})\mathbf{K}_{\mathrm{Rx2}}\mathbf{n}^*. \end{aligned} \tag{3.4}$$

Scaling caused by $\mathbf{K}_{\mathrm{Rx1}}$ in the first term can be easily suppressed if it is taken into account when generating the weight vector $\mathbf{w}(\theta_{\mathrm{d}})$. However, if not addressed properly, $\mathbf{K}_{\mathrm{Rx1}}$ can cause severe distortion to the signal. What is even more interesting, is the presence of the second term $\mathbf{w}^{\mathrm{H}}(\theta_{\mathrm{d}})\mathbf{K}_{\mathrm{Rx2}}\mathbf{a}^*(\theta)r^*$ caused by RX I/Q imbalance. It is important to note that whereas the effects of additional noise can be mitigated by improving the SNR, e.g. by increasing the TX power, the power of the second term is linearly dependent on the signal power. Moreover, the second term includes a conjugated version of the steering vector $\mathbf{a}(\theta)$ and is processed by the same weights as the first term. Consequently, mitigation of this self interference becomes a challenging task.

In order to further evaluate the effects of the signal distortion and specially the effects in the spatial domain, we next formulate the radiation pattern of an antenna array under RX I/Q imbalance. Assuming that the original signal r is circular or proper, which is true for many of the communications signals such as single-carrier M-quadrature amplitude modulation (QAM) [13], the radiation pattern of an antenna array under RX I/Q imbalance can be expressed as [P3–P4]

$$D_{\mathrm{Rxi}}(\theta) = \left|\mathbf{w}^{\mathrm{H}}(\theta_{\mathrm{d}})\mathbf{K}_{\mathrm{Rx1}}\mathbf{a}(\theta)\right|^2 + \left|\mathbf{w}^{\mathrm{H}}(\theta_{\mathrm{d}})\mathbf{K}_{\mathrm{Rx2}}\mathbf{a}^*(\theta)\right|^2. \tag{3.5}$$

When the radiation pattern in (3.5) is compared with the ideal one in (2.25), we notice that RX I/Q imbalance affects also the radiation properties of an antenna array. If the beamforming weight vector $\mathbf{w}(\theta_{\mathrm{d}})$ is defined without taking I/Q imbalance into consideration, coherent combining of the components in $\left|\mathbf{w}^{\mathrm{H}}(\theta_{\mathrm{d}})\mathbf{K}_{\mathrm{Rx1}}\mathbf{a}(\theta)\right|^2$ do not necessarily happen anymore with respect to DoA $\theta = \theta_{\mathrm{d}}$. In fact, the phase changes caused by the individual elements of $\mathbf{K}_{\mathrm{Rx1}}$ can affect the direction and magnitude of the array maximum gain. In addition, the term $\left|\mathbf{w}^{\mathrm{H}}(\theta_{\mathrm{d}})\mathbf{K}_{\mathrm{Rx2}}\mathbf{a}^*(\theta)\right|^2$ is, in general, non-zero and its impacts are emphasized in a case of ULA where the conjugated steering vector is of the form $\mathbf{a}^*(\theta) = \left[1, e^{-jd\kappa\cos\theta}, e^{-j2d\kappa\cos\theta}, \ldots, e^{-j(N-1)d\kappa\cos\theta}\right]^{\mathrm{T}} = \mathbf{a}(180^\circ - \theta)$. When additionally assuming that the I/Q imbalance parameters are equal in all RX branches, i.e. $\mathbf{K}_{\mathrm{Rx2}} = K_{\mathrm{Rx2}}\mathbf{I}$, the second term in (3.5) becomes equal to $\left|K_{\mathrm{Rx2}}\mathbf{w}^{\mathrm{H}}(\theta_{\mathrm{d}})\mathbf{a}(180^\circ - \theta)\right|^2$. Practically, it reaches its maximum value when the weights match with the conjugated

steering vector, i.e., when $\theta = 180^\circ - \theta_\mathrm{d}$. Consequently, *systematic RX I/Q imbalance generates an additional mirror beam to the radiation pattern of a ULA*. While being just an example with the given antenna array structure, the above discussion clearly shows the limitations of the plain linear beamforming. In the next subsection, we alleviate this via WL beamforming whereas the performance of both methods are illustrated later with numerical examples in Section 3.5.

Similar derivations are next shortly summarized for a TX beamformer under TX I/Q imbalance. According to (2.24), the transmitted effective signal towards direction θ under ideal I/Q balance is equal to $s_\mathrm{TX}(\theta) = \mathbf{a}^\mathrm{H}(\theta)\mathbf{w}(\theta_\mathrm{d})x$. However, taking TX I/Q imbalance into consideration, the signal vector at the antennas becomes equal to [P2]

$$\mathbf{s}_\mathrm{Txi} = \mathbf{K}_\mathrm{Tx1}\mathbf{s} + \mathbf{K}_\mathrm{Tx2}\mathbf{s}^* = \mathbf{K}_\mathrm{Tx1}\mathbf{w}(\theta_\mathrm{d})x + \mathbf{K}_\mathrm{Tx2}\mathbf{w}^*(\theta_\mathrm{d})x^*. \tag{3.6}$$

Consequently, the effective transmitted signal towards direction θ and under TX I/Q imbalance can be expressed as [P2]

$$s_\mathrm{Txi}(\theta) = \mathbf{a}^\mathrm{H}(\theta)\mathbf{s}_\mathrm{Txi} = \mathbf{a}^\mathrm{H}(\theta)\mathbf{K}_\mathrm{Tx1}\mathbf{w}(\theta_\mathrm{d})x + \mathbf{a}^\mathrm{H}(\theta)\mathbf{K}_\mathrm{Tx2}\mathbf{w}^*(\theta_\mathrm{d})x^*. \tag{3.7}$$

This has obvious similarities with the corresponding formulation for RX beamformer signal given in (3.4). In fact, the biggest difference is that the steering vector $\mathbf{a}(\theta)$ and the beamformer weights $\mathbf{w}(\theta_\mathrm{d})$ have swapped places. This is visible also in the radiation pattern, which is given for a TX beamformer under TX I/Q imbalance by [P2]

$$D_\mathrm{Txi}(\theta) = \left|\mathbf{a}^\mathrm{H}(\theta)\mathbf{K}_\mathrm{Tx1}\mathbf{w}(\theta_\mathrm{d})\right|^2 + \left|\mathbf{a}^\mathrm{H}(\theta)\mathbf{K}_\mathrm{Tx2}\mathbf{w}^*(\theta_\mathrm{d})\right|^2. \tag{3.8}$$

Due to having so much in common, the distorted radiation patterns of RX and TX beamformers under I/Q imbalances behave in the same way. In particular, if the TX beamformer is equipped with a ULA and the I/Q imbalance parameters are equal in all TX branches, the mirror beam is created also in the TX side. As a result, transmitted antenna signals are added up coherently not only in the RXs locating in the desired direction θ_d but also in the mirror direction $180^\circ - \theta_\mathrm{d}$. In order to avoid such a harmful signal and radiation distortion, we focus on WL TX beamforming in Section 3.4.

3.3 WL RX Beamforming

WL processing is an efficient and powerful tool for I/Q imbalance mitigation. In this section, we focus on WL processing in multiantenna RXs providing the concept of WL RX beamforming which is depicted in Fig. 3.1. As introduced in Section 3.1, the WL method consists of joint processing of the signal and its conjugate. Whereas the weights for these terms in a single transceiver branch are equal to w_1 and w_2, the spatial multiantenna processing results in beamforming weight vectors $\mathbf{w}_1(\theta_\mathrm{d}) \in \mathbb{C}^{N\times 1}$ and $\mathbf{w}_2(\theta_\mathrm{d}) \in \mathbb{C}^{N\times 1}$. In order to formulate the overall processing in a compact form, we stack the weight vectors into the single WL weight vector, i.e. $\widetilde{\mathbf{w}}(\theta_\mathrm{d}) = [\mathbf{w}_1^\mathrm{T}(\theta_\mathrm{d}), \mathbf{w}_2^\mathrm{T}(\theta_\mathrm{d})]^\mathrm{T} \in \mathbb{C}^{2N\times 1}$. Moreover, the received antenna signal vector and its complex conjugate are stacked resulting in $\widetilde{\mathbf{r}}(\theta) = [\mathbf{r}^\mathrm{T}(\theta), \mathbf{r}^\mathrm{H}]^\mathrm{T}(\theta) \in \mathbb{C}^{2N\times 1}$. With these preliminaries, the output of a WL RX beamformer can be given straightforwardly by [P3–P4]

$$\widetilde{y}_\mathrm{RX}(\theta) = \widetilde{\mathbf{w}}^\mathrm{H}(\theta_\mathrm{d})\widetilde{\mathbf{r}}(\theta) = \left[\mathbf{w}_1^\mathrm{H}(\theta_\mathrm{d}), \mathbf{w}_2^\mathrm{H}(\theta_\mathrm{d})\right] \begin{bmatrix} \mathbf{a}(\theta)r + \mathbf{n} \\ \mathbf{a}^*(\theta)r^* + \mathbf{n}^* \end{bmatrix}. \tag{3.9}$$

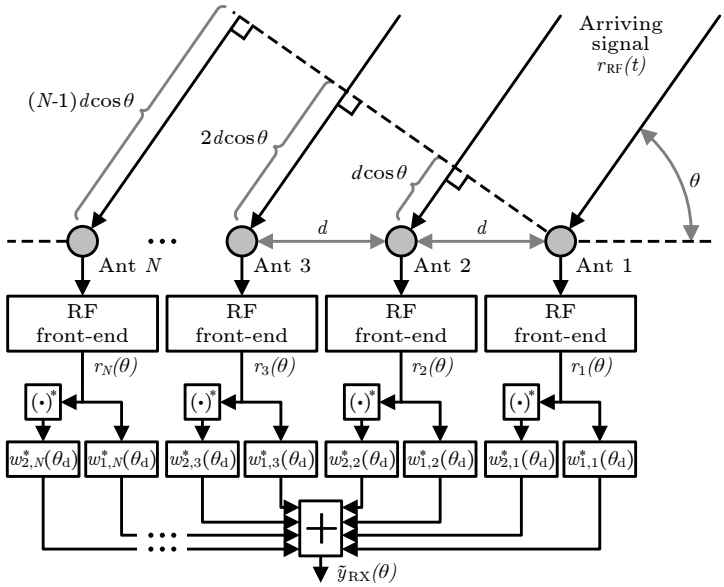

Figure 3.1: Illustration of a conceptual WL RX beamformer with the ULA structure.

Such processing can be implemented purely digitally, and thus no additional analog components are required. Furthermore, as $\widetilde{\mathbf{w}}^{\mathrm{H}}(\theta_\mathrm{d})\widetilde{\mathbf{r}}(\theta)$ clearly implicates, WL processing has a similar structure than the conventional beamforming, i.e. $\mathbf{w}^{\mathrm{H}}(\theta_\mathrm{d})\mathbf{r}(\theta)$, but now just with doubled dimensions. As a result WL beamformer provides also doubled degrees of freedom which can be beneficial, e.g., for I/Q imbalance mitigation purposes as is demonstrated in the following.

Under I/Q imbalance in multiple parallel RX branches, the augmented antenna signal vector gets a form of $\widetilde{\mathbf{r}}_{\mathrm{Rxi}}(\theta) = [\mathbf{r}^{\mathrm{T}}_{\mathrm{Rxi}}(\theta), \mathbf{r}^{\mathrm{H}}_{\mathrm{Rxi}}(\theta)]^{\mathrm{T}} \in \mathbb{C}^{2N\times 1}$ where $\mathbf{r}_{\mathrm{Rxi}}$ is given according to (3.3). Consequently, the output of such WL beamformer becomes equal to [P3–P4]

$$\widetilde{y}_{\mathrm{Rxi}}(\theta) = \widetilde{\mathbf{w}}^{\mathrm{H}}(\theta_\mathrm{d})\widetilde{\mathbf{r}}_{\mathrm{Rxi}}(\theta) = \left[\mathbf{w}_1^{\mathrm{H}}(\theta_\mathrm{d}), \mathbf{w}_2^{\mathrm{H}}(\theta_\mathrm{d})\right] \begin{bmatrix} \mathbf{K}_{\mathrm{Rx1}} & \mathbf{K}_{\mathrm{Rx2}} \\ \mathbf{K}^*_{\mathrm{Rx2}} & \mathbf{K}^*_{\mathrm{Rx1}} \end{bmatrix} \begin{bmatrix} \mathbf{a}(\theta)r + \mathbf{n} \\ \mathbf{a}^*(\theta)r^* + \mathbf{n}^* \end{bmatrix}. \quad (3.10)$$

Evidently, I/Q imbalance creates signal distortion, which is visible in (3.10) as an additional matrix having a single RX I/Q imbalance matrix in each of its quadrants. The distortion is visible also in the radiation pattern which is given under RX I/Q imbalance by [P3–P4]

$$\begin{aligned} \widetilde{D}_{\mathrm{Rxi}}(\theta) = &\left|\mathbf{w}_1^{\mathrm{H}}(\theta_\mathrm{d})\mathbf{K}_{\mathrm{Rx1}}\mathbf{a}(\theta) + \mathbf{w}_2^{\mathrm{H}}(\theta_\mathrm{d})\mathbf{K}^*_{\mathrm{Rx2}}\mathbf{a}(\theta)\right|^2 \\ &+ \left|\mathbf{w}_1^{\mathrm{H}}(\theta_\mathrm{d})\mathbf{K}_{\mathrm{Rx2}}\mathbf{a}^*(\theta) + \mathbf{w}_2^{\mathrm{H}}(\theta_\mathrm{d})\mathbf{K}^*_{\mathrm{Rx1}}\mathbf{a}^*(\theta)\right|^2. \end{aligned} \quad (3.11)$$

Similarly to the radiation pattern of a linear beamformer in (3.5), also now the first term corresponds to the desired signal term whereas the second term is the harmful component. However, due to the doubled number of weights, WL processing provides a more flexible weighting than its linear counterpart where the terms including the SOI

and its complex conjugate are processed with the same weights. In fact, in [P4] we show analytically that in a case of SMF, as a simple example, WL processing can suppress the harmful signal component completely while it is impossible with the plain linear SMF.

Next we address the actual optimization of the WL RX beamforming weights. Following the work in [P4] we focus now on the RF-aware WL-MVDR concept as an example. Note that the WL weights can be formulated also according to multiple other algorithms such as the Wiener filter and LMS used in [P3], normalized LMS (NLMS) introduced in [P1] and SMF presented in [P4].

The main idea of MVDR beamforming is to minimize the variance of a beamformer output while maintaining distortionless response towards the desired spatial direction [73, p. 406]. Consequently, a MVDR beamformer has a built-in capability to suppress incoming interference. In this respect, we extend our signal model to cover also the interference coming from co-channel TXs nearby. In particular, we substitute the RX noise vector $\mathbf{n}$ in the signal model with the interference plus noise vector $\mathbf{z} \in \mathbb{C}^{N\times 1}$ which is equal to

$$\mathbf{z} = \sum_{l=1}^{L} \mathbf{a}(\theta_{\mathrm{int},l}) r_{\mathrm{int},l} + \mathbf{n}. \tag{3.12}$$

Here L denotes the number of external interferers whereas $r_{\mathrm{int},l}$ is the received signal of the l^{th} interferer and $\mathbf{a}(\theta_{\mathrm{int},l})$ is the steering vector corresponding to the same interferer. Note that the beamformer is required to know neither the steering vectors $\mathbf{a}(\theta_{\mathrm{int},l}), l \in \{1,\ldots,L\}$ nor the powers of the interferers. In fact, the RF-aware WL-MVDR beamformer introduced in [P4] can be given as a function of the I/Q imbalance parameters, the steering vector corresponding to the desired direction and the covariance matrix of the received signal as summarized next.

Assuming that information of the RX I/Q imbalance parameters is provided in the BS RX by any available I/Q imbalance estimation algorithm, we can form the augmented RF-aware steering matrix $\widetilde{\mathbf{A}}_{\mathrm{Rxi}}(\theta_{\mathrm{d}}) \in \mathbb{C}^{2N\times 2}$ as [P4]

$$\widetilde{\mathbf{A}}_{\mathrm{Rxi}}(\theta_{\mathrm{d}}) = \begin{bmatrix} \mathbf{K}_{\mathrm{Rx1}}\mathbf{a}(\theta_{\mathrm{d}}) & \mathbf{K}_{\mathrm{Rx2}}\mathbf{a}^{*}(\theta_{\mathrm{d}}) \\ \mathbf{K}^{*}_{\mathrm{Rx2}}\mathbf{a}(\theta_{\mathrm{d}}) & \mathbf{K}^{*}_{\mathrm{Rx1}}\mathbf{a}^{*}(\theta_{\mathrm{d}}) \end{bmatrix}. \tag{3.13}$$

Different quadrants of $\widetilde{\mathbf{A}}_{\mathrm{Rxi}}(\theta_{\mathrm{d}})$ are formed in such a manner that they compensate the harmful effects of I/Q imbalance occurring in the BS RX branches and visible, e.g., in (3.10). The WL-MVDR weight vector $\widetilde{\mathbf{w}}^{\mathrm{MVDR}}_{\mathrm{Rxi}}(\theta_{\mathrm{d}}) \in \mathbb{C}^{2N\times 1}$ under RX I/Q imbalance is then written as [P4]

$$\widetilde{\mathbf{w}}^{\mathrm{MVDR}}_{\mathrm{Rxi}}(\theta_{\mathrm{d}}) = \widetilde{\mathbf{R}}^{-1}_{\mathrm{Rxi}}\widetilde{\mathbf{A}}_{\mathrm{Rxi}}(\theta_{\mathrm{d}}) \left[\widetilde{\mathbf{A}}^{\mathrm{H}}_{\mathrm{Rxi}}(\theta_{\mathrm{d}})\widetilde{\mathbf{R}}^{-1}_{\mathrm{Rxi}}\widetilde{\mathbf{A}}_{\mathrm{Rxi}}(\theta_{\mathrm{d}})\right]^{-1} \begin{bmatrix} 1 \\ 0 \end{bmatrix} \tag{3.14}$$

where $\widetilde{\mathbf{R}}_{\mathrm{Rxi}} = \mathbb{E}[\widetilde{\mathbf{r}}_{\mathrm{Rxi}}(\theta)\widetilde{\mathbf{r}}^{\mathrm{H}}_{\mathrm{Rxi}}(\theta)] \in \mathbb{C}^{2N\times 2N}$ denotes the covariance matrix of the augmented received signal under RX I/Q imbalance. In the beamforming weight optimization, the awareness of the surrounding radio conditions are obtained through the covariance matrix while the RF-awareness is achieved with the help of the augmented steering vector. In such a way, the RF-aware WL-MVDR beamformer is able to provide good performance despite RX I/Q imbalance. We illustrate the performance of the RF-aware

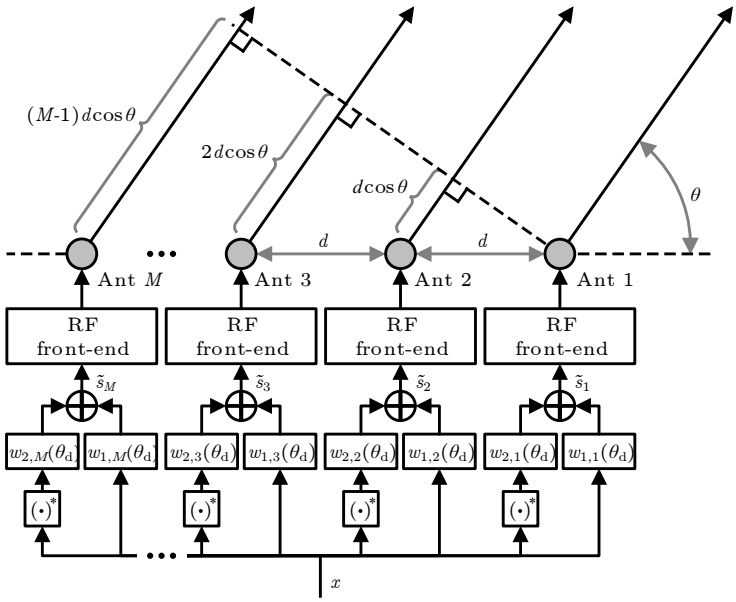

Figure 3.2: Illustration of a conceptual WL TX beamformer with the ULA structure.

WL-MVDR as well as other WL beamforming methods with numerical examples later in Section 3.5.

3.4 WL TX Beamforming

WL TX beamforming is based on WL signal processing prior to analog RF front-ends as illustrated in Fig. 3.2. In fact, the method can be considered also as a signal predistortion which is a common TX signal processing principle, e.g., for mitigating amplifier nonlinearities, see [9, 12, 14]. The basic approach is to feed each RF front-end with a WL signal $\widetilde{s}_i$ which consists not only of the properly weighted actual TX signal x but also of jointly processed complex conjugate x^*. The resulting WL antenna signal vector can then be expressed as $\widetilde{\mathbf{s}} = [\mathbf{w}_1(\theta_\mathrm{d}), \mathbf{w}_2(\theta_\mathrm{d})][x, x^*]^\mathrm{T} \in \mathbb{C}^{N\times 1}$ yielding the effective transmitted WL signal towards direction θ given by [P2]

$$\widetilde{s}_\mathrm{TX}(\theta) = \mathbf{a}^\mathrm{H}(\theta)\widetilde{\mathbf{s}} = \mathbf{a}^\mathrm{H}(\theta)[\mathbf{w}_1(\theta_\mathrm{d}), \mathbf{w}_2(\theta_\mathrm{d})] \begin{bmatrix} x \\ x^* \end{bmatrix}. \tag{3.15}$$

Based on the signal distortion in parallel TX branches, the WL antenna signal under TX I/Q imbalance becomes equal to $\widetilde{\mathbf{s}}_\mathrm{Txi} = \mathbf{K}_\mathrm{Tx1}\widetilde{\mathbf{s}} + \mathbf{K}_\mathrm{Tx2}\widetilde{\mathbf{s}}^* \in \mathbb{C}^{N\times 1}$. That, in turn, results in the effective transmitted WL signal towards θ which can be written as [P2]

$$\widetilde{s}_\mathrm{Txi}(\theta) = \mathbf{a}^\mathrm{H}(\theta)\widetilde{\mathbf{s}}_\mathrm{Txi} = \mathbf{a}^\mathrm{H}(\theta)\left[\mathbf{K}_\mathrm{Tx1}, \mathbf{K}_\mathrm{Tx2}\right] \begin{bmatrix} \mathbf{w}_1(\theta_\mathrm{d}) & \mathbf{w}_2(\theta_\mathrm{d}) \\ \mathbf{w}_2^*(\theta_\mathrm{d}) & \mathbf{w}_1^*(\theta_\mathrm{d}) \end{bmatrix} \begin{bmatrix} x \\ x^* \end{bmatrix}. \tag{3.16}$$

By comparing (3.16) with (3.15), we notice that TX I/Q imbalance causes signal distortion through the I/Q imbalance matrices $\mathbf{K}_{\mathrm{Tx1}}$ and $\mathbf{K}_{\mathrm{Tx2}}$ as well as through the conjugated versions of $\mathbf{w}_1(\theta_\mathrm{d})$ and $\mathbf{w}_2(\theta_\mathrm{d})$. Whereas this phenomenon is slightly different than that in (3.10) with RX I/Q imbalance, the radiation patterns of these cases have more in common. Particularly, the radiation pattern of a WL TX beamformer under TX I/Q imbalance is equal to [P2]

$$\begin{aligned}\widetilde{D}_{\mathrm{Txi}}(\theta) = &\left|\mathbf{a}^{\mathrm{H}}(\theta)\left(\mathbf{K}_{\mathrm{Tx1}}\mathbf{w}_1(\theta_\mathrm{d}) + \mathbf{K}_{\mathrm{Tx2}}\mathbf{w}_2^*(\theta_\mathrm{d})\right)\right|^2 \\ &+ \left|\mathbf{a}^{\mathrm{H}}(\theta)\left(\mathbf{K}_{\mathrm{Tx1}}\mathbf{w}_2(\theta_\mathrm{d}) + \mathbf{K}_{\mathrm{Tx2}}\mathbf{w}_1^*(\theta_\mathrm{d})\right)\right|^2\end{aligned} \tag{3.17}$$

which has very similar structure to the one in (3.11) given for the corresponding RX beamformer.

TX beamforming weights can be optimized by several methods. One of the conventional TX beamforming approaches is based on the concept of null-steering. There, a single beam is steered towards the desired direction θ_d whereas the transmission is minimized to the undesired directions $\theta_{\mathrm{un},1},\ldots,\theta_{\mathrm{un},P}$ by setting nulls to the corresponding places in the spatial response. This kind of method can be used, e.g., in secondary TXs in CRs where the data is to be sent to a secondary RX while interfering the primary devices is strictly forbidden. In [P2], we provide a detailed derivation for the WL null-steering weights and the method is shortly summarized below.

The WL null-steering principle is formulated mathematically as [P2]

$$\max_{\widetilde{\mathbf{w}}_{\mathrm{Txi}}} \left|\widetilde{\mathbf{w}}_{\mathrm{Txi}}^{\mathrm{H}}\widetilde{\mathbf{a}}_{\mathrm{Txi}}(\theta_\mathrm{d})\right|^2 \quad \text{subject to} \quad \begin{cases} \widetilde{\mathbf{w}}_{\mathrm{Txi}}^{\mathrm{H}}\widetilde{\mathbf{A}}_{\mathrm{Txi}} &= \mathbf{0} \\ \widetilde{\mathbf{w}}_{\mathrm{Txi}}^{\mathrm{H}}\widetilde{\mathbf{w}}_{\mathrm{Txi}} &\leq \sqrt{\widetilde{\alpha}} \end{cases} \tag{3.18}$$

where $\widetilde{\mathbf{a}}_{\mathrm{Txi}}(\theta_\mathrm{d}) = [(\mathbf{K}_{\mathrm{Tx1}}^{\mathrm{H}}\mathbf{a}(\theta_\mathrm{d}))^{\mathrm{T}}, (\mathbf{K}_{\mathrm{Tx2}}^{\mathrm{H}}\mathbf{a}(\theta_\mathrm{d}))^{\mathrm{T}}]^{\mathrm{T}} \in \mathbb{C}^{2M\times 1}$ is the RF-aware steering vector ensuring transmission to the desired direction θ_d. Additionally, $\widetilde{\mathbf{A}}_{\mathrm{Txi}} \in \mathbb{C}^{2M\times 2P+1}$ guarantees the nulls in the response and it is equal to [P2]

$$\widetilde{\mathbf{A}}_{\mathrm{Txi}} = \left[\widetilde{\mathbf{A}}_{\mathrm{Txi}}(\theta_{\mathrm{un},1}),\ldots,\widetilde{\mathbf{A}}_{\mathrm{Txi}}(\theta_{\mathrm{un},P}),\widetilde{\mathbf{a}}_{\mathrm{Txi,SI}}(\theta_\mathrm{d})\right] \tag{3.19}$$

where $\theta_{\mathrm{un},i}, i \in 1,\ldots,P$ denote the undesired spatial directions and the resulting steering matrices are denoted by $\widetilde{\mathbf{A}}_{\mathrm{Txi}}(\theta_{\mathrm{un},i}) \in \mathbb{C}^{2M\times 2}$. Moreover, $\widetilde{\mathbf{a}}_{\mathrm{Txi,SI}}(\theta_\mathrm{d}) = [(\mathbf{K}_{\mathrm{Tx2}}^{\mathrm{T}}\mathbf{a}^*(\theta_\mathrm{d}))^{\mathrm{T}}, (\mathbf{K}_{\mathrm{Tx1}}^{\mathrm{T}}\mathbf{a}^*(\theta_\mathrm{d}))^{\mathrm{T}}]^{\mathrm{T}} \in \mathbb{C}^{2M\times 1}$ is an additional steering vector whose purpose is to control and mitigate the undesired self interference due to TX I/Q imbalance. Finally, $\widetilde{\alpha}$ denotes the TX power scaling factor. A solution for the weight optimization task described above is then given by [P2]

$$\widetilde{\mathbf{w}}_{\mathrm{Txi}}^{\mathrm{NS}}(\theta_\mathrm{d}) = \frac{\sqrt{\widetilde{\alpha}}}{\left|\left|\left(\mathbf{I} - \mathbf{P}_{\widetilde{\mathbf{A}}_{\mathrm{Txi}}}\right)\widetilde{\mathbf{a}}_{\mathrm{Txi}}(\theta_\mathrm{d})\right|\right|}\left(\mathbf{I} - \mathbf{P}_{\widetilde{\mathbf{A}}_{\mathrm{Txi}}}\right)\widetilde{\mathbf{a}}_{\mathrm{Txi}}(\theta_\mathrm{d}). \tag{3.20}$$

Here $\mathbf{P}_{\widetilde{\mathbf{A}}_{\mathrm{Txi}}} \in \mathbb{C}^{2P+1\times 2P+1}$ denotes the orthogonal projection matrix of $\widetilde{\mathbf{A}}_{\mathrm{Txi}}$ and is equal to [P2]

$$\mathbf{P}_{\widetilde{\mathbf{A}}_{\mathrm{Txi}}} = \widetilde{\mathbf{A}}_{\mathrm{Txi}}\left[\widetilde{\mathbf{A}}_{\mathrm{Txi}}^{\mathrm{H}}\widetilde{\mathbf{A}}_{\mathrm{Txi}}\right]^{-1}\widetilde{\mathbf{A}}_{\mathrm{Txi}}^{\mathrm{H}}. \tag{3.21}$$

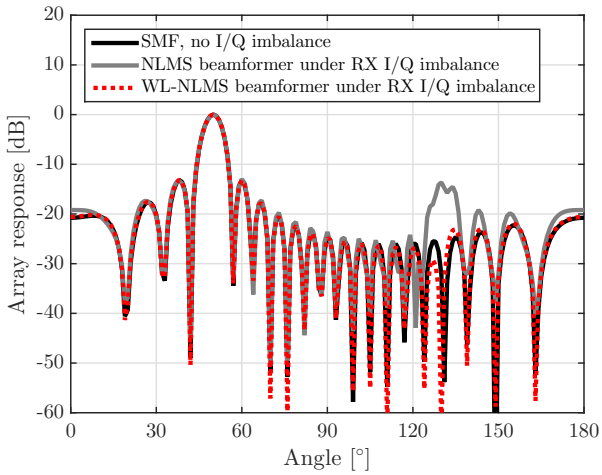

Figure 3.3: Radiation patterns of the NLMS and WL-NLMS beamforming methods with 20 antenna elements when $\theta_{\mathrm{d}} = 50°$, SNR $= 40\,\mathrm{dB}$, $g = 0.8$, and $\phi = -20°$. Iterative training was based on 3000 16-QAM symbols.

The solution given in (3.20) fulfills the requirements in (3.18). However, $\widetilde{\mathbf{w}}_{\mathrm{Txi}}^{\mathrm{NS}}(\theta_{\mathrm{d}})$ is not directly applicable to be used in WL processing described in (3.15) due to dimensional mismatches. Consequently, we substitute the weights for signal x with the first M elements of the WL null-steering weight vector while the rest of the elements are used for the conjugated signal x^*, i.e., $\mathbf{w}_1(\theta_{\mathrm{d}}) = \widetilde{\mathbf{w}}_{\mathrm{Txi}}^{\mathrm{NS}}(\theta_{\mathrm{d}})[1:M]$ and $\mathbf{w}_2(\theta_{\mathrm{d}}) = \widetilde{\mathbf{w}}_{\mathrm{Txi}}^{\mathrm{NS}}(\theta_{\mathrm{d}})$ [M+1:2M]. Due to joint processing of the signal and its conjugate, this solution can provide the desired radiation characteristics even when being under severe TX I/Q imbalance as illustrated by a numerical example in the next section.

3.5 Numerical Examples of Beamforming Performance

We start the numerical evaluations with a simple example in Fig. 3.3 illustrating the mirror beam effect in a RX beamformer under I/Q imbalance. The setup consist of a ULA with $N = 20$ RX antennas and associated RX branches. The gain imbalance is set to 0.8 in all branches whereas the phase imbalance is equal to $-20°$. Such a case could happen in closely located RX branches that share, e.g., common LO signals that dominate the harmful effects of I/Q imbalance. The desired direction $\theta_{\mathrm{d}} = 50°$ resulting in the mirror direction $180° - 50° = 130°$. Beamforming is implemented with the WL-NLMS algorithm described in detail in [P1], and the conventional NLMS method, both using 3000 16-QAM symbols for iterative training. Moreover, the SNR is set to 40 dB. Finally, SMF under ideal I/Q balance is included to the setup as a reference. As the results show, all beamformers can successfully steer the main beam towards $\theta_{\mathrm{d}} = 50°$ and have close to identical response around the desired direction. What is interesting, however, is that the response of NLMS has a high peak also towards the

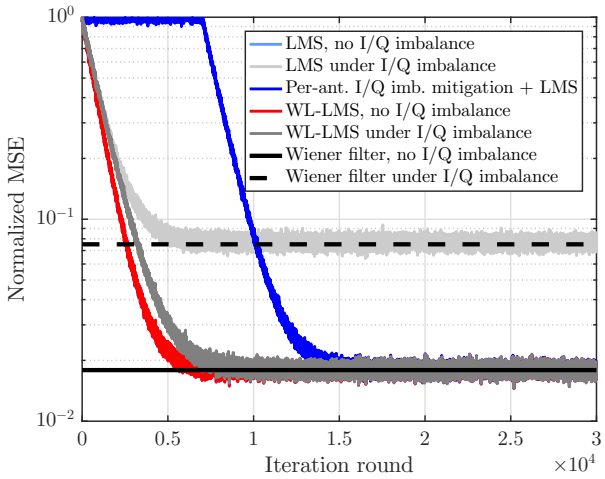

Figure 3.4: Beamforming weight convergence of the LMS and WL-LMS methods. $N = 6$, $\theta_{\mathrm{d}} = 65°$, $\theta_{\mathrm{int},1} = 22°$, $\theta_{\mathrm{int},2} = 115°$, SNR $= 10\,\mathrm{dB}$, $g \sim \mathcal{U}(0.82, 0.88)$, and $\phi \sim \mathcal{U}(7°, 13°)$. Iterative training was based on 16-QAM symbols and the results are averaged over 500 channel and I/Q imbalance parameter realizations. The curves with light blue and red overlap each other, and consequently only the red curve is properly visible.

mirror direction which is caused purely by equal I/Q imbalance in the RX branches as discussed in Section 3.2. Such a peak is not visible in the case of WL-NLMS indicating that it is able to provide error free radiation properties even when being under RX I/Q imbalance.

RX beamforming is further illustrated in Fig. 3.4 where the weight convergence of the adaptive WL-LMS and LMS algorithms is shown. The RX consists now of a ULA with $N = 6$ antennas and RX branches. Modeling a setup with some shared and some branch dependent processing blocks, the gain imbalance parameters are drawn from $\mathcal{U}(0.82, 0.88)$ whereas the phase imbalance coefficient are drawn from $\mathcal{U}(7°, 13°)$. The iterative training is again based on 16-QAM symbols and the results are averaged over 500 realizations. The desired direction is equal to $\theta_{\mathrm{d}} = 65°$ while external interferers are located at directions $\theta_{\mathrm{int},1} = 22°$ and $\theta_{\mathrm{int},2} = 115°$. Finally, the SNR is set to 10 dB and each of the interferers is 6 dB stronger than the desired signal. First of all, the horizontal lines of the Wiener filter show that the normalized mean square error (MSE) is more than 3.5 times better under ideal I/Q balance than the corresponding value under RX I/Q imbalance. Second of all, we see that the performance of LMS with and without RX I/Q imbalance converges close to the corresponding results of the optimal minimum mean square error (MMSE) Wiener filter as expected. The error level of WL-LMS, however, is not dependent on the I/Q imbalance scheme. In fact, WL-LMS under ideal I/Q balance as well as under I/Q imbalance provides the same normalized MSE as the Wiener filter without I/Q imbalance. The only difference between the two cases of WL-LMS is that the convergence takes slightly longer under I/Q imbalance. As a reference, we compare here the cases above also to the conventional setup where I/Q imbalance mitigation is first done in each of the individual RX branches by the blind, circularity-based, adaptive

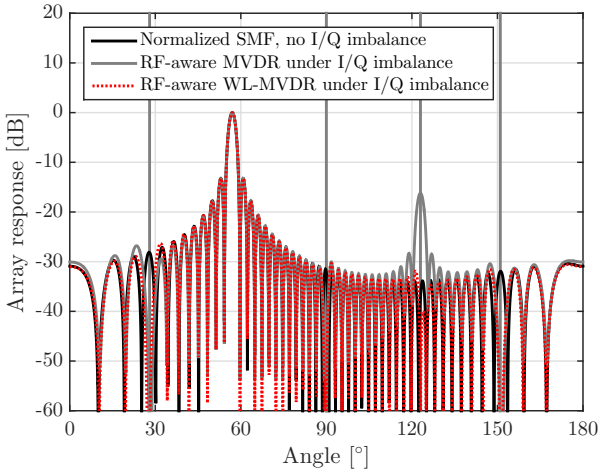

Figure 3.5: Radiation patterns of the SMF, RF-aware MVDR and RF-aware WL-MVDR methods under systematic I/Q imbalance. $N = 50$, $\theta_{\mathrm{d}} = 57°$, $\theta_{\mathrm{int},1-4} = 28°$, $90°$, $123°$, and $151°$. SNR $= 10\,\mathrm{dB}$, $g = 0.85$, and $\phi = -15°$.

algorithm proposed in [10, 11], and the actual LMS-based beamforming operates then across the antenna signals where the harmful I/Q imbalance effects have been pushed down. The step size of the I/Q imbalance mitigation algorithm is chosen such that the algorithm converges quickly, in this case after 7000 iterations. Once the I/Q imbalance mitigation algorithm has reached a steady state operation, the beamformer is turned on. The results show that also this method provides a performance close to that of the Wiener filter. However, the total time required for the convergence of the LMS beamformer preceded by per-antenna branch I/Q imbalance mitigation is higher than with WL-LMS due to the adaptation of the I/Q imbalance mitigation algorithm. Since both of these approaches can be implemented with $12N$ real-valued multiplications per output sample, WL-LMS can be considered as a more suitable solution for practical systems than the conventional method with per-antenna branch I/Q imbalance mitigation.

The following four examples are based on a case where the RX consists of ULA with $N = 50$ antennas and the RF-aware WL-MVDR as well as the RF-aware MVDR, described in detail in [P4], are applied. In addition, SMF is included as a benchmark. The desired direction $\theta_{\mathrm{d}} = 57°$ while the interferers locate at directions $\theta_{\mathrm{int},1-4} = 28°$, $90°$, $123°$, and $151°$ and are marked with gray vertical lines. In addition, the SNR is set to $10\,\mathrm{dB}$. The case with systematic I/Q imbalance is depicted in Fig. 3.5. There the gain and phase imbalance coefficients are equal in all RX branches and are set to $g = 0.85$ and $\theta = -15°$, respectively. Obviously, all beamformers provide the same response towards the desired signal. Moreover, both MVDR methods can effectively place a null towards the interferers at $\theta_{\mathrm{int},1} = 28°$, $\theta_{\mathrm{int},2} = 90°$ and $\theta_{\mathrm{int},4} = 151°$. However, their responses at $\theta_{\mathrm{int},3} = 180° - \theta_{\mathrm{d}} = 123°$ have significant differences. In particular, even though the RF-aware MVDR knows the I/Q imbalance parameters, it cannot steer a null for $\theta_{\mathrm{int},3}$ and results only in some $16\,\mathrm{dB}$ attenuation for that particular interferer. Consequently, the combiner output signal is heavily distorted if a strong interferer is transmitting at

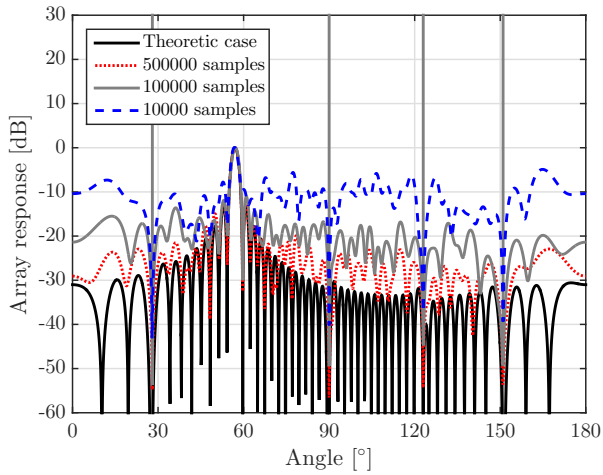

Figure 3.6: Dependency of the training signal length on the RF-aware WL-MVDR radiation pattern under systematic I/Q imbalance. $N = 50$, $\theta_{\mathrm{d}} = 57°$, $\theta_{\mathrm{int},1-4} = 28°$, $90°$, $123°$, and $151°$. SNR $= 10\,\mathrm{dB}$, $g = 0.85$, and $\phi = -15°$.

the mirror direction. Our further simulations in [P4] have shown that the mirror beam is much stronger with $N = 50$ than with $N = 8$. Interestingly, this implicates that the bigger the array, the more sensitive it gets for RX I/Q imbalance in terms of the mirror beam phenomenon. Such performance degradation does not occur with the RF-aware WL-MVDR since it does not suffer from the mirror beam effect. Instead, it steers a deep null also to the mirror direction, and thus ensures reliable operation for all considered interference locations. Additionally, as shown in [P4], WL-MVDR provides the same performance with all practically reasonable gain and phase coefficient values and is hence independent on I/Q imbalance.

The same setup is considered also in Fig. 3.6. However, whereas the RF-aware WL-MVDR weight optimization in Fig. 3.5 was based on deploying theoretical ideal ensemble averaged covariance matrix, now we use estimated covariance matrix based on finite signal lengths. In particular, the covariance matrix is now calculated with 10000, 100000 and 500000 signal samples. First of all, we notice that in all cases the main beam is successfully steered towards the desired direction. Additionally, all schemes provide nulls at the interference directions. Nonetheless, the deepness of the nulls is heavily dependent on the number of samples, i.e., the more samples are used, the deeper null can be created by the RF-aware WL-MVDR. What is also interesting, is that the response at "don't care" regions have remarkable differences where a higher number of samples results in better control. Whereas these regions are not very significant with fixed device locations, this phenomenon needs to be kept in mind when considering the weight update rate in mobile networks.

The next example given in Fig. 3.7 addresses the awareness of the I/Q imbalance parameters. In earlier examples we assumed that the RX has a perfect knowledge of the I/Q imbalance matrices. Instead of such an unrealistic assumption, we add now some uncertainties to the I/Q imbalance matrices. The actual gain and phase imbalance

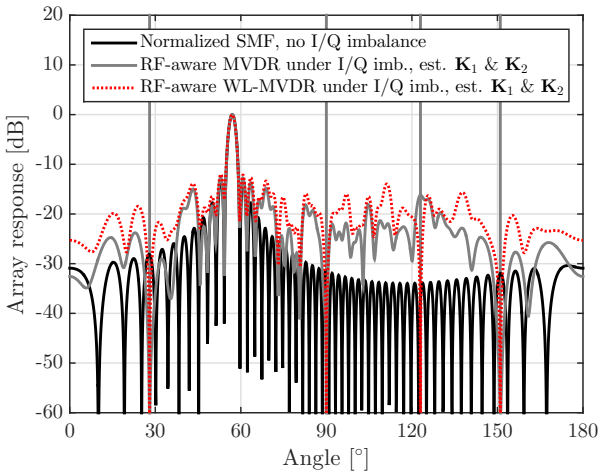

Figure 3.7: The effects of the estimated I/Q imbalance parameters on the radiation patterns of the SMF, RF-aware MVDR and RF-aware WL-MVDR methods under systematic I/Q imbalance. $N = 50$, $\theta_{\mathrm{d}} = 57°$, $\theta_{\mathrm{int},1-4} = 28°$, $90°$, $123°$, and $151°$. SNR $= 10\,\mathrm{dB}$, $g = 0.85$, and $\phi = -15°$.

uncertainties are set to $\pm 0.1\,\%$ (relative to the real value) and $\pm 0.1\,°$, respectively. These values match in a case where the IRR after I/Q compensation is equal to 60 dB, a value which has been reported for a single transceiver branch, e.g., in [11, 12]. Again, the response towards the desired direction is equal in all cases. However, the uncertainty of I/Q imbalance causes now a high ripple in other directions. Fortunately, the nulls can be still steered towards the interferers. The only exception to that is seen with the RF-aware MVDR when considering the mirror beam in direction $180° - 57° = 123°$ caused by equal I/Q imbalances in parallel RX branches. Consequently, the RF-aware WL-MVDR is the only beamformer among the considered ones which provides good beamforming performance in practical scenarios.

In Fig. 3.8, the same basic scenario as above is considered but now the gain and phase imbalance coefficients are drawn from $\mathcal{U}(0.85, 1.15)$ and $\mathcal{U}(-15°, 15°)$, respectively, being an example of a case where the RX branches have all hardware blocks of their own. Now the response of the RF-aware MVDR has some ripples in the "don't care" regions but it does not suffer of the mirror beam effect. This stems from the fact that now the effects of I/Q imbalances do not add up coherently with respect to spatial directions. Consequently, under random RX I/Q imbalance both of the considered beamformers, i.e. the RF-aware MVDR and the RF-aware WL-MVDR, are able to perform sufficiently in terms of interference suppression. However, an issue which is not very well visible in the figure is that the nulls of the RF-aware MVDR towards the interferers provide an attenuation of 53 dB–66 dB while the corresponding range for the RF-aware WL-MVDR is equal to 88 dB–98 dB.

Finally, we change the viewpoint to TX beamforming. The setup consists of $M = 8$ parallel TX antennas and the associated TX branches whose gain imbalance parameters are drawn from $\mathcal{U}(0.85, 1.15)$ whereas the phase imbalance parameters are drawn from

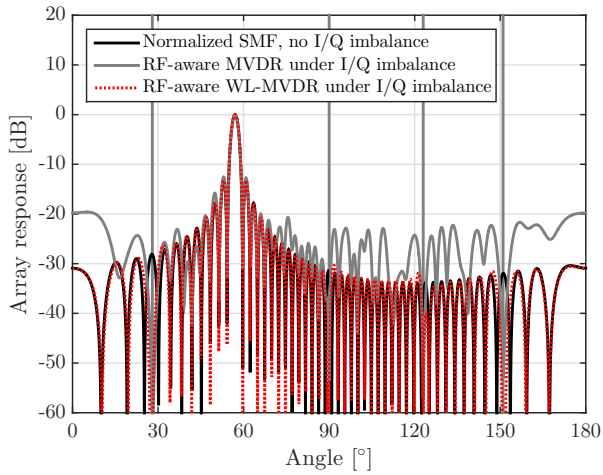

Figure 3.8: Radiation patterns of the SMF, RF-aware MVDR and RF-aware WL-MVDR methods under random I/Q imbalance. $N = 50$, $\theta_{\mathrm{d}} = 57°$, $\theta_{\mathrm{int},1-4} = 28°$, $90°$, $123°$, and $151°$. SNR $= 10\,\mathrm{dB}$, $g \sim \mathcal{U}(0.85, 1.15)$, and $\phi \sim \mathcal{U}(-15°, 15°)$.

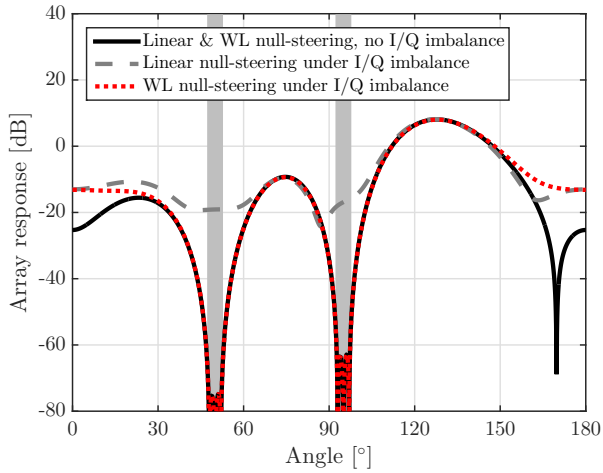

Figure 3.9: Radiation patterns of the linear and WL TX null-steering beamforming methods with 8 antenna elements when $\theta_{\mathrm{d}} = 130°$, $\theta_{\mathrm{PU},1} = 50° \pm 2°$, $\theta_{\mathrm{PU},2} = 95° \pm 2°$, $g \sim \mathcal{U}(0.85, 1.15)$, and $\phi \sim \mathcal{U}(-15°, 15°)$.

$\mathcal{U}(-15°, 15°)$. The desired direction is equal to $\theta_{\mathrm{d}} = 130°$ whereas transmission towards $\theta_{\mathrm{PU},1} = 50° \pm 2°$, $\theta_{\mathrm{PU},2} = 95° \pm 2°$ is considered to be forbidden. Fig. 3.9 illustrates the performance of the WL null-steering method compared to its linear counterpart with and without TX I/Q imbalance. The results show that transmission towards the desired direction is well reached in all cases. Furthermore, WL null-steering creates deep null towards the undesired direction, and thus protects devices in those directions

from additional interference. The conventional linear null-steering, in turn, is not able to provide proper nulls towards these forbidden directions. In fact, the attenuation at those points is only 18 dB–20 dB compared to the main direction, meaning that sensitive RX devices can suffer significantly especially when the total TX power is high. To conclude, this example demonstrates that WL beamforming is a useful tool not only in the RX side but also in multiantenna TXs where the transmission is desired to be concentrated spatially towards a certain direction while simultaneously keeping the undesired or forbidden directions free of interference.

CHAPTER 4

Spatial RX Processing in Multiantenna OFDM/OFDMA Systems under I/Q Imbalance: Modeling, Analysis and Digital Mitigation

This chapter is based on the work in [P5–P8] and extends the modeling, analysis and mitigation of I/Q imbalance into wideband OFDM and OFDMA waveforms as well as into full MIMO communications where not only the BS RX but also the UE TXs can operate with multiple parallel antennas. We also incorporate external interferers into the signal models to model heterogeneous networks. After that we introduce the concept of augmented subcarrier processing and formulate its analytical output SINR in order to evaluate the performance of the combiner. Moreover, we provide extensive numerical examples to show the expected performance as a function of multiple system parameters while more examples can be found from [P5–P8]. Finally, we provide some practical aspects regarding real world implementations of the considered processing methods.

4.1 Background and State of the Art

I/Q imbalance in systems utilizing OFDM waveforms is an extensively studied topic as can be seen from Table 4.1. Since our aim is to investigate I/Q imbalance especially in multiantenna systems, we group the existing studies based on the considered antenna configurations. Note that, in order to prevent misunderstandings, we define a scheme where multiple single-antenna UEs communicate with a multiantenna BS either as MU-MISO (in downlink) or as MU-SIMO (in uplink) since the link between a single UE and the BS is purely a MISO or SIMO connection.

A majority of the research regarding I/Q imbalance in OFDM systems has been done for SU-SISO connections. One of the first publications addressing this issue was [162]

Table 4.1: Summary of essential studies regarding I/Q imbalance with OFDM-based waveforms.

	SISO	MISO	SIMO	MIMO
TX I/Q imbalance	[9, 12, 14, 114, 195, 209]	-	[96, 107], [P5]	[P6–P8]
RX I/Q imbalance	[10, 11, 20, 77, 98, 162, 171, 203, 205]	[70]	[97, 123, 202], [P5]	[40, 172], [P6–P8]
TX+RX I/Q imbalance	[43,52,65,67,83, 84, 130, 136, 138, 154, 169, 173]	[23, 26, 112, 113, 135, 206]	[23, 26], [P5]	[87, 118, 129, 137, 155–158, 170, 207], [P6–P8]
Single-user	[9–12, 14, 20, 52, 65, 77, 98, 130, 136, 138, 154, 162, 169, 171, 173, 203, 205, 209]	[23, 70, 112, 113, 135, 206]	[23, 123, 202], [P5]	[40, 87, 118, 129, 137, 155–158, 170, 172, 207]
Multiuser*	[43, 67, 83, 84, 114, 195]	[23, 26]	[23, 26, 96, 97, 107]	[170], [P6–P8]
Massive MIMO	-	[23, 26]	[23, 26, 97]	[P6–P8]
Other RF impairments	[9, 14, 20, 43, 52, 65, 77, 203]	[23, 26, 70]	[23, 26, 96, 123, 202]	[40, 87, 129, 170]
Augmented subcarrier processing	[20, 77, 83, 84, 114, 130, 162, 169, 171, 173, 195, 203, 209]	-	[96, 202], [P5]	[87, 118, 129, 137, 156, 157, 170, 172, 207], [P6–P8]
OFDM	[9, 14, 20, 52, 65, 98, 130, 136, 138, 154, 162, 169, 171, 173, 203, 205, 209]	[70, 112, 113, 135, 206]	[97, 123, 202], [P5]	[40, 87, 118, 129, 137, 155–158, 170, 172, 207], [P7–P8]
OFDMA	[43, 77, 84, 114, 195]	-	[96]	[P6–P8]
SC-FDMA	[14, 43, 67, 83, 195]	-	[96, 107]	-
Other waveform†	[10–12]	[23, 26]	[23, 26]	-

* Multiuser scheme includes spatial as well as frequency domain UE multiplexing.
† Waveform is not specified but it is compatible with OFDM.

which focused on RX I/Q imbalance and its frequency domain mitigation. Similar theme can be found also from [171] where, in addition to frequency domain equalizer, also a time domain method was developed. RX I/Q imbalance was addressed also in [10] where a blind estimation method was developed. The work in [169, 173] extended the I/Q imbalance scheme to joint TX+RX I/Q imbalances and their compensation in the RX side. Another frequency-domain compensation method was developed in [20]

but this time for the joint effects of RX I/Q imbalance and CFO. The study in [98], in turn, concentrated on the capacity of an OFDM link under RX I/Q imbalance whereas [11] provided circularity-based compensation method for RX I/Q imbalance. TX I/Q imbalance was, in turn, considered in [12] where a calibration method for frequency selective TX I/Q imbalance was developed. The study in [130] considered frequency dependent TX+RX I/Q imbalances under high mobility causing Doppler spread. The work in [77] investigated the joint effects of RX I/Q imbalance and amplifier nonlinearities and developed RX signal processing methods for impairment mitigation in LTE systems. Channel estimation and data detection algorithms under RX I/Q imbalance and phase noise were considered in [203]. The studies in [9, 14] focused on developing a TX predistorter against frequency-dependent PA nonlinearities and TX I/Q imbalance. Analytical performance in terms of detection error rate, ergodic capacity and outage capacity under RX I/Q imbalance was evaluated in [205]. Mutual information analysis under TX+RX I/Q imbalance and phase noise was, in turn, given in [65]. The studies in [136, 138] provided exact average SINR formulation for an OFDM link under TX +RX I/Q imbalances. Other aspects were considered in [52] where an error rate analysis for an OFDM link under TX+RX I/Q imbalances jointly with CFO and phase noise was provided. Furthermore, in [154] a preamble based channel and I/Q imbalance estimation was considered.

Due to the single antenna equipment in both ends of the connection, SISO links do not support spatial UE multiplexing. However, UEs can be multiplexed in frequency domain through the OFDMA [121, p. 439] and single-carrier frequency-division multiple access (SC-FDMA) [127] principles. Consequently, there exist I/Q imbalance studies also in these areas and [114] is one of them considering pilot patterns under TX I/Q imbalance in OFDMA uplink. TX I/Q imbalance was considered also in [195] where the UE multiplexing is done through OFDMA as well as SC-FDMA and I/Q imbalance mitigation is implemented in the RX. The study in [67] provided error vector magnitude analysis for SC-FDMA links under TX+RX I/Q imbalances while [83] presented a capacity analysis for a similar setup. Optimization of pilot patterns in an uplink OFDMA scheme under TX+RX I/Q imbalances was, in turn, considered in [84]. Finally, in [43] I/Q imbalance and CFO were studied in OFDMA/SC-FDMA uplink transmission.

Extending the SISO link to have multiple antennas in the TX results in a MISO connection and the work in [206] provided performance analysis for TX+RX I/Q imbalances in space-time coded MISO-OFDM systems. TX+RX I/Q imbalances were considered also in [112] which focuses on downlink antenna selection, and in [113] concentrating on TX diversity in terms of the outage probability. Furthermore, [135] provided accurate analytical approximation for the per-subcarrier average SINR under TX+RX I/Q imbalances. Finally, [70] considered the joint effects of RX I/Q imbalance and phase noise in downlink transmission.

In contrast to the MISO scheme, SIMO link has only one TX antenna but multiple RX antennas. The study in [123] concentrated on such an antenna scenario under I/Q imbalance, phase noise, amplifier nonlinearities and DC offset in terms of simulations and practical performance measurements. Compensation of RX I/Q imbalance and phase noise were, in turn, considered in [202]. The single user SIMO (SU-SIMO) scheme was extended to MU-SIMO in [107] where the UE multiplexing was carried out with the SC-FDMA and the focus was on turbo equalization in LTE RXs when the TXs

suffer from I/Q imbalance. SC-FDMA as well as OFDMA were considered also in [96] analyzing TX I/Q imbalance and CFO in uplink transmission.

When both the TX and RX are equipped with multiple antenna we get a MIMO connection. In a SU-MIMO context, [172] provided an extensive analysis of RX I/Q imbalance in OFDM systems. The studies in [156, 157] were, in turn, focused on estimation and compensation of TX+RX I/Q imbalances while probability of erroneous detection under the same scenario was investigated in [155, 157, 158]. Furthermore, the work in [207] concentrated on estimation and compensation of TX+RX I/Q imbalances in space-time coded OFDM systems. TX+RX I/Q imbalances were considered also in [118] where the focus was on pilot designs for channel estimation. Similar aspects were studied in [129] where methods for the pilot design and actual channel estimation were provided for a SU-MIMO system under TX+RX I/Q imbalances, CFO and the Doppler effect. The work in [40] was, in turn, focused on estimation of the wireless channel as well as the RX I/Q imbalance and CFO parameters in SU-MIMO OFDM systems. A joint I/Q imbalance and phase noise estimation/compensation scheme was provided in [87] while [137] resulted in analytical approximation for the per-subcarrier SINR. Finally, the work in [170] focused mainly on I/Q imbalance and CFO in SU-MIMO but extends the study partly also to MU-MIMO.

The effects of I/Q imbalance have been studied also in the massive MIMO framework. RX I/Q imbalance in uplink MU-SIMO transmission was investigated in [97] where the compensation of I/Q imbalance is carried out in each of the antenna branches before the channel equalization. The study in [23], in turn, considered the effects of residual TX and RX RF impairments after their mitigation as an additive distortion noise with Gaussian distribution and focused on the achievable performance in terms of energy efficiency, estimation accuracy and capacity. Moreover, spectral efficiency issues under similar impairment models, but now only for the UEs, were studied for downlink and uplink in [26]. RF impairments were also recognized as an issue in massive MIMO systems in [99, 110] although not investigated in detail there. Massive MIMO and OFDM-based waveforms was the main theme also in publications [P6–P7] and considered in a smaller scale in [P8].

Stemming from the nature of the signal distortion caused by I/Q imbalance in OFDM systems and based on the observations made in the studies listed above, the so-called augmented subcarrier processing for I/Q imbalance mitigation has been developed. Therein, each subcarrier signal is processed jointly with the corresponding signal at the mirror subcarrier. Taking an example of augmented RX processing under RX I/Q imbalance, the mathematical formulation for the augmented output signal $\widetilde{y}_{\mathrm{Rxi},c}$ at subcarrier c can be expressed as [77, 157, 162]

$$\widetilde{y}_{\mathrm{Rxi},c} = w_{1,c} r_{\mathrm{Rxi},c} + w_{2,c} r^{*}_{\mathrm{Rxi},c'}. \tag{4.1}$$

Here $r_{\mathrm{Rxi},c}$ and $r_{\mathrm{Rxi},c'}$ denote the frequency domain received data samples at subcarrier c and at the corresponding mirror subcarrier c', respectively. Moreover, $w_{1,c}$ and $w_{2,c}$ are the processing weights at subcarrier c. Note that we have omitted the OFDM symbol index i from the signal variables for notational convenience and consistency with the publications. Note also that despite being frequency domain variables, all terms here are written in lowercase in order to distinguish them later from matrices. The method described in (4.1) is very close to WL time-domain processing discussed

in Chapter 3. In fact, the augmented frequency domain processing corresponds to WL processing in time domain since $\mathscr{F}\{w_1(t) \star x(t) + w_2(t) \star x^*(t)\} = W_1(f)X(f) + W_2(f)X^*(-f)$. The augmented subcarrier processing has been utilized in some form for signals under I/Q imbalance in the TX side in [9, 14, 209] and in the RX side, e.g., in [43, 77, 83, 87, 96, 97, 107, 130, 137, 156, 157, 162, 169–173, 195, 202, 203, 207]. Due to being an efficient and popular tool for I/Q imbalance mitigation, *we exploit the augmented subcarrier approach for I/Q imbalance mitigation in multiantenna systems* in publications [P5–P8] and do the same also in this chapter.

4.2 Extended Uplink Signal Model and Frequency Domain Analysis

In the following, we introduce a signal model which was used in publications [P6–P8] and is compatible also with the work in [P5]. The setup consists of a full MU-MIMO scheme where the UEs are multiplexed spatially as well as in frequency domain through the OFDMA principle. That is, multiple active UE TXs are transmitting simultaneously at each of the subcarriers. Such a multiple-access scheme is already adopted to Institute of Electrical and Electronics Engineers (IEEE) 802.16 Worldwide Interoperability for Microwave Access (WiMAX) advanced air interface specification [78] and has been considered to be a potential air interface technology for the future wireless local area network (WLAN) implementations within the IEEE 802.11ax/HEW framework [79, 80]. In addition, the considered model can be easily applied to other multicarrier systems such as LTE and LTE-A which, in terms of uplink, are based on SC-FDMA waveform having many similarities with OFDMA.

The considered MU-MIMO setup is illustrated in Fig. 4.1. As discussed in Section 2.2.1, it makes sense to analyze OFDM-based systems at the subcarrier level. Consequently, we focus on a subcarrier pair consisting of an arbitrary subcarrier c and its mirror subcarrier c'. The number of active UEs at subcarrier c is denoted with U while the number of UEs at the mirror subcarrier is equal to V. The UEs at the corresponding subcarriers are indexed with $u \in \{1, \ldots, U\}$ and $v \in \{1, \ldots, V\}$, respectively. Depending on the subcarrier allocation between different UEs, u and v might sometimes refer to the same UE. Furthermore, the number of TX antennas of UE u and v is equal to M_u and M_v, respectively. In order to model increasingly popular heterogeneous networks, we include also external interferers to the considered setup. The number of interferers at all subcarriers is denoted with L and they are indexed by $l \in \{1, \ldots, L\}$. Moreover, the number of TX antennas of the l^{th} interferer is equal to J_l.

The transmitted signal vector of UE u at subcarrier c is equal to $\mathbf{s}_{u,c} = \mathbf{G}_{u,c}\mathbf{x}_{u,c} \in \mathbb{C}^{M_u \times 1}$ where $\mathbf{x}_{u,c} \in \mathbb{C}^{Q_{\mathrm{u},c} \times 1}$ denotes the parallel data streams to be transmitted, $Q_{\mathrm{u},c}$ is the number of those streams, and $\mathbf{G}_{u,c} \in \mathbb{C}^{M_u \times Q_{\mathrm{u},c}}$ is the TX precoder matrix which maps the data streams to the TX antennas. The corresponding signal vector of UE v at the mirror subcarrier c' is given by $\mathbf{s}_{v,c'} = \mathbf{G}_{v,c'}\mathbf{x}_{v,c'} \in \mathbb{C}^{M_v \times 1}$ where the TX data stream vector, the number of TX streams and the precoder matrix are equal to $\mathbf{x}_{v,c'}$, $Q_{\mathrm{v},c'}$ and $\mathbf{G}_{v,c'}$, respectively. The total number of transmitted data streams at subcarrier c is denoted with $S = \sum_{u=1}^{U} Q_{\mathrm{u},c}$.

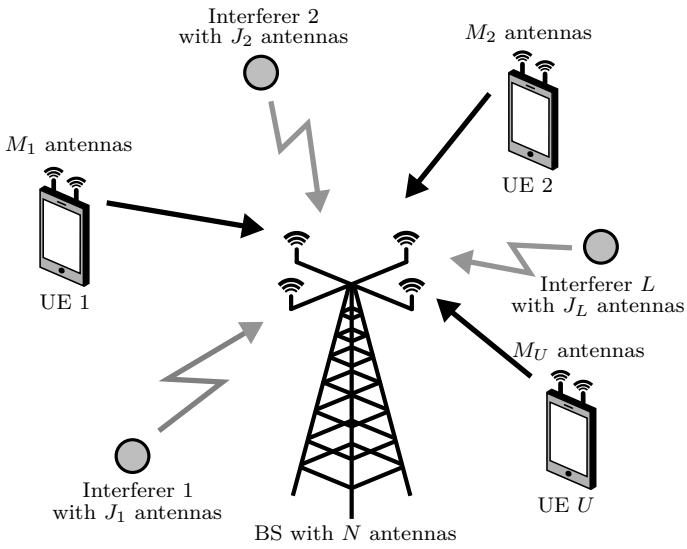

Figure 4.1: Illustration of the considered MU-MIMO scenario with external interferers. All devices in the figure are active simultaneously at subcarrier c. Further UE multiplexing takes place in frequency domain which, however, is not illustrated here for clarity.

Based on the formulation of TX I/Q imbalance in (2.12), the transmitted signal vector of a single UE u at subcarrier c under TX I/Q imbalance can be expressed as [P6–P8]

$$\mathbf{s}_{\mathrm{Txi},u,c} = \mathbf{K}_{\mathrm{Tx1},u,c}\mathbf{s}_{u,c} + \mathbf{K}_{\mathrm{Tx2},u,c}\mathbf{s}^*_{u,c'} = \mathbf{K}_{\mathrm{Tx1},u,c}\mathbf{G}_{u,c}\mathbf{x}_{u,c} + \mathbf{K}_{\mathrm{Tx2},u,c}\mathbf{G}^*_{u,c'}\mathbf{x}^*_{u,c'} \quad (4.2)$$

where the UE and subcarrier specific diagonal TX I/Q imbalance matrices $\mathbf{K}_{\mathrm{Tx1},u,c}$ and $\mathbf{K}_{\mathrm{Tx2},u,c}$, both $\in \mathbb{C}^{M_u \times M_u}$, are given by [P6–P8]

$$\begin{aligned} \mathbf{K}_{\mathrm{Tx1},u,c} &= \mathrm{diag}(K_{\mathrm{Tx1},1,u,c}, \cdots, K_{\mathrm{Tx1},M_u,u,c}), \\ \mathbf{K}_{\mathrm{Tx2},u,c} &= \mathrm{diag}(K_{\mathrm{Tx2},1,u,c}, \cdots, K_{\mathrm{Tx2},M_u,u,c}). \end{aligned} \quad (4.3)$$

When subcarriers c and c' are both allocated to a single UE, the transmitted signal is distorted due to the mirror interference discussed in Section 2.2.1. However, in the OFDMA scheme where the UEs are multiplexed to different subcarriers, subcarrier c' is not necessarily allocated to UE u. Thus the second term in (4.2) is equal to zero and no mirror interference is generated. Nevertheless, if subcarrier c' is allocated to another UE v, its effective transmitted signal at subcarrier c is equal to $\mathbf{s}_{\mathrm{Txi},v,c} = \mathbf{K}_{\mathrm{Tx2},v,c}\mathbf{s}^*_{v,c'} = \mathbf{K}_{\mathrm{Tx2},v,c}\mathbf{G}^*_{v,c'}\mathbf{x}^*_{v,c'}$. Consequently, TX I/Q imbalance causes interference between the UEs at mirror subcarrier pairs when inspecting from the RX point of view.

Spatially and frequency multiplexed uplink signals propagate through the wireless channels and are eventually received in the BS. Taking into account that I/Q imbalance occurs also in the BS RX electronics, the received signal $\mathbf{r}_{\mathrm{TxRxi},c} \in \mathbb{C}^{N\times 1}$ under joint

TX+RX I/Q imbalances is given by [P6–P8]

$$\begin{aligned}\mathbf{r}_{\mathrm{TxRxi},c} &= \mathbf{K}_{\mathrm{Rx1},c}\mathbf{r}_{\mathrm{Txi},c} + \mathbf{K}_{\mathrm{Rx2},c}\mathbf{r}^{*}_{\mathrm{Txi},c'} \\ &= \sum_{u=1}^{U} \widetilde{\mathbf{\Psi}}_{u,c}\mathbf{G}_{u,c}\mathbf{x}_{u,c} + \sum_{v=1}^{V} \widetilde{\mathbf{\Omega}}_{v,c}\mathbf{G}^{*}_{v,c'}\mathbf{x}^{*}_{v,c'} + \mathbf{K}_{\mathrm{Rx1},c}\mathbf{z}_{c} + \mathbf{K}_{\mathrm{Rx2},c}\mathbf{z}^{*}_{c'}.\end{aligned} \tag{4.4}$$

Here, perfect time and frequency synchronization is assumed between the BS RX and UE TXs. The subcarrier specific diagonal RX I/Q imbalance matrices $\mathbf{K}_{\mathrm{Rx1},c}$ and $\mathbf{K}_{\mathrm{Rx2},c}$, both $\in \mathbb{C}^{N\times N}$, are of the form [P6–P8]

$$\begin{aligned}\mathbf{K}_{\mathrm{Rx1},c} &= \mathrm{diag}(K_{\mathrm{Rx1},1,c}, \cdots, K_{\mathrm{Rx1},N,c}), \\ \mathbf{K}_{\mathrm{Rx2},c} &= \mathrm{diag}(K_{\mathrm{Rx2},1,c}, \cdots, K_{\mathrm{Rx2},N,c}).\end{aligned} \tag{4.5}$$

In addition, the effective channel matrices $\widetilde{\mathbf{\Psi}}_{u,c} \in \mathbb{C}^{N\times M_u}$ and $\widetilde{\mathbf{\Omega}}_{v,c} \in \mathbb{C}^{N\times M_v}$ including the aggregate effects of the wireless channels as well as of TX+RX I/Q imbalances are given by [P6–P8]

$$\begin{aligned}\widetilde{\mathbf{\Psi}}_{u,c} &= \begin{bmatrix}\mathbf{K}_{\mathrm{Rx1},c} & \mathbf{K}_{\mathrm{Rx2},c}\end{bmatrix} \begin{bmatrix}\mathbf{H}_{u,c} & \mathbf{0} \\ \mathbf{0} & \mathbf{H}^{*}_{u,c'}\end{bmatrix} \begin{bmatrix}\mathbf{K}_{\mathrm{Tx1},u,c} \\ \mathbf{K}^{*}_{\mathrm{Tx2},u,c'}\end{bmatrix}, \\ \widetilde{\mathbf{\Omega}}_{v,c} &= \begin{bmatrix}\mathbf{K}_{\mathrm{Rx1},c} & \mathbf{K}_{\mathrm{Rx2},c}\end{bmatrix} \begin{bmatrix}\mathbf{H}_{v,c} & \mathbf{0} \\ \mathbf{0} & \mathbf{H}^{*}_{v,c'}\end{bmatrix} \begin{bmatrix}\mathbf{K}_{\mathrm{Tx2},v,c} \\ \mathbf{K}^{*}_{\mathrm{Tx1},v,c'}\end{bmatrix}\end{aligned} \tag{4.6}$$

where $\mathbf{H}_{u,c} \in \mathbb{C}^{N\times M_u}$ and $\mathbf{H}_{v,c} \in \mathbb{C}^{N\times M_v}$ present the wireless channels of UEs u and v at subcarrier c. Due to the OFDM signal structure, the channel matrices are assumed to be constants within each narrowband subcarrier. Finally, the external interference plus noise vector $\mathbf{z}_c \in \mathbb{C}^{N\times 1}$ at subcarrier c is equal to [P6–P8]

$$\mathbf{z}_c = \sum_{l=1}^{L} \mathbf{H}_{\mathrm{int},l,c}\mathbf{s}_{\mathrm{int},l,c} + \mathbf{n}_c. \tag{4.7}$$

Here, $\mathbf{H}_{\mathrm{int},l,c} \in \mathbb{C}^{N\times J_l}$ denotes the wireless channel matrix between the l^{th} interferer and the BS. Additionally, $\mathbf{s}_{\mathrm{int},l,c} \in \mathbb{C}^{J_l\times 1}$ presents the interference signal of the same interferer. Note that we assume neither synchronization between the non-collaborative interferers and the BS nor any specific waveform for the interference. Consequently, $\mathbf{s}_{\mathrm{int},l,c}$ is the result of the interference after the RX FFT processing and can be modeled, e.g., as white Gaussian noise. However, the external interference has a spatial response through channel $\mathbf{H}_{\mathrm{int},l,c}$, which is a key element for the interference mitigation. In contrast to the interference, the RX noise vector $\mathbf{n}_c \in \mathbb{C}^{N\times 1}$ is modeled as additive Gaussian noise without any spatial response. The elements of $\mathbf{n}_c$ are assumed to be complex circular and mutually uncorrelated.

When analyzing the signal distortion visible in (4.4), we note that the received signal consists of four different terms. The first sum term includes the contribution of all UEs allocated to subcarrier c and their signals are to be separated in the BS through the spatial RX processing. The second sum term, in turn, includes the effects of mirror UEs at the mirror subcarrier whose signals leak to subcarrier c due to TX

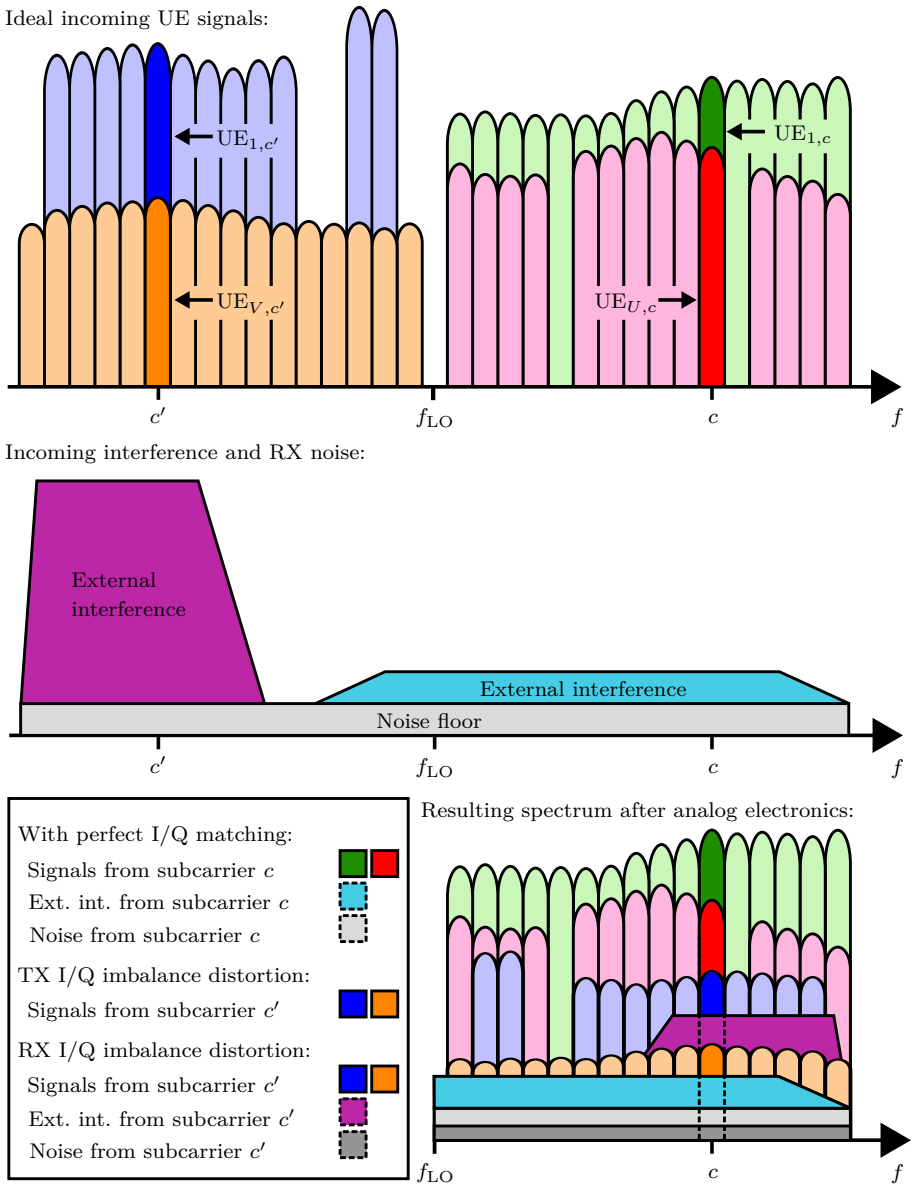

Figure 4.2: Spectral illustration of the received MU-MIMO OFDMA signal under TX and RX I/Q imbalances.

and RX I/Q imbalance, and thus cause inter-user interference between the UEs at the mirror subcarrier pairs. The third term consists of the inevitable co-channel external interference as well as the RX noise. Practically, their effects and especially the effects of strong interferers are to be suppressed in the BS by multiantenna spatial processing. Finally, the fourth term present the interference and noise leaking from the mirror

subcarrier due to RX I/Q imbalance only whereas TX I/Q imbalance is not involved at all in this phenomenon. A detailed frequency domain illustration of the received signal is given in Fig. 4.2 where the behavior of different signal terms is clearly visible. Note that the provided signal model reduces to a setup with TX only I/Q imbalance when substituting $\mathbf{K}_{\mathrm{Rx1},c} = \mathbf{I}$ and $\mathbf{K}_{\mathrm{Rx2},c} = \mathbf{0}$ for all c. Similarly, the case with RX only I/Q imbalance is obtained by substituting $\mathbf{K}_{\mathrm{Tx1},i,j} = \mathbf{I}$ and $\mathbf{K}_{\mathrm{Tx2},i,j} = \mathbf{0}$ for all $i \in \{u, v\}$ and $j \in \{c, c'\}$.

The highly flexible signal model provided in (4.4) enables the use of separate I/Q imbalance parameters for each transceiver branch. Therefore, the model is applicable also for increasingly popular remote radio unit implementations where the RF front-ends locate in a close proximity of the BS antennas and are thus distributed in space while the baseband processing is carried out in a centralized manner. In addition, the I/Q imbalance parameters can be set separately for each subcarrier, which, in turn, makes it possible to model frequency-selective I/Q imbalance in wideband systems. The model addresses also the presence of co-channel external interferers, a scenario which might happen in heterogeneous networks where, e.g., UEs at the edge of a macro cell strongly interfere with the reception in a neighboring femto cell.

4.3 Augmented Subcarrier Processing in Multiantenna BS RXs

In Chapter 3, we focused on multiantenna processing performing beamforming in narrowband systems. In contrast, now the focus is on multicarrier type of signals where each subcarrier channel is considered to be narrowband but the whole signal band is, indeed, much wider and has frequency dependent channel characteristics due to multipath propagation. Consequently, in the following, we exploit the spatial processing principle where the response for a single spatial direction is replaced with a generic channel response. Starting with conventional multiantenna-based spatial RX processing, the combiner output signal vector $\mathbf{y}_c \in \mathbb{C}^{S\times 1}$ at subcarrier c can be expressed as [P6–P8]

$$\mathbf{y}_c = \mathbf{W}_c^{\mathrm{H}}\mathbf{r}_c = \sum_{u=1}^{U} \mathbf{W}_c^{\mathrm{H}}\mathbf{H}_{u,c}\mathbf{G}_{u,c}\mathbf{x}_{u,c} + \mathbf{W}_c^{\mathrm{H}}\mathbf{z}_c \tag{4.8}$$

where $\mathbf{W}_c = [\mathbf{w}_{1,1,c}, \ldots, \mathbf{w}_{Q_U,U,c}] \in \mathbb{C}^{N\times S}$ denotes the combiner weight matrix and includes an individual column for each data stream to be separated. In addition, the received signal under ideal I/Q balance is equal to $\mathbf{r}_c = \sum_{u=1}^{U} \mathbf{H}_{u,c}\mathbf{G}_{u,c}\mathbf{x}_{u,c} + \mathbf{z}_c \in \mathbb{C}^{N\times 1}$. However, under TX+RX I/Q imbalances the received signal is distorted as seen in (4.4) and the combiner output $\mathbf{y}_{\mathrm{TxRxi},c} \in \mathbb{C}^{S\times 1}$ at subcarrier c gets a form of [P6–P8]

$$\begin{aligned}\mathbf{y}_{\mathrm{TxRxi},c} &= \mathbf{W}_c^{\mathrm{H}}\mathbf{r}_{\mathrm{TxRxi},c} \\ &= \sum_{u=1}^{U} \mathbf{W}_c^{\mathrm{H}}\widetilde{\mathbf{\Psi}}_{u,c}\mathbf{G}_{u,c}\mathbf{x}_{u,c} + \sum_{v=1}^{V} \mathbf{W}_c^{\mathrm{H}}\widetilde{\mathbf{\Omega}}_{v,c}\mathbf{G}^*_{v,c'}\mathbf{x}^*_{v,c'} \\ &\quad + \mathbf{W}_c^{\mathrm{H}}\mathbf{K}_{\mathrm{Rx1},c}\mathbf{z}_c + \mathbf{W}_c^{\mathrm{H}}\mathbf{K}_{\mathrm{Rx2},c}\mathbf{z}^*_{c'}.\end{aligned} \tag{4.9}$$

No matter how the weight matrix is optimized, the most essential aim of the combining process is to separate all S transmitted data streams from U UEs while suppressing the effects of the interference and noise. However, under TX and RX I/Q imbalances the task is more challenging than usual since the imperfections generate additional interference terms as visible in (4.9). That is, the inter-user interference as well as the external interference and noise, all originating from the mirror subcarrier, leak to subcarrier c. This results in a situation where the degrees of freedom of plain linear processing techniques run out easily. This issue is even emphasized when the number of UEs, data streams or external interferers is increased.

In the following, due to the challenges of linear methods under I/Q imbalance and based on the observations made in studies regarding I/Q imbalance in OFDM-based systems, we concentrate on the augmented subcarrier processing principle. Although it is utilized in various ways for signal processing under I/Q imbalance in the literature, augmented processing has not been investigated in the MU context where the UEs are multiplexed spatially. In addition, none of the studies in the literature include external interference to the signal models or to performance evaluations. Therefore, our focus is on a very generic MU-MIMO setup where we combine the extended uplink signal model introduced in Section 4.2 and the augmented subcarrier processing discussed in the SU-SISO context in Section 4.1. In this way, we can model and evaluate the performance of OFDM-based systems under frequency selective TX and RX I/Q imbalances while varying the number of spatially multiplexed UEs and their transmitted data streams, the number of TX and RX antennas as well as the influence of external interferers.

The augmented BS RX processing is depicted in Fig. 4.3. The BS has N parallel antenna branches, which are followed by the associated RF front-ends. After the parallel ADCs, the antenna signals go through the CP removal and FFT processing. Note that all these processing blocks are the same for both the conventional per-subcarrier and the augmented subcarrier processing. The difference is seen after the FFTs where an augmented combiner processes mirror subcarrier signals jointly. That is, signals at subcarrier c, i.e. $\mathbf{r}_c$, are combined with their counterparts at the mirror subcarrier, i.e. $\mathbf{r}_{c'}$, but the vectors are processed by different weights. We denote the weights for data stream q of UE u by $\mathbf{w}_{\mathrm{A},q,u,c} \in \mathbb{C}^{N\times 1}$ and $\mathbf{w}_{\mathrm{B},q,u,c'} \in \mathbb{C}^{N\times 1}$, and stack them into the augmented weight vector $\mathbf{w}_{q,u,c} = [\mathbf{w}_{\mathrm{A},q,u,c}^{\mathrm{T}}, \mathbf{w}_{\mathrm{B},q,u,c'}^{\mathrm{T}}]^{\mathrm{T}} \in \mathbb{C}^{2N\times 1}$. Under TX+RX I/Q imbalances this results in the combiner output signal $\widetilde{\mathbf{y}}_{\mathrm{TxRxi},c} \in \mathbb{C}^{S\times 1}$ equal to [P6–P8]

$$\begin{aligned}\widetilde{\mathbf{y}}_{\mathrm{TxRxi},c} &= \widetilde{\mathbf{W}}_c^{\mathrm{H}} \widetilde{\mathbf{r}}_{\mathrm{TxRxi},c} \\ &= \sum_{u=1}^{U} \widetilde{\mathbf{W}}_c^{\mathrm{H}} \widetilde{\boldsymbol{\Xi}}_{u,c} \mathbf{G}_{u,c} \mathbf{x}_{u,c} + \sum_{v=1}^{V} \widetilde{\mathbf{W}}_c^{\mathrm{H}} \widetilde{\boldsymbol{\Phi}}_{v,c} \mathbf{G}_{v,c'}^{*} \mathbf{x}_{v,c'}^{*} \\ &\quad + \widetilde{\mathbf{W}}_c^{\mathrm{H}} \widetilde{\mathbf{K}}_{\mathrm{RxA},c} \mathbf{z}_c + \widetilde{\mathbf{W}}_c^{\mathrm{H}} \widetilde{\mathbf{K}}_{\mathrm{RxB},c} \mathbf{z}_{c'}^{*}\end{aligned} \tag{4.10}$$

where $\widetilde{\mathbf{W}}_c = [\widetilde{\mathbf{w}}_{1,1,c}, \cdots, \widetilde{\mathbf{w}}_{Q_U,U,c}] \in \mathbb{C}^{2N\times S}$ is the augmented weight matrix and $\widetilde{\mathbf{r}}_{\mathrm{TxRxi},c} = \left[\mathbf{r}_{\mathrm{TxRxi},c}^{\mathrm{T}}, \mathbf{r}_{\mathrm{TxRxi},c'}^{\mathrm{H}}\right] \in \mathbb{C}^{2N\times 1}$ denotes the augmented signal vector under TX+RX I/Q imbalances. The augmented effective channel matrices $\widetilde{\boldsymbol{\Xi}}_{u,c} \in \mathbb{C}^{2N\times M_u}$

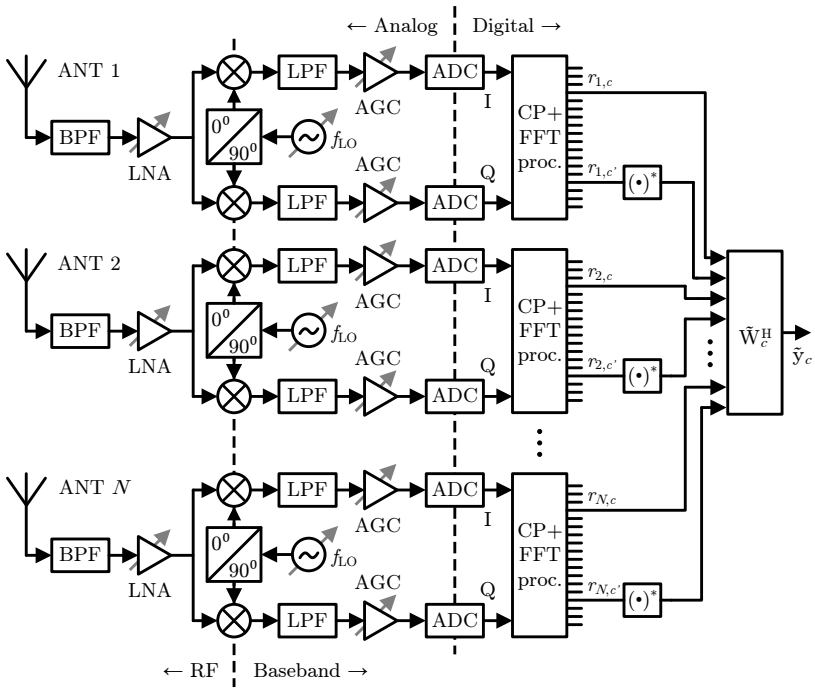

Figure 4.3: Illustration of multiple parallel RF front-ends and the augmented RX processing in MU-MIMO systems utilizing OFDMA waveforms.

and $\widetilde{\mathbf{\Phi}}_{v,c} \in \mathbb{C}^{2N \times M_v}$ are, in turn, given by [P6–P8]

$$\begin{aligned} \widetilde{\mathbf{\Xi}}_{u,c} &= \begin{bmatrix} \mathbf{K}_{\mathrm{Rx1},c} & \mathbf{K}_{\mathrm{Rx2},c} \\ \mathbf{K}^*_{\mathrm{Rx2},c'} & \mathbf{K}^*_{\mathrm{Rx1},c'} \end{bmatrix} \begin{bmatrix} \mathbf{H}_{u,c} & \mathbf{0} \\ \mathbf{0} & \mathbf{H}^*_{u,c'} \end{bmatrix} \begin{bmatrix} \mathbf{K}_{\mathrm{Tx1},u,c} \\ \mathbf{K}^*_{\mathrm{Tx2},u,c'} \end{bmatrix}, \\ \widetilde{\mathbf{\Phi}}_{v,c} &= \begin{bmatrix} \mathbf{K}_{\mathrm{Rx1},c} & \mathbf{K}_{\mathrm{Rx2},c} \\ \mathbf{K}^*_{\mathrm{Rx2},c'} & \mathbf{K}^*_{\mathrm{Rx1},c'} \end{bmatrix} \begin{bmatrix} \mathbf{H}_{v,c} & \mathbf{0} \\ \mathbf{0} & \mathbf{H}^*_{v,c'} \end{bmatrix} \begin{bmatrix} \mathbf{K}_{\mathrm{Tx2},v,c} \\ \mathbf{K}^*_{\mathrm{Tx1},v,c'} \end{bmatrix}. \end{aligned} \tag{4.11}$$

In addition, the augmented RX I/Q imbalance matrices $\mathbf{K}_{\mathrm{RxA},c}$ and $\mathbf{K}_{\mathrm{RxB},c}$, both $\in \mathbb{C}^{2N \times N}$, are expressed as [P6–P8]

$$\widetilde{\mathbf{K}}_{\mathrm{RxA},c} = \begin{bmatrix} \mathbf{K}_{\mathrm{Rx1},c} \\ \mathbf{K}^*_{\mathrm{Rx2},c'} \end{bmatrix}, \qquad \widetilde{\mathbf{K}}_{\mathrm{RxB},c} = \begin{bmatrix} \mathbf{K}_{\mathrm{Rx2},c} \\ \mathbf{K}^*_{\mathrm{Rx1},c'} \end{bmatrix}. \tag{4.12}$$

The formulation in (4.10) looks very similar to the output of the per-subcarrier processing in (4.9). In fact, the differences are only in the effective channel matrices and the combining weights. However, it is important to notice that the augmented processing method has significantly more degrees of freedom to separate the desired data streams while suppressing the interference and noise terms. Moreover, the augmented method has a built-in capability for exploiting information regarding the channel and I/Q imbalance parameters at the mirror subcarrier. Whereas this brings additional costs in terms of the

computational complexity in DSP, the costly RF branches and FFT processing blocks are the same as in the per-subcarrier method. Practical aspects, such as computational complexity, are discussed in detail in Section 4.6.

So far, the combining weights have been considered as arbitrary coefficients whereas their optimization has not been addressed yet. In practice, the optimization is based on information about the effective channels, which is, in turn, estimated in the BS RX with the help of uplink pilot or training signals transmitted by the UEs. The pilots propagate through the TX and RX RF front-ends as well as over the air, and consequently the channel estimates include, indeed, the joint effects of the RF imperfections and the wireless channels. It is also important to note that the uplink channels cannot be estimated accurately based on the downlink-uplink channel reciprocity since although the wireless channel might be reciprocal, RF imperfections in the TXs and RXs are, in general, unequal.

The actual estimation algorithms are based either on adaptive or statistical techniques. In the following, we exemplify the augmented processing principle with the Wiener filter, which provides the optimal linear solution for the augmented signal model in the MMSE sense. The algorithm is based on the statistical variables, namely the covariance matrix of the received signal and the cross-correlation vector between the received signal and transmitted pilots. Whereas such information might be hard to gather in practice, Wiener filter can be approximated by adaptive methods such as the LMS, NLMS and RLS algorithms as discussed in [P5, P8] and illustrated later with numerical examples in Section 4.6. However, here we prefer the augmented Wiener algorithm because it provides performance bounds in terms of the MMSE, and thus can clearly demonstrate the benefits of the augmented processing principle.

Under TX+RX I/Q imbalances, the mathematical formulation for the weight matrix $\widetilde{\mathbf{W}}_{\mathrm{TxRxi},c}^{\mathrm{LMMSE}} = [\widetilde{\mathbf{w}}_{1,1,c}^{\mathrm{LMMSE}}, \ldots, \widetilde{\mathbf{w}}_{Q_U,U,c}^{\mathrm{LMMSE}}] \in \mathbb{C}^{2N \times S}$ following the Wiener principle is given by [P7–P8]

$$\widetilde{\mathbf{W}}_{\mathrm{TxRxi},c}^{\mathrm{LMMSE}} = \widetilde{\mathbf{R}}_{\mathrm{TxRxi},c}^{-1} \widetilde{\mathbf{V}}_{\mathrm{TxRxi},c} \tag{4.13}$$

where $\widetilde{\mathbf{R}}_{\mathrm{TxRxi},c} = \mathbb{E}\left[\widetilde{\mathbf{r}}_{\mathrm{TxRxi},c} \widetilde{\mathbf{r}}_{\mathrm{TxRxi},c}^{\mathrm{H}}\right] \in \mathbb{C}^{2N \times 2N}$ is the augmented covariance matrix given in detail in the next section. Moreover, $\widetilde{\mathbf{V}}_{\mathrm{TxRxi},c} = [\widetilde{\mathbf{v}}_{\mathrm{TxRxi},1,1,c}, \cdots, \widetilde{\mathbf{v}}_{\mathrm{TxRxi},Q_U,U,c}] \in \mathbb{C}^{2N \times S}$ denotes the augmented cross-correlation matrix whose columns are of the form [P7–P8]

$$\widetilde{\mathbf{v}}_{\mathrm{TxRxi},q,u,c} = \mathbb{E}\left[\widetilde{\mathbf{r}}_{\mathrm{TxRxi},c} x_{q,u,c}^{*}\right] = \sigma_{x,u,c}^{2} \widetilde{\boldsymbol{\Xi}}_{u,c} \mathbf{G}_{u,c} \mathbf{e}_q. \tag{4.14}$$

Here $x_{q,u,c}$ is the known transmitted data stream and $\sigma_{x,u,c}^2 = \mathbb{E}[|x_{u,c}\|^2]$ denotes the TX power of a single data stream of UE u at subcarrier c.

The solution given in (4.13) can effectively suppress the inter-stream interference, inter-user interference, as well as the external interference, all at subcarrier c, in the optimal MMSE sense. What is even more interesting, however, is that it can suppress also the corresponding interference components, which are leaking from the mirror subcarrier due to TX+RX I/Q imbalances. This is a clear difference when compared to the classical per-subcarrier processing methods as illustrated in Section 4.5 with numerical examples. In fact, the augmented processing can be expected to gain increasing interest in future

heterogeneous MU-MIMO networks where the capability of interference suppression is one of the key issues.

4.4 Combiner Output SINR

In order to quantify the performance of the augmented combiners, we next formulate the instantaneous per-data-stream SINR. It includes the effects of the TX and RX devices, wireless propagation channel as well as the augmented BS RX processing with given, yet arbitrary combining weights, i.e., the provided SINR is independent of the weight optimization algorithm.

Since the SINR is a ratio of powers, we concentrate first on the power of a single data stream at the combiner output. The total output power of an arbitrary data stream q of UE u at subcarrier c can be expressed as [P8]

$$\widetilde{P}_{q,u,c} = \mathbb{E}\left[|\widetilde{y}_{\mathrm{TxRxi},q,u,c}|^2\right] = \widetilde{\mathbf{w}}_{q,u,c}^{\mathrm{H}} \widetilde{\mathbf{R}}_{\mathrm{TxRxi},c} \widetilde{\mathbf{w}}_{q,u,c} \tag{4.15}$$

where $\widetilde{\mathbf{w}}_{q,u,c}$ refers to the augmented combining weights of the corresponding data stream. In addition, the augmented covariance matrix $\widetilde{\mathbf{R}}_{\mathrm{TxRxi},c} \in \mathbb{C}^{2N \times 2N}$ is equal to [P8]

$$\begin{aligned} \widetilde{\mathbf{R}}_{\mathrm{TxRxi},c} &= \mathbb{E}\left[\widetilde{\mathbf{r}}_{\mathrm{TxRxi},c} \widetilde{\mathbf{r}}_{\mathrm{TxRxi},c}^{\mathrm{H}}\right] \\ &= \sum_{u=1}^{U} \sigma_{\mathrm{x},u,c}^2 \widetilde{\boldsymbol{\Xi}}_{u,c} \mathbf{G}_{u,c} \mathbf{G}_{u,c}^{\mathrm{H}} \widetilde{\boldsymbol{\Xi}}_{u,c}^{\mathrm{H}} + \sum_{v=1}^{V} \sigma_{\mathrm{x},v,c'}^2 \widetilde{\boldsymbol{\Phi}}_{v,c} \mathbf{G}_{v,c'}^{*} \mathbf{G}_{v,c'}^{\mathrm{T}} \widetilde{\boldsymbol{\Phi}}_{v,c}^{\mathrm{H}} \\ &\quad + \widetilde{\mathbf{K}}_{\mathrm{RxA},c} \mathbf{R}_{\mathrm{z},c} \widetilde{\mathbf{K}}_{\mathrm{RxA},c}^{\mathrm{H}} + \widetilde{\mathbf{K}}_{\mathrm{RxB},c} \mathbf{R}_{\mathrm{z},c'}^{*} \widetilde{\mathbf{K}}_{\mathrm{RxB},c}^{\mathrm{H}}. \end{aligned} \tag{4.16}$$

Here, $\sigma_{\mathrm{x},u,c}^2 = \mathbb{E}[|x_{u,c}|^2]$ and $\sigma_{\mathrm{x},v,c'}^2 = \mathbb{E}[|x_{v,c'}|^2]$ denote the TX power of a single data stream of UE u and UE v, respectively. Furthermore, $\mathbf{R}_{\mathrm{z},c} \in \mathbb{C}^{N \times N}$ is the covariance matrix of the external interference and noise and is equal to [P8]

$$\mathbf{R}_{\mathrm{z},c} = \mathbb{E}\left[\mathbf{z}_c \mathbf{z}_c^{\mathrm{H}}\right] = \sum_{l=1}^{L} \sigma_{\mathrm{int},l,c}^2 \mathbf{H}_{\mathrm{int},l,c} \mathbf{H}_{\mathrm{int},l,c}^{\mathrm{H}} + \sigma_{\mathrm{n},c}^2 \mathbf{I} \tag{4.17}$$

where $\sigma_{\mathrm{int},l,c}^2$ and $\sigma_{\mathrm{n},c}^2$ refer to the power of the l^{th} external interferer and to the additional RX noise, respectively, both at subcarrier c. The first sum term in (4.16) corresponds to the UEs at subcarrier c whereas the second sum term is caused by the leakage of the mirror UE signals. The third term, in turn, is generated due to the external interference and noise at subcarrier c while the last term represents the corresponding impact originating from the mirror subcarrier. Note that, the covariance matrix with the conventional per-subcarrier combiner is given as the top-left quadrant of (4.16).

The total per-data-stream power is next split to useful signal and interference and noise terms as follows [P8]

$$\widetilde{P}_{q,u,c} = \widetilde{P}_{x,q,u,c} + \widetilde{P}_{\mathrm{ISI},q,u,c} + \widetilde{P}_{\mathrm{IUI},u,c} + \widetilde{P}_{\mathrm{IUI},c'} + \widetilde{P}_{\mathrm{z},c} + \widetilde{P}_{\mathrm{z},c'}. \tag{4.18}$$

Here, $\widetilde{P}_{x,q,u,c}$ represents the output power of the desired data stream q and $\widetilde{P}_{\mathrm{ISI},q,u,c}$ denotes the effect of the inter-stream interference originating from the other streams

of the same UE. Both of these terms are originating from UE u, but they need to be separated in the analysis because when examining the received signal from an individual but arbitrary stream q of UE u point of view, the other streams of the same UE are treated as interference. Furthermore, $\widetilde{P}_{\mathrm{IUI},u,c}$ and $\widetilde{P}_{\mathrm{IUI},u,c'}$ denote the inter-user interference from subcarriers c and c', respectively. Finally, $\widetilde{P}_{z,c}$ and $\widetilde{P}_{z,c'}$ are the output powers of the external interference and noise originating from subcarriers c and c', respectively. The detailed formulations for these power terms can, in turn, be given based on the signal term grouping in the augmented covariance matrix in (4.16). Additionally, we need two stream selection matrices, namely $\mathbf{\Gamma}_{q,u,c} = \mathrm{diag}(\mathbf{e}_q) \in \mathbb{R}^{Q_{u,c} \times Q_{u,c}}$ and $\mathbf{\Delta}_{q,u,c} = \mathbf{I} - \mathbf{\Gamma}_{q,u,c} \in \mathbb{R}^{Q_{u,c} \times Q_{u,c}}$, which refer to the desired data stream q of UE u at subcarrier c, and to the interfering other data streams of the same UE, respectively. The power terms are then equal to [P8]

$$\widetilde{P}_{x,q,u,c} = \sigma^2_{\mathrm{x},u,c} \widetilde{\mathbf{w}}^{\mathrm{H}}_{q,u,c} \widetilde{\mathbf{\Xi}}_{u,c} \mathbf{G}_{u,c} \mathbf{\Gamma}_{q,u,c} \mathbf{G}^{\mathrm{H}}_{u,c} \widetilde{\mathbf{\Xi}}^{\mathrm{H}}_{u,c} \widetilde{\mathbf{w}}_{q,u,c} \tag{4.19}$$

$$\widetilde{P}_{\mathrm{ISI},q,u,c} = \sigma^2_{\mathrm{x},u,c} \widetilde{\mathbf{w}}^{\mathrm{H}}_{q,u,c} \widetilde{\mathbf{\Xi}}_{u,c} \mathbf{G}_{u,c} \mathbf{\Delta}_{q,u,c} \mathbf{G}^{\mathrm{H}}_{u,c} \widetilde{\mathbf{\Xi}}^{\mathrm{H}}_{u,c} \widetilde{\mathbf{w}}_{q,u,c} \tag{4.20}$$

$$\widetilde{P}_{\mathrm{IUI},u,c} = \sum_{i=1, i \neq u}^{U} \sigma^2_{\mathrm{x},i,c} \widetilde{\mathbf{w}}^{\mathrm{H}}_{q,u,c} \widetilde{\mathbf{\Xi}}_{i,c} \mathbf{G}_{i,c} \mathbf{G}^{\mathrm{H}}_{i,c} \widetilde{\mathbf{\Xi}}^{\mathrm{H}}_{i,c} \widetilde{\mathbf{w}}_{q,u,c} \tag{4.21}$$

$$\widetilde{P}_{\mathrm{IUI},c'} = \sum_{v=1}^{V} \sigma^2_{\mathrm{x},v,c'} \widetilde{\mathbf{w}}^{\mathrm{H}}_{q,u,c} \widetilde{\mathbf{\Phi}}_{v,c} \mathbf{G}^{*}_{v,c'} \mathbf{G}^{\mathrm{T}}_{v,c'} \widetilde{\mathbf{\Phi}}^{\mathrm{H}}_{v,c} \widetilde{\mathbf{w}}_{q,u,c} \tag{4.22}$$

$$\widetilde{P}_{\mathrm{z},c} = \widetilde{\mathbf{w}}^{\mathrm{H}}_{q,u,c} \widetilde{\mathbf{K}}_{\mathrm{RxA},c} \mathbf{R}_{\mathrm{z},c} \widetilde{\mathbf{K}}^{\mathrm{H}}_{\mathrm{RxA},c} \widetilde{\mathbf{w}}_{q,u,c} \tag{4.23}$$

$$\widetilde{P}_{\mathrm{z},c'} = \widetilde{\mathbf{w}}^{\mathrm{H}}_{q,u,c} \widetilde{\mathbf{K}}_{\mathrm{RxB},c} \mathbf{R}^{*}_{\mathrm{z},c'} \widetilde{\mathbf{K}}^{\mathrm{H}}_{\mathrm{RxB},c} \widetilde{\mathbf{w}}_{q,u,c}. \tag{4.24}$$

Finally, the instantaneous per-data-stream SINR of an augmented combiner under TX+RX I/Q imbalances can be written as [P8]

$$\widetilde{\mathrm{SINR}}_{\mathrm{TxRxi},q,u,c} = \frac{\widetilde{P}_{x,q,u,c}}{\widetilde{P}_{\mathrm{ISI},q,u,c} + \widetilde{P}_{\mathrm{IUI},u,c} + \widetilde{P}_{\mathrm{IUI},c'} + \widetilde{P}_{\mathrm{z},c} + \widetilde{P}_{\mathrm{z},c'}}. \tag{4.25}$$

The SINR given above quantifies the instantaneous performance of a single data stream after BS RX processing with given, yet arbitrary combining weights. As discussed in [P8], averaging the instantaneous SINR over the channel fading variables in the considered MU-MIMO OFDMA scenario is infeasible due to intractable algebraic representation. However, in the next section, we illustrate the expected combining performance by averaging the instantaneous SINR numerically across the fading variables and I/Q imbalance parameters as well as over all UEs and data streams through Monte-Carlo simulations.

4.5 Numerical SINR Performance

In this section, we illustrate the performance of the augmented subcarrier processing and compare it to the performance of the conventional per-subcarrier processing. The comparison is done with respect to several parameters in order to demonstrate various aspects of the considered MU-MIMO setup.

Table 4.2: Basic simulation parameters for the OFDMA setup.

Parameter	Symbol	Value
RX antennas	N	20
Number of UEs	U, V	5
TX antennas in UEs	M_u, M_v	2
Data streams in UEs	$Q_{u,c}$, $Q_{v,c'}$	2
Number of external interferers	L	8
TX antennas in external interferers	J_l	1
Signal-to-noise ratio	SNR	20 dB
Signal-to-interference ratio	SIR_c, $\mathrm{SIR}_{c'}$	-20 dB
Minimum image rejection ratio	$\mathrm{IRR}_{\min}$	25 dB

The basic simulation parameters are summarized in Table 4.2 whereas the setup is also varied in the evaluations in terms of a single parameter at a time. The considered setup consists of a BS equipped with $N = 20$ RX antennas. Subcarriers c and c' have $U = 5$ and $V = 5$ active UEs, respectively. Each UE has $M_u = M_v = 2$ TX antennas and $Q_{u,c} = Q_{v,c'} = 2$ data streams to be transmitted. Moreover, the precoding matrices $\mathbf{G}_{u,c}$ and $\mathbf{G}_{v,c'}$ are selected to be 2×2 identity matrices performing a simple one-to-one mapping between the data streams and TX antennas. The SNR is defined as the ratio between the total averaged RX power from all data streams of a single UE, and the noise power. We set SNR = 20 dB and model the RX noise with circular symmetric complex Gaussian distributed variables. Both of the considered subcarriers have $L = 8$ external interferers equipped with a single antenna. We define the signal-to-interference ratio (SIR) at a given subcarrier as the ratio between the total averaged RX power from all data streams of a single UE, and the total averaged RX power originating from all external interferers. The TX powers of all external interferers are assumed to be equal and we set $\mathrm{SIR}_c = \mathrm{SIR}_{c'} = -20$ dB. The wireless propagation channels between the TX-RX antenna pairs are independent and Rayleigh distributed. Finally, TX as well as RX I/Q imbalances are defined in terms of the minimum allowable IRR ($\mathrm{IRR}_{\min}$) which is set to 25 dB. The actual I/Q imbalance parameters for an individual transceiver branch are, in turn, selected in the following way. First, the phase imbalance coefficient is drawn from $\mathcal{U}(-\alpha, \alpha)$ so that α guarantees the selected $\mathrm{IRR}_{\min}$ if the gain imbalance was set to zero. After that, the gain imbalance coefficient is selected from the conditional distribution $\mathcal{U}(g_{\min}, g_{\max})$ where $g_{\min}$ and $g_{\max}$ correspond to the $\mathrm{IRR}_{\min}$ with the selected phase imbalance coefficient.

Fig. 4.4 depicts the per-data-stream SINR as a function of the SNR under various I/Q imbalance schemes for both the classical per-subcarrier Wiener method and the augmented Wiener method. With ideal I/Q balance both methods provide a linear increase in the SINR. From those lines we notice that the effects of the inter-user and external interference can be suppressed very effectively. In fact, the combiners are even able to suppress the additional noise since the resulting SINR is some 5 dB better than the SNR in the combiner inputs (note that the per-UE SNR in the x-axis maps to 3 dB lower per-data-stream SNR in the considered setup). However, under I/Q imbalances the SINR curves of the per-subcarrier Wiener method saturate. TX I/Q imbalance results in the SINR saturation to a level of 25 dB. Since TX I/Q imbalance does not

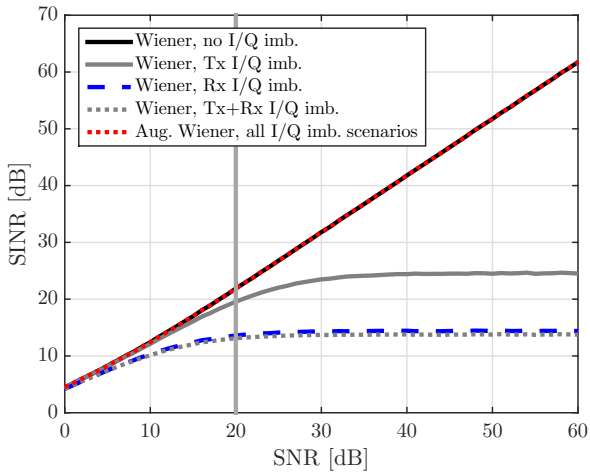

Figure 4.4: Average SINR as a function of the SNR for the MU-MIMO OFDMA scenario. The gray vertical line shows the operation point matching the parameters given in Table 4.2.

affect the external interference and noise in the mirror subcarrier, the SINR degradation is here purely caused by the mirroring effect in the UE TXs. RX I/Q imbalance, in turn, degrades the SINR even more due to the leakage of the inter-user and external interference originating from the mirror subcarrier. The worst performance is seen with TX+RX I/Q imbalances, which yield the saturated SINR to be slightly worse than under RX I/Q imbalance only. When considering the augmented subcarrier processing, the results are much better. With that method the SINR is not dependent on the considered I/Q imbalance scenario. Consequently, it provides the SINR equal to the one under ideal I/Q balance, even when being under TX+RX I/Q imbalances and in the challenging MU-MIMO OFDMA scenario.

The SINR behavior under the same setup is further illustrated in Fig. 4.5 as a function of the SIR at subcarriers c and c'. The first thing to notice is that the SINR saturates at the low and high SIRs in all cases. In the high SIR region, the effects of the external interference are basically negligible and the performance is limited by the data stream and UE separation capabilities of the combiners. Naturally, the ideal I/Q balance yields the best SINR among the considered cases whereas TX or RX I/Q imbalance with the per-subcarrier combiner result to some 2 dB lower SINR. The worst SINR is again obtained under TX+RX I/Q imbalances due to the highest levels of the inter-user and inter-stream interferences. As the SIR decreases, the effects of the external interference become more dominant. Consequently, the combiners put more effort into spatial interference suppression through the spatial responses of the external interferers and the SINRs decreases. Under RX and TX+RX I/Q imbalances the case is in fact very severe. The performance is heavily affected by the external interference and the SINR drops drastically. As noticed in [P8], with additional simulations, the drop in the SINR is caused particularly by the strong external interferers at the mirror subcarrier. In fact, the per-subcarrier combiner does not have capability for handling the leaking interference, and hence the received signal gets strongly distorted. When

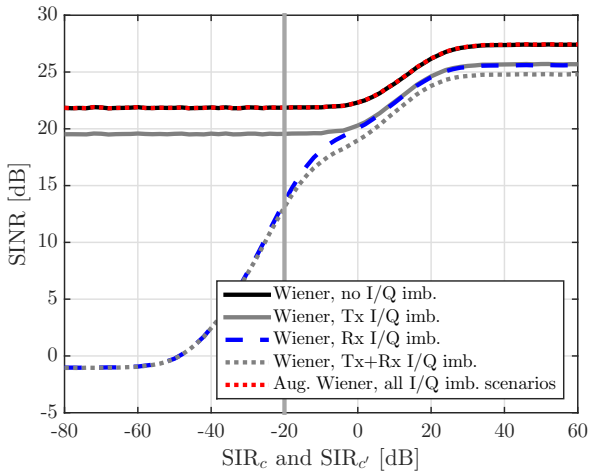

Figure 4.5: Average SINR as a function of the SIR$_c$ and SIR$_{c'}$ for the MU-MIMO OFDMA scenario. The gray vertical line shows the operation point matching the parameters given in Table 4.2.

changing to the augmented subcarrier under all I/Q imbalance cases, we notice that its performance follows that of the ideal case and the SINR decreases quickly to a saturated level of 22 dB. The SINR of the per-subcarrier combiner under TX I/Q imbalance is pretty similar to the ideal case but just with a small negative offset. The performance there is degraded, again, purely due to the mirroring in the TXs. The saturation of the SINRs in the low SIR region with all considered cases is, in fact, quite surprising. As the SIR decreases, one could expect also decreasing SINRs since the external interference becomes more dominant. However, the SINR saturation shows that the combiners can reach a stable state where they can suppress the interferers completely by nulling their response in locations that correspond to the spatial signatures of the external interferers. Unfortunately, this requires lots of resources, and consequently lots of the data stream and UE separation capabilities are sacrificed. This is particularly visible with RX I/Q imbalance where the SINR goes below 0 dB. Fig. 4.5 depicts clearly the limitations of the per-subcarrier combiner and guides us towards augmented subcarrier principle, especially in interference-limited networks.

The influence of the external interference is presented also in Fig. 4.6 where the SINR is shown as a function of the number of external interferers. In the considered scenario, the BS has $N = 20$ RX antennas, and consequently it can generate in total 20 maxima/minima to its spatial response. Assuming that each UE has $M_u = 2$ TX antennas and there are $L = 8$ external interferers nearby, the BS RX should be able to separate all data streams of $(N - L)/M_u = 6$ UE without degradations in the SINR, as long as the spatial responses do not overlap. However, as visible in the figure, the SINR decreases in all cases as the number of external interferers increases. This is explained by the built-in feature of the Wiener combiner which seeks for an optimal balance between the data stream separation and interference suppression. The worst performance among the simulated cases is obtained with the per-subcarrier Wiener

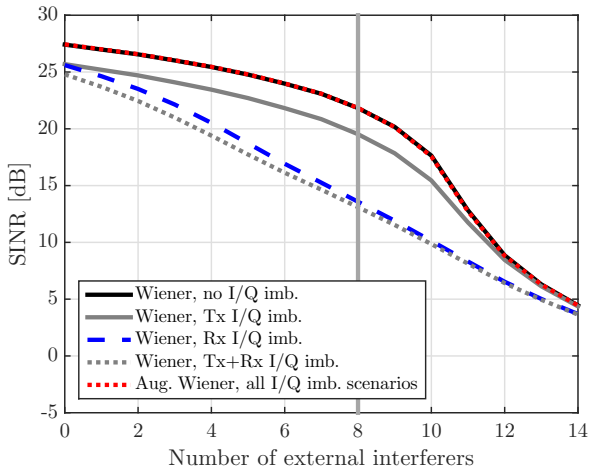

Figure 4.6: Average SINR as a function of the number of external interferers L for the MU-MIMO OFDMA scenario. The gray vertical line shows the operation point matching the parameters given in Table 4.2.

combiner when I/Q imbalance occurs in the RX electronics due to the interference leakage from the mirror subcarrier. Under TX I/Q imbalance the signal distortion is caused purely in the TX side and the resulting SINR is much better than that under RX or TX+RX I/Q imbalances. The augmented combiner under all I/Q imbalance schemes has, again, equal SINR when compared to the case under ideal I/Q balance. The results directly implicate that the augmented processing can provide clear performance improvements in terms of the external interferers as long as the number of external interferers stays on reasonable levels. When the total number of incoming signals goes beyond the number of RX antennas, all cases end up with low SINRs due to lacking degrees of freedom as expected.

The performance of the considered MU-MIMO OFDMA setup is depicted also in Fig. 4.7, which illustrates the SINR as a function of the $\mathrm{IRR}_{\mathrm{min}}$. As can be expected based on the figures above, the augmented combiner under all I/Q imbalance cases provides equal performance with the ideal I/Q balance. In such a case, the SINR behaves as a flat line since it is not dependent on the $\mathrm{IRR}_{\mathrm{min}}$. The per-subcarrier combiner, in turn, suffers when being under I/Q imbalances. TX I/Q imbalance results in visible SINR degradation when the $\mathrm{IRR}_{\mathrm{min}}$ goes under 35 dB whereas the same happen under RX or TX+RX I/Q imbalances already at $\mathrm{IRR}_{\mathrm{min}} = 45$ dB. Note that neither of those values may be reached in practice as discussed in Section 2.2.1. When considering $\mathrm{IRR}_{\mathrm{min}}$ equal to 25 dB, which is the minimum UE IRR, e.g., in the LTE/LTE-A specification [1], the SINR deterioration is some 2.5 dB under TX I/Q imbalance and roughly 9 dB under RX as well as under TX+RX I/Q imbalances. That implicates that the augmented subcarrier processing can improve the performance significantly in MU-MIMO networks, which have similar specification with the existing systems.

In addition to the MU-MIMO OFDMA setup discussed above, we evaluate the performance of the augmented subcarrier processing also in the massive MIMO framework.

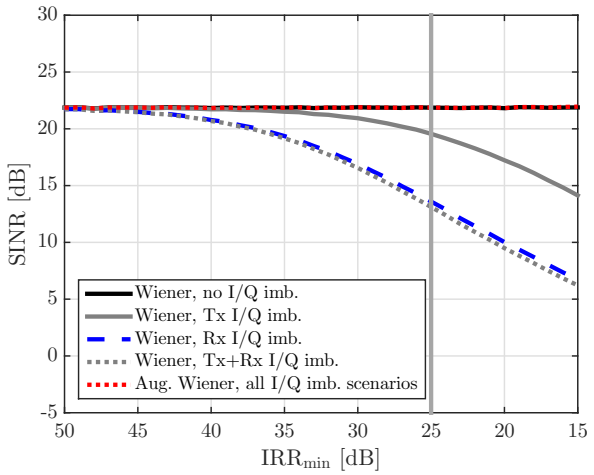

Figure 4.7: Average SINR as a function of the IRR_{min} for the MU-MIMO OFDMA scenario. The gray vertical line shows the operation point matching the parameters given in Table 4.2.

Towards that end, we modify the scenario so that the BS has now $N = 100$ RX antennas. Moreover, we no longer multiplex the UEs in frequency domain and consequently utilize only OFDM waveforms with $U = 5$ spatially multiplexed UEs. Each UE has $M_u = 1$ TX antenna transmitting a single data stream, thus enabling also the use of very simple and cost-effective UEs that are expected to be common in IoT-based networks. Due to the low-cost UEs and the vast number of RX antennas we also decrease the level of IRR to 20 dB. Furthermore, since the massive MIMO setup is often expected to be used in the mmWaves where the propagation losses are much higher than in the conventionally used frequency bands, we remove the external interferers from the setup. Parameters of the resulting massive MIMO OFDM simulation scenario are summarized in Table 4.3. Finally, since the massive MIMO systems require simplicity in the associated hardware as well as in the DSP side, we use the performance of the MRC method as a benchmark in the comparisons. In the considered setup, the MRC weight matrix is equal to $\mathbf{W}^{\text{MRC}}_{\text{TxRxi},c} = [\widetilde{\mathbf{\Psi}}_{1,c}, \ldots, \widetilde{\mathbf{\Psi}}_{U,c}] \in \mathbb{C}^{N \times U}$ [P7–P8]. Being such a simple method, MRC can adapt the RX processing weights of a single UE to the effective channel of that UE but can take into account neither the inter-user interference nor the external interference. Note also that MRC weights $\mathbf{W}^{\text{MRC}}_{\text{TxRxi},c}$ are used to process the plain linear RX signal given in (4.4), and hence they cannot process signals at the mirror subcarrier pairs jointly.

The performance of the massive MIMO setup is depicted first in Fig. 4.8 where the SINR is shown as a function of the number of RX antennas. Here, we select the maximum number of antennas to be equal to 3000 even though it won't be realistic, at least in the near future, in order to illustrate some interesting things in the SINR behavior. After reaching enough degrees of freedom, we see a linear increase equal to $10\log_{10}(N)$ in the cases with ideal I/Q balance. The per-subcarrier and the augmented subcarrier combiner are able to exploit channel information regarding the inter-user and external interference, and hence they can suppress the interference efficiently. MRC, in

Table 4.3: Basic simulation parameters for the massive MIMO OFDM setup.

Parameter	Symbol	Value
RX antennas	N	100
Number of UEs	U	5
TX antennas in UEs	M_u	1
Data streams in UEs	$Q_{u,c}$	1
Number of external interferers	L	0
Signal-to-noise ratio	SNR	20 dB
Image rejection ratio	IRR	20 dB

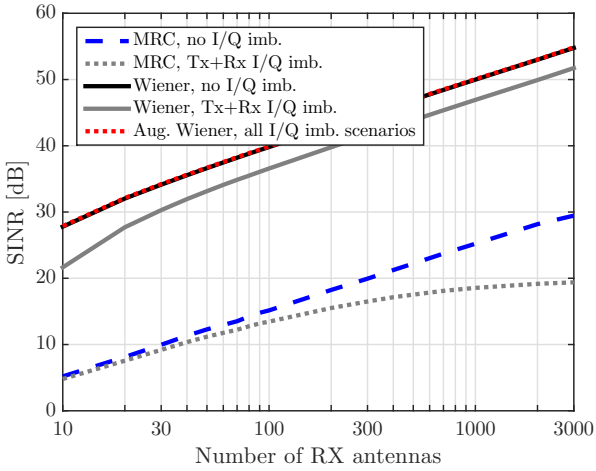

Figure 4.8: Average SINR as a function of the number of RX antennas N for the massive MIMO OFDM scenario parameterized in Table 4.3. Note the logarithmic scale on the x-axis.

turn, is not able to do that, and consequently the incoming interference causes -25 dB offset to the SINR. In practice, it means that in order to reach the same output SINR, MRC requires more than 300 times more RX antennas than Wiener combiners. When considering TX+RX I/Q imbalances, the augmented subcarrier processing provides the same SINR as with ideal I/Q balance. The per-subcarrier Wiener combiner, in turn, has 3 dB lower SINR than in the ideal case. Since now there are no external interferers, the SINR degradation is caused solely by the mirroring in the UE TXs. The SINR of MRC under TX+RX I/Q imbalances, in turn, looks very interesting. In particular, we notice that the SINR saturates to 20 dB, which is exactly the same as the TX IRR. The root of this lies in the fact that the MRC weights of UE u match to the effective channel matrix $\widetilde{\mathbf{\Psi}}_{u,c}$ which is dominated by the term $\mathbf{K}_{\mathrm{Rx1},c}\mathbf{H}_{u,c}K_{\mathrm{Tx1},u,c}$. The desired signal $x_{u,c}$ which is, indeed, propagated through $\widetilde{\mathbf{\Psi}}_{u,c}$ is hence combined in the RX in terms of the maximum ratio principle. However, now also the mirror subcarrier is allocated to the same UE and due to TX I/Q imbalance, the mirror subcarrier signal $x_{u,c'}$ leaks to subcarrier c via the effective channel $\widetilde{\mathbf{\Omega}}_{u,c}$ including a term equal to $\mathbf{K}_{\mathrm{Rx1},c}\mathbf{H}_{u,c}K_{\mathrm{Tx2},u,c}$. As a result, the only difference between those two elements in

the propagation channels is on the TX I/Q imbalance parameters. The ratio of these parameters is given by $10\log_{10}(|K_{\mathrm{Tx1},u,c}|^2/|K_{\mathrm{Tx2},u,c}|^2)$, which is exactly the same as the $\mathrm{IRR}_{\mathrm{Tx},c}$ of UE u. Summarizing the discussion above, the SINR of MRC with OFDM waveforms and under TX+RX I/Q imbalances is strictly limited to $\mathrm{IRR}_{\mathrm{Tx},c}$ even with limitless number of RX antennas. Note that our further simulations in [P7] have shown that such a phenomenon does not happen with OFDMA where subcarriers c and c' are allocated to different UEs. The phenomenon does neither occur with the Wiener combiners, as visible in Fig. 4.8, since their weights for a single UE are not matched only with the effective channel of that specific UE but optimized in terms of the overall setup including, e.g., inter-user interference.

The massive MIMO setup is finally evaluated in Fig. 4.9 showing the SINR as a function of the number of UEs U. Naturally, all cases result in decreasing SINR as the number of UEs increases. Again, MRC yields the worst SINR performance among the considered combiners and the difference between ideal I/Q balance and TX+RX I/Q imbalance schemes is small. The per-subcarrier Wiener combiner provides 10 dB–25 dB better SINR under TX+RX I/Q imbalances. The steepest SINR degradation is seen around $U = 50$ where 50 desired UE signals income to the BS RX at subcarrier c and 50 signals leak from the mirror subcarrier. In total, that results in 100 incoming signals, which match also the number of RX antennas meaning that the SINR degradation is strongly affected by lacking degrees of freedom. In contrast, the per-subcarrier Wiener combiner under ideal I/Q balance and the augmented Wiener combiner under all I/Q imbalance schemes provide fairly slow decrease in the SINR until the number of UEs approaches 100 where also their degrees of freedom are running out. The figure indisputably shows that I/Q imbalance limits the capacity of a single BS in terms of the active UEs in its coverage area. In addition, the augmented Wiener combiner provides performance equal to the case with ideal I/Q balance, and thus offers additional performance boost compared to the per-subcarrier combiners.

4.6 Notes on Practical Aspects

In this section, the focus is on practical aspects of the provided signal model and the proposed augmented subcarrier processing. In particular, we first address the assumption of perfect time and frequency synchronization and discuss the validity of the signal model and the augmented processing method with real world signals. After that we continue to adaptive weight optimization, which is based on uplink training signals, instead of assuming that statistical *a priori* information is available. Finally, we evaluate the computational complexity issues regarding the augmented subcarrier combiner.

4.6.1 Time and Frequency Synchronization

In the signal model given in (4.4), we assumed that there is a perfect time and frequency synchronization between the UE TXs and the BS RX. However, such a perfection is an unrealistic assumption since the transceivers in OFDM-based systems have, in general, small synchronization offsets. Considering first the frequency synchronization, the maximum CFO is typically relatively small. As an example, in the common LTE/LTE-A systems, the CFO of a UE needs to be within ± 0.1 PPM observed over a period of one

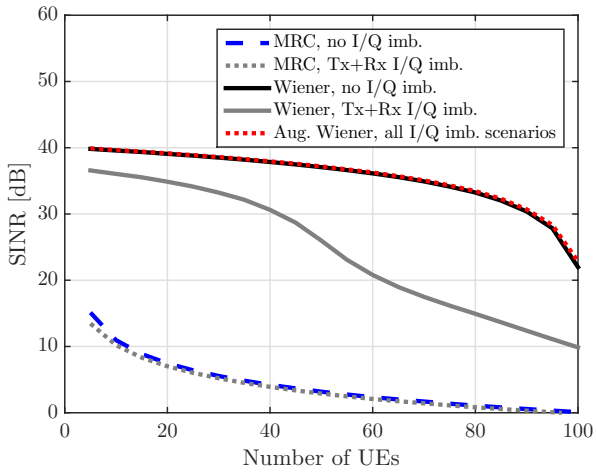

Figure 4.9: Average SINR as a function of the number of UEs U for the massive MIMO OFDM scenario parameterized in Table 4.3.

time slot (0.5 ms) compared to the carrier frequency of the BS [1, 2]. Hence, a carrier frequency of 2 GHz, as a typical example, results in the maximum CFO of ±200 Hz. That is very small relative to 15 kHz subcarrier spacing (maximum of 1.3 %) and the resulting inter-carrier and inter-user interferences are small. Additionally, according to the simplest approximation of the CFO, small offsets in the frequency synchronization map only to common phase error per UE per OFDMA symbol. Thus, they are just parts of the effective propagation channels, which are structurally processed in the BS RX. Second of all, assuming practical timing offset, i.e. being within the cyclic prefix length for all UEs, also they map to being parts of the effective frequency selective channels. Therefore, we conclude that the considered signal model and the associated signal processing methods are valid and suitable for practical signals as long as the time and frequency synchronization are within reasonable limits.

4.6.2 Adaptive Weight Optimization

Up to now, the discussion in this chapter has assumed that the combining weights are solved mainly according to the Wiener principle. Whereas the Wiener weights, that are based on statistical information such as the covariance and cross-correlation matrices, are good for illustration purposes, they may be hard to obtain in practice especially with UEs under high mobility. Therefore, we next address the weight optimization task with the data-aided adaptive NLMS algorithms described in detail in [P5]. Fig. 4.10 illustrates how the SINRs of the per-subcarrier and augmented subcarrier combiners converge under various I/Q imbalance schemes in a SU-SIMO OFDM setup with external interferers. First of all, we notice that NLMS under difference I/Q imbalance schemes reaches a performance close to that of the corresponding Wiener combiner. With ideal I/Q balance and under TX I/Q imbalance the performance of NLMS is converged already after 500 iterations whereas the SINRs under RX and TX+RX I/Q imbalances still

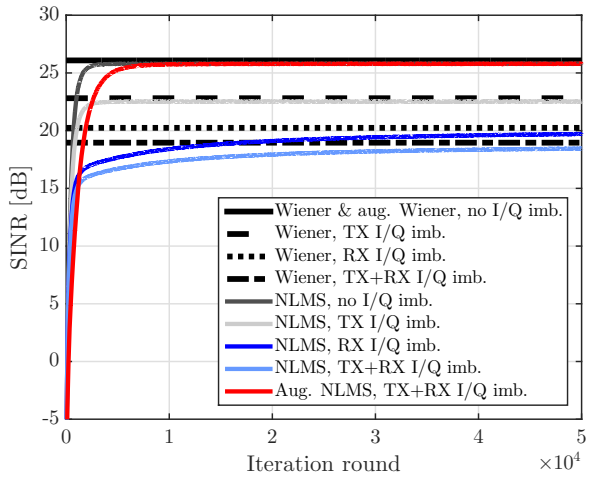

Figure 4.10: Convergence of the SINR with the NLMS and augmented NLMS methods. $N = 8$, SNR $= 20\,\text{dB}$, SIR$=-15\,\text{dB}$, $g \sim \mathcal{U}(0.9, 1.1)$, and $\phi \sim \mathcal{U}(-10^\circ, 10^\circ)$. Iterative training was based on 16-QAM symbols and the results are averaged over 500 channel and I/Q imbalance parameter realizations.

increase slowly after 50000 iterations. The augmented subcarrier NLMS, in turn, yields the SINR close to that of the per-subcarrier and augmented Wiener combiners under ideal I/Q balance. Moreover, now the convergence under TX+RX I/Q imbalances is much faster than with the per-subcarrier method under the same scheme. In fact and as further depicted in [P5], the augmented subcarrier NLMS has almost the same fast pace of convergence under all I/Q imbalance schemes, which is beneficial in cases with high mobility and quickly varying channels. We have also noticed that the SIR affects the convergence heavily through its dominance in the received signal. The higher the SIR, the slower the convergence is with all considered weight optimizing algorithms. As a summary, in terms of the performance, the Wiener combiners can be substituted with adaptive data-aided algorithms in practical BS RX implementations at the cost of only slight SINR degradations.

4.6.3 Computational Complexity

In order to evaluate the feasibility of the augmented subcarrier processing in real world transceivers, we finally focus on its features in terms of the computational complexity. We compare the complexity of the augmented subcarrier methods and compare them with the corresponding per-subcarrier methods. The comparison includes the joint effects of the channel equalization, data stream separation and I/Q imbalance mitigation. Particularly, we focus on the computational complexity of all the associated signal processing blocks, namely the FFT processing, weight optimization and digital data combining. As a complexity metric we use real-valued floating point operations (flops) and for an easy comparison between the methods, we define N_{in}, which is the total number of the parallel input samples of a combiner. For the per-subcarrier combiner

$N_{\text{in}} = N$ while for the augmented subcarrier combiner $N_{\text{in}} = 2N$ due to joint processing of the mirror subcarrier pairs.

The total per-subcarrier computational complexity of a digital combiner can be expressed as

$$\Theta_{\text{tot},c} = \frac{N}{C}\Theta_{\text{FFT}} + S\Theta_{\text{weights},c} + S\Theta_{\text{combining},c}. \tag{4.26}$$

Here, Θ_{FFT} denotes the complexity of the FFT processing in a single RX branch and with the state-of-the-art split-radix implementation it is equal to [89]

$$\Theta_{\text{FFT}} = \frac{34}{9}C\log_2 C - \frac{124}{27}C - 2\log_2 C - \frac{2}{9}(-1)^{\log_2 C}\log_2 C + \frac{16}{27}(-1)^{\log_2 C} + 8. \tag{4.27}$$

Note that in (4.26) Θ_{FFT} is multiplied with N since the FFT block is included in each of the RX chains. Moreover, it is divided by C in order to quantify the computational complexity from a single subcarrier point of view. The combining weights, in turn, are here considered to be solved with adaptive algorithms. With respect to the conventional LMS [73, p. 238] and RLS [73, p. 442] as practical examples, the computational loads of per-data-stream weight optimization in a single iteration round can be expressed as

$$\Theta^{\text{LMS}}_{\text{weights},c} = 16N_{\text{in}} + 6, \qquad \Theta^{\text{RLS}}_{\text{weights},c} = 32N_{\text{in}}^2 + 20N_{\text{in}}. \tag{4.28}$$

Finally, the digital combining results in a computational complexity equal to

$$\Theta_{\text{combining},c} = 8N_{\text{in}} - 2. \tag{4.29}$$

Since the complexities of the weight optimization and combining processes are here given for a single data stream, they need to be multiplied by S in (4.26) in order to obtain the total computational load of all data streams to be separated in the BS.

Table 4.4a shows the ratios between the overall computational complexities of the augmented subcarrier combiner and the per-subcarrier combiner when the weights are estimated according to the LMS method. Based on the results, the augmented subcarrier processing has 33 %–98 % higher complexity than the per-subcarrier method. The higher the size of the FFT, i.e. the higher the number of subcarriers, the lower the additional complexity. This is caused by the fact that the impact of the computationally heavy FFT, being exactly the same for the per-subcarrier and augmented subcarrier methods, is emphasized with higher number of subcarriers. Moreover, less RX antennas and data streams to be separated we have, smaller the difference between the augmented and per-subcarrier methods.

The corresponding results with the RLS algorithm are given in Table 4.4b. Also now the general trends are the same as with LMS. However, the additional complexity caused by the augmented processing method is now in the range of 121 %–298 %. The reason for this lies in $\Theta^{\text{RLS}}_{\text{weights},c}$ which increases quadratically with N_{in}. The complexity of RLS is thus much higher than with LMS, and consequently RLS might even become unfeasible in BSs with large antenna arrays used in massive MIMO systems.

While the examples above are based on the basic LMS and RLS algorithms, other variants of LMS/RLS or completely other estimation methods could have been selected

Table 4.4: The ratio of the computational complexities between the augmented subcarrier processing and the linear per-subcarrier processing as a function of the number of RX antennas N and the number of data streams S. Comparison includes FFT processing, weight estimation with the given algorithm as well as digital combining.

(a) Weights solved by the augmented/per-subcarrier LMS.

N	S	FFT size				
		64	256	1024	2048	8192
1	1	1.52	1.45	1.39	1.37	1.33
10	5	1.86	1.81	1.77	1.75	1.72
20	10	1.92	1.90	1.87	1.86	1.84
100	50	1.98	1.98	1.97	1.97	1.96

(b) Weights solved by the augmented/per-subcarrier RLS.

N	S	FFT size				
		64	256	1024	2048	8192
1	1	2.63	2.48	2.36	2.31	2.21
10	5	3.81	3.80	3.79	3.78	3.77
20	10	3.91	3.91	3.90	3.90	3.90
100	50	3.98	3.98	3.98	3.98	3.98

as well. Naturally, this kind of substitution would have resulted in changes in the exact computational complexities of the weight optimization blocks. However, our intention here is just to emphasize that the additional computational complexity due to the augmented subcarrier processing can vary from only a few tens to several hundreds of percentages when compared with its per-subcarrier counterpart. Consequently, we conclude that use of the augmented subcarrier processing needs careful consideration when searching for a balance between the performance and computational complexity.

CHAPTER 5

Summary

Future radio networks require significant developments in several technological fields. In this respect, this thesis is focused on the utilization of multiantenna technologies based on flexible radio transceivers which suffer from inevitable imperfections in the associated analog RF electronics. In particular, we concentrated on the effects of one of the most severe RF imperfections in direct-conversion transceivers, namely I/Q imbalance. Moreover, we studied how to improve the performance of a system under I/Q imbalance by following the dirty RF principle where the analog imperfections are mitigated with the help of DSP algorithms.

Chapter 3 and publications [P1–P4] focused on I/Q imbalance in antenna arrays performing narrowband beamforming. Starting from the known issues caused by I/Q imbalance in single antenna devices, we extended the analysis into joint effects of multiple transceiver branches operating in parallel. One of the key findings in this respect was that I/Q imbalance distorts not only the antenna signals but affects also the radiation properties of antenna arrays. Based on these observations and a common I/Q imbalance mitigation principle in single antenna systems, we applied the WL beamforming principle into the problem. WL beamforming was shown to be more flexible in terms of I/Q imbalance mitigation than its linear counterpart. In addition, by several numerical examples imitating real world use cases we showed that WL beamforming can provide good performance, desired radiation characteristics and reliable operation even when being under severe I/Q imbalance.

In Chapter 4 and publications [P5–P8], the focus was turned to wideband systems utilizing spatial UE multiplexing. Moreover, UE multiplexing took place also in frequency domain through the OFDMA principle. We included also external interference sources to our analysis in order to model possible challenges in increasingly popular heterogeneous networks. The provided uplink signal models, analysis as well as the developments for BS RX I/Q imbalance mitigation methods were all based on full MIMO scheme where not only the BS but also the UEs can be equipped with multiple antennas. The detailed frequency domain analysis revealed that I/Q imbalance causes crosstalk between UEs at the mirror subcarrier pairs, and that the received uplink signal at an individual subcarrier is severely distorted by external interferers and noise at the considered subcarrier as well

as at the mirror subcarrier. As a solution for such an issue, we utilized the augmented subcarrier processing principle in the RX combiner and formulated a concrete combiner example following the LMMSE method. Moreover, we derived the instantaneous per-data-stream SINR in order to quantify the effects of the wireless channel, I/Q imbalance parameters and RX combining in a simple manner. Our numerical examples showed that the proposed augmented subcarrier processing is able to provide the same performance as the per-subcarrier under ideal I/Q matching, no matter if the augmented combiner is affected by I/Q imbalance or not. Consequently, the augmented processing enhances the performance under I/Q imbalance in terms of the number of active UEs, the required number of RX antennas, as well as the robustness against external interference, noise and high I/Q imbalance levels.

Altogether, this thesis emphasizes that even though multiantenna systems will indisputably provide big advantages in future radio communications, they will encounter also some challenges regarding the actual hardware implementations. As a concrete example, I/Q imbalance in TXs and RXs needs to be taken properly into account if all the desired benefits of multiantenna and array processing are wanted to be reached. The analysis and I/Q imbalance mitigation principles provided in this thesis can be used as guidelines for transceiver designs. Furthermore, the contributions of the thesis constitute a good starting point for future research regarding, e.g., hybrid beamforming, reduced complexity or joint effects of I/Q imbalance and other RF impairments such as TX PA nonlinearities, array perturbation and synchronization errors in multiantenna systems. In this way, this thesis work can enhance the performance of future wireless communications systems and can help to use low-cost structures and components in the associated analog RF electronics.

APPENDIX A

Equivalence of Symmetrical and Asymmetrical I/Q Imbalance Models

A.1 TX I/Q Imbalance

Following the symmetrical TX I/Q imbalance model, the distorted frequency-independent time-domain signal can be written as [130, 135–138]

$$x_{\mathrm{Txi}}(t) = \alpha_{\mathrm{Tx}} x_{\mathrm{L}}(t) + \beta_{\mathrm{Tx}} x_{\mathrm{L}}^{*}(t) \tag{A.1}$$

where the I/Q imbalance coefficients are equal to

$$\begin{aligned} \alpha_{\mathrm{Tx}} &= \cos\left(\frac{\phi_{\mathrm{Tx}}}{2}\right) - j\epsilon_{\mathrm{Tx}} \sin\left(\frac{\phi_{\mathrm{Tx}}}{2}\right), \\ \beta_{\mathrm{Tx}} &= \epsilon_{\mathrm{Tx}} \cos\left(\frac{\phi_{\mathrm{Tx}}}{2}\right) - j \sin\left(\frac{\phi_{\mathrm{Tx}}}{2}\right). \end{aligned} \tag{A.2}$$

Applying the well-known trigonometric identities $\cos(\theta) = (e^{j\theta} + e^{-j\theta})/2$ and $\sin(\theta) = (e^{j\theta} - e^{-j\theta})/2j$ to α_{Tx} and β_{Tx} in (A.1) results in

$$\begin{aligned} x_{\mathrm{Txi}}(t) &= \left(\frac{e^{j\frac{\phi_{\mathrm{Tx}}}{2}} + e^{-j\frac{\phi_{\mathrm{Tx}}}{2}}}{2} - j\epsilon_{\mathrm{Tx}} \frac{e^{j\frac{\phi_{\mathrm{Tx}}}{2}} - e^{-j\frac{\phi_{\mathrm{Tx}}}{2}}}{2j} \right) x_{\mathrm{L}}(t) \\ &\quad + \left(\epsilon_{\mathrm{Tx}} \frac{e^{j\frac{\phi_{\mathrm{Tx}}}{2}} + e^{-j\frac{\phi_{\mathrm{Tx}}}{2}}}{2} - j \frac{e^{j\frac{\phi_{\mathrm{Tx}}}{2}} - e^{-j\frac{\phi_{\mathrm{Tx}}}{2}}}{2j} \right) x_{\mathrm{L}}^{*}(t) \\ &= \frac{1}{2}\left((1-\epsilon_{\mathrm{Tx}}) e^{j\frac{\phi_{\mathrm{Tx}}}{2}} + (1+\epsilon_{\mathrm{Tx}}) e^{-j\frac{\phi_{\mathrm{Tx}}}{2}} \right) x_{\mathrm{L}}(t) \\ &\quad + \frac{1}{2}\left(-(1-\epsilon_{\mathrm{Tx}}) e^{j\frac{\phi_{\mathrm{Tx}}}{2}} + (1+\epsilon_{\mathrm{Tx}}) e^{-j\frac{\phi_{\mathrm{Tx}}}{2}} \right) x_{\mathrm{L}}^{*}(t). \end{aligned} \tag{A.3}$$

After some simple algebraic operations, the signal can be written as

$$\begin{aligned} x_{\mathrm{Txi}}(t) &= (1+\epsilon_{\mathrm{Tx}})\, e^{-j\frac{\phi_{\mathrm{Tx}}}{2}} \left[\frac{1}{2} \cdot \frac{e^{j\frac{\phi_{\mathrm{Tx}}}{2}}}{1+\epsilon_{\mathrm{Tx}}} \left((1-\epsilon_{\mathrm{Tx}}) e^{j\frac{\phi_{\mathrm{Tx}}}{2}} + (1+\epsilon_{\mathrm{Tx}}) e^{-j\frac{\phi_{\mathrm{Tx}}}{2}} \right) x_{\mathrm{L}}(t) \right. \\ &\qquad \left. + \frac{1}{2} \cdot \frac{e^{j\frac{\phi_{\mathrm{Tx}}}{2}}}{1+\epsilon_{\mathrm{Tx}}} \left(-(1-\epsilon_{\mathrm{Tx}}) e^{j\frac{\phi_{\mathrm{Tx}}}{2}} + (1+\epsilon_{\mathrm{Tx}}) e^{-j\frac{\phi_{\mathrm{Tx}}}{2}} \right) x_{\mathrm{L}}^*(t) \right] \\ &= (1+\epsilon_{\mathrm{Tx}})\, e^{-j\frac{\phi_{\mathrm{Tx}}}{2}} \left(\frac{1+\frac{1-\epsilon_{\mathrm{Tx}}}{1+\epsilon_{\mathrm{Tx}}} e^{j\phi_{\mathrm{Tx}}}}{2} x_{\mathrm{L}}(t) + \frac{1-\frac{1-\epsilon_{\mathrm{Tx}}}{1+\epsilon_{\mathrm{Tx}}} e^{j\phi_{\mathrm{Tx}}}}{2} x_{\mathrm{L}}^*(t) \right). \end{aligned} \tag{A.4}$$

When substituting $g_{\mathrm{Tx}} = \frac{1-\epsilon_{\mathrm{Tx}}}{1+\epsilon_{\mathrm{Tx}}}$ to the final form of $x_{\mathrm{Txi}}(t)$ in (A.4), we finally get

$$\begin{aligned} x_{\mathrm{Txi}}(t) &= (1+\epsilon_{\mathrm{Tx}})\, e^{-j\frac{\phi_{\mathrm{Tx}}}{2}} \left(\frac{1+g_{\mathrm{Tx}} e^{j\phi_{\mathrm{Tx}}}}{2} x_{\mathrm{L}}(t) + \frac{1-g_{\mathrm{Tx}} e^{j\phi_{\mathrm{Tx}}}}{2} x_{\mathrm{L}}^*(t) \right) \\ &= (1+\epsilon_{\mathrm{Tx}})\, e^{-j\frac{\phi_{\mathrm{Tx}}}{2}} \left(K_{\mathrm{Tx1}} x_{\mathrm{L}}(t) + K_{\mathrm{Tx2}} x_{\mathrm{L}}^*(t) \right) \end{aligned} \tag{A.5}$$

which is very similar to the corresponding asymmetrical model given in (2.16). In fact, the only difference between these two models is $(1+\epsilon_{\mathrm{Tx}})e^{-j\frac{\phi_{\mathrm{Tx}}}{2}}$ visible in (A.5). Such a factor is equal for $x_{\mathrm{L}}(t)$ and $x_{\mathrm{L}}^*(t)$, and thus can be considered as a part of the common impulse response of the TX, having no effect on the IRR. As a consequence, the symmetrical and asymmetrical TX I/Q imbalance models are equivalent from the I/Q imbalance perspective.

A.2 RX I/Q Imbalance

The analysis for RX I/Q imbalance follows similar principles as for the TX side. The symmetrical I/Q imbalance model for an RX signal can be written as [135–138, 172, 173]

$$r_{\mathrm{Rxi}}(t) = \alpha_{\mathrm{Rx}} r_{\mathrm{L}}(t) + \beta_{\mathrm{Rx}} r_{\mathrm{L}}^*(t) \tag{A.6}$$

where the I/Q imbalance coefficients are equal to

$$\begin{aligned} \alpha_{\mathrm{Rx}} &= \cos\left(\frac{\phi_{\mathrm{Rx}}}{2}\right) + j\epsilon_{\mathrm{Rx}} \sin\left(\frac{\phi_{\mathrm{Rx}}}{2}\right), \\ \beta_{\mathrm{Rx}} &= \epsilon_{\mathrm{Rx}} \cos\left(\frac{\phi_{\mathrm{Rx}}}{2}\right) - j \sin\left(\frac{\phi_{\mathrm{Rx}}}{2}\right). \end{aligned} \tag{A.7}$$

By applying the trigonometric identities now to α_{Rx} and β_{Rx} in (A.6), we get

$$\begin{aligned} r_{\mathrm{Rxi}}(t) &= \left(\frac{e^{j\frac{\phi_{\mathrm{Rx}}}{2}} + e^{-j\frac{\phi_{\mathrm{Rx}}}{2}}}{2} + j\epsilon_{\mathrm{Rx}} \frac{e^{j\frac{\phi_{\mathrm{Rx}}}{2}} - e^{-j\frac{\phi_{\mathrm{Rx}}}{2}}}{2j} \right) r_{\mathrm{L}}(t) \\ &\quad + \left(\epsilon_{\mathrm{Rx}} \frac{e^{j\frac{\phi_{\mathrm{Rx}}}{2}} + e^{-j\frac{\phi_{\mathrm{Rx}}}{2}}}{2} - j \frac{e^{j\frac{\phi_{\mathrm{Rx}}}{2}} - e^{-j\frac{\phi_{\mathrm{Rx}}}{2}}}{2j} \right) r_{\mathrm{L}}^*(t) \\ &= \frac{1}{2} \left((1+\epsilon_{\mathrm{Rx}}) e^{j\frac{\phi_{\mathrm{Rx}}}{2}} + (1-\epsilon_{\mathrm{Rx}}) e^{-j\frac{\phi_{\mathrm{Rx}}}{2}} \right) r_{\mathrm{L}}(t) \\ &\quad + \frac{1}{2} \left(-(1-\epsilon_{\mathrm{Rx}}) e^{j\frac{\phi_{\mathrm{Rx}}}{2}} + (1+\epsilon_{\mathrm{Rx}}) e^{-j\frac{\phi_{\mathrm{Rx}}}{2}} \right) r_{\mathrm{L}}^*(t). \end{aligned} \tag{A.8}$$

That can be modified further into a form of

$$\begin{aligned} r_{\mathrm{Rxi}}(t) &= \left[\frac{1}{2} \cdot \frac{e^{-j\frac{\phi_{\mathrm{Rx}}}{2}}}{1+\epsilon_{\mathrm{Rx}}} \left((1+\epsilon_{\mathrm{Rx}}) e^{j\frac{\phi_{\mathrm{Rx}}}{2}} + (1-\epsilon_{\mathrm{Rx}}) e^{-j\frac{\phi_{\mathrm{Rx}}}{2}} \right) \right] (1+\epsilon_{\mathrm{Rx}})\, e^{j\frac{\phi_{\mathrm{Rx}}}{2}} r_{\mathrm{L}}(t) \\ &\quad + \left[\frac{1}{2} \cdot \frac{e^{j\frac{\phi_{\mathrm{Rx}}}{2}}}{1+\epsilon_{\mathrm{Rx}}} \left(-(1-\epsilon_{\mathrm{Rx}}) e^{j\frac{\phi_{\mathrm{Rx}}}{2}} + (1+\epsilon_{\mathrm{Rx}}) e^{-j\frac{\phi_{\mathrm{Rx}}}{2}} \right) \right] (1+\epsilon_{\mathrm{Rx}})\, e^{-j\frac{\phi_{\mathrm{Rx}}}{2}} r_{\mathrm{L}}^*(t) \\ &= \left(\frac{1 + \frac{1-\epsilon_{\mathrm{Rx}}}{1+\epsilon_{\mathrm{Rx}}} e^{-j\phi_{\mathrm{Rx}}}}{2} \right) (1+\epsilon_{\mathrm{Rx}})\, e^{j\frac{\phi_{\mathrm{Rx}}}{2}} r_{\mathrm{L}}(t) \\ &\quad + \left(\frac{1 - \frac{1-\epsilon_{\mathrm{Rx}}}{1+\epsilon_{\mathrm{Rx}}} e^{j\phi_{\mathrm{Rx}}}}{2} \right) (1+\epsilon_{\mathrm{Rx}})\, e^{-j\frac{\phi_{\mathrm{Rx}}}{2}} r_{\mathrm{L}}^*(t). \end{aligned} \tag{A.9}$$

When marking $g_{\mathrm{Rx}} = \frac{1-\epsilon_{\mathrm{Rx}}}{1+\epsilon_{\mathrm{Rx}}}$ and $b_{\mathrm{Rx}} = (1+\epsilon_{\mathrm{Rx}}) e^{j\frac{\phi_{\mathrm{Rx}}}{2}}$, the distorted signal can be finally written as

$$\begin{aligned} r_{\mathrm{Rxi}}(t) &= \left(\frac{1 + g_{\mathrm{Rx}} e^{-j\phi_{\mathrm{Rx}}}}{2} \right) b_{\mathrm{Rx}} r_{\mathrm{L}}(t) + \left(\frac{1 - g_{\mathrm{Rx}} e^{j\phi_{\mathrm{Rx}}}}{2} \right) \left(b_{\mathrm{Rx}} r_{\mathrm{L}}(t) \right)^* \\ &= K_{\mathrm{Rx1}} b_{\mathrm{Rx}} r_{\mathrm{L}}(t) + K_{\mathrm{Rx2}} \left(b_{\mathrm{Rx}} r_{\mathrm{L}}(t) \right)^*. \end{aligned} \tag{A.10}$$

Considering b_{Rx} as a part of the common impulse response of the RX chain prior the down-conversion, and thus not affecting the ratio of $r_{\mathrm{L}}(t)$ and $r_{\mathrm{L}}^*(t)$, the final form of $r_{\mathrm{Rxi}}(t)$ in (A.10) and the asymmetrical model in (2.17) are equivalent from the I/Q imbalance perspective.

References

[1] *Evolved Universal Terrestrial Radio Access (E-UTRA); User Equipment (UE) radio transmission and reception*, The 3rd Generation Partnership Project (3GPP), TS36.101, version 11.8.0, release 11, Mar. 2014.

[2] *Evolved Universal Terrestrial Radio Access (E-UTRA); User Equipment (UE) conformance specification; Radio transmission and reception*, The 3rd Generation Partnership Project (3GPP), TS36.521.-1, version 11.2.0, release 11, Sep. 2013.

[3] A. A. Abidi, "Direct-conversion radio transceivers for digital communications," *IEEE Journal of Solid-State Circuits*, vol. 30, no. 12, pp. 1399–1410, Dec. 1995.

[4] T. Adali, P. J. Schreier, and L. L. Scharf, "Complex-valued signal processing: The proper way to deal with impropriety," *IEEE Transactions on Signal Processing*, vol. 59, no. 11, pp. 5101–5125, Nov. 2011.

[5] S. Afsardoost, T. Eriksson, and C. Fager, "Digital predistortion using a vector-switched model," *IEEE Transactions on Microwave Theory and Techniques*, vol. 60, no. 4, pp. 1166–1174, Apr. 2012.

[6] S. Alamouti, "A simple transmit diversity technique for wireless communications," *IEEE Journal on Selected Areas in Communications*, vol. 16, no. 8, pp. 1451–1458, Oct. 1998.

[7] Analog Devices, "RF and Microwave IC Selection Guide," 2015. [Online]. Available: http://www.analog.com/media/en/news-marketing-collateral/product-selection-guide/RF-and-Microwave-ICs-Selection-Guide.pdf

[8] J. G. Andrews, S. Buzzi, W. Choi, S. V. Hanly, A. Lozano, A. C. K. Soong, and J. C. Zhang, "What will 5G be?" *IEEE Journal of Selected Areas in Communications*, vol. 32, no. 6, pp. 1065–1082, Jun. 2014.

[9] L. Anttila, P. Händel, and M. Valkama, "Joint mitigation of power amplifier and I/Q modulator impairments in broadband direct-conversion transmitters," *IEEE*

Transactions on Microwave Theory and Techniques, vol. 58, no. 4, pp. 730–739, Apr. 2010.

[10] L. Anttila, M. Valkama, and M. Renfors, "Blind moment estimation techniques for I/Q imbalance compensation in quadrature receivers," in *Proc. IEEE 17th International Symposium on Personal, Indoor and Mobile Radio Communications (PIMRC)*, Sep. 2006, pp. 1–5.

[11] L. Anttila, M. Valkama, and M. Renfors, "Circularity-based I/Q imbalance compensation in wideband direct-conversion receivers," *IEEE Transactions on Vehicular Technology*, vol. 57, no. 4, pp. 2099–2113, Jul. 2008.

[12] L. Anttila, M. Valkama, and M. Renfors, "Frequency-selective I/Q mismatch calibration of wideband direct-conversion transmitters," *IEEE Transactions on Circuits and Systems II: Express Briefs*, vol. 55, no. 4, pp. 359–363, Apr. 2008.

[13] L. Anttila, "Digital Front-End Signal Processing with Widely-Linear Signal Models in Radio Devices," Ph.D. dissertation, Tampere University of Technology, Finland, Oct. 2011. [Online]. Available: http://URN.fi/URN:ISBN:978-952-15-2978-8

[14] L. Anttila, P. Händel, O. Mylläri, and M. Valkama, "Recursive learning-based joint digital predistorter for power amplifier and I/Q modulator impairments," *International Journal of Microwave and Wireless Technologies*, vol. 2, no. 2, pp. 173–182, Apr. 2010.

[15] K. Appaiah, A. Ashikhmin, and T. L. Marzetta, "Pilot contamination reduction in multi-user TDD systems," in *Proc. IEEE International Conference on Communications (ICC)*, May 2010, pp. 1–5.

[16] A. G. Armada and M. Calvo, "Phase noise and sub-carrier spacing effects on the performance of an OFDM communication system," *IEEE Communications Letters*, vol. 2, no. 1, pp. 11–13, Jan. 1998.

[17] E. H. Armstrong, "A new system of short wave amplification," *Proceedings of the Institute of Radio Engineers*, vol. 9, no. 1, pp. 3–11, Feb. 1921.

[18] A. Ashikhmin and T. Marzetta, "Pilot contamination precoding in multi-cell large scale antenna systems," in *Proc. IEEE International Symposium on Information Theory Proceedings (ISIT)*, Jul. 2012, pp. 1137–1141.

[19] R. Baldemair, T. Irnich, K. Balachandran, E. Dahlman, G. Mildh, Y. Selen, S. Parkvall, M. Meyer, and A. Osseiran, "Ultra-dense networks in millimeter-wave frequencies," *IEEE Communications Magazine*, vol. 53, no. 1, pp. 202–208, Jan. 2015.

[20] I. Barhumi and M. Moonen, "IQ-imbalance compensation for OFDM in the presence of IBI and carrier-frequency offset," *IEEE Transactions on Signal Processing*, vol. 55, no. 1, pp. 256–266, Jan. 2007.

[21] N. Bhushan, J. Li, D. Malladi, R. Gilmore, D. Brenner, A. Damnjanovic, R. Sukhavasi, C. Patel, and S. Geirhofer, "Network densification: The dominant theme for wireless evolution into 5G," *IEEE Communications Magazine*, vol. 52, no. 2, pp. 82–89, Feb. 2014.

[22] E. Biglieri, R. Calderbank, A. Constantinides, A. Goldsmith, A. Paulraj, and V. H. Poor, *MIMO Wireless Communications*. Cambridge University Press, 2007.

[23] E. Björnson, J. Hoydis, M. Kountouris, and M. Debbah, "Massive MIMO systems with non-ideal hardware: Energy efficiency, estimation, and capacity limits," *IEEE Transactions on Information Theory*, vol. 60, no. 11, pp. 7112–7139, Nov. 2014.

[24] E. Björnson, M. Matthaiou, and M. Debbah, "Massive MIMO systems with hardware-constrained base stations," in *Proc. IEEE International Conference on Acoustics, Speech and Signal Processing (ICASSP)*, May 2014, pp. 3142–3146.

[25] E. Björnson, M. Matthaiou, A. Pitarokoilis, and E. G. Larsson, "Distributed massive MIMO in cellular networks: Impact of imperfect hardware and number of oscillators," in *Proc. 23rd European Signal Processing Conference (EUSIPCO)*, Aug. 2015, pp. 2436–2440.

[26] E. Björnson, E. G. Larsson, and M. Debbah, "Massive MIMO for maximal spectral efficiency: How many users and pilots should be allocated?" *IEEE Transactions on Wireless Communications*, vol. 15, no. 2, pp. 1293–1308, Feb. 2016.

[27] E. Björnson, E. G. Larsson, and T. L. Marzetta, "Massive MIMO: Ten myths and one critical question," *IEEE Communications Magazine*, vol. 54, no. 2, pp. 114–123, Feb. 2016.

[28] D. W. Bliss and S. Govindasamy, *Adaptive Wireless Communications: MIMO Channels and Networks*. Cambridge University Press, May 2013.

[29] F. Boccardi, R. W. Heath, A. Lozano, T. L. Marzetta, and P. Popovski, "Five disruptive technology directions for 5G," *IEEE Communications Magazine*, vol. 52, no. 2, pp. 74–80, Feb. 2014.

[30] H. Bogucka, P. Kryszkiewicz, and A. Kliks, "Dynamic spectrum aggregation for future 5G communications," *IEEE Communications Magazine*, vol. 53, no. 5, pp. 35–43, May 2015.

[31] W. M. Brown and R. B. Crane, "Conjugate linear filtering," *IEEE Transactions on Information Theory*, vol. 15, no. 4, pp. 462–465, Jul. 1969.

[32] H. Cao, A. S. Tehrani, C. Fager, T. Eriksson, and H. Zirath, "I/Q imbalance compensation using a nonlinear modeling approach," *IEEE Transactions on Microwave Theory and Techniques*, vol. 57, no. 3, pp. 513–518, Mar. 2009.

[33] S. Carpenter, D. Nopchinda, M. Abbasi, Z. S. He, M. Bao, T. Eriksson, and H. Zirath, "A D-band 48-Gbit/s 64-QAM/QPSK direct-conversion I/Q transceiver chipset," *IEEE Transactions on Microwave Theory and Techniques*, vol. 64, no. 4, pp. 1285–1296, Apr. 2016.

[34] P. Chevalier, "Optimal array processing for non-stationary signals," in *Proc. IEEE International Conference on Acoustics, Speech, and Signal Processing (ICASSP)*, May 1996, pp. 2868–2871.

[35] P. Chevalier and A. Blin, "Widely linear MVDR beamformers for the reception of an unknown signal corrupted by noncircular interferences," *IEEE Transactions on Signal Processing*, vol. 55, no. 11, pp. 5323–5336, Nov. 2007.

[36] P. Chevalier, J. P. Delmas, and A. Oukaci, "Performance analysis of the optimal widely linear MVDR beamformer," in *Proc. 17th European Signal Processing Conference (EUSIPCO)*, Aug. 2009, pp. 587–591.

[37] P. Chevalier, J.-P. Delmas, and A. Oukaci, "Optimal widely linear MVDR beamforming for noncircular signals," in *Proc. IEEE International Conference on Acoustics, Speech and Signal Processing (ICASSP)*, Apr. 2009, pp. 3573–3576.

[38] P. Chevalier and A. Maurice, "Constrained beamforming for cyclostationary signals," in *Proc. IEEE International Conference on Acoustics, Speech, and Signal Processing (ICASSP)*, Apr. 1997, pp. 3789–3792.

[39] J. Choi and R. W. Heath, "Near maximum-likelihood detector with one-bit ADCs for multiuser massive MIMO systems," in *Proc. IEEE 6th International Workshop on Computational Advances in Multi-Sensor Adaptive Processing (CAMSAP)*, Dec. 2015, pp. 397–400.

[40] Y.-H. Chung and S.-M. Phoong, "Joint estimation of I/Q imbalance, CFO and channel response for MIMO OFDM systems," *IEEE Transactions on Communications*, vol. 58, no. 5, pp. 1485–1492, May 2010.

[41] F. M. Colebrook, "Homodyne," *Wireless World and Radio Review*, no. 13, pp. 645–648, 1924.

[42] L. Cottatellucci, R. R. Müller, and M. Vehkaperä, "Analysis of pilot decontamination based on power control," in *Proc. IEEE Vehicular Technology Conference (VTC-Spring)*, Jun. 2013, pp. 1–5.

[43] D. Darsena, L. Di Virgilio, G. Gelli, and F. Verde, "Widely-linear frequency-shift compensation of CFO and I/Q imbalance in OFDMA/SC-FDMA systems," in *Proc. IEEE International Conference on Communications (ICC)*, Jun. 2015, pp. 2686–2691.

[44] D. Darsena, G. Gelli, L. Paura, and F. Verde, "Widely-linear beamforming/combining techniques for MIMO wireless systems," in *Proc. 5th International Symposium on Communications Control and Signal Processing (ISCCSP)*, May 2012, pp. 1–5.

[45] S. S. Das, E. de Carvalho, and R. Prasad, "Performance analysis of OFDM systems with adaptive sub carrier bandwidth," *IEEE Transactions on Wireless Communications*, vol. 7, no. 4, pp. 1117–1122, Apr. 2008.

[46] L. Ding, Z. Ma, D. R. Morgan, M. Zierdt, and G. T. Zhou, "Compensation of frequency-dependent gain/phase imbalance in predistortion linearization systems," *IEEE Transactions on Circuits and Systems I: Regular Papers*, vol. 55, no. 1, pp. 390–397, Feb. 2008.

[47] S. C. Douglas, "Widely-linear recursive least-squares algorithm for adaptive beamforming," in *Proc. IEEE International Conference on Acoustics, Speech and Signal Processing (ICASSP)*, Apr. 2009, pp. 2041–2044.

[48] Y. Egashira, Y. Tanabe, and K. Sato, "A novel IQ imbalance compensation method with pilot-signals for OFDM system," in *Proc. IEEE 64th Vehicular Technology Conference (VTC-Fall)*, Sep. 2006, pp. 1–5.

[49] O. Elijah, C. Leow, T. Rahman, S. Nunoo, and S. Iliya, "A comprehensive survey of pilot contamination in massive MIMO - 5G system," *IEEE Communications Surveys Tutorials*, 2015.

[50] Ericsson AB, "5G radio access (white paper)," February 2015. [Online]. Available: http://www.ericsson.com/res/docs/whitepapers/wp-5g.pdf

[51] T. Eriksson and C. Fager, "Digital predistortion of concurrent multiband communication systems," in *Proc. IEEE International Conference on Acoustics, Speech and Signal Processing (ICASSP)*, May 2014, pp. 3918–3922.

[52] N. Y. Ermolova, Y. Zou, M. Valkama, and O. Tirkkonen, "Error-rate analysis of OFDM radio link over mobile Rayleigh channel under multiple RF impairments," *IEEE Transactions on Vehicular Technology*, vol. 63, no. 2, pp. 930–936, Feb. 2014.

[53] F. Fernandes, A. Ashikhmin, and T. L. Marzetta, "Inter-cell interference in noncooperative TDD large scale antenna systems," *IEEE Journal on Selected Areas in Communications*, vol. 31, no. 2, pp. 192–201, Feb. 2013.

[54] G. Fettweis, M. Lohning, D. Petrovic, M. Windisch, P. Zillmann, and W. Rave, "Dirty RF: A new paradigm," in *Proc. 16th International Symposium on Personal, Indoor and Mobile Radio Communications (PIMRC)*, vol. 4, Sep. 2005, pp. 2347–2355 Vol. 4.

[55] M. Filippou, D. Gesbert, and H. Yin, "Decontaminating pilots in cognitive massive MIMO networks," in *Proc. International Symposium on Wireless Communication Systems (ISWCS)*, Aug. 2012, pp. 816–820.

[56] X. Gao, O. Edfors, F. Rusek, and F. Tufvesson, "Massive MIMO performance evaluation based on measured propagation data," *IEEE Transactions on Wireless Communications*, vol. 14, no. 7, pp. 3899–3911, Jul. 2015.

[57] X. Gao, "Massive MIMO in Real Propagation Environments," Ph.D. dissertation, Lund University, Sweden, Feb. 2016. [Online]. Available: http://lup.lub.lu.se/record/8567483/file/8569798.pdf

[58] X. Gao, O. Edfors, F. Tufvesson, and E. G. Larsson, "Massive MIMO in real propagation environments: Do all antennas contribute equally?" *IEEE Transactions on Communications*, vol. 63, no. 11, pp. 3917–3928, Nov. 2015.

[59] M. Gavell, "Advanced Analog MMICs for mm-wave Communication and Remote Sensing in 0.15μm mHEMT Technology," Licentiate Thesis, Chalmers University of Technology, Sweden, Aug. 2013. [Online]. Available: http://publications.lib.chalmers.se/records/fulltext/182498/182498.pdf

[60] M. Gavell, M. Ferndahl, S. E. Gunnarsson, M. Abbasi, and H. Zirath, "An image reject mixer for high-speed E-band (71-76, 81-86 GHz) wireless communication," in *Proc. IEEE Compound Semiconductor Integrated Circuit Symposium (CISC)*, Oct. 2009, pp. 1–4.

[61] D. Gesbert, M. Kountouris, R. W. Heath, C.-B. Chae, and T. Salzer, "Shifting the MIMO paradigm," *IEEE Signal Processing Magazine*, vol. 24, no. 5, pp. 36–46, Sep. 2007.

[62] A. Ghosh, T. A. Thomas, M. C. Cudak, R. Ratasuk, P. Moorut, F. W. Vook, T. S. Rappaport, G. R. Maccartney, S. Sun, and S. Nie, "Millimeter-wave enhanced local area systems: A high-data-rate approach for future wireless networks," *IEEE Journal of Selected Areas in Communications*, vol. 32, no. 6, pp. 1152–1163, Jun. 2014.

[63] L. C. Godara, "Application of antenna arrays to mobile communications. I: Performance improvement, feasibility, and system considerations," *Proceedings of the IEEE*, vol. 85, no. 7, pp. 1031–1060, Jul. 1997.

[64] L. C. Godara, "Application of antenna arrays to mobile communications. II: Beamforming and direction-of-arrival considerations," *Proceedings of the IEEE*, vol. 85, no. 8, pp. 1195–1245, Aug. 1997.

[65] A. Gokceoglu, Y. Zou, M. Valkama, P. C. Sofotasios, P. Mathecken, and D. Cabric, "Mutual information analysis of OFDM radio link under phase noise, IQ imbalance and frequency-selective fading channel," *IEEE Transactions on Wireless Communications*, vol. 12, no. 6, pp. 3048–3059, Jun. 2013.

[66] A. Goldsmith, *Wireless Communications*. Cambridge University Press, 2005.

[67] A. Gomaa and N. Al-Dhahir, "Multi-user SC-FDMA systems under IQ imbalance: EVM and subcarrier mapping impact," in *Proc. IEEE Global Telecommunications Conference (GLOBECOM)*, Dec. 2011, pp. 1–5.

[68] Q. Gu, *RF System Design of Transceivers for Wireless Communications*. Springer, 2005.

[69] U. Gustavsson, C. Sanchez-Perez, T. Eriksson, F. Athley, G. Durisi, P. Landin, K. Hausmair, C. Fager, and L. Svensson, "On the impact of hardware impairments on massive MIMO," in *Proc. IEEE Global Communications Conference (GLOBECOM) Workshops*, Dec. 2014, pp. 294–300.

[70] R. Hamila, Ö. Özdemir, and N. Al-Dhahir, "Beamforming OFDM performance under joint phase noise and I/Q imbalance," *IEEE Transactions on Vehicular Technology*, 2015.

[71] N. C. Hamilton, "Aspects of direct conversion receiver design," in *Proc. Fifth International Conference on HF Radio Systems and Techniques*, Jul. 1991, pp. 299–303.

[72] F. Harris, "Digital filter equalization of analog gain and phase mismatch in I-Q receivers," in *Proc. 5th IEEE International Conference on Universal Personal Communications (ICUPC)*, Sep. 1996, pp. 793–796.

[73] S. Haykin, *Adaptive Filter Theory*, 4th ed. Prentice Hall, 2002.

[74] J. Hoydis, S. ten Brink, and M. Debbah, "Massive MIMO: How many antennas do we need?" in *Proc. 49th Annual Allerton Conference on Communication, Control, and Computing (Allerton)*, Sep. 2011, pp. 545 –550.

[75] J. Hoydis, S. ten Brink, and M. Debbah, "Massive MIMO in the UL/DL of cellular networks: How many antennas do we need?" *IEEE Journal of Selected Areas in Communications*, vol. 31, no. 2, pp. 160–171, Feb. 2013.

[76] Huawei Technologies Co. Ltd., "5G: A technology vision (white paper)," 2013. [Online]. Available: http://www.huawei.com/5gwhitepaper

[77] G. Hueber, Y. Zou, K. Dufrene, R. Stuhlberger, and M. Valkama, "Smart front-end signal processing for advanced wireless receivers," *IEEE Journal of Selected Topics in Signal Processing*, vol. 3, no. 3, pp. 472–487, Jun. 2009.

[78] IEEE Standards Association, *IEEE Standard for WirelessMAN-Advanced Air Interface for Broadband Wireless Access Systems*, Standard 802.16.1-2012, Sep. 2012. [Online]. Available: http://standards.ieee.org/getieee802/download/802.16.1-2012.pdf

[79] IEEE Standards Association. (2014) IEEE 802.11 documents. [Online]. Available: https://mentor.ieee.org/802.11/documents

[80] Institute of Electrical and Electronics Engineers, Inc. (2014) Status of IEEE 802.11 HEW study group. [Online]. Available: http://www.ieee802.org/11/Reports/hew_update.htm

[81] International Telecommunications Union - Radiocommunication Sector (ITU-R), *Provisional Final Acts - World Radiocommunication Conference (WRC-15)*, Nov. 2015. [Online]. Available: http://www.itu.int/en/ITU-R/conferences/wrc/2015/

[82] International Telecommunications Union - Telecommunications Standardization Sector (ITU-T), *Recommendation ITU-T Y.2060 - Overview of the Internet of Things*, Series Y: Global Information Infrastructure, Internet Protocol Aspects and Next-Generation Networks, Jun. 2012. [Online]. Available: https://www.itu.int/rec/T-REC-Y.2060-201206-I

[83] A. Ishaque, P. Sakulkar, and G. Ascheid, "Capacity analysis of uplink multi-user SC-FDMA system with frequency-dependent I/Q imbalance," in *Proc. 51st Annual Allerton Conference on Communication, Control, and Computing (Allerton)*, Oct. 2013, pp. 1067–1074.

[84] A. Ishaque, P. Sakulkar, and G. Ascheid, "Multiuser pilot pattern for uplink multicarrier systems with frequency-dependent I/Q imbalance," in *Proc. IEEE Wireless Communications and Networking Conference (WCNC)*, Apr. 2014, pp. 936–941.

[85] S. Jacobsson, G. Durisi, M. Coldrey, U. Gustavsson, and C. Studer, "One-bit massive MIMO: Channel estimation and high-order modulations," in *Proc. IEEE International Conference on Communications (ICC) Workshop*, Jun. 2015, pp. 1304–1309.

[86] G. James, D. Burley, D. Clements, P. Dyke, J. Searl, N. Steele, and J. Wright, *Advanced Modern Engineering Mathematics*, 4th ed. Pearson Education Ltd., 2011.

[87] S. Jnawali, S. Beygi, and H. R. Bahrami, "A low-complexity method to compensate IQ-imbalance and phase noise in MIMO-OFDM systems," in *Proc. IEEE Global Telecommunications Conference (GLOBECOM)*, Dec. 2011, pp. 1–6.

[88] M. Joham, W. Utschick, and J. A. Nossek, "Linear transmit processing in MIMO communications systems," *IEEE Transactions on Signal Processing*, vol. 53, no. 8, pp. 2700–2712, Aug. 2005.

[89] S. G. Johnson and M. Frigo, "A modified split-radix FFT with fewer arithmetic operations," *IEEE Transactions on Signal Processing*, vol. 55, no. 1, pp. 111–119, Jan. 2007.

[90] J. Jose, A. Ashikhmin, T. L. Marzetta, and S. Vishwanath, "Pilot contamination and precoding in multi-cell TDD systems," *IEEE Transactions on Wireless Communications*, vol. 10, no. 8, pp. 2640–2651, Aug. 2011.

[91] V. Jungnickel, K. Manolakis, W. Zirwas, B. Panzner, V. Braun, M. Lossow, M. Sternad, R. Apelfröjd, and T. Svensson, "The role of small cells, coordinated multipoint, and massive MIMO in 5G," *IEEE Communications Magazine*, vol. 52, no. 5, pp. 44–51, May 2014.

[92] T. Kaiser, A. Bourdoux, H. Boche, J. R. Fonollosa, J. B. Andersen, and W. Utschick, Eds., *Smart Antennas – State of the Art*, ser. Signal Processing and Communications. Hindawi Publishing Corporation, 2005, vol. 3.

[93] P. Kela, J. Turkka, and M. Costa, "Borderless mobility in 5G outdoor ultra-dense networks," *IEEE Access*, vol. 3, pp. 1462–1476, 2015.

[94] Z. Khan, H. Ahmadi, E. Hossain, M. Coupechoux, L. DaSilva, and J. Lehtomäki, "Carrier aggregation/channel bonding in next generation cellular networks: Methods and challenges," *IEEE Network*, vol. 28, no. 6, pp. 34–40, Nov. 2014.

[95] A. Kiayani, L. Anttila, O. Mylläri, and M. Valkama, "Prototype implementation and RF performance measurements of DSP based transmitter I/Q imbalance calibration," in *Proc. 7th International Symposium on Communication Systems Networks and Digital Signal Processing (CSNDSP)*, Jul. 2010, pp. 484–489.

[96] A. Kiayani, L. Anttila, Y. Zou, and M. Valkama, "Channel estimation and equalization in multiuser uplink OFDMA and SC-FDMA systems under transmitter RF impairments," *IEEE Transactions on Vehicular Technology*, vol. 65, no. 1, pp. 82–99, Jan. 2016.

[97] N. Kolomvakis, M. Matthaiou, J. Li, M. Coldrey, and T. Svensson, "Massive MIMO with IQ imbalance: Performance analysis and compensation," in *Proc. IEEE International Conference on Communications (ICC)*, Jun. 2015, pp. 1703–1709.

[98] S. Krone and G. Fettweis, "On the capacity of OFDM systems with receiver I/Q imbalance," in *Proc. IEEE International Conference on Communications (ICC)*, May 2008, pp. 1317–1321.

[99] E. G. Larsson, O. Edfors, F. Tufvesson, and T. L. Marzetta, "Massive MIMO for next generation wireless systems," *IEEE Communications Magazine*, vol. 52, no. 2, pp. 186–195, Feb. 2014.

[100] E. G. Larsson and H. V. Poor, "Joint beamforming and broadcasting in massive MIMO," *IEEE Transactions on Wireless Communications*, vol. 15, no. 4, pp. 3058–3070, Apr. 2016.

[101] E. A. Lee and D. G. Messerschmitt, *Digital Communication*, 2nd ed. Kluwer Academic Publishers, 1994.

[102] T. A. Levanen, J. Pirskanen, T. Koskela, J. Talvitie, and M. Valkama, "Radio interface evolution towards 5G and enhanced local area communications," *IEEE Access*, vol. 2, pp. 1005–1029, 2014.

[103] L. Li, A. Ashikhmin, and T. Marzetta, "Pilot contamination precoding for interference reduction in large scale antenna systems," in *Proc. 51st Annual Allerton Conference on Communication, Control, and Computing (Allerton)*, Oct. 2013, pp. 226–232.

[104] Linear Technology, "Wireless & RF solutions," 2011. [Online]. Available: http://www.linear.com/docs/12457

[105] J. Litva, *Digital Beamforming in Wireless Communications*. Artech House Publishers, Aug. 1996.

[106] C.-L. Liu, "Impacts of I/Q imbalance on QPSK-OFDM-QAM detection," *IEEE Transactions on Consumer Electronics*, vol. 44, no. 3, pp. 984–989, Aug. 1998.

[107] R. Liu, X. Li, L. Ding, and X. Gao, "Low complexity turbo equalization for LTE uplink with transmitter IQ imbalance," in *Proc. International Conference on Wireless Communications and Signal Processing (WCSP)*, Oct. 2010, pp. 1–6.

[108] W. Liu and S. Weiss, *Wideband Beamforming: Concepts and Techniques*, ser. Wireless Communications and Mobile Computing. Wiley, Mar. 2010.

[109] I.-T. Lu and J. Chang, "Joint transmitter and receiver IQ imbalance estimation and compensation for OFDM systems," in *Proc. IEEE Radio and Wireless Symposium (RWS)*, Jan. 2010, pp. 476–479.

[110] L. Lu, G. Y. Li, A. L. Swindlehurst, A. Ashikhmin, and R. Zhang, "An overview of massive MIMO: Benefits and challenges," *IEEE Journal of Selected Topics in Signal Processing*, vol. 8, no. 5, pp. 742–758, Oct. 2014.

[111] F.-L. Luo, *Digital Front-End in Wireless Communications and Broadcasting: Circuits and Signal Processing*. Cambridge University Press, Sep. 2011.

[112] B. Maham and O. Tirkkonen, "Transmit antenna selection OFDM systems with transceiver I/Q imbalance," *IEEE Transactions on Vehicular Technology*, vol. 61, no. 2, pp. 865–871, Feb. 2012.

[113] B. Maham, O. Tirkkonen, and A. Hjørungnes, "Impact of transceiver I/Q imbalance on transmit diversity of beamforming OFDM systems," *IEEE Transactions on Communications*, vol. 60, no. 3, pp. 643–648, Mar. 2012.

[114] H. A. Mahmoud, H. Arslan, M. K. Ozdemir, and F. E. Retnasothie, "IQ imbalance correction for OFDMA uplink systems," in *Proc. IEEE International Conference on Communications (ICC)*, Jun. 2009, pp. 1–5.

[115] P.-I. Mak, S.-P. U, and R. P. Martins, "Transceiver architecture selection: Review, state-of-the-art survey and case study," *IEEE Circuits and Systems Magazine*, vol. 7, no. 2, pp. 6–25, 2007.

[116] T. L. Marzetta, "Noncooperative cellular wireless with unlimited numbers of base station antennas," *IEEE Transactions on Wireless Communications*, vol. 9, no. 11, pp. 3590–3600, Nov. 2010.

[117] T. McWhorter and P. Schreier, "Widely-linear beamforming," in *Proc. 37th Asilomar Conference on Signals, Systems and Computers*, vol. 1, Nov. 2003, pp. 753–759.

[118] H. Minn and D. Munoz, "Pilot designs for channel estimation of MIMO OFDM systems with frequency-dependent I/Q imbalances," *IEEE Transactions on Communications*, vol. 58, no. 8, pp. 2252–2264, Aug. 2010.

[119] S. Mirabbasi and K. Martin, "Classical and modern receiver architectures," *IEEE Communications Magazine*, vol. 38, no. 11, pp. 132–139, Nov. 2000.

[120] J. Mitola and G. Q. Maguire Jr., "Cognitive radio: Making software radios more personal," *IEEE Personal Communications*, vol. 6, no. 4, pp. 13–18, Aug. 1999.

[121] A. F. Molisch, *Wireless Communications*, 2nd ed. John Wiley & Sons, 2011.

[122] M. Morelli and M. Moretti, "Carrier frequency offset estimation for OFDM direct-conversion receivers," *IEEE Transactions on Wireless Communications*, vol. 11, no. 7, pp. 2670–2679, Jul. 2012.

[123] P. F. Morlat, J. C. N. Perez, G. Villemaud, J. Verdier, and J. M. Gorce, "On the compensation of RF impairments with multiple antennas in SIMO OFDM systems," in *Proc. IEEE 64th Vehicular Technology Conference (VTC-Fall)*, Sep. 2006, pp. 1–5.

[124] R. R. Müller, L. Cottatellucci, and M. Vehkaperä, "Blind pilot decontamination," *IEEE Journal of Selected Topics in Signal Processing*, vol. 8, no. 5, pp. 773–786, Oct. 2014.

[125] R. R. Müller, M. Vehkaperä, and L. Cottatellucci, "Analysis of blind pilot decontamination," in *Proc. Asilomar Conference on Signals, Systems and Computers*, Nov. 2013, pp. 1016–1020.

[126] F. Munier, T. Eriksson, and A. Svensson, "An ICI reduction scheme for OFDM system with phase noise over fading channels," *IEEE Transactions on Communications*, vol. 56, no. 7, pp. 1119–1126, Jul. 2008.

[127] H. G. Myung, J. Lim, and D. J. Goodman, "Single carrier FDMA for uplink wireless transmission," *IEEE Vehicular Technology Magazine*, vol. 1, no. 3, pp. 30–38, Sep. 2006.

[128] W. Namgoong and T. H. Meng, "Direct-conversion RF receiver design," *IEEE Transactions on Communications*, vol. 49, no. 3, pp. 518–529, Mar. 2001.

[129] B. Narasimhan, S. Narayanan, H. Minn, and N. Al-Dhahir, "Reduced-complexity baseband compensation of joint Tx/Rx I/Q imbalance in mobile MIMO-OFDM," *IEEE Transactions on Wireless Communications*, vol. 9, no. 5, pp. 1720–1728, May 2010.

[130] B. Narasimhan, D. Wang, S. Narayanan, H. Minn, and N. Al-Dhahir, "Digital compensation of frequency-dependent joint Tx/Rx I/Q imbalance in OFDM systems under high mobility," *IEEE Journal of Selected Topics in Signal Processing*, vol. 3, no. 3, pp. 405–417, Jun. 2009.

[131] H. Q. Ngo and E. G. Larsson, "EVD-based channel estimation in multicell multiuser MIMO systems with very large antenna arrays," in *Proc. IEEE International Conference on Acoustics, Speech and Signal Processing (ICASSP)*, Mar. 2012, pp. 3249–3252.

[132] H. C. Nguyen, E. de Carvalho, and R. Prasad, "Multi-user interference cancellation schemes for carrier frequency offset compensation in uplink OFDMA," *IEEE Transactions on Wireless Communications*, vol. 13, no. 3, pp. 1164–1171, Mar. 2014.

[133] Nokia Solutions and Networks, "Looking ahead to 5G (white paper)," 2014. [Online]. Available: http://networks.nokia.com/sites/default/files/document/5g_white_paper_0.pdf

[134] A. Osseiran, F. Boccardi, V. Braun, K. Kusume, P. Marsch, M. Maternia, O. Queseth, M. Schellmann, H. Schotten, H. Taoka, H. Tullberg, M. A. Uusitalo, B. Timus,

and M. Fallgren, "Scenarios for 5G mobile and wireless communications: The vision of the METIS project," *IEEE Communications Magazine*, vol. 52, no. 5, pp. 26–35, May 2014.

[135] Ö. Özdemir, R. Hamila, and N. Al-Dhahir, "SINR analysis for beamforming OFDM systems under joint transmit-receive I/Q imbalance," in *Proc. IEEE 23rd International Symposium on Personal Indoor and Mobile Radio Communications (PIMRC)*, Sep. 2012, pp. 1896–1901.

[136] Ö. Özdemir, R. Hamila, and N. Al-Dhahir, "Exact SINR analysis of OFDM systems under joint Tx/RX I/Q imbalance," in *Proc. IEEE 24th International Symposium on Personal Indoor and Mobile Radio Communications (PIMRC)*, Sep. 2013, pp. 646–650.

[137] Ö. Özdemir, R. Hamila, and N. Al-Dhahir, "I/Q imbalance in multiple beamforming OFDM transceivers: SINR analysis and digital baseband compensation," *IEEE Transactions on Communications*, vol. 61, no. 5, pp. 1914–1925, May 2013.

[138] Ö. Özdemir, R. Hamila, and N. Al-Dhahir, "Exact average OFDM subcarrier SINR analysis under joint transmit-receive I/Q imbalance," *IEEE Transactions on Vehicular Technology*, vol. 63, no. 8, pp. 4125–4130, Oct. 2014.

[139] H. G. Park, C. Park, H. Oh, and M. G. Kyeong, "RF gain/phase and I/Q imbalance error correction technique for multi-channel array antenna systems," in *Proc. IEEE 53rd Vehicular Technology Conference (VTC-Spring)*, May 2001, pp. 175–179.

[140] J. Park, C.-H. Lee, B.-S. Kim, and J. Laskar, "Design and analysis of low flicker-noise CMOS mixers for direct-conversion receivers," *IEEE Transactions on Microwave Theory and Techniques*, vol. 54, no. 12, pp. 4372–4380, Dec. 2006.

[141] B. Picinbono and P. Chevalier, "Widely linear estimation with complex data," *IEEE Transactions on Signal Processing*, vol. 43, no. 8, pp. 2030–2033, Aug. 1995.

[142] T. Pollet, M. Van Bladel, and M. Moeneclaey, "BER sensitivity of OFDM systems to carrier frequency offset and Wiener phase noise," *IEEE Transactions on Communications*, vol. 43, no. 2/3/4, pp. 191–193, Feb. 1995.

[143] J. G. Proakis, *Digital Communications*, 4th ed. McGraw-Hill, 2001.

[144] J. G. Proakis and M. Salehi, *Digital Communications*, 5th ed. McGraw-Hill, 2008.

[145] K. P. Pun, J. E. Franca, C. Azeredo-Leme, C. F. Chan, and C. S. Choy, "Correction of frequency-dependent I/Q mismatches in quadrature receivers," *Electronics Letters*, vol. 37, no. 23, pp. 1415–1417, Nov. 2001.

[146] J. Qi and S. Aïssa, "Compensation for HPA nonlinearity and I/Q imbalance in MIMO beamforming systems," in *Proc. IEEE 6th International Conference on Wireless and Mobile Computing, Networking and Communications (WiMob)*, Oct. 2010, pp. 78–82.

[147] S. Rangan, T. S. Rappaport, and E. Erkip, "Millimeter-wave cellular wireless networks: Potentials and challenges," *Proceedings of the IEEE*, vol. 102, no. 3, pp. 366–385, Mar. 2014.

[148] T. S. Rappaport, S. Sun, R. Mayzus, H. Zhao, Y. Azar, K. Wang, G. N. Wong, J. K. Schulz, M. Samimi, and F. Gutierrez, "Millimeter wave mobile communications for 5G cellular: It will work!" *IEEE Access*, vol. 1, pp. 335–349, 2013.

[149] B. Razavi, "Design considerations for direct-conversion receivers," *IEEE Transactions on Circuits and Systems II: Analog and Digital Signal Processing*, vol. 44, no. 6, pp. 428–435, Jun. 1997.

[150] B. Razavi, "Cognitive Radio Design Challenges and Techniques," *IEEE Journal of Solid-State Circuits*, vol. 45, no. 8, pp. 1542–1553, Aug. 2010.

[151] B. Razavi, *RF Microelectronics*. Prentice Hall, 1998.

[152] W. Roh, J.-Y. Seol, J. Park, B. Lee, J. Lee, Y. Kim, J. Cho, K. Cheun, and F. Aryanfar, "Millimeter-wave beamforming as an enabling technology for 5G cellular communications: Theoretical feasibility and prototype results," *IEEE Communications Magazine*, vol. 52, no. 2, pp. 106–113, Feb. 2014.

[153] F. Rusek, D. Persson, B. K. Lau, E. G. Larsson, T. L. Marzetta, O. Edfors, and F. Tufvesson, "Scaling up MIMO: Opportunities and challenges with very large arrays," *IEEE Signal Processing Magazine*, vol. 30, no. 1, pp. 40–60, Jan. 2013.

[154] M. Sakai, H. Lin, and K. Yamashita, "Joint estimation of channel and I/Q imbalance in OFDM/OQAM systems," *IEEE Communications Letters*, vol. 20, no. 2, pp. 284–287, Feb. 2016.

[155] T. C. W. Schenk, E. R. Fledderus, and P. F. M. Smulders, "Performance impact of IQ mismatch in direct-conversion MIMO OFDM transceivers," in *Proc. IEEE Radio and Wireless Symposium (RWS)*, Jan. 2007, pp. 329–332.

[156] T. C. W. Schenk, P. F. M. Smulders, and E. R. Fledderus, "Estimation and compensation of frequency selective TX/RX IQ imbalance in MIMO OFDM systems," in *Proc. IEEE International Conference on Communications (ICC)*, Jun. 2006, pp. 251–256.

[157] T. Schenk, *RF Imperfections in High-rate Wireless Systems: Impact and Digital Compensation*. Springer, 2008.

[158] T. C. W. Schenk, E. R. Fledderus, and P. F. M. Smulders, "Performance analysis of zero-IF MIMO OFDM transceivers with IQ imbalance," *Journal of Communications*, vol. 2, no. 7, pp. 9–19, Dec. 2007.

[159] T. M. Schmidl and D. C. Cox, "Robust frequency and timing synchronization for OFDM," *IEEE Transactions on Communications*, vol. 45, no. 12, pp. 1613–1621, Dec. 1997.

[160] P. J. Schreier and L. L. Scharf, "Second-order analysis of improper complex random vectors and processes," *IEEE Transactions on Signal Processing*, vol. 51, no. 3, pp. 714–725, Mar. 2003.

[161] P. J. Schreier and L. L. Scharf, *Statistical Signal Processing of Complex-Valued Data*. Cambridge, UK: Cambridge University Press, Mar. 2010.

[162] A. Schuchert, R. Hasholzner, and P. Antoine, "A novel IQ imbalance compensation scheme for the reception of OFDM signals," *IEEE Transactions on Consumer Electronics*, vol. 47, no. 3, pp. 313–318, Aug. 2001.

[163] A. Shahed hagh ghadam, "Contributions to Analysis and DSP-based Mitigation of Nonlinear Distortion in Radio Transceivers," Ph.D. dissertation, Tampere University of Technology, Finland, Oct. 2011. [Online]. Available: http://URN.fi/URN:ISBN:978-952-15-2794-4

[164] Y.-M. Shi, L. Huang, C. Qian, and H. C. So, "Shrinkage linear and widely linear complex-valued least mean squares algorithms for adaptive beamforming," *IEEE Transactions on Signal Processing*, vol. 63, no. 1, pp. 119–131, Jan. 2015.

[165] N. Song, J. Steinwandt, L. Wang, R. C. de Lamare, and M. Haardt, "Non-data-aided adaptive beamforming algorithm based on the widely linear auxiliary vector filter," in *Proc. IEEE International Conference on Acoustics, Speech and Signal Processing (ICASSP)*, May 2011, pp. 2636–2639.

[166] J. H. Sørensen and E. de Carvalho, "Pilot decontamination through pilot sequence hopping in massive MIMO systems," in *Proc. IEEE Global Communications Conference (GLOBECOM)*, Dec. 2014, pp. 3285–3290.

[167] W. L. Stutzman and G. A. Thiele, *Antenna Theory and Design*, 2nd ed. John Wiley & Sons, 1997.

[168] V. Syrjälä, "Analysis and Mitigation of Oscillator Impairments in Modern Receiver Architectures," Ph.D. dissertation, Tampere University of Technology, Finland, Jun. 2012. [Online]. Available: http://URN.fi/URN:ISBN:978-952-15-2855-2

[169] D. Tandur and M. Moonen, "Joint adaptive compensation of transmitter and receiver IQ imbalance under carrier frequency offset in OFDM-based systems," *IEEE Transactions on Signal Processing*, vol. 55, no. 11, pp. 5246–5252, Nov. 2007.

[170] D. Tandur and M. Moonen, "Compensation of RF impairments in MIMO OFDM systems," in *Proc. IEEE International Conference on Acoustics, Speech and Signal Processing (ICASSP)*, Mar. 2008, pp. 3097–3100.

[171] A. Tarighat, R. Bagheri, and A. H. Sayed, "Compensation schemes and performance analysis of IQ imbalances in OFDM receivers," *IEEE Transactions on Signal Processing*, vol. 53, no. 8, pp. 3257–3268, Aug. 2005.

[172] A. Tarighat and A. H. Sayed, "MIMO OFDM receivers for systems with IQ imbalances," *IEEE Transactions on Signal Processing*, vol. 53, no. 9, pp. 3583–3596, Sep. 2005.

[173] A. Tarighat and A. H. Sayed, "Joint compensation of transmitter and receiver impairments in OFDM systems," *IEEE Transactions on Wireless Communications*, vol. 6, no. 1, pp. 240–247, Jan. 2007.

[174] D. Tse and P. Viswanath, *Fundamentals of Wireless Communication*. Cambridge University Press, 2005.

[175] H. Tsurumi and T. Maeda, "Design study on a direct conversion receiver front-end for 280 MHz, 900 MHz, and 2.6 GHz band radio communication systems," in *Proc. IEEE 41st Vehicular Technology Conference (VTC)*, May 1991, pp. 457–462.

[176] J. Tubbax, B. Come, L. Van der Perre, L. Deneire, S. Donnay, and M. Engels, "Compensation of IQ imbalance in OFDM systems," in *Proc. IEEE International Conference on Communications (ICC)*, May 2003, pp. 3403–3407.

[177] J. Tubbax, B. Come, L. Van der Perre, S. Donnay, M. Engels, H. De Man, and M. Moonen, "Compensation of IQ imbalance and phase noise in OFDM systems," *IEEE Transaction on Wireless Communications*, vol. 4, no. 3, pp. 872–877, May 2005.

[178] D. G. Tucker, "The history of the homodyne and synchrodyne," *Journal of the British Institution of Radio Engineers*, vol. 14, no. 4, pp. 143–154, Apr. 1954.

[179] U. Tureli, D. Kivanc, and H. Liu, "Experimental and analytical studies on a high-resolution OFDM carrier frequency offset estimator," *IEEE Transactions on Vehicular Technology*, vol. 50, no. 2, pp. 629–643, Mar. 2001.

[180] M. Valkama and M. Renfors, "Advanced DSP for I/Q imbalance compensation in a low-IF receiver," in *Proc. IEEE International Conference on Communications (ICC)*, Jun. 2000, pp. 768–772.

[181] M. Valkama, M. Renfors, and V. Koivunen, "Advanced methods for I/Q imbalance compensation in communication receivers," *IEEE Transactions on Signal Processing*, vol. 49, no. 10, pp. 2335–2344, Oct. 2001.

[182] M. Valkama, M. Renfors, and V. Koivunen, "Blind signal estimation in conjugate signal models with application to I/Q imbalance compensation," *IEEE Signal Processing Letters*, vol. 12, no. 11, pp. 733–736, Nov. 2005.

[183] M. Valkama, A. Shahed Hagh Ghadam, L. Anttila, and M. Renfors, "Advanced digital signal processing techniques for compensation of nonlinear distortion in wideband multicarrier radio receivers," *IEEE Transactions on Microwave Theory and Techniques*, vol. 54, no. 6, pp. 2356–2366, Jun. 2006.

[184] M. Valkama, Y. Zou, and M. Renfors, "On I/Q imbalance effects in MIMO space-time coded transmission systems," in *Proc. IEEE Radio and Wireless Symposium (RWS)*, Jan. 2006, pp. 223–226.

[185] M. Valkama, "Advanced I/Q Signal Processing for Wideband Receivers: Models and Algorithms," Ph.D. dissertation, Tampere University of Technology, Finland, Nov. 2001. [Online]. Available: http://URN.fi/URN:NBN:fi:tty-200810021094

[186] J.-J. van de Beek, M. Sandell, and P. O. Börjesson, "ML estimation of time and frequency offset in OFDM systems," *IEEE Transactions on Signal Processing*, vol. 45, no. 7, pp. 1800–1805, Jul. 1997.

[187] B. D. Van Veen and K. M. Buckley, "Beamforming: A versatile approach to spatial filtering," *IEEE Acoustics, Speech, and Signal Processing (ASSP) Magazine*, vol. 5, no. 2, pp. 4–24, Apr. 1988.

[188] J. Vieira, S. Malkowsky, K. Nieman, Z. Miers, N. Kundargi, L. Liu, I. Wong, V. Öwall, O. Edfors, and F. Tufvesson, "A flexible 100-antenna testbed for massive MIMO," in *Proc. IEEE Global Communication Conference (GLOBECOM) Workshops*, Dec. 2014, pp. 287–293.

[189] C.-X. Wang, F. Haider, X. Gao, X.-H. You, Y. Yang, D. Yuan, H. Aggoune, H. Haas, S. Fletcher, and E. Hepsaydir, "Cellular architecture and key technologies for 5G wireless communication networks," *IEEE Communications Magazine*, vol. 52, no. 2, pp. 122–130, Feb. 2014.

[190] S. Wang, Y. Li, and J. Wang, "Multiuser detection in massive spatial modulation MIMO with low-resolution ADCs," *IEEE Transactions on Wireless Communications*, vol. 14, no. 4, pp. 2156–2168, Apr. 2015.

[191] M. Windisch, "Estimation and Compensation of IQ Imbalance in Broadband Communications Receivers," Ph.D. dissertation, Technische Universität Dresden, Germany, 2007.

[192] D. Xu, L. Huang, X. Xu, and Z. Ye, "Widely linear MVDR beamformers for noncircular signals based on time-averaged second-order noncircularity coefficient estimation," *IEEE Transactions on Vehicular Technology*, vol. 62, no. 7, pp. 3219–3227, Sep. 2013.

[193] H. Yin, D. Gesbert, M. Filippou, and Y. Liu, "A coordinated approach to channel estimation in large-scale multiple-antenna systems," *IEEE Journal on Selected Areas in Communications*, vol. 31, no. 2, pp. 264–273, Feb. 2013.

[194] H. Yin, D. Gesbert, M. Filippou, and Y. Liu, "Decontaminating pilots in massive MIMO systems," in *Proc. IEEE International Conference on Communications (ICC)*, Jun. 2013, pp. 3170–3175.

[195] Y. Yoshida, K. Hayashi, H. Sakai, and W. Bocquet, "Analysis and compensation of transmitter IQ imbalances in OFDMA and SC-FDMA systems," *IEEE Transactions on Signal Processing*, vol. 57, no. 8, pp. 3119–3129, Aug. 2009.

[196] S. Zarei, W. Gerstacker, J. Aulin, and R. Schober, "I/Q imbalance aware widely-linear receiver for uplink multi-cell massive MIMO systems: Design and sum rate analysis," *IEEE Transactions on Wireless Communications*, vol. 15, no. 5, pp. 3393–3408, May 2016.

[197] S. Zarei, W. Gerstacker, and R. Schober, "I/Q imbalance aware widely-linear precoding for downlink massive MIMO systems," in *Proc. IEEE Global Communications Conference (GLOBECOM) Workshops*, Dec. 2014, pp. 301–307.

[198] S. Zarei, W. Gerstacker, and R. Schober, "I/Q imbalance aware widely-linear channel estimation and detection for uplink massive MIMO systems," in *Proc. Twelfth Internation Symposium on Wireless Communication Systems (ISWCS)*, Aug. 2015, pp. 646–650.

[199] J. Zhang, B. Zhang, S. Chen, X. Mu, M. El-Hajjar, and L. Hanzo, "Pilot contamination elimination for large-scale multiple-antenna aided OFDM systems," *IEEE Journal of Selected Topics in Signal Processing*, vol. 8, no. 5, pp. 759–772, Oct. 2014.

[200] W. Zhang, R. C. de Lamare, C. Pan, and M. Chen, "Widely linear block-diagonalization type precoding in massive MIMO systems with IQ imbalance," in *Proc. IEEE International Conference on Communications (ICC)*, Jun. 2015, pp. 1789–1794.

[201] S. Zhou and M.-C. F. Chang, "A CMOS passive mixer with low flicker noise for low-power direct-conversion receiver," *IEEE Journal of Solid-State Circuits*, vol. 40, no. 5, pp. 1084–1093, May 2005.

[202] Q. Zou, A. Tarighat, and A. H. Sayed, "On the joint compensation of IQ imbalances and phase noise in MIMO-OFDM systems," in *Proc. IEEE International Symposium on Circuits and Systems (ISCAS)*, May 2007, pp. 37–40.

[203] Q. Zou, A. Tarighat, and A. H. Sayed, "Joint compensation of IQ imbalance and phase noise in OFDM wireless systems," *IEEE Transactions on Communications*, vol. 57, no. 2, pp. 404–414, Feb. 2009.

[204] Y. Zou, "Analysis and Mitigation of I/Q Imbalances in Multi-Antenna Transmission Systems," Ph.D. dissertation, Tampere University of Technology, Finland, Nov. 2009. [Online]. Available: http://URN.fi/URN:NBN:fi:tty-200911257153

[205] Y. Zou, M. Valkama, N. Y. Ermolova, and O. Tirkkonen, "Analytical performance of OFDM radio link under RX I/Q imbalance and frequency-selective Rayleigh fading channel," in *Proc. IEEE 12th International Workshop on Signal Processing Advances in Wireless Communications (SPAWC)*, Jun. 2011, pp. 251–255.

[206] Y. Zou, M. Valkama, and M. Renfors, "Performance analysis of space-time coded MIMO-OFDM systems under I/Q imbalance," in *Proc. IEEE International Conference on Acoustics, Speech and Signal Processing (ICASSP)*, Apr. 2007, pp. 341–344.

[207] Y. Zou, M. Valkama, and M. Renfors, "Compensation of frequency-selective I/Q imbalances in space-time coded multi-antenna OFDM systems," in *Proc. 3rd International Symposium on Communications, Control and Signal Processing (ISCCSP)*, Mar. 2008, pp. 123–128.

[208] Y. Zou, M. Valkama, and M. Renfors, "Digital compensation of I/Q imbalance effects in space-time coded transmit diversity systems," *IEEE Transactions on Signal Processing*, vol. 56, no. 6, pp. 2496–2508, Jun. 2008.

[209] Y. Zou, M. Valkama, and M. Renfors, "Pilot-based compensation of frequency-selective I/Q imbalances in direct-conversion OFDM transmitters," in *Proc. IEEE 68th Vehicular Technology Conference (VTC-Fall)*, Sep. 2008, pp. 1–5.

Publications

Publication 1

A. Hakkarainen, J. Werner, and M. Valkama, "RF Imperfections in Antenna Arrays: Response Analysis and Widely-Linear Digital Beamforming," in *Proceedings of the IEEE Radio and Wireless Symposium (RWS)*, Austin, TX, USA, 20–23 Jan. 2013. DOI: 10.1109/rws.2013.6486683

RF Imperfections in Antenna Arrays: Response Analysis and Widely-Linear Digital Beamforming

Aki Hakkarainen, Janis Werner, and Mikko Valkama

Department of Communication Engineering, Tampere University of Technology
P.O. Box 553, 33101 Tampere, Finland, phone: +358 3 3115 11, fax: +358 3 364 1449
email: {aki.hakkarainen, janis.werner, mikko.e.valkama}@tut.fi

***Abstract*— In this paper, we analyze the impact of radio frequency (RF) circuit imperfections on the digital beamforming capabilities of linear antenna arrays. Special emphasis is on the I/Q imbalances and common channel responses of all individual parallel radio chains, and their impact on the radiation pattern is analyzed in closed form. We also propose an extension on the digital signal processing side, called widely-linear (WL) digital beamforming, in order to mitigate the influence of RF I/Q imbalances in digital beamforming processing instead of individually calibrating all the parallel radio chains. This is shown to efficiently recover the desired beamforming capabilities and directional properties which are initially corrupted by RF imperfections. As a practical example, a widely linear normalized least-mean square (WL-NLMS) algorithm with a known training signal is formulated to get optimal weights for signals from different antennas. The proposed method enables more accurate direction of arrival (DOA) estimations and beam steering properties even when operating under substantial RF imperfections in the RF circuits of a receiver.**

***Index Terms*— adaptive signal processing, antenna arrays, antenna radiation patterns, beam steering, cognitive radio, I/Q imbalance, radio transceivers**

I. Introduction

Radio spectrum is strongly regulated all over the world. However, there are big variations in the spatial and temporal usage of frequencies in practice [1], [2]. Consequently, the concept of cognitive radio (CR) is needed to improve the spectral efficiency by using the scarce spectrum dynamically [3]. The idea is an adaptation to the radio environment in terms of time, frequency and location. Based on the spectrum occupancy measurements or existing databases, CRs use the radio spectrum opportunistically without interfering with any primary user [3], [4]. The spectral efficiency can be further increased by exploiting the directional properties of communications. Thus antenna arrays and efficient beamforming are essential components to sense and utilize the available radio spectrum in CR [5], [6].

One of the most promising radio structures for cognitive transceivers in terms of low costs and frequency flexibility is the direct-conversion radio (DCR) architecture [7]. However, it requires a very versatile RF front-end, i.e. analog electronic components, which are difficult and expensive to implement. In practice, this leads to system performance degradation due to the RF imperfections. One of them is the RF I/Q imbalance, which exists due to non-ideal behavior in RF mixers. In this paper, the influence of this unwanted phenomenon is studied in the context of digital beamforming and antenna arrays. A novel array signal processing method is also developed to mitigate the spurious response without individual calibrations for all the parallel receiver branches.

This paper is organized as follows. In Section II, the principal antenna array response with digital linear beamforming is formulated shortly. Section III introduces I/Q imbalance effects on the RF chains and derives the corresponding array response and radiation pattern of a beamformer in closed-form. In Section IV, a WL digital beamforming structure is developed to suppress the spurious response, without separate RF chain calibrations. Section V gives example simulation results and finally conclusions are drawn in Section VI.

II. Antenna Array Response

The output signal of a digital beamformer is defined by

$$y = \sum_{i=1}^{N} w_i^* x_i = \mathbf{w}^H \mathbf{x} \tag{1}$$

where $\mathbf{w} = [w_1, w_2, ..., w_N]^T$ refers to the combining weights and $\mathbf{x} = [x_1, x_2, ..., x_N]^T$ to the signal snapshots from each antenna element [8]. The snapshots are given by

$$\mathbf{x} = s\mathbf{a}(\theta) \tag{2}$$

where s is the arriving signal and $\mathbf{a}(\theta)$ is the steering vector to direction θ. In case of a uniform linear array, the steering vector is defined as $\mathbf{a}(\theta) = [1, e^{j\kappa\cos\theta}, e^{j\kappa 2\cos\theta}, \cdots, e^{j\kappa(N-1)\cos\theta}]^T$, where $\kappa = \frac{2\pi}{\lambda}d$, d is the distance between antenna elements and λ denotes the wavelength. The conceptual beamformer and the used notation are depicted in Fig. 1. Furthermore, $\mathbf{w}$ should be matched to θ, so we need to use $\mathbf{w}(\theta_d)$, where θ_d is the desired direction of arrival. When substituting (2) and $\mathbf{w}(\theta_d)$ in (1), we get the output signal as a function of angle θ with the weights for the desired direction

$$y(\theta) = s\mathbf{w}^H(\theta_d)\mathbf{a}(\theta). \tag{3}$$

Based on (3), the spatial response of an antenna array can be presented as a radiation pattern where the effect of the input signal power has been removed by normalization. With ideal omni-directional antenna elements, the radiation pattern with the given weights is described by

$$D(\theta) = |y(\theta)| \,/\, |s| = \left|\mathbf{w}^H(\theta_d)\mathbf{a}(\theta)\right|. \tag{4}$$

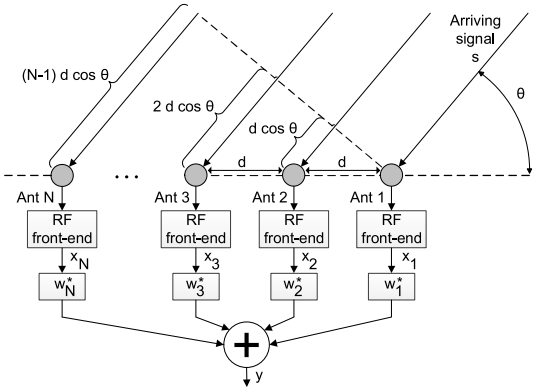

Fig. 1. The conceptual digital beamformer and the used notation.

III. RF I/Q Imbalance Effects

DCR down-converts the received RF signal to two real-valued baseband signals, called in-phase (I) and quadrature-phase (Q) components. Ideally, the conversion is done with two local oscillator signals and mixers, which have equal gains and exactly 90 degrees phase difference. However, in practice oscillator signals and mixers have a gain mismatch and they are not in perfect phase quadrature [9]. The effect is called I/Q imbalance and can be modeled for an individual signal or radio chain at baseband equivalent level as [10]

$$x_{imb}(t) = K_1 x(t) + K_2 x^*(t) \tag{5}$$

where $K_1 = \frac{(1+ge^{-j\phi})}{2}$ and $K_2 = \frac{1-ge^{j\phi}}{2}$ and $x(t)$ is the baseband equivalent signal under ideal I/Q matching. Here, g presents the relative gain mismatch and ϕ presents the phase mismatch between the I- and Q-branch. In the context of antenna array with multiple parallel DCR's (one per antenna), (2) and (5) can be combined, leading to signal snapshots with I/Q imbalance given by

$$\mathbf{x}_{imb} = \mathbf{K}_1\mathbf{x} + \mathbf{K}_2\mathbf{x}^* = \mathbf{K}_1 s\mathbf{a}(\theta) + \mathbf{K}_2 s^*\mathbf{a}(\pi-\theta) \tag{6}$$

where $\mathbf{K}_1 = \text{diag}(K_{1,1}, K_{1,2}, \cdots, K_{1,N})$ and $\mathbf{K}_2 = \text{diag}(K_{2,1}, K_{2,2}, \cdots, K_{2,N})$ are referring to the I/Q imbalance coefficients in each parallel antenna branch. When the ideal signal snapshots in (3) are then substituted with the signal snapshots with I/Q imbalance in (6), we get the combiner output signal with I/Q imbalance of the form

$$\begin{aligned} y_{imb}(\theta) &= \mathbf{w}^H(\theta_d)\mathbf{K}_1 s\mathbf{a}(\theta) + \mathbf{w}^H(\theta_d)\mathbf{K}_2 s^*\mathbf{a}(\pi-\theta) \\ &= |s|\,(e^{j\phi_s}\mathbf{w}^H(\theta_d)\mathbf{K}_1\mathbf{a}(\theta) \\ &\quad + e^{-j\phi_s}\mathbf{w}^H(\theta_d)\mathbf{K}_2\mathbf{a}(\pi-\theta)) \end{aligned} \tag{7}$$

where ϕ_s denotes the phase of s. Stemming from (7), the radiation pattern of a beamformer including RF I/Q imbalance is given in (11) at the bottom of the page. Due to the effect of RF I/Q imbalance, the radiation pattern is clearly corrupted and consists of two terms. More specifically, the second term relative to $\mathbf{a}(\pi-\theta)$ corresponds to the undesired mirror beam towards angle $180^\circ - \theta$. This will be illustrated more clearly in Section V.

IV. Widely-Linear Beamforming against RF Imperfections

In general, WL beamforming is defined as [11]

$$y_{wl} = \mathbf{w}_1^H\mathbf{x} + \mathbf{w}_2^H\mathbf{x}^* = \mathbf{w}_{wl}^H\mathbf{x}_{tot} \tag{8}$$

where $\mathbf{w}_{wl} = [\mathbf{w}_1^T, \mathbf{w}_2^T]^T$ and $\mathbf{x}_{tot} = [\mathbf{x}^T, \mathbf{x}^H]^T$. In words, opposed to plain linear beamforming, the WL structure combines both the direct signal snapshot $\mathbf{x}$ and its complex conjugate $\mathbf{x}^*$ (with weights $\mathbf{w}_1$ and $\mathbf{w}_2$, respectively) and has therefore doubled computational complexity compared to the conventional beamforming. When combining (2) and (8), the output signal of a WL beamformer with the given weights, and ideal RF chains, is given as a function of θ by

$$\begin{aligned} y_{wl}(\theta) &= s\mathbf{w}_1^H(\theta_d)\mathbf{a}(\theta) + s^*\mathbf{w}_2^H(\theta_d)\mathbf{a}^*(\theta) \\ &= s\mathbf{w}_1^H(\theta_d)\mathbf{a}(\theta) + s^*\mathbf{w}_2^H(\theta_d)\mathbf{a}(\pi-\theta) \\ &= |s|\,(e^{j\phi_s}\mathbf{w}_1^H(\theta_d)\mathbf{a}(\theta) + e^{-j\phi_s}\mathbf{w}_2^H(\theta_d)\mathbf{a}(\pi-\theta)). \end{aligned} \tag{9}$$

The radiation pattern of the WL beamformer (still assuming perfect RF chains) is then

$$\begin{aligned} D_{wl}(\theta) &= |y_{wl}(\theta)|\,/\,|s| \\ &= \left|e^{j\phi_s}\mathbf{w}_1^H(\theta_d)\mathbf{a}(\theta) + e^{-j\phi_s}\mathbf{w}_2^H(\theta_d)\mathbf{a}(\pi-\theta))\right|. \end{aligned} \tag{10}$$

Similarly, equations for the output signal and radiation pattern of the WL beamformer under RF I/Q imbalance can be derived by substituting the signal snapshot vector $\mathbf{x}$ in (8) with its counterpart with I/Q imbalance in (6). The resulting output signal and radiation pattern are given by (12) and (13) at the bottom of the page. Based on (12) and (13), it is clear that with proper selection of the weights $\mathbf{w}_1$ and $\mathbf{w}_2$, the undesired mirror beam (term relative to $\mathbf{a}(\pi-\theta)$) can be suppressed. It stems from the rich nature of WL structure which processes both $\mathbf{x}_{imb}$ and $\mathbf{x}_{imb}^*$.

The weight optimization task for the above WL beamformer can be solved in several ways. As an example, the NLMS algorithm, described in more details in [12], is one good starting point due to its simple implementation and

$$D_{imb}(\theta) = |y_{imb}(\theta)|\,/\,|s| = \left|e^{j\phi_s}\mathbf{w}^H(\theta_d)\mathbf{K}_1\mathbf{a}(\theta) + e^{-j\phi_s}\mathbf{w}^H(\theta_d)\mathbf{K}_2\mathbf{a}(\pi-\theta)\right| \tag{11}$$

$$y_{wl,imb}(\theta) = |s|\,(e^{j\phi_s}(\mathbf{w}_1^H(\theta_d)\mathbf{K}_1 + \mathbf{w}_2^H(\theta_d)\mathbf{K}_2^*)\mathbf{a}(\theta) + e^{-j\phi_s}(\mathbf{w}_1^H(\theta_d)\mathbf{K}_2 + \mathbf{w}_2^H(\theta_d)\mathbf{K}_1^*)\mathbf{a}(\pi-\theta)) \tag{12}$$

$$D_{wl,imb}(\theta) = \frac{|y_{wl,imb}(\theta)|}{|s|} = \left|e^{j\phi_s}(\mathbf{w}_1^H(\theta_d)\mathbf{K}_1 + \mathbf{w}_2^H(\theta_d)\mathbf{K}_2^*)\mathbf{a}(\theta) + e^{-j\phi_s}(\mathbf{w}_1^H(\theta_d)\mathbf{K}_2 + \mathbf{w}_2^H(\theta_d)\mathbf{K}_1^*)\mathbf{a}(\pi-\theta)\right| \tag{13}$$

low computational complexity. The WL-NLMS algorithm is iteratively solving the weights by

$$y_{wl}(n) = \mathbf{w}_{wl}^H(n)\mathbf{x}_{tot}(n) \quad (14)$$

$$e_{wl}(n) = s_t(n) - y_{wl}(n) \quad (15)$$

$$\mathbf{w}_{wl}(n+1) = \mathbf{w}_{wl}(n) + \mu \frac{\mathbf{x}_{tot}(n)e_{wl}^*(n)}{||\mathbf{x}_{tot}(n)||^2} \quad (16)$$

where $\mathbf{x}_{tot} = [\mathbf{x}_{imb}^T, \mathbf{x}_{imb}^H]^T$, $s_t(n)$ denotes the known training signal, $e_{wl}(n)$ presents the estimation error and μ is the step-size coefficient.

A novel training solution to mitigate the mirror beam, is to use a dual-angle input signal in the coefficient learning phase, where an additional signal is injected locally into the array input at the mirror angle $180^\circ - \theta$. This corresponds to the ideal signal snapshots of the form

$$\mathbf{x}_t = s_t\mathbf{a}(\theta) + s_m\mathbf{a}(\pi - \theta) \quad (17)$$

where s_m denotes the injected mirror signal. To enable such mirror injection, a rough estimate of desired signal DOA is needed first. Then, the mirror signal is artificially generated in the receiver and injected in the receiver branches with phase shifts corresponding to the mirror direction. While coefficient learning is progressing, and thus more accurate DOA estimates are available, the phase shifts of the mirror injection can be finetuned as well.

V. Simulation Example

In the simulations, 20 antenna elements with $\lambda/2$ spacing were used. For the weight training phase, 16-QAM single-carrier waveform with the raised cosine pulse (50% rolloff) was generated. In addition, additive white Gaussian noise (SNR 40dB) and I/Q imbalance were included to the received signals. I/Q imbalance amplitude mismatch coefficients were 0.8 while phase mismatch coefficients were -20° for all receiver branches. Equal I/Q imbalance coefficients were used because in practice only a single oscillator would be used for the IQ demodulators in all branches. Relatively high imbalance values were used for illustration purposes. In total, 3000 symbols (16-QAM) were used as the reference signal s_t to train the WL-NLMS and NLMS weights.

Results are depicted in Fig. 2. The conventional NLMS algorithm performs well in the main direction but has a high sidelobe to the mirror direction due to I/Q imbalance. This is exactly in line with the earlier analytical analysis given in Section III. The proposed WL-NLMS with the additional signal component injection in the training phase is equal to NLMS near the desired direction. However, the proposed WL-NLMS clearly outperforms NLMS in the mirror direction, having close to perfect radiation pattern despite of RF imperfections.

VI. Conclusions

In this paper, the influence of common RF imperfection called I/Q imbalance for the antenna array response was studied. The radiation pattern equations for the beamformer were derived with and without I/Q imbalance and the existence of a mirror beam element in the radiation pattern was shown. Then, widely-linear beamforming with an additional signal component injection in the training phase was proposed to mitigate the mirror beam. Computer simulation results were shown for a linear antenna array with 20 antenna elements with both conventional NLMS algorithm as well as with the proposed WL-NLMS algorithm. Results showed that the proposed WL-NLMS method outperforms NLMS and successfully mitigates the unwanted mirror beam.

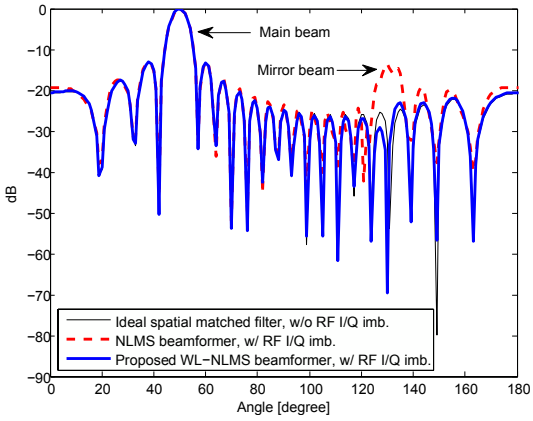

Fig. 2. Radiation patterns with uniform linear antenna array of 20 elements with the desired signal direction of 50°.

References

[1] FCC, "Spectrum policy task force report," *ET Docket No. 02-135*, Nov. 2002.

[2] V. Valenta et al., "Towards cognitive radio networks: Spectrum utilization measurements in suburb environment," in *Proc. IEEE RWS 2009*, Jan. 2009, pp. 352 –355.

[3] S. Haykin, "Cognitive radio: brain-empowered wireless communications," *IEEE J. on Selected Areas in Communications*, vol. 23, no. 2, pp. 201 – 220, Feb. 2005.

[4] A. Hayar et al., "Cognitive radio research and implementation challenges," in *Proc. ACSSC 2007*, Nov. 2007, pp. 782 –786.

[5] H. Sarvanko et al., "Exploiting spatial dimension in cognitive radios and networks," in *Proc. CROWNCOM 2011*, Jun. 2011, pp. 360 –364.

[6] S. Huang et al., "Non-Intrusive cognitive radio networks based on smart antenna technology," in *Proc. IEEE GLOBECOM 2007*, Nov. 2007, pp. 4862 –4867.

[7] P. Mak et al., "Transceiver architecture selection: Review, state-of-the-art survey and case study," *IEEE Circuits and Systems Magazine*, vol. 7, no. 2, pp. 6 –25, 2007.

[8] J. Litva, *Digital Beamforming in Wireless Communications*. Artech House Publishers, Aug. 1996.

[9] A. Baier, "Quadrature mixer imbalances in digital TDMA mobile radio receivers," in *Proc. Int. Zurich Seminar on Digital Communications, 1990. Electronic Circuits and Systems for Communications*, Mar. 1990, pp. 147 –162.

[10] M. Valkama et al., "Blind signal estimation in conjugate signal models with application to I/Q imbalance compensation," *IEEE Signal Processing Letters*, vol. 12, no. 11, pp. 733 – 736, Nov. 2005.

[11] P. Chevalier, "Optimal array processing for non-stationary signals," in *Proc. IEEE ICASSP 1996.*, vol. 5, May 1996, pp. 2868 –2871 vol. 5.

[12] S. Haykin, *Adaptive Filter Theory*, 3rd ed. Prentice Hall, Dec. 1995.

Publication 2

A. Hakkarainen, J. Werner, K. R. Dandekar, and M. Valkama, "RF-Aware Widely-Linear Beamforming and Null-Steering in Cognitive Radio Transmitters," in *Proceedings of the 8th International Conference on Cognitive Radio Oriented Wireless Networks (CROWNCOM)*, Washington, DC, USA, 8–10 July 2013. DOI: 10.4108/icst.crowncom.2013.252052

RF-Aware Widely-Linear Beamforming and Null-Steering in Cognitive Radio Transmitters

Aki Hakkarainen*, Janis Werner*, Kapil R. Dandekar† and Mikko Valkama*
*Department of Electronics and Communications Engineering
Tampere University of Technology, P.O. Box 553, FI-33101 Tampere, Finland
Email: {aki.hakkarainen, janis.werner, mikko.e.valkama}@tut.fi
†Department of Electrical and Computer Engineering
Drexel University, Philadelphia, PA 19104, USA
Email: dandekar@drexel.edu

***Abstract*—Protection of the primary users (PUs) from interference stemming from secondary user (SU) transmissions is one of the key issues in dynamic cognitive radio systems. Assuming elementary direction of arrival (DOA) or location estimation of PU devices can be carried out in the SU devices, appropriate directional transmission utilizing e.g. antenna arrays and null-steering can then be deployed to avoid interference by steering nulls towards the PUs. In this paper, we study such transmitter digital beamforming and null-steering under practical limitations of the associated radio frequency (RF) circuits, namely the amplitude and phase mismatches between the in-phase and quadrature (I/Q) rails of the parallel up-conversion chains. Closed-form analysis of the available beamforming and null-steering capabilities is first provided, showing that the transmitter null-steering capabilities are heavily degraded due to RF circuit imperfections. Motivated by this, we will then propose and formulate a widely-linear (WL) digital beamforming and null-steering solution which is shown to efficiently suppress the RF circuit imperfection effects from the radiation pattern. Based on the obtained results, the developed solution can provide efficient null-steering and interference suppression characteristics, despite of the imperfections in the RF circuits, and can thus enable, e.g., the use of cost-efficient RF chains in the SU transmitters.**

I. Introduction

While most existing and emerging radio communication systems, like mobile cellular networks and broadcast networks, build on heavily regulated radio spectrum use, recent measurement campaigns have revealed (see, e.g., [1]–[5]) that there are big temporal and spatial variations in the truly realized radio spectrum use. This, in turn, indicates that sophisticated or cognitive radio (CR) devices, being able to identify time-, frequency- and/or space-dependent under-utilized chunks of the radio spectrum, could use them in a dynamic manner for communication purposes [6]. Thus the efficiency and flexibility of the overall radio spectrum use would be greatly improved, offering also the possibility of overlay type secondary radio systems.

This work was supported by the Finnish Funding Agency for Technology and Innovation (Tekes) under the project "Reconfigurable Antenna-based Enhancement of Dynamic Spectrum Access Algorithms", the Industrial Research Fund of Tampere University of Technology (Tuula and Yrjö Neuvo Fund), and the Doctoral Programme of the President of Tampere University of Technology.

This work was also supported by the National Science Foundation (NSF) under award number 1147838.

One the most central requirements in dynamic secondary user (SU) spectrum access systems is the ability to control interference towards primary user (PU) devices. One interesting recently-established idea in this context is to carry out direction of arrival (DOA) and/or location estimation of the PU devices and use that information in the SU access system in controlling the interference. Such ideas have been described at concept, signal processing and network levels, e.g., in [7]–[9]. At physical layer, one interesting possibility is to use novel reconfigurable antenna systems, like transmitter null-steering through digital beamforming [10] or leaky-wave antenna (LWA) structures [11], for directional transmission such that interference towards identified PU devices is minimized.

In this paper, motivated by the ever-increasing digital signal processing capabilities in radio devices, we focus on digital beamforming based transmitter null-steering and the associated radio frequency (RF) hardware challenges in SU transmitters. Assuming that the parallel RF chains deploy the well-known direct-conversion transmitter (DCT) topology [12], known to suffer from the amplitude and phase mismatches between the I and Q rails of the individual RF chains [13], we will first provide closed-form radiation pattern analysis of the overall transmitter including the effects of such practical RF imperfections. The analysis shows that the beamforming capabilities, and especially the null-steering performance, are heavily degraded due to the imperfections in the transmitter RF circuits. This is especially emphasized when the number of antennas is fairly high and thus high angular resolution is targeted. Stemming from this, we will then formulate and propose an augmented or widely-linear (WL) signal processing based beamforming solution which has the structural capability to automatically suppress the effects of the practical RF circuit imperfections. Optimum RF-aware widely-linear beamforming coefficients are derived and demonstrated through extensive simulations to yield beamforming and null-steering performance practically identical to the case with ideal RF circuits. Thus based on the obtained results, the proposed RF-aware beamforming principle can offer high-performance null-steering and physical layer interference protection solution, despite of practical limitations in the deployed RF circuits. This can then enable the use of cost-efficient RF circuits in

the SU devices without sacrificing the interference control capabilities towards PUs.

The rest of the paper is organized as follows. In Section II, the fundamental array signal and system models, including also I/Q imbalance models and WL processing, are provided. Then, in Section III, the classical linear null-steering method is reviewed and based on that, the proposed RF-aware WL null-steering beamforming is formulated. Next, in Section IV, simulations and numerical results are given for illustrating the capabilities of the conventional and proposed WL null-steering methods under RF I/Q imbalance. Finally, the paper is concluded in Section V.

Notation: Throughout the paper, vectors and matrices are written with bold characters. The superscripts $(\cdot)^T$, $(\cdot)^H$, $(\cdot)^*$ and $(\cdot)^{-1}$ represent transpose, hermitian (conjugate) transpose, conjugate and matrix inverse, respectively. The tilde sign $\sim$ above variables is used to present a WL (augmented) quantity and the results obtained by the WL processing.

II. Fundamental Signal and Array Models

A. Spatial Response of Transmitter Beamformer

The digital baseband signal snapshots $\mathbf{x} = [x_1, x_2, ..., x_N]^T \in \mathbb{C}^{N\times 1}$ in a transmit beamformer with N antenna elements can be presented as

$$\mathbf{x} = \mathbf{w}(\theta_\mathrm{d})s \tag{1}$$

where $\mathbf{w}(\theta_\mathrm{d}) = [w_1(\theta_\mathrm{d}), w_2(\theta_\mathrm{d}), ..., w_N(\theta_\mathrm{d})]^T \in \mathbb{C}^{N\times 1}$ refers to the precoding weights under a given optimization criteria towards the desired direction θ_d [14]. In addition, s is the transmitted complex signal snapshot. The conceptual digital transmit beamformer and the used notation is depicted in Fig. 1. When the transmitted signal snapshots are eventually received by the receiver located in direction θ, the corresponding received snapshot is equal to

$$y(\theta) = \mathbf{a}^H(\theta)\mathbf{x} + n = \mathbf{a}^H(\theta)\mathbf{w}(\theta_\mathrm{d})s + n \tag{2}$$

where $\mathbf{a}(\theta) \in \mathbb{C}^{N\times 1}$ is the steering vector and n denotes the additive white Gaussian noise (AWGN) due to the transmission channel and receiver equipment. Here, the noise is assumed to be complex circular. Note that we have excluded the actual propagation related effects in (2) since with closely-spaced antenna elements, the effective channels between different transmit antennas and the receiver only differ by the phase shifts included in $\mathbf{a}(\theta)$. The steering vector of the transmitter is defined e.g. for a uniform linear array (ULA) as $\mathbf{a}(\theta) = [1, e^{j d\kappa \cos\theta}, e^{j 2d\kappa \cos\theta}, ..., e^{j(N-1)d\kappa\cos\theta}]^T$. Here, $\kappa = \frac{2\pi}{\lambda}$ where λ is the wavelength of the RF signal frequency. Further, the signal power in the receiver is given by

$$\mathbb{E}\left[|y(\theta)|^2\right] = \sigma_s^2 \left|\mathbf{a}^H(\theta)\mathbf{w}(\theta_\mathrm{d})\right|^2 + \sigma_n^2 \tag{3}$$

where $\sigma_s^2 = \mathbb{E}\left[|s|^2\right]$ denotes the signal power and $\sigma_n^2 = \mathbb{E}\left[|n|^2\right]$ is the noise power. Finally, the spatial response of the transmit beamformer with given precoding weights can be presented as the radiation pattern. It is defined as the spatial dependency of the received signal power seen by the receiver located in direction θ. Thus, the radiation pattern is given by

$$D(\theta) = \left|\mathbf{a}^H(\theta)\mathbf{w}(\theta_\mathrm{d})\right|^2. \tag{4}$$

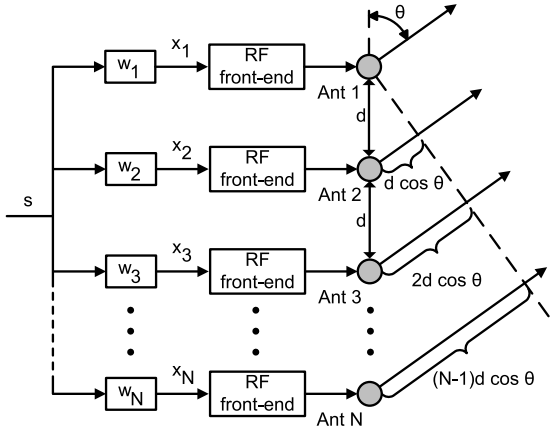

Fig. 1. The conceptual digital transmit beamformer and the used notation.

B. I/Q Imbalance in Transmitter

DCTs (also known as zero-IF transmitters) up-convert two real-valued baseband signals, namely in-phase (I) and quadrature-phase (Q) signals, straight to the RF frequency [12]. These RF signals are then combined and the resulting RF signal is finally amplified and transmitted through the antenna [15]. Ideally the up-conversion is done with two local oscillators (LOs) and mixers which have equal gains and exactly 90° phase difference. This is unfortunately not the case in practice resulting in gain and phase mismatches between the up-converted RF signals [13]. This effect is known as I/Q imbalance and can be modeled for a single radio chain at baseband equivalent level as [16]

$$x_\mathrm{imb}(t) = K_1 x(t) + K_2 x^*(t) \tag{5}$$

where $K_1 = (1 + ge^{j\phi})/2$ and $K_2 = (1 - ge^{j\phi})/2$. In addition, $x(t)$ is the baseband equivalent signal under perfect I/Q matching, and g and ϕ denote relative gain and phase mismatches in the transmitter chain, respectively. Note that the I/Q imbalance creates a WL transformation to the signal which is our main motivation for the WL processing discussed in Section II.C.

In an antenna array transmitter utilizing digital beamforming, several transmitter chains are used in parallel and the corresponding baseband equivalent signal snapshots (one for each transmitter chain) under transmitter I/Q imbalance can be modeled as

$$\begin{aligned}\mathbf{x}_\mathrm{imb} &= \mathbf{K}_1\mathbf{x} + \mathbf{K}_2\mathbf{x}^* \\ &= \left[\mathbf{K}_1, \mathbf{K}_2\right]\begin{bmatrix}\mathbf{w}(\theta_\mathrm{d}) & \mathbf{0}_N \\ \mathbf{0}_N & \mathbf{w}^*(\theta_\mathrm{d})\end{bmatrix}\begin{bmatrix}s \\ s^*\end{bmatrix}\end{aligned} \tag{6}$$

where matrices

$$\mathbf{K}_1 = \mathrm{diag}\left(K_{1,1}, K_{1,2}, ..., K_{1,N}\right) \quad (7)$$

$$\mathbf{K}_2 = \mathrm{diag}\left(K_{2,1}, K_{2,2}, ..., K_{2,N}\right) \quad (8)$$

present the I/Q imbalance coefficients of each parallel transmitter chain. The corresponding signal snapshot observed by the receiver in direction θ is then given by

$$\begin{aligned} y_{\text{imb}}(\theta) &= \mathbf{a}^H(\theta)\mathbf{x}_{\text{imb}} + n \\ &= \mathbf{a}^H(\theta)\left[\mathbf{K}_1, \mathbf{K}_2\right]\begin{bmatrix}\mathbf{w}(\theta_\text{d}) & \mathbf{0}_N \\ \mathbf{0}_N & \mathbf{w}^*(\theta_\text{d})\end{bmatrix}\begin{bmatrix}s \\ s^*\end{bmatrix} + n \\ &= \mathbf{a}^H(\theta)\mathbf{K}_1\mathbf{w}(\theta_\text{d})s + \mathbf{a}^H(\theta)\mathbf{K}_2\mathbf{w}^*(\theta_\text{d})s^* + n. \end{aligned} \quad (9)$$

This result means that the received signal is on the one hand corrupted by the common response $\mathbf{K}_1$ and on the other hand suffers from the self interference due to the complex conjugate term. Since in realistic scenarios $|K_{1,i}| \gg |K_{2,i}| \; \forall \, i$ [16] and $\left|\mathbf{a}^H(\theta)\mathbf{w}(\theta_\text{d})\right| \gg \left|\mathbf{a}^H(\theta)\mathbf{w}^*(\theta_\text{d})\right|$, the self interference term is weak but cannot be neglected, especially with high-order modulations. Actually, the self interference creates a twist to the constellation diagram and the symbol detection in the receiver side becomes more difficult.

To quantify the signal properties further, the power of the received signal under transmitter I/Q imbalance is written as

$$\begin{aligned} \mathbb{E}\left[\left|y_{\text{imb}}(\theta)\right|^2\right] &= \sigma_s^2\left|\mathbf{a}^H(\theta)\mathbf{K}_1\mathbf{w}(\theta_\text{d})\right|^2 \\ &\quad + \sigma_s^2\left|\mathbf{a}^H(\theta)\mathbf{K}_2\mathbf{w}^*(\theta_\text{d})\right|^2 + \sigma_n^2. \end{aligned} \quad (10)$$

In addition, the radiation pattern of the transmit beamformer under I/Q imbalance can be given by

$$D_{\text{imb}}(\theta) = \left|\mathbf{a}^H(\theta)\mathbf{K}_1\mathbf{w}(\theta_\text{d})\right|^2 + \left|\mathbf{a}^H(\theta)\mathbf{K}_2\mathbf{w}^*(\theta_\text{d})\right|^2. \quad (11)$$

It is clear that I/Q imbalance is affecting the radiation properties since the coefficients $\mathbf{K}_1$ and $\mathbf{K}_2$ are present in (11). More importantly, the latter term, which is totally new compared to (4), includes conjugated precoding weight $\mathbf{w}^*(\theta_\text{d})$. Interestingly in case of ULAs and equal I/Q imbalance in all transmitter branches, this creates an additional beam to the mirror direction $180° - \theta$ as is shown in Section IV. This is of course a harmful effect and should be suppressed, especially if null-steering towards the mirror-angle is targeted.

C. Widely-Linear Beamforming

WL processing precodes not only the signal s itself but also its complex conjugate s^* with individual weights [17] as follows

$$\tilde{\mathbf{x}} = \mathbf{W}(\theta_\text{d})\tilde{\mathbf{s}} = \left[\mathbf{w}_1(\theta_\text{d}), \mathbf{w}_2(\theta_\text{d})\right]\begin{bmatrix}s \\ s^*\end{bmatrix}. \quad (12)$$

Here, the weight matrix $\mathbf{W} = [\mathbf{w}_1(\theta_\text{d}), \mathbf{w}_2(\theta_\text{d})] \in \mathbb{C}^{N\times 2}$ and the augmented signal vector $\tilde{\mathbf{s}} = [s, s^*]^T \in \mathbb{C}^{2\times 1}$. Weights $\mathbf{w}_1(\theta_\text{d})$ and $\mathbf{w}_2(\theta_\text{d})$ are the WL precoding weights for the signal snapshot and its complex conjugate, respectively, optimized under a given optimization criteria towards the desired direction θ_d. The conceptual WL digital transmit beamformer is depicted in Fig. 2. The corresponding signal snapshot observed by the receiver in direction θ is equal to

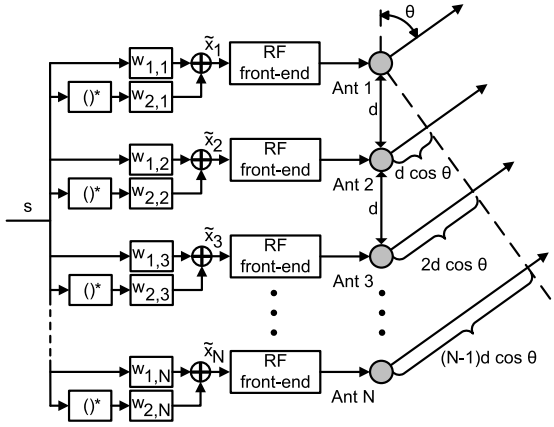

Fig. 2. The conceptual WL digital transmit beamformer.

$$\begin{aligned} \tilde{y}(\theta) &= \mathbf{a}^H(\theta)\tilde{\mathbf{x}} + n \\ &= \mathbf{a}^H(\theta)\left[\mathbf{w}_1(\theta_\text{d}), \mathbf{w}_2(\theta_\text{d})\right]\begin{bmatrix}s \\ s^*\end{bmatrix} + n \\ &= \mathbf{a}^H(\theta)\mathbf{w}_1(\theta_\text{d})s + \mathbf{a}^H(\theta)\mathbf{w}_2(\theta_\text{d})s^* + n. \end{aligned} \quad (13)$$

In case of circular signals, the conjugate of the signal does not include any additional information for the beamforming and thus WL processing does not offer significant performance gain, when perfect RF hardware with perfect I/Q balance is assumed. However, since I/Q imbalance structurally creates WL transformation to the signal, WL beamforming becomes a natural choice for the beamforming problem under I/Q imbalance. It results in doubled computational load (compared to the linear case) but also offers doubled degrees of freedom for the I/Q imbalance mitigation, and makes separate I/Q calibration loops in parallel transmit chains unnecessary.

The baseband equivalent transmit signal snapshots obtained by WL precoding under I/Q imbalance are modeled as

$$\begin{aligned} \tilde{\mathbf{x}}_{\text{imb}} &= \mathbf{K}_1\tilde{\mathbf{x}} + \mathbf{K}_2\tilde{\mathbf{x}}^* \\ &= \left[\mathbf{K}_1, \mathbf{K}_2\right]\begin{bmatrix}\mathbf{w}_1(\theta_\text{d}) & \mathbf{w}_2(\theta_\text{d}) \\ \mathbf{w}_2^*(\theta_\text{d}) & \mathbf{w}_1^*(\theta_\text{d})\end{bmatrix}\begin{bmatrix}s \\ s^*\end{bmatrix}. \end{aligned} \quad (14)$$

Further, the corresponding signal snapshot observed by the receiver in direction θ is now equal to

$$\begin{aligned} \tilde{y}_{\text{imb}}(\theta) &= \mathbf{a}^H(\theta)\tilde{\mathbf{x}}_{\text{imb}} + n \\ &= \mathbf{a}^H(\theta)\left[\mathbf{K}_1, \mathbf{K}_2\right]\begin{bmatrix}\mathbf{w}_1(\theta_\text{d}) & \mathbf{w}_2(\theta_\text{d}) \\ \mathbf{w}_2^*(\theta_\text{d}) & \mathbf{w}_1^*(\theta_\text{d})\end{bmatrix}\begin{bmatrix}s \\ s^*\end{bmatrix} + n \\ &= \mathbf{a}^H(\theta)\left(\mathbf{K}_1\mathbf{w}_1(\theta_\text{d}) + \mathbf{K}_2\mathbf{w}_2^*(\theta_\text{d})\right)s \\ &\quad + \mathbf{a}^H(\theta)\left(\mathbf{K}_1\mathbf{w}_2(\theta_\text{d}) + \mathbf{K}_2\mathbf{w}_1^*(\theta_\text{d})\right)s^* + n. \end{aligned} \quad (15)$$

Still, both s and s^* exist in the received signal but now with a more flexible weighting than in the plain linear case. In fact, with proper transmit weight selection it is now possible to

eliminate the conjugated term completely while preserving the desired term, which is not possible with the linear beamformer.

The power of the received signal under transmit I/Q imbalance is now given by

$$\mathbb{E}\left[\left|\tilde{y}_{\text{imb}}(\theta)\right|^2\right] = \sigma_s^2 \left|\mathbf{a}^H(\theta)\left(\mathbf{K}_1\mathbf{w}_1(\theta_\text{d}) + \mathbf{K}_2\mathbf{w}_2^*(\theta_\text{d})\right)\right|^2 + \sigma_s^2 \left|\mathbf{a}^H(\theta)\left(\mathbf{K}_1\mathbf{w}_2(\theta_\text{d}) + \mathbf{K}_2\mathbf{w}_1^*(\theta_\text{d})\right)\right|^2 + \sigma_n^2. \quad (16)$$

Finally, the radiation pattern of the WL beamformer under I/Q imbalance is equal to

$$\tilde{D}_{\text{imb}}(\theta) = \left|\mathbf{a}^H(\theta)\left(\mathbf{K}_1\mathbf{w}_1(\theta_\text{d}) + \mathbf{K}_2\mathbf{w}_2^*(\theta_\text{d})\right)\right|^2 + \left|\mathbf{a}^H(\theta)\left(\mathbf{K}_1\mathbf{w}_2(\theta_\text{d}) + \mathbf{K}_2\mathbf{w}_1^*(\theta_\text{d})\right)\right|^2. \quad (17)$$

Here, the first term presents the power of the wanted signal term whereas the latter term is due to the unwanted conjugated signal term. Therefore, the magnitude of the first term should be maximized (under the maximum output power constraints) while the latter term should be attenuated as much as possible in order to minimize the spurious responses. This will be addressed next, including also additional null-steering constraints towards PUs.

III. RF-Aware WL Null-Steering Beamforming

A. Conventional Null-Steering Method

Beamforming methods which have the wanted response characteristics to the desired direction while minimizing the transmitted power to the forbidden direction(s) (or the received power from the interference source direction), are commonly referred as null-steering beamforming methods [18]–[20]. The conventional null-steering approach for the transmitter side can be formulated as

$$\max_{\mathbf{w}} \left|\mathbf{w}^H\mathbf{a}(\theta_\text{d})\right|^2 \quad \text{subject to} \quad \begin{cases} \mathbf{w}^H\mathbf{A} & = \mathbf{0} \\ \mathbf{w}^H\mathbf{w} & \leq \sqrt{\alpha} \end{cases} \quad (18)$$

where $\mathbf{A} = [\mathbf{a}(\theta_{\text{PU},1}), \mathbf{a}(\theta_{\text{PU},2}), \cdots, \mathbf{a}(\theta_{\text{PU},M})] \in \mathbb{C}^{N\times M}$ is the null-steering matrix consisting of steering vectors for M PU directions [10]. The transmitted power of the array is equal to $\alpha\sigma_s^2$. The classical optimum solution for the optimization task above is given by

$$\mathbf{w}_{\text{NS}} = \frac{\sqrt{\alpha}}{||(\mathbf{I} - \mathbf{P}_\text{A})\,\mathbf{a}(\theta_\text{d})||}\left(\mathbf{I} - \mathbf{P}_\text{A}\right)\mathbf{a}(\theta_\text{d}) \quad (19)$$

where $\mathbf{I} \in \mathbb{C}^{N\times N}$ is an identity matrix and $\mathbf{P}_\mathbf{A} \in \mathbb{C}^{N\times N}$, defined as

$$\mathbf{P}_\text{A} = \mathbf{A}\left[\mathbf{A}^H\mathbf{A}\right]^{-1}\mathbf{A}^H, \quad (20)$$

is the orthogonal projection matrix onto the subspace spanned by the columns of $\mathbf{A}$. Intuitively, the solution corresponds to the spatial matched filter solution with additional null-steering constraints. However, this method cannot take transmitter I/Q imbalance into account and is therefore suffering from the problems discussed in Section II.B. This gives us the motivation to develope a WL beamforming method, which is not only mitigating the unwanted I/Q imbalance effects but also steering nulls towards the forbidden PU directions.

B. Proposed RF-Aware WL Null-Steering Method

I/Q imbalance corrupts the output of the beamformer as shown in (15). In order to eliminate this unwanted behavior without individual I/Q imbalance cancellation in all parallel transmitter branches, the null-steering method has to be modified. Based on (17), the requirements for all PU directions $\theta_{\text{PU},i},\ i = 1, ..., M$ should be set as

$$\mathbf{a}^H(\theta_{\text{PU},i})\mathbf{K}_1\mathbf{w}_1 + \mathbf{a}^H(\theta_{\text{PU},i})\mathbf{K}_2\mathbf{w}_2^* = 0 \quad (21)$$

$$\mathbf{a}^H(\theta_{\text{PU},i})\mathbf{K}_1\mathbf{w}_2 + \mathbf{a}^H(\theta_{\text{PU},i})\mathbf{K}_2\mathbf{w}_1^* = 0. \quad (22)$$

Now, we can take conjugate transpose of (21) and transpose of (22). Then after reorganizing terms, the requirements can be given by

$$\mathbf{w}_1^H\mathbf{K}_1^H\mathbf{a}(\theta_{\text{PU},i}) + \mathbf{w}_2^T\mathbf{K}_2^H\mathbf{a}(\theta_{\text{PU},i}) = 0 \quad (23)$$

$$\mathbf{w}_1^H\mathbf{K}_2^T\mathbf{a}^*(\theta_{\text{PU},i}) + \mathbf{w}_2^T\mathbf{K}_1^T\mathbf{a}^*(\theta_{\text{PU},i}) = 0 \quad (24)$$

which can be further combined and expressed as

$$\tilde{\mathbf{w}}^H\tilde{\mathbf{A}}(\theta_{\text{PU},i}) = \begin{bmatrix} \mathbf{w}_1 \\ \mathbf{w}_2^* \end{bmatrix}^H \begin{bmatrix} \mathbf{K}_1^H\mathbf{a}(\theta_{\text{PU},i}) & \mathbf{K}_2^T\mathbf{a}^*(\theta_{\text{PU},i}) \\ \mathbf{K}_2^H\mathbf{a}(\theta_{\text{PU},i}) & \mathbf{K}_1^T\mathbf{a}^*(\theta_{\text{PU},i}) \end{bmatrix} = \mathbf{0}_{1\times 2} \quad (25)$$

where $\tilde{\mathbf{w}} \in \mathbb{C}^{2N\times 1}$ and $\tilde{\mathbf{A}}(\theta_{\text{PU},i}) \in \mathbb{C}^{2N\times 2}$. In addition to the null-steering, we also want to eliminate the self interference of the signal, i.e the conjugated signal term in (15). This can be interpreted as an additional null constraint given by

$$\tilde{\mathbf{w}}^H\tilde{\mathbf{a}}_{\text{SI}}(\theta_\text{d}) = \tilde{\mathbf{w}}^H \begin{bmatrix} \mathbf{K}_2^T\mathbf{a}^*(\theta_\text{d}) \\ \mathbf{K}_1^T\mathbf{a}^*(\theta_\text{d}) \end{bmatrix} = 0 \quad (26)$$

where $\tilde{\mathbf{a}}_{\text{SI}}(\theta_\text{d}) \in \mathbb{C}^{2N\times 1}$. Now the final null-steering matrix $\tilde{\mathbf{A}} \in \mathbb{C}^{2N\times 2M+1}$, including the PU null-steering constraints as well as the self-interference elimination, can be given by

$$\tilde{\mathbf{A}} = \left[\tilde{\mathbf{A}}(\theta_{\text{PU},1}), \tilde{\mathbf{A}}(\theta_{\text{PU},2}), \cdots, \tilde{\mathbf{A}}(\theta_{\text{PU},M}), \tilde{\mathbf{a}}_{\text{SI}}(\theta_\text{d})\right]. \quad (27)$$

Then, based on the previous sub-section, the proposed RF-aware WL null-steering method can be seen as maximizing the first term in (17) under the null-steering constraints in $\tilde{\mathbf{A}}$, or equivalently expressed as

$$\max_{\mathbf{w}} \left|\tilde{\mathbf{w}}^H\tilde{\mathbf{a}}(\theta_\text{d})\right|^2 \quad \text{subject to} \quad \begin{cases} \tilde{\mathbf{w}}^H\tilde{\mathbf{A}} & = \mathbf{0} \\ \tilde{\mathbf{w}}^H\tilde{\mathbf{w}} & \leq \sqrt{\tilde{\alpha}} \end{cases} \quad (28)$$

where $\tilde{\mathbf{a}}(\theta_\text{d}) = \left[\left(\mathbf{K}_1^H\mathbf{a}(\theta_\text{d})\right)^T, \left(\mathbf{K}_2^H\mathbf{a}(\theta_\text{d})\right)^T\right]^T \in \mathbb{C}^{2N\times 1}$. Note that this is an augmented version of the conventional null-steering method. The optimum solution for this optimization task is given by

$$\tilde{\mathbf{w}}_{\text{NS}} = \frac{\sqrt{\tilde{\alpha}}}{||(\mathbf{I} - \mathbf{P}_{\tilde{\text{A}}})\,\tilde{\mathbf{a}}(\theta_\text{d})||}\left(\mathbf{I} - \mathbf{P}_{\tilde{\text{A}}}\right)\tilde{\mathbf{a}}(\theta_\text{d}). \quad (29)$$

Here, $\mathbf{P}_{\tilde{\text{A}}} \in \mathbb{C}^{2M+1\times 2M+1}$ is the orthogonal projection matrix (based on the augmented null-steering matrix) and is given by

$$\mathbf{P}_{\tilde{\text{A}}} = \tilde{\mathbf{A}}\left[\tilde{\mathbf{A}}^H\tilde{\mathbf{A}}\right]^{-1}\tilde{\mathbf{A}}^H. \quad (30)$$

Finally, for any given weights $\tilde{\mathbf{w}}$, the transmit power of the array is $\left(||\mathbf{K}_1\mathbf{w}_1 + \mathbf{K}_2\mathbf{w}_2^*||^2 + ||\mathbf{K}_1\mathbf{w}_2 + \mathbf{K}_2\mathbf{w}_1^*||^2\right)\sigma_s^2$. Thus

for any $\tilde{\alpha}$ used in (29), appropriate weight scaling can always be easily determined to set the desired total transmit power.

Note that the solution obtained by (29) automatically deploys the RF imperfection knowledge properly to suppress unwanted degradation of the radiation pattern. As a consequence, the actual I/Q imbalance cancellation in the parallel transmitter branches is not needed at all. In practice, the information of RF imperfections can be obtained, e.g. with the help of feedback loops which are anyways present in the transmitter hardware due to e.g. gain control.

Finally, the WL null-steering weight matrix $\mathbf{W}_{\text{NS}}(\theta_{\text{d}}) \in \mathbb{C}^{N\times 2}$, to be used for signal precoding under I/Q imbalance, is given by

$$\mathbf{W}_{\text{NS}}(\theta_{\text{d}}) = [\tilde{\mathbf{w}}_{\text{NS}}(1:N), \tilde{\mathbf{w}}^{*}_{\text{NS}}(N+1:2N)]\,. \qquad (31)$$

The results of this method compared with the conventional null-steering method with and without I/Q imbalance are next illustrated using computer simulations.

IV. Simulations and Numerical Examples

Numerical examples and performance results are based on MATLAB simulations where an ULA with 8 antenna elements is used. The element spacing d is equal to half of the RF signal wavelength λ. The desired direction is selected to be $\theta_{\text{d}} = 130°$, while the forbidden PU directions are equal to $\theta_{\text{PU},1} = 50°$ and $\theta_{\text{PU},2} = 95°$. Since the information of the PU directions is based on e.g. DOA estimation which is not necessarily exact, two additional null constraints are set around ($\pm 2°$) the actual PU directions. The total transmit power is set to be equal to 1 for both beamforming methods.

I/Q imbalance in the RF chains is implemented in two different ways; as a random unequal I/Q imbalance in the transmitter branches (g and ϕ are uniformly distributed in the range of 0.85–1.15 and -15–15°, respectively), and as a systematic I/Q imbalance where the I/Q imbalance coefficients are equal in all transmitter branches (g is 0.85 and ϕ is 15°). In the former case, all parallel transmitter branches have their own hardware which is the most probable solution in distributed array structures. In the latter case, transmitter branches are sharing hardware resources, such as RF LO. In reality, the behavior is most likely somewhere in-between, that is I/Q imbalance has common and independent subcomponents (from one transmitter branch to another). However, these two scenarios represent the two limiting cases.

Fig. 3 shows the radiation pattern of the conventional null-steering method in case of random I/Q imbalance. The response to the desired direction is well maintained but the nulls towards the PUs are even 58 dB weaker than without I/Q imbalance. This means that the beamformer is effectively transmitting energy to the forbidden PU directions and thus causing severe interference to the primary communication system. This can be prevented by using the proposed WL null-steering method whose results are depicted in Fig. 4. The results show that the desired radiation characteristics are now well maintained, not only to the desired direction, but also to the forbidden PU directions.

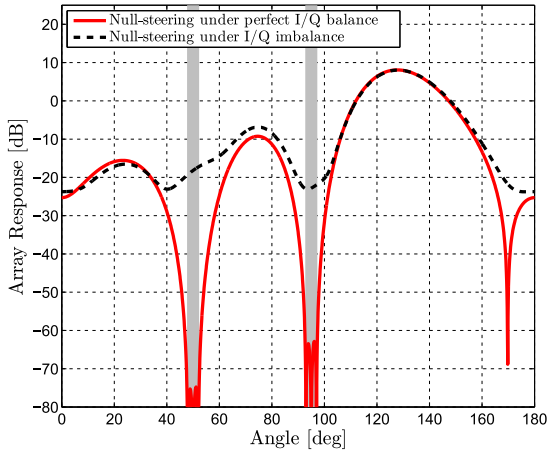

Fig. 3. Radiation patterns of the conventional null-steering method under random I/Q imbalance, 8 antenna elements. $\theta_{\text{d}} = 130°$, $\theta_{\text{PU},1} = 50° \pm 2°$ and $\theta_{\text{PU},2} = 95° \pm 2°$.

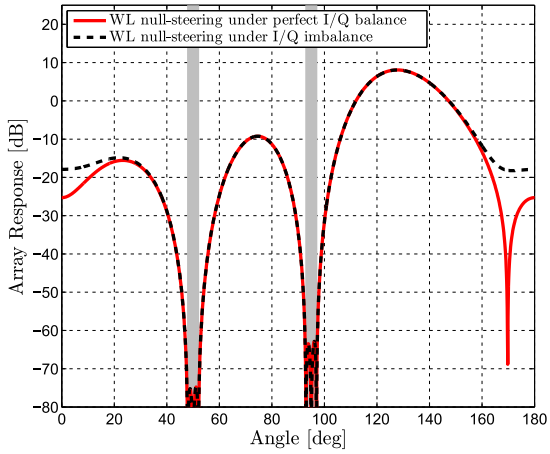

Fig. 4. Radiation patterns of the proposed WL null-steering method under random I/Q imbalance, 8 antenna elements. $\theta_{\text{d}} = 130°$, $\theta_{\text{PU},1} = 50° \pm 2°$ and $\theta_{\text{PU},2} = 95° \pm 2°$.

The radiation pattern of the conventional null-steering method under systematic I/Q imbalance is illustrated in Fig. 5. Again, the classical beamformer is transmitting more energy to both PU directions than without I/Q imbalance. The most severe problem is the mirror direction $180° - \theta_{\text{d}}$ where a strong mirror peak can be seen. This is actually due to the existence of the conjugated precoding weights in (11). In addition, the beamformer loses 0.8 dB of its gain to the desired direction due to the scaling of the first term in (11) with $\mathbf{K}_1$. The results of the proposed WL null-steering method are depicted in Fig. 6. They show, again, that the proposed method is able to maintain the wanted radiation characteristics to the desired direction while steering strong nulls towards the PUs.

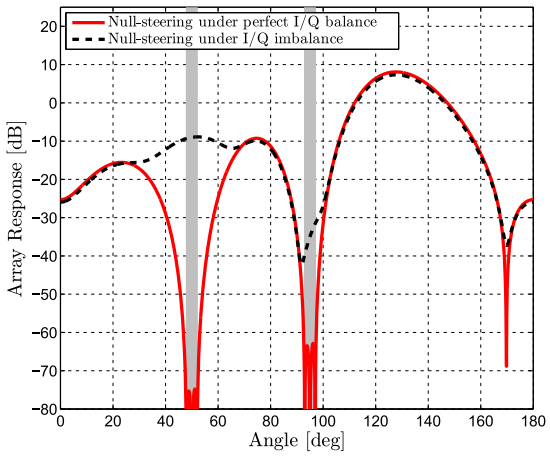

Fig. 5. Radiation patterns of the conventional null-steering method under systematic I/Q imbalance, 8 antenna elements. $\theta_{\mathrm{d}} = 130°$, $\theta_{\mathrm{PU},1} = 50° \pm 2°$ and $\theta_{\mathrm{PU},2} = 95° \pm 2°$.

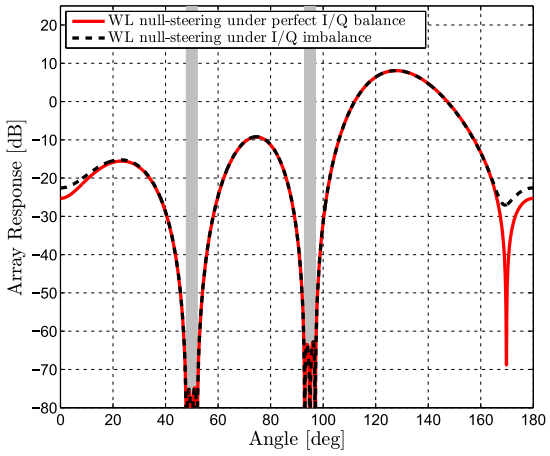

Fig. 6. Radiation patterns of the proposed WL null-steering method under systematic I/Q imbalance, 8 antenna elements. $\theta_{\mathrm{d}} = 130°$, $\theta_{\mathrm{PU},1} = 50° \pm 2°$ and $\theta_{\mathrm{PU},2} = 95° \pm 2°$.

V. Conclusion

Transmitter digital beamforming and null-steering characteristics are heavily affected by the imperfections in the associated RF circuits. In this paper, effects of one common RF imperfection, namely I/Q imbalance, were studied. Firstly, closed-form analysis of the available beamforming and null-steering capabilities under RF I/Q imbalance was carried out. Secondly, the RF-aware WL beamforming method was proposed and formulated for suppressing the unwanted behavior due to RF I/Q imbalance without individual I/Q imbalance cancellation in all parallel transmitter branches. Simulation results under random as well as systematic I/Q imbalance showed that the proposed WL beamforming method successfully mitigates the unwanted I/Q imbalance effects and thus restores the wanted radiation properties, despite of imperfect RF circuits, whereas the conventional null-steering method loses its capabilities to steer strong nulls towards forbidden directions. This offers an efficient null-steering solution for SU transmitters in cognitive radio systems such that efficient interference protection towards PUs can be maintained even if operating with low cost RF chains that are commonly subject to substantial RF imperfections.

References

[1] M. Islam et al, "Spectrum survey in Singapore: Occupancy measurements and analyses," in *Proc. CROWNCOM 2008*, May 2008, pp. 1 –7.

[2] V. Valenta et al., "Towards cognitive radio networks: Spectrum utilization measurements in suburb environment," in *Proc. IEEE RWS 2009*, Jan. 2009, pp. 352 –355.

[3] M. Lopez-Benitez, A. Umbert, and F. Casadevall, "Evaluation of spectrum occupancy in Spain for cognitive radio applications," in *Proc. 69th IEEE VTC 2009.*, Apr. 2009, pp. 1 –5.

[4] T. Taher et al., "Dynamic spectrum access opportunities for public safety in land mobile radio bands," in *Proc. CROWNCOM 2011*, Jun. 2011, pp. 355 –359.

[5] K. Patil et al., "Spectrum occupancy statistics in the context of cognitive radio," in *Proc. 14th International Symposium on Wireless Personal Multimedia Communications*, Oct. 2011, pp. 1 –5.

[6] S. Haykin, "Cognitive radio: brain-empowered wireless communications," *IEEE J. Sel. Areas Commun.*, vol. 23, no. 2, pp. 201 – 220, Feb. 2005.

[7] R. Martin and R. Thomas, "Algorithms and bounds for estimating location, directionality, and environmental parameters of primary spectrum users," *IEEE Trans. Wireless Commun.*, vol. 8, no. 11, pp. 5692 –5701, Nov. 2009.

[8] F. Penna and D. Cabric, "Bounds and tradeoffs for cooperative DoA-Only localization of primary users," in *Proc. IEEE GLOBECOM 2011*, Dec. 2011, pp. 1 –5.

[9] L. De Nardis, M. Di Benedetto, A. Akhtar, and O. Holland, "Combination of DOA and beamforming in position-based routing for underlay cognitive wireless networks," in *Proc. CROWNCOM 2012*, Jun. 2012, pp. 218 –223.

[10] K. Zarifi, S. Affes, and A. Ghrayeb, "Collaborative null-steering beamforming for uniformly distributed wireless sensor networks," *IEEE Trans. Signal Process.*, vol. 58, no. 3, pp. 1889 –1903, Mar. 2010.

[11] D. Piazza, D. Michele, and K. Dandekar, "Two port reconfigurable CRLH leaky wave antenna with improved impedance matching and beam tuning," in *Proc. 3rd European Conference on Antennas and Propagation, 2009.*, Mar. 2009, pp. 2046 –2049.

[12] S. Mirabbasi and K. Martin, "Classical and modern receiver architectures," *IEEE Commun. Mag.*, vol. 38, no. 11, pp. 132 – 139, Nov. 2000.

[13] T. Schenk and J.-P. Linnartz, *RF Imperfections in High-Rate Wireless Systems: Impact and Digital Compensation*. Springer, 2008.

[14] K. Karakayali et al., "Optimum zero-forcing beamforming with per-antenna power constraints," in *Proc. IEEE ISIT 2007*, Jun., pp. 101–105.

[15] B. Razavi, "RF transmitter architectures and circuits," in *Proc. IEEE Custom Integrated Circuits, 1999.*, 1999, pp. 197 –204.

[16] L. Anttila, M. Valkama, and M. Renfors, "Frequency-selective I/Q mismatch calibration of wideband direct-conversion transmitters," *IEEE Trans. Circuits Syst. II, Exp. Briefs*, vol. 55, no. 4, pp. 359 –363, Apr. 2008.

[17] D. Darsena et al., "Widely-linear beamforming/combining techniques for MIMO wireless systems," in *Proc. ISCCSP 2012*, May, pp. 1–5.

[18] M. Y. Frankel and R. D. Esman, "Dynamic null steering in an ultra-wideband time-steered array antenna," *Applied Optics*, vol. 37, no. 23, pp. 5488–5494, Aug. 1998.

[19] B. Friedlander and B. Porat, "Performance analysis of a null-steering algorithm based on direction-of-arrival estimation," *IEEE Trans. Acoust., Speech, Signal Process.*, vol. 37, no. 4, pp. 461 –466, Apr. 1989.

[20] L. Godara, "Application of antenna arrays to mobile communications. II. beam-forming and direction-of-arrival considerations," *Proc. IEEE*, vol. 85, no. 8, pp. 1195 –1245, Aug. 1997.

Publication 3

A. Hakkarainen, J. Werner, M. Renfors, K. Dandekar, and M. Valkama, "RF-Aware Widely-Linear MMSE Beamforming," in *Proceedings of the 10th International Symposium on Wireless Communication Systems (ISWCS)*, Ilmenau, Germany, 27–30 Aug. 2013. ISBN: 978-3-8007-3529-7.

RF-Aware Widely-Linear MMSE Beamforming

Aki Hakkarainen*, Janis Werner*, Markku Renfors*, Kapil Dandekar† and Mikko Valkama*
*Department of Electronics and Communications Engineering, Tampere University of Technology, Tampere, Finland
Emails: {aki.hakkarainen, janis.werner, markku.renfors, mikko.e.valkama}@tut.fi
†Department of Electrical and Computer Engineering, Drexel University, Philadelphia, PA 19104, USA
Email: dandekar@drexel.edu

***Abstract*—Beamforming offers good spatial resolution for the wireless communication systems and thus enables sophisticated transmission and interference suppression scenarios. In this paper, data-aided receiver beamforming is studied under practical limitations in the associated radio frequency (RF) circuits, namely the amplitude and phase imbalance between the in-phase and quadrature-phase (I/Q) rails. Closed-form analysis of the available beamforming capabilities is provided, showing that the beamformer performance degrades heavily due to the I/Q imbalance. Motivated by the widely-linear (WL) structure of the I/Q imbalance, we then propose deploying data-aided WL minimum mean squared error (MMSE) beamforming solution for the beamforming task. Simulation results show that the proposed WL beamforming solution is able to efficiently suppress the unwanted I/Q imbalance effects and thus provides good overall performance, even under severe imperfections in the RF circuits.**

***Keywords*—adaptive signal processing, antenna arrays, antenna radiation patterns, beam steering, circular signals, I/Q imbalance, radio transceivers, widely-linear processing**

I. Introduction

The ever-increasing demands for the wireless communication systems are contradicting with the limitations in the available physical communication resources, e.g. frequency, time and space. One promising solution for the problem is beamforming where communication devices steer their transmission and/or reception to the desired direction under given optimization requirements. Beamforming can be implemented in several ways, e.g. with antenna arrays combined with digital signal processing [1]. However, such digital beamforming needs multiple parallel transceiver chains and thus the size and total cost of the hardware can increase significantly. In this paper, we focus on the receiver side digital beamforming under practical RF circuit imperfections.

For decreasing the hardware size and cost, the direct-conversion receiver (DCR) [2] can be used. It is flexible and it does not require RF image rejection filter nor intermediate frequency stages. Thus, it also has a lower implementation cost and smaller size than e.g. the classical super-heterodyne receiver [3]. However, it is commonly known that DCR suffers from the imperfections in the associated RF circuits, e.g. I/Q imbalance [2]. The mitigation of I/Q imbalance is widely studied for single radio chains, e.g. in [4], but the effects of such RF imperfections in beamforming have not been studied systematically so far.

In this paper, we continue the authors' work in [5] where very preliminary results for I/Q imbalance mitigation were given. At first, in this paper, radiation properties of the beamformer are given in closed-form and the effects of I/Q imbalance on the radiation characteristics are studied. Then, motivated by the WL structure of the I/Q imbalance, the WL MMSE beamforming principle is proposed. This way, I/Q imbalance can be taken into account in the beamforming process and thus separate I/Q imbalance calibration in individual receiver chains is not needed. It is shown by the simulation results that the proposed WL beamforming provides significant performance improvements under RF I/Q imbalance compared to the corresponding linear beamforming methods. It should be noticed that WL beamforming has certainly been proposed earlier in the literature, e.g. in [6]–[8]. However, the focus in prior work has been on processing of non-circular signals or interference while here we deploy the increased degrees of freedom and modeling capabilities of WL beamforming to explicitly suppress RF circuit imperfections in the beamforming process. Hence we call it RF-aware WL beamforming.

The rest of this paper is organized as follows. In Section 2, a short review for the signal and array models is given. Then, in Section 3, we present optimal linear and WL MMSE solutions for the beamforming task with and without RF I/Q imbalance. In Section 4, numerical examples and simulation results are given and finally, in Section 5, the paper is concluded.

Notation: Throughout the paper, vectors and matrices are written in bold. The superscripts $(\cdot)^T$, $(\cdot)^H$, $(\cdot)^*$ and $(\cdot)^{-1}$ represent transpose, hermitian (conjugate) transpose, conjugate and matrix inverse, respectively. The tilde sign $\sim$ above variables is used to present a WL (augmented) quantity and the results obtained by the WL processing. The statistical expectation is denoted with $\mathbb{E}[\cdot]$. A complex random variable x is called circular if $\mathbb{E}[x^2] = 0$.

II. Fundamental Signal and Array Models

A. Digital Linear Beamformer Response

The received baseband signal snapshots $\mathbf{x} = [x_1, x_2, ..., x_N] \in \mathbb{C}^{N\times 1}$ of a beamformer with N antenna elements can be presented as [7]

$$\mathbf{x} = s\mathbf{a}(\theta) + \mathbf{n}. \quad (1)$$

Here, s is the arriving signal and $\mathbf{a}(\theta) \in \mathbb{C}^{N\times 1}$ is the steering vector defined e.g. for a uniform linear array (ULA) as $\mathbf{a}(\theta) = [1, e^{jd\kappa\cos\theta}, e^{j2d\kappa\cos\theta}, ..., e^{j(N-1)d\kappa\cos\theta}]^T$. The wavenumber $\kappa = \frac{2\pi}{\lambda}$ where λ is the RF signal wavelength.

This work was supported by the Finnish Funding Agency for Technology and Innovation (Tekes) under the project "Reconfigurable Antenna-based Enhancement of Dynamic Spectrum Access Algorithms", the Industrial Research Fund of Tampere University of Technology (Tuula and Yrjö Neuvo Fund), the Academy of Finland under the project 251138 "Digitally-Enhanced RF for Cognitive Radio Devices", and the Doctoral Programme of the President of Tampere University of Technology.

The work was also supported by National Science Foundation (NSF) under award number 1147838.

In addition, $\mathbf{n} \in \mathbb{C}^{N\times 1}$ models the additive white Gaussian noise (AWGN) in the receiver. Noise components are assumed to be complex circular and mutually uncorrelated.

When the received signal snapshots are combined with a digital linear beamformer, the output signal is given by [1]

$$y = \mathbf{w}^H \mathbf{x} \tag{2}$$

where $\mathbf{w} = [w_1, w_2, ..., w_N]^T \in \mathbb{C}^{N\times 1}$ refers to the combining weights. The output signal can be further presented as a function of direction θ by

$$y(\theta) = \mathbf{w}^H(\theta_\mathrm{d})\mathbf{x} = s\mathbf{w}^H(\theta_\mathrm{d})\mathbf{a}(\theta) + \mathbf{w}^H(\theta_\mathrm{d})\mathbf{n} \tag{3}$$

where $\mathbf{w}(\theta_\mathrm{d})$ stand for the weights optimized under a given optimization criteria towards the desired direction θ_d (here d denotes "desired"). The power of this output signal is then given by

$$\mathbb{E}\left[|y(\theta)|^2\right] = \sigma_s^2 \left|\mathbf{w}^H(\theta_\mathrm{d})\mathbf{a}(\theta)\right|^2 + \mathbf{w}^H(\theta_\mathrm{d})\mathbf{R_n}\mathbf{w}(\theta_\mathrm{d}) \tag{4}$$

where $\sigma_s^2 = \mathbb{E}\left[|s|^2\right]$ is the signal power and $\mathbf{R_n} = \mathbb{E}\left[\mathbf{n}\mathbf{n}^H\right] \in \mathbb{C}^{N\times N}$ is the covariance matrix of the noise.

Finally, the spatial response of the beamformer can be presented as the radiation pattern. It is defined for given weights as the spatial dependency of the received signal power. The radiation pattern under the practical assumption of uncorrelated signal and noise is presented by

$$D(\theta) = \left|\mathbf{w}^H(\theta_d)\mathbf{a}(\theta)\right|^2. \tag{5}$$

B. RF I/Q Imbalance

DCR down-converts the received RF signal directly to two real-valued baseband signals, namely in-phase (I) and quadrature-phase (Q) signals [3]. Ideally, the conversion is done by two mixers with equal gains, and two local oscillator signals with exactly 90° phase difference. Unfortunately, this is not the case in practice and consequently I and Q signals have gain and phase mismatch [2]. This is called I/Q imbalance and can be modeled for an individual radio chain at baseband equivalent level as [4]

$$x_\mathrm{imb}(t) = K_1 x(t) + K_2 x^*(t) \tag{6}$$

where $x(t)$ is the baseband equivalent signal under perfect I/Q matching, and $K_1 = (1 + ge^{-j\phi})/2$ and $K_2 = (1 - ge^{j\phi})/2$. Further, g and ϕ denote the relative gain and phase mismatches between I and Q branches.

When beamforming is implemented by antenna arrays and digital combining, several receiver chains are used in parallel. Then, the received signal snapshots under I/Q imbalance are given by

$$\mathbf{x}_\mathrm{imb} = \mathbf{K}_1\mathbf{x} + \mathbf{K}_2\mathbf{x}^* = [\mathbf{K}_1, \mathbf{K}_2]\begin{bmatrix} s\mathbf{a}(\theta) + \mathbf{n} \\ s^*\mathbf{a}^*(\theta) + \mathbf{n}^* \end{bmatrix} \tag{7}$$

where matrices $\mathbf{K}_1 = \mathrm{diag}\left(K_{1,1}, K_{1,2}, ..., K_{1,N}\right)$ and $\mathbf{K}_2 = \mathrm{diag}\left(K_{2,1}, K_{2,2}, ..., K_{2,N}\right)$ present I/Q imbalance coefficients of each parallel receiver chain. The resulting output signal of the beamformer is then given by

$$\begin{aligned} y_\mathrm{imb}(\theta) &= \mathbf{w}^H(\theta_\mathrm{d})\mathbf{x}_\mathrm{imb} \\ &= \mathbf{w}^H(\theta_\mathrm{d})\left[\mathbf{K}_1, \mathbf{K}_2\right]\begin{bmatrix} s\mathbf{a}(\theta) + \mathbf{n} \\ s^*\mathbf{a}^*(\theta) + \mathbf{n}^* \end{bmatrix} \\ &= \mathbf{w}^H(\theta_\mathrm{d})\mathbf{K}_1\left(s\mathbf{a}(\theta) + \mathbf{n}\right) \\ &\quad + \mathbf{w}^H(\theta_\mathrm{d})\mathbf{K}_2\left(s^*\mathbf{a}^*(\theta) + \mathbf{n}^*\right). \end{aligned} \tag{8}$$

Note that the output signal consists not only of the wanted signal term but also its complex conjugate. This gives us motivation towards WL processing, introduced in the next subsection. Assuming circular signal and noise, the power of the output signal is now equal to

$$\begin{aligned} \mathbb{E}\left[|y_\mathrm{imb}(\theta)|^2\right] &= \sigma_s^2\left|\mathbf{w}^H(\theta_\mathrm{d})\mathbf{K}_1\mathbf{a}(\theta)\right|^2 \\ &\quad + \sigma_s^2\left|\mathbf{w}^H(\theta_\mathrm{d})\mathbf{K}_2\mathbf{a}^*(\theta)\right|^2 \\ &\quad + \mathbf{w}^H(\theta_\mathrm{d})\mathbf{K}_1\mathbf{R_n}\mathbf{K}_1^H\mathbf{w}(\theta_\mathrm{d}) \\ &\quad + \mathbf{w}^H(\theta_\mathrm{d})\mathbf{K}_2\mathbf{R}_\mathbf{n}^*\mathbf{K}_2^H\mathbf{w}(\theta_\mathrm{d}) \end{aligned} \tag{9}$$

and finally the radiation pattern of the beamformer under RF I/Q imbalance can be given by

$$D_\mathrm{imb}(\theta) = \left|\mathbf{w}^H(\theta_\mathrm{d})\mathbf{K}_1\mathbf{a}(\theta)\right|^2 + \left|\mathbf{w}^H(\theta_\mathrm{d})\mathbf{K}_2\mathbf{a}^*(\theta)\right|^2. \tag{10}$$

Now, it is clear that I/Q imbalance is really affecting the radiation properties of the beamformer. This is further illustrated in Section IV with the simulation results.

C. Widely-Linear Beamforming

WL beamforming [6] combines the received signal snapshots $\mathbf{x}$ and the complex conjugates $\mathbf{x}^*$ with individual weights. Thus, the resulting signal snapshot in the output, first without RF I/Q imbalance, can be modeled as

$$\tilde{y} = \mathbf{w}_1^H\mathbf{x} + \mathbf{w}_2^H\mathbf{x}^* = \tilde{\mathbf{w}}^H\tilde{\mathbf{x}} \tag{11}$$

where $\mathbf{w}_1 \in \mathbb{C}^{N\times 1}$ and $\mathbf{w}_2 \in \mathbb{C}^{N\times 1}$ are the beamforming weights, $\tilde{\mathbf{w}} = [\mathbf{w}_1^T, \mathbf{w}_2^T]^T \in \mathbb{C}^{2N\times 1}$ is the augmented weight vector and $\tilde{\mathbf{x}} = [\mathbf{x}^T, \mathbf{x}^H]^T \in \mathbb{C}^{2N\times 1}$ presents the augmented signal snapshots. The output signal can be represented as a function of direction θ as

$$\begin{aligned} \tilde{y}(\theta) &= \left[\mathbf{w}_1^H(\theta_\mathrm{d}), \mathbf{w}_2^H(\theta_\mathrm{d})\right]\begin{bmatrix} s\mathbf{a}(\theta) + \mathbf{n} \\ s^*\mathbf{a}^*(\theta) + \mathbf{n}^* \end{bmatrix} \\ &= \mathbf{w}_1^H(\theta_\mathrm{d})\left(s\mathbf{a}(\theta) + \mathbf{n}\right) + \mathbf{w}_2^H(\theta_\mathrm{d})\left(s^*\mathbf{a}^*(\theta) + \mathbf{n}^*\right) \end{aligned} \tag{12}$$

Again, the weights are optimized under a given optimization criteria towards the desired direction θ_d.

WL processing does not offer significant benefits in case of circular signals. However, since I/Q imbalance structurally creates non-circularity for the received signals (which are assumed to be originally circular), WL beamforming becomes beneficial. The output signal of the WL beamformer under I/Q imbalance is given by (14) in the bottom of the next page. Again, s and s^* are present in the output, but now with more flexible weighting than in the plain linear case. The power of this signal is given by (15), also in the bottom of the next page. Finally, the radiation pattern for the WL beamformer under I/Q imbalance can be written as

$$\begin{aligned} \tilde{D}_\mathrm{imb}(\theta) &= \left|\mathbf{w}_1^H(\theta_\mathrm{d})\mathbf{K}_1\mathbf{a}(\theta) + \mathbf{w}_2^H(\theta_\mathrm{d})\mathbf{K}_2^*\mathbf{a}(\theta)\right|^2 \\ &\quad + \left|\mathbf{w}_1^H(\theta_\mathrm{d})\mathbf{K}_2\mathbf{a}^*(\theta) + \mathbf{w}_2^H(\theta_\mathrm{d})\mathbf{K}_1^*\mathbf{a}^*(\theta)\right|^2. \end{aligned} \tag{16}$$

It is obvious that the radiation characteristics of the WL beamformer can be modified and optimized more easily than in (10) due to the individual weights for $\mathbf{x}$ and $\mathbf{x}^*$. Due to the 5-page limitation in this paper, more extensive analysis of WL beamforming under I/Q imbalance is given in [9].

III. Optimal RF-Aware MMSE Beamforming

In order to evaluate the performance of the beamforming algorithms in realistic radio environment with interference, the interfering signals are now added explicitly to the signal model. The received signal snapshots are then given by

$$\mathbf{x} = s\mathbf{a}(\theta) + \mathbf{z} \tag{17}$$

where the total interference plus noise term $\mathbf{z}$ is equal to

$$\mathbf{z} = \sum_{j=1}^{M_{\text{int}}} s_{\text{int},j}\mathbf{a}(\theta_{\text{int},j}) + \mathbf{n}. \tag{18}$$

Here, M_{int} denotes the total amount of interfering signals, and $s_{\text{int},j}$ and $\mathbf{a}(\theta_{\text{int},j})$ present the signal waveform and steering vector of the j^{th} interfering signal coming from the direction $\theta_{\text{int},j}$. Similarly as earlier, the signal snapshots under I/Q imbalance are equal to $\mathbf{x}_{\text{imb}} = \mathbf{K}_1\mathbf{x} + \mathbf{K}_2\mathbf{x}^*$.

A. Wiener Filters

Wiener filters give the optimal MMSE solution for stationary signal estimation problems [10]. They base on comparing the filter output signal to the desired signal [11], and hence typically results in data-aided learning. In beamforming, the MMSE solution for the beamformer weights is equal to

$$\mathbf{w}_o = \mathbf{R}_{\mathbf{x}}^{-1}\mathbf{p}. \tag{19}$$

Here, $\mathbf{R}_{\mathbf{x}} = \mathbb{E}\left[\mathbf{x}\mathbf{x}^H\right] \in \mathbb{C}^{N\times N}$ is the covariance matrix of $\mathbf{x}$, and $\mathbf{p} = \mathbb{E}[\mathbf{x}d^*] \in \mathbb{C}^{N\times 1}$ is the cross-correlation vector between the received signal snapshots and the desired signal d. Note that d denotes the transmitted pilot signal snapshot (assumed to be known in the receiver), whereas $s = hd$ presents the corresponding received snapshot. Here h models the channel between the transmitter and receiver for the narrow-band signal (e.g. OFDM subcarrier).

When taking a detailed look to the covariance matrix $\mathbf{R}_{\mathbf{x}}$ under practical assumption of circular signals, it can be presented as

$$\begin{aligned}\mathbf{R}_{\mathbf{x}} &= \mathbb{E}\left[\mathbf{x}\mathbf{x}^H\right] \\ &= \sigma_s^2\mathbf{a}(\theta_{\text{d}})\mathbf{a}^H(\theta_{\text{d}}) + \sigma_n^2\mathbf{I}_N \\ &\quad + \sum_{j=1}^{M_{\text{int}}} \sigma_{\text{int},j}^2\mathbf{a}(\theta_{\text{int},j})\mathbf{a}^H(\theta_{\text{int},j})\end{aligned} \tag{20}$$

where $\sigma_s^2 = |h|^2\sigma_d^2$ denote the power of the useful signal, and σ_n^2 and $\sigma_{\text{int},j}^2$ are the powers of the noise and interfering signal j, respectively. In addition, $\mathbf{I}_N \in \mathbb{R}^{N\times N}$ is a unit matrix. However, under I/Q imbalance the circularity property of the signals is violated and also the covariance matrix is shaped. The covariance matrix then reads

$$\begin{aligned}\mathbf{R}_{\mathbf{x},\text{imb}} &= \mathbb{E}\left[\mathbf{x}_{\text{imb}}{\mathbf{x}_{\text{imb}}}^H\right] \\ &= \sigma_s^2\mathbf{K}_1\mathbf{a}(\theta_{\text{d}})\mathbf{a}^H(\theta_{\text{d}})\mathbf{K}_1^H + \sigma_n^2\mathbf{K}_1\mathbf{K}_1^H \\ &\quad + \sum_{j=1}^{M_{\text{int}}} \sigma_{\text{int},j}^2\mathbf{K}_1\mathbf{a}(\theta_{\text{int},j})\mathbf{a}^H(\theta_{\text{int},j})\mathbf{K}_1^H \\ &\quad + \sigma_s^2\mathbf{K}_2\mathbf{a}^*(\theta_{\text{d}})\mathbf{a}^T(\theta_{\text{d}})\mathbf{K}_2^H + \sigma_n^2\mathbf{K}_2\mathbf{K}_2^H \\ &\quad + \sum_{j=1}^{M_{\text{int}}} \sigma_{\text{int},j}^2\mathbf{K}_2\mathbf{a}^*(\theta_{\text{int},j})\mathbf{a}^T(\theta_{\text{int},j})\mathbf{K}_2^H.\end{aligned} \tag{21}$$

Now the covariance matrix includes totally new terms relative to $\mathbf{K}_2$. In addition, the desired terms are now scaled by $\mathbf{K}_1$. Furthermore, also the complementary covariance of $\mathbf{x}_{\text{imb}}$, defined below in (24), is now nonzero and thus the linear Wiener filter becomes suboptimal. To overcome this problem, the WL-Wiener filter can be used since it can structurally take signal non-circularity into account.

The beamforming problem under RF I/Q imbalance can now be solved by the WL-Wiener filter as [12], [13]

$$\tilde{\mathbf{w}}_o = \tilde{\mathbf{R}}_{\mathbf{x}}^{-1}\tilde{\mathbf{p}} \tag{22}$$

where the augmented covariance matrix $\tilde{\mathbf{R}}_{\mathbf{x}} = \mathbb{E}\left[\tilde{\mathbf{x}}\tilde{\mathbf{x}}^H\right] \in \mathbb{C}^{2N\times 2N}$, and the augmented cross-correlation vector $\tilde{\mathbf{p}} = \mathbb{E}[\tilde{\mathbf{x}}d^*] \in \mathbb{C}^{2N\times 1}$. Here, the augmented covariance matrix can be represented as

$$\tilde{\mathbf{R}}_{\mathbf{x}} = \begin{bmatrix} \mathbf{R}_{\mathbf{x}} & \mathbf{C}_{\mathbf{x}} \\ \mathbf{C}_{\mathbf{x}}^* & \mathbf{R}_{\mathbf{x}}^* \end{bmatrix} \tag{23}$$

where $\mathbf{C}_{\mathbf{x}} = \mathbb{E}\left[\mathbf{x}\mathbf{x}^T\right] \in \mathbb{C}^{N\times N}$ denotes the complementary covariance matrix of $\mathbf{x}$. Under the assumption of circular signals, $\mathbf{C}_{\mathbf{x}} = 0$ and the WL-Wiener filter reduces to the conventional Wiener filter [14]. However, since the received signals become non-circular due to I/Q imbalance, the complementary covariance matrix is no longer all zero. In fact, it is now given by

$$\begin{aligned}\mathbf{C}_{\mathbf{x},\text{imb}} &= \mathbb{E}\left[\mathbf{x}_{\text{imb}}\mathbf{x}_{\text{imb}}^T\right] \\ &= \sigma_s^2\mathbf{K}_1\mathbf{a}(\theta_{\text{d}})\mathbf{a}^H(\theta_{\text{d}})\mathbf{K}_2^T + \sigma_n^2\mathbf{K}_1\mathbf{K}_2^T \\ &\quad + \sum_{j=1}^{M_{\text{int}}} \sigma_{\text{int},j}^2\mathbf{K}_1\mathbf{a}(\theta_{\text{int},j})\mathbf{a}^H(\theta_{\text{int},j})\mathbf{K}_2^T \\ &\quad + \sigma_s^2\mathbf{K}_2\mathbf{a}^*(\theta_{\text{d}})\mathbf{a}^T(\theta_{\text{d}})\mathbf{K}_1^T + \sigma_n^2\mathbf{K}_2\mathbf{K}_1^T \\ &\quad + \sum_{j=1}^{M_{\text{int}}} \sigma_{\text{int},j}^2\mathbf{K}_2\mathbf{a}^*(\theta_{\text{int},j})\mathbf{a}^T(\theta_{\text{int},j})\mathbf{K}_1^T\end{aligned} \tag{24}$$

$$\begin{aligned}\tilde{y}_{\text{imb}}(\theta) &= \tilde{\mathbf{w}}^H(\theta_{\text{d}})\tilde{\mathbf{x}}_{\text{imb}} = \left[\mathbf{w}_1^H(\theta_{\text{d}}), \mathbf{w}_2^H(\theta_{\text{d}})\right]\begin{bmatrix}\mathbf{K}_1 & \mathbf{K}_2 \\ \mathbf{K}_2^* & \mathbf{K}_1^*\end{bmatrix}\begin{bmatrix}s\mathbf{a}(\theta)+\mathbf{n} \\ s^*\mathbf{a}^*(\theta)+\mathbf{n}^*\end{bmatrix} \\ &= \left(\mathbf{w}_1^H(\theta_{\text{d}})\mathbf{K}_1 + \mathbf{w}_2^H(\theta_{\text{d}})\mathbf{K}_2^*\right)(s\mathbf{a}(\theta)+\mathbf{n}) + \left(\mathbf{w}_1^H(\theta_{\text{d}})\mathbf{K}_2 + \mathbf{w}_2^H(\theta_{\text{d}})\mathbf{K}_1^*\right)(s^*\mathbf{a}^*(\theta)+\mathbf{n}^*)\end{aligned} \tag{14}$$

$$\begin{aligned}\mathbb{E}\left[\left|\tilde{y}_{\text{imb}}(\theta)\right|^2\right] &= \sigma_s^2\left|\mathbf{w}_1^H(\theta_{\text{d}})\mathbf{K}_1\mathbf{a}(\theta) + \mathbf{w}_2^H(\theta_{\text{d}})\mathbf{K}_2^*\mathbf{a}(\theta)\right|^2 + \sigma_s^2\left|\mathbf{w}_1^H(\theta_{\text{d}})\mathbf{K}_2\mathbf{a}^*(\theta) + \mathbf{w}_2^H(\theta_{\text{d}})\mathbf{K}_1^*\mathbf{a}^*(\theta)\right|^2 \\ &\quad + \mathbf{w}_1^H(\theta_{\text{d}})\mathbf{K}_1\mathbf{R}_{\mathbf{n}}\mathbf{K}_1^H\mathbf{w}_1(\theta_{\text{d}}) + \mathbf{w}_2^H(\theta_{\text{d}})\mathbf{K}_2^*\mathbf{R}_{\mathbf{n}}\mathbf{K}_2^T\mathbf{w}_2(\theta_{\text{d}}) + \mathbf{w}_1^H(\theta_{\text{d}})\mathbf{K}_2\mathbf{R}_{\mathbf{n}}^*\mathbf{K}_2^H\mathbf{w}_1(\theta_{\text{d}}) \\ &\quad + \mathbf{w}_2^H(\theta_{\text{d}})\mathbf{K}_1^*\mathbf{R}_{\mathbf{n}}^*\mathbf{K}_1^T\mathbf{w}_2(\theta_{\text{d}}) + \mathbf{w}_1^H(\theta_{\text{d}})\mathbf{K}_1\mathbf{R}_{\mathbf{n}}\mathbf{K}_2^T\mathbf{w}_2(\theta_{\text{d}}) + \mathbf{w}_2^H(\theta_{\text{d}})\mathbf{K}_2^*\mathbf{R}_{\mathbf{n}}\mathbf{K}_1^H\mathbf{w}_1(\theta_{\text{d}}) \\ &\quad + \mathbf{w}_1^H(\theta_{\text{d}})\mathbf{K}_2\mathbf{R}_{\mathbf{n}}^*\mathbf{K}_1^T\mathbf{w}_2(\theta_{\text{d}}) + \mathbf{w}_2^H(\theta_{\text{d}})\mathbf{K}_1^*\mathbf{R}_{\mathbf{n}}^*\mathbf{K}_2^H\mathbf{w}_1(\theta_{\text{d}})\end{aligned} \tag{15}$$

and thus the augmented covariance matrix under I/Q imbalance can be finally presented by

$$\tilde{\mathbf{R}}_{\mathbf{x},\text{imb}} = \begin{bmatrix} \mathbf{R}_{\mathbf{x},\text{imb}} & \mathbf{C}_{\mathbf{x},\text{imb}} \\ \mathbf{C}^*_{\mathbf{x},\text{imb}} & \mathbf{R}^*_{\mathbf{x},\text{imb}} \end{bmatrix}. \tag{25}$$

The corruption of the augmented covariance matrix also naturally affects the operation of the beamformer. In addition, the cross-correlation vectors are shaped similarly as the covariance matrices. This is summarized in **Table 1** where the cross-correlation vectors with and without I/Q imbalance are presented. However, the WL-Wiener filter can suppress the unwanted I/Q imbalance effects due to the doubled degrees of freedom and this way enables better performance than the linear structure. This is further demonstrated in Section IV with simulation results.

B. Practical Data-Aided Learning

The optimal MMSE solution needs the calculation of the covariance matrix and its inverse. These are computationally heavy operations consuming lots of time and power which may be problematic in wireless communication devices.

Fortunately, the MMSE solution can be approximated with simple adaptive methods, e.g. least mean squares (LMS) algorithm [15] which converges close to the Wiener filter solution, assuming that the signals are stationary [11]. Although the convergence of LMS might be slower than e.g. with recursive least squares algorithm, we have selected LMS for an exemplary approach due to its intuitiveness and low computational complexity. It solves the estimation problem iteratively by

$$y(i) = \mathbf{w}^H_{\text{LMS}}(i)\mathbf{x}(i) \tag{26}$$

$$e(i) = d(i) - y(i) \tag{27}$$

$$\mathbf{w}_{\text{LMS}}(i+1) = \mathbf{w}_{\text{LMS}}(i) + \mu\mathbf{x}(i)e^*(i) \tag{28}$$

where $\mathbf{w}_{\text{LMS}} \in \mathbb{C}^{N\times 1}$ denotes the LMS weights, e is the estimation error and μ stands for the step-size coefficient. All parameters present the values on the i^{th} iteration round.

In order to estimate the MMSE solution of the WL-Wiener filter, the WL extension of the LMS (WL-LMS) [16] can be used. It is given, similarly as for linear case in (26-28), by

$$\tilde{y}(i) = \tilde{\mathbf{w}}^H_{\text{LMS}}(i)\tilde{\mathbf{x}}(i) \tag{29}$$

$$\tilde{e}(i) = d(i) - \tilde{y}(i) \tag{30}$$

$$\tilde{\mathbf{w}}_{\text{LMS}}(i+1) = \tilde{\mathbf{w}}_{\text{LMS}}(i) + \tilde{\mu}\tilde{\mathbf{x}}(i)\tilde{e}^*(i) \tag{31}$$

where $\tilde{\mathbf{w}}_{\text{LMS}} \in \mathbb{C}^{2N\times 1}$ now denotes the WL-LMS weights. When operating under RF I/Q imbalance, the observation $\tilde{\mathbf{x}}$ above is simply replaced with $\tilde{\mathbf{x}}_{\text{imb}}$. The performance of the LMS methods are next illustrated with simulations under both ideal I/Q matching and I/Q imbalance. Additionally, the Wiener filter solutions are presented for the comparison.

IV. Simulations and Numerical Examples

Performance results are based on extensive MATLAB simulations where ULA with 6 antenna elements is used. The element spacing $d = \lambda/2$. A 16-QAM waveform is used to model consecutive received signal snapshots and two complex circular Gaussian interfering signals are generated for modeling interference. The desired signal is coming from direction $\theta_{\text{d}} = 65^\circ$ while the interfering signals are coming from directions $\theta_{\text{int},1} = 22^\circ$ and $\theta_{\text{int},2} = 115^\circ$. Interfering signals are 6 dB stronger than the desired signal and signal to noise ratio SNR=10 dB. The exact channel realization is not relevant in this study and hence we set $h = 1$.

TABLE I. Cross-correlation vectors for the Wiener filters.

	Perfect I/Q matching	Under I/Q imbalance
$\mathbf{p}$	$\sigma_d^2 h\mathbf{a}(\theta_{\text{d}})$	$\mathbf{K}_1\sigma_d^2 h\mathbf{a}(\theta_{\text{d}})$
$\tilde{\mathbf{p}}$	$\begin{bmatrix}\sigma_d^2 h\mathbf{a}(\theta_{\text{d}}) \\ \mathbf{0}_{\text{N}\times 1}\end{bmatrix}$	$\begin{bmatrix}\mathbf{K}_1\sigma_d^2 h\mathbf{a}(\theta_{\text{d}}) \\ \mathbf{K}_2^*\sigma_d^2 h\mathbf{a}(\theta_{\text{d}})\end{bmatrix}$

To implement I/Q imbalance, the gain imbalance coefficient g for the n^{th} receiver branch is randomly selected from the range 0.85 ± 0.03 while the phase imbalance coefficient ϕ is taken from the range $10^\circ\pm3^\circ$ and thus the non-circularity rate ρ [17] in individual receiver branches is in the range 0.176...0.300. This models beamformer where parallel receiver branches are consisting of similar components which have some performance fluctuation due to e.g. manufacturing process.

Reference results, obtained by the Wiener filters, are based on the covariance matrix and cross-correlation vector models in Section 3.1. The LMS algorithms are initialized with all zero weights, they iterate $50\,000$ rounds and the step-size $\mu = \tilde{\mu} = 0.00001$. Convergence results of the LMS algorithms are averaged over 500 realizations.

Radiation patterns of the linear and WL Wiener filters are depicted in **Figure 1**. All cases have slight attenuation to the desired direction which is common in MMSE filters for obtaining proper noise and interference suppression. Under perfect I/Q matching, both methods are steering strong nulls towards the interference sources. However, under I/Q imbalance, the linear Wiener filter fails in the null steering and is therefore effectively receiving energy from the interference directions. As discussed already in Section 3.1, this problem can be prevented by using the WL-Wiener filter. It can take I/Q imbalance into account already at the structural level and therefore is able to give good radiation properties also under severe I/Q imbalance which is proven by the results. Notice that the WL beamformer does not know the I/Q imbalance properties of the individual radio chains, but is implicitly building such RF awareness to the beamforming weights in the learning phase.

Performance of the LMS and WL-LMS methods after $50\,000$ iterations are shown in **Figure 2**. Results with perfect I/Q balance differ slightly from the results of the Wiener filters. This comes from the fact that the Wiener filters calculate deterministic MMSE beamforming weights (for given variances and imbalance coefficients) while the LMS weights are slightly fluctuating (even after the convergence) and thus leading to different results. Again, the linear method under I/Q imbalance fails in null steering task whereas the WL-LMS is able to attenuate interference efficiently. Differences between the WL-LMS results under perfect I/Q matching and I/Q imbalance are again explained by the fluctuating weights.

Finally, the convergence of the LMS algorithms is depicted in **Figure 3**. The conventional LMS method approaches the Wiener filter results with and without I/Q imbalance (note that without I/Q imbalance LMS and WL-LMS are almost equal and therefore the results of LMS are not visible). The WL-LMS gets close to the ideal Wiener filter solution (with perfect I/Q matching) no matter if I/Q imbalance is present or not. This confirms that WL processing is able to take I/Q imbalance

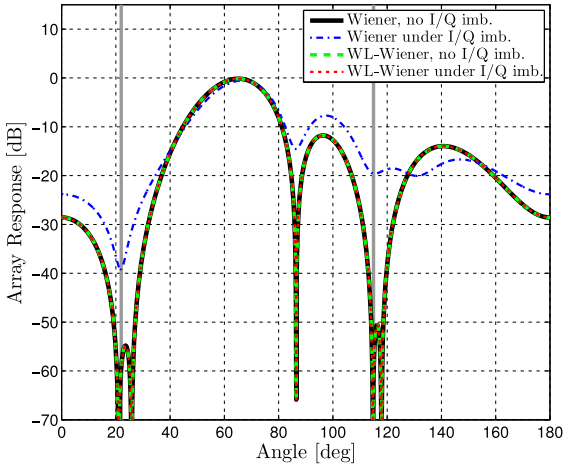

Fig. 1. Radiation patterns of the Wiener and WL-Wiener filters, 6 antenna elements, $\theta_{\mathrm{d}} = 65°$, $\theta_{\mathrm{int},1} = 22°$ and $\theta_{\mathrm{int},2} = 115°$. One realization for each method.

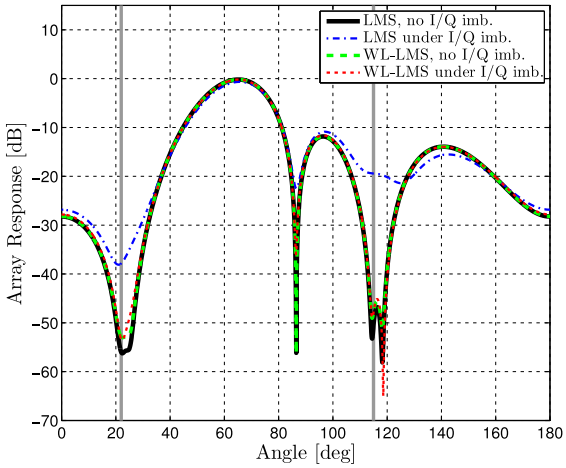

Fig. 2. Radiation patterns of LMS and WL-LMS, 6 antenna elements, $\theta_{\mathrm{d}} = 65°$, $\theta_{\mathrm{int},1} = 22°$ and $\theta_{\mathrm{int},2} = 115°$. One realization for each method. $\mu = \tilde{\mu} = 0.00001$.

into account at the structural level and therefore can reach the optimum performance even under severe I/Q imbalance.

V. Conclusion

In this paper, the effects of RF I/Q imbalance on digital beamforming were studied and analyzed. It was shown that I/Q imbalance corrupts output signal properties and degrades radiation characteristics of the beamformer, even in case of data-aided beamforming methods. For mitigating the unwanted I/Q imbalance effects, WL beamforming methods, namely WL-Wiener filter and WL-LMS, were formulated. MATLAB simulation results showed that the proposed methods can operate efficiently and provide the wanted signal and beamforming properties, even under severe I/Q imbalance in the RF circuits. This avoids the need for separate I/Q calibration loops in the parallel receiver chains, and thus RF awareness is efficiently built in to the beamforming process.

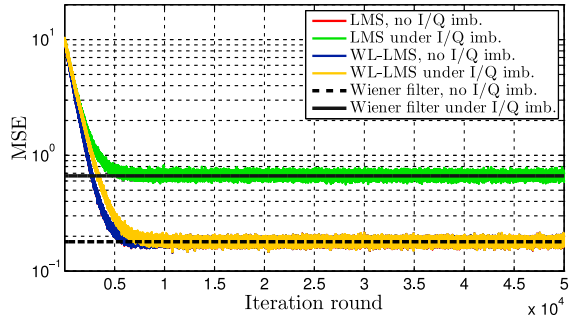

Fig. 3. Convergence of the mean-squared error with LMS and WL-LMS, averaged over 500 realizations. $\mu = \tilde{\mu} = 0.00001$. Note that without I/Q imbalance LMS (red) and WL-LMS (blue) are almost equal and therefore the results of LMS are not visible.

References

[1] J. Litva, *Digital Beamforming in Wireless Communications*. Artech House Publishers, Aug. 1996.

[2] S. Mirabbasi and K. Martin, "Classical and modern receiver architectures," *IEEE Communications Mag.*, vol. 38, no. 11, pp. 132–139, Nov. 2000.

[3] A. Mashmour, W. Domino, and N. Beamish, "On the direct conversion receiver – a tutorial," *Microwave Journal*, vol. 44, no. 6, pp. 114–128, Jun. 2001.

[4] M. Valkama, M. Renfors, and V. Koivunen, "Advanced methods for I/Q imbalance compensation in communication receivers," *IEEE Trans. Signal Process.*, vol. 49, no. 10, pp. 2335–2344, Oct. 2001.

[5] A. Hakkarainen, J. Werner, and M. Valkama, "RF imperfections in antenna arrays: Response analysis and widely-linear digital beamforming," in *Proc. IEEE RWS 2013*, Jan. 2013, pp. 187 –189.

[6] P. Chevalier and A. Maurice, "Constrained beamforming for cyclostationary signals," in *Proc. IEEE ICASSP 1997*, vol. 5, 1997, pp. 3789–3792.

[7] T. McWhorter and P. Schreier, "Widely-linear beamforming," in *Proc. Thirty-Seventh Asilomar Conference on Signals, Systems and Computers, 2004*, vol. 1, Nov. 2003, pp. 753 – 759 Vol.1.

[8] P. Chevalier and A. Blin, "Widely linear MVDR beamformers for the reception of an unknown signal corrupted by noncircular interferences," *IEEE Trans. Signal Process.*, vol. 55, no. 11, pp. 5323 –5336, Nov. 2007.

[9] A. Hakkarainen, J. Werner, K. R. Dandekar, and M. Valkama, "Widely-linear beamforming and RF impairment suppression in massive antenna arrays," *Journal of Communications and Networks*, no. Special Issue on Massive MIMO, Aug. 2013 (under review).

[10] H. L. V. Trees, *Detection, Estimation, and Modulation Theory, Optimum Array Processing*. John Wiley & Sons, Apr. 2004.

[11] S. Haykin, *Adaptive Filter Theory*, 3rd ed. Prentice Hall, 1995.

[12] P. Chevalier, "Optimal array processing for non-stationary signals," in *Proc. IEEE ICASSP 1996*, vol. 5, May 1996, pp. 2868 –2871.

[13] P. Chevalier and F. Pipon, "New insights into optimal widely linear array receivers for the demodulation of BPSK, MSK, and GMSK signals corrupted by noncircular interferences-application to SAIC," *IEEE Trans. Signal Process.*, vol. 54, no. 3, pp. 870–883, 2006.

[14] J. Benesty, J. Chen, and Y. (Arden) Huang, "On widely linear wiener and tradeoff filters for noise reduction," *Speech Communication*, vol. 52, no. 5, pp. 427–439, May 2010.

[15] B. Widrow et al., "Adaptive antenna systems," *Proc. IEEE*, vol. 55, no. 12, pp. 2143–2159, Dec. 1967.

[16] D. Mandic and V. S. L. Goh, *Complex Valued Nonlinear Adaptive Filters: Noncircularity, Widely Linear and Neural Models*. John Wiley & Sons, Apr. 2009.

[17] J.-P. Delmas and H. Abeida, "On the degree of second-order noncircularity of complex random variables," in *Proc. IEEE ICASSP 2008*, Apr. 2008, pp. 3905–3908.

Publication 4

A. Hakkarainen, J. Werner, K. R. Dandekar, and M. Valkama, "Widely-Linear Beamforming and RF Impairment Suppression in Massive Antenna Arrays," in *Journal of Communications and Networks*, vol. 15, no. 4, pp. 383–397, Aug. 2013. DOI: 10.1109/jcn.2013.000069

Widely-Linear Beamforming and RF Impairment Suppression in Massive Antenna Arrays

Aki Hakkarainen, Janis Werner, Kapil R. Dandekar, and Mikko Valkama

Abstract: **In this paper, the sensitivity of massive antenna arrays and digital beamforming to radio frequency (RF) chain in-phase quadrature-phase (I/Q) imbalance is studied and analyzed. The analysis shows that massive antenna arrays are increasingly sensitive to such RF chain imperfections, corrupting heavily the radiation pattern and beamforming capabilities. Motivated by this, novel RF-aware digital beamforming methods are then developed for automatically suppressing the unwanted effects of the RF I/Q imbalance without separate calibration loops in all individual receiver branches. More specifically, the paper covers closed-form analysis for signal processing properties as well as the associated radiation and beamforming properties of massive antenna arrays under both systematic and random RF I/Q imbalances. All analysis and derivations in this paper assume ideal signals to be circular. The well-known minimum variance distortionless response (MVDR) beamformer and a widely-linear (WL) extension of it, called WL-MVDR, are analyzed in detail from the RF imperfection perspective, in terms of interference attenuation and beamsteering. The optimum RF-aware WL-MVDR beamforming solution is formulated and shown to efficiently suppress the RF imperfections. Based on the obtained results, the developed solutions and in particular the RF-aware WL-MVDR method can provide efficient beamsteering and interference suppressing characteristics, despite of the imperfections in the RF circuits. This is seen critical especially in the massive antenna array context where the cost-efficiency of individual RF chains is emphasized.**

Index Terms: **Antenna arrays, antenna radiation patterns, beam steering, circular signals, in-phase quadrature-phase (I/Q) imbalance, massive multiple input multiple output (MIMO), radio transceivers.**

I. Introduction

Data transmission over wireless networks has been increasing rapidly during the last five years and it is predicted that this trend will continue also in the coming years [1]. However, physical resources (e.g. frequencies, number of time slots, spatial distribution of the users) for data transmission will remain the same, so new technologies have to be developed in order to enable this growth also in the future. One of these technologies is the multiple input multiple output (MIMO) principle and advanced antenna arrays in physical layer data transmission. Such multiantenna technologies enable simultaneous transmissions between two or more devices through multiple antennas on both ends, the transmitter(s) and the receiver(s), and are therefore offering a significant increase in transmission rates. Furthermore, antenna arrays can offer sophisticated interference suppression mechanisms which is especially critical in interference-limited systems such as mobile cellular radio at cell edges. Traditionally MIMO has been implemented or specified with up to eight antennas on both ends [2].

Massive MIMO (also known as very large MIMO) is defined as a system which has from tens to hundreds of antenna elements, at least in one/some of the involved devices [3, 4]. One common use case is a base station with a massive antenna array serving several user terminals equipped only with a single or few antennas. The implementation of the base station antenna structure can be arbitrary, but in practice some regular collocated structures, such as linear arrays, are used for antenna placement. The most fundamental aim of massive MIMO is to offer all the benefits of conventional MIMO, but on a larger scale, by simple, cheap and low-power hardware implementation. To put it in another way, when increasing the number of parallel antennas and associated radio frequency (RF) chains, the size and cost-efficiency of individual RF chains becomes more and more critical.

A good candidate for the massive MIMO transceiver structure is the direct-conversion radio (DCR) architecture [5] due to the following facts. On the one hand, it is flexible and thus able to operate with several different air interfaces, frequency bands and waveforms [6]. On the other hand, it neither requires RF image rejection filter nor intermediate frequency stages [7] and therefore has a lower implementation cost and a smaller size than e.g. the classic super-heterodyne structure [8]. Unfortunately, DCR suffers from a common RF imperfection, called in-phase quadrature-phase (I/Q) imbalance [9], due to non-ideal properties of analog electronics, specifically in RF mixers. This leads to a degradation in the overall performance and therefore also to a deteriorated user experience. Interestingly, the impacts of such RF imperfections have not been studied systematically so far, especially in the massive antenna array context.

At behavioral baseband equivalent modeling level, RF I/Q imbalance maps to widely-linear (WL) signal transformation, i.e. the ideal signal and its complex conjugate are effectively added up with separate complex weights [10]. This changes the signal properties and the resulting signal becomes non-circular [11], even though typical communication waveforms are of cir-

Manuscript received January 31.

This work was supported by the Finnish Funding Agency for Technology and Innovation (Tekes) under the project "Reconfigurable Antenna-based Enhancement of Dynamic Spectrum Access Algorithms", the Industrial Research Fund of Tampere University of Technology (Tuula and Yrjö Neuvo Fund), the Academy of Finland under the project 251138 "Digitally-Enhanced RF for Cognitive Radio Devices", and the Doctoral Programme of the President of Tampere University of Technology. The work was also supported by the National Science Foundation (NSF) under award number 1147838.

A. Hakkarainen, J. Werner and M. Valkama are with the Department of Electronics and Communications Engineering, Tampere University of Technology, Tampere, Finland, emails: {aki.hakkarainen, janis.werner, mikko.e.valkama}@tut.fi.

K. R. Dandekar is with the Department of Electrical and Computer Engineering, Drexel University, Philadelphia, PA, USA, email: dandekar@drexel.edu.

Digital object identier 10.1109/JCN.2013.000069

cular nature. It has been shown that this unwanted behavior can be compensated in a single receiver chain by WL processing [12]. However, the overall impacts and suppression of such RF I/Q imbalance have not been studied systematically in the literature so far in the antenna array and beamforming context. The WL beamforming concept, in turn, has been studied in the literature as such, e.g. in [13–19], but only from the perspective of non-circular desired signals or non-circular interferers, with no connection to RF imperfections. Since in practice most of the modern communication signals are anyway circular, we propose and demonstrate the applicability of WL beamforming for compensating the unwanted effects of the internal source of non-circularity, here RF I/Q imbalance.

In this paper, the sensitivity of massive antenna arrays to RF I/Q imbalance is studied and analyzed in the beamforming context. In addition, novel RF-aware digital beamforming methods are developed for mitigating the unwanted effects of I/Q imbalance. The main emphasis is on the radiation properties of the beamformer as well as on the output signal properties. The work extends strongly the authors' work in [20] where very preliminary treatment of these issues was given and a simple training-based beamforming solution was studied. There the signal model was assumed to be noiseless, radio environment was assumed to be free of interference, the effects of I/Q imbalance were studied only with the systematic imbalance model and very limited amount of examples were given. Contrary to the work in [20], more sophisticated minimum variance distortionless response (MVDR) and WL-MVDR methods with covariance matrix analysis are studied in this paper. In addition, detailed analysis of both systematic and random I/Q imbalance between different RF chains are provided without need for explicit training in the beamformer weight optimization. It is also shown, that WL processing provides significant improvements in the overall performance under I/Q imbalance as compared to plain linear beamforming. The above aspects are studied with analytical signal models and closed-form radiation pattern analysis deploying well-defined closed-form beamformer output power expressions. Also, extensive numerical results are provided with both conventional sized antenna array (eight antenna elements) and massive antenna array (50 antenna elements). Some practical aspects of the beamformer implementations are discussed and presented as well, dealing with I/Q imbalance uncertainty, in order to illustrate the feasibility of the proposed methods for realistic beamforming problems.

The remainder of this paper is structured as follows. In section II, the response of the digital linear beamformer is first shortly reviewed. Then, I/Q imbalance models for individual RF chains are deployed and the response analysis and radiation patterns for both linear and WL digital beamformers are carried out and derived in closed form. Next in section III, the structural capability of linear and WL beamforming to suppress RF imperfection is studied by comparing the responses under RF I/Q imbalance to the ideal response of a classical spatial matched filter (SMF) under perfect I/Q balance. This shows that WL processing has the structural ability to suppress the RF imperfections better than classical linear processing. Then, in section IV, MVDR and WL-MVDR methods are introduced and the effects of I/Q imbalance on the covariance and complementary covariance matrix structures are derived. In addition, the proposed RF-aware MVDR and RF-aware WL-MVDR are introduced for I/Q imbalance mitigation under the assumption of known I/Q imbalance coefficients. Extensive numerical examples, under systematic and random I/Q imbalances, and result analysis can be found in section V. Furthermore, the impact of practical I/Q imbalance uncertainty is addressed. Finally, in section VI, conclusions of the paper are drawn.

Notation: Throughout this paper, vectors and matrices are written with bold characters. The superscripts $(\cdot)^T$, $(\cdot)^H$, $(\cdot)^*$ and $(\cdot)^{-1}$ represent transpose, Hermitian (conjugate) transpose, conjugate and matrix inverse, respectively. The tilde sign $\tilde{(\cdot)}$ is used to present a WL (augmented) quantity and the results obtained by the WL processing. The statistical expectation is denoted with $\mathbb{E}[\cdot]$. A complex random variable x is called circular if $\mathbb{E}\left[x^2\right] = 0$.

II. Fundamental Signal and Array Models

A. Spatial Response of a Digital Linear Beamformer

The output signal snapshot of a digital linear beamformer with N antenna elements is given by

$$y = \sum_{i=1}^{N} w_i^* x_i = \mathbf{w}^H \mathbf{x} \tag{1}$$

where $\mathbf{w} = [w_1, w_2, ..., w_N]^T \in \mathbb{C}^{N\times 1}$ refers to the combining weights and $\mathbf{x} = [x_1, x_2, ..., x_N]^T \in \mathbb{C}^{N\times 1}$ to the baseband signal snapshots from each antenna element $i = 1 \cdots N$ [21]. Note that the signal model and analysis in this paper are focusing on classical narrowband signals due to more simple presentation and notations. However, the presentation and developments can also be generalized to wideband signals, since e.g. wideband orthogonal frequency-division multiplexing (OFDM) signal is a combination of several independent narrowband subsignals which can be processed individually [22], assuming that the angular spread is reasonably small. This is the case e.g. with above roof-top level base station antennas of macro cellular radio networks. Furthermore, even in a rich multipath environment, if the angular spread is small, the effects of multipath propagation can be efficiently suppressed by processing OFDM signals in post-FFT per subcarrier manner (see [23]).

Stemming from the above assumptions, the instantaneous baseband snapshots are given by

$$\mathbf{x} = s\mathbf{a}(\theta) + \mathbf{n} \tag{2}$$

where s is the arriving signal, θ is the spatial direction, $\mathbf{a}(\theta) \in \mathbb{C}^{N\times 1}$ is the steering vector and $\mathbf{n} \in \mathbb{C}^{N\times 1}$ models the additive noise in the receiver branches. The steering vector is defined e.g. for a uniform linear array (ULA) as $\mathbf{a}(\theta) = [1, e^{jd\kappa\cos\theta}, e^{j2d\kappa\cos\theta}, ..., e^{j(N-1)d\kappa\cos\theta}]^T$ where the wavenumber $\kappa = 2\pi/\lambda$. Here, λ stands for the wavelength of the RF signal frequency.

The output signal can be presented as a function of the direction θ by

$$y(\theta) = \mathbf{w}^H(\theta_\mathrm{d})\mathbf{x} = s\mathbf{w}^H(\theta_\mathrm{d})\mathbf{a}(\theta) + \mathbf{w}^H(\theta_\mathrm{d})\mathbf{n} \tag{3}$$

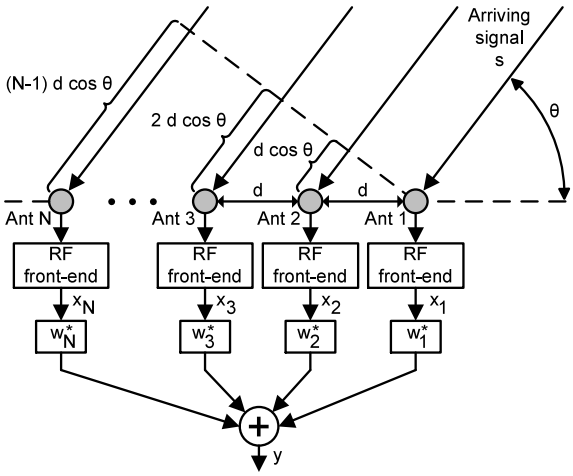

Fig. 1. The conceptual digital beamformer with a uniform linear array and the used notation. The flow of the arriving signal is presented by arrows.

where $\mathbf{w}(\theta_{\mathrm{d}})$ are the weights optimized under a given optimization criterion towards the desired direction θ_{d}. The conceptual beamformer with ULA implementation and the used notation is illustrated in Fig. 1.

Next, the power of the output signal of the digital linear beamformer is defined. Under the typical assumption of uncorrelated signal and noise, the power of the output signal is given by

$$\mathbb{E}\left[|y(\theta)|^2\right] = \sigma_s^2 \left|\mathbf{w}^H(\theta_{\mathrm{d}})\mathbf{a}(\theta)\right|^2 + \mathbf{w}^H(\theta_{\mathrm{d}})\mathbf{R}_{\mathbf{n}}\mathbf{w}(\theta_{\mathrm{d}}) \quad (4)$$

where $\sigma_s^2 = \mathbb{E}\left[|s|^2\right]$ denotes signal power and $\mathbf{R}_{\mathbf{n}} = \mathbb{E}\left[\mathbf{n}\mathbf{n}^H\right] \in \mathbb{C}^{N\times N}$ is the covariance matrix of the noise. Further, the spatial response of the beamformer is expressed using the radiation pattern. The radiation pattern is based on the signal model in (2) and is defined for given weights as the spatial dependency of the desired signal output power. Here, the term relative to the noise can be neglected since it is independent of the direction θ. The radiation pattern is given by

$$D(\theta) = \left|\mathbf{w}^H(\theta_d)\mathbf{a}(\theta)\right|^2. \quad (5)$$

B. RF I/Q imbalance

DCR down-converts the received RF signal to two real-valued baseband signals, called in-phase (I) and quadrature-phase (Q) components [24]. Ideally, the conversion is done with two local oscillator signals and mixers, which have equal gains and exactly 90 degrees phase difference. However, in practice oscillator signals and mixers have a gain mismatch and they are not in perfect phase quadrature [9]. For this reason, the characteristics and statistics of the resulting signal are changed and the corresponding complex signal, even if originally circular, becomes non-circular [11]. This effect is called I/Q imbalance and can be modeled for an individual signal or radio chain at baseband equivalent level as [10]

$$x_{\mathrm{imb}}(t) = K_1 x(t) + K_2 x^*(t) \quad (6)$$

where

$$K_1 = \frac{(1+ge^{-j\phi})}{2} \quad \text{and} \quad K_2 = \frac{1-ge^{j\phi}}{2} \quad (7)$$

and $x(t)$ is the baseband equivalent signal under ideal I/Q matching. Here, g presents the relative gain mismatch and ϕ presents the phase mismatch between the I- and Q-branch. Ideally $g = 1$ and $\phi = 0°$. In the context of antenna arrays with multiple parallel DCRs (one per antenna), (2) and (6) can be combined, leading to signal snapshots with I/Q imbalance given by

$$\mathbf{x}_{\mathrm{imb}} = \mathbf{K}_1\mathbf{x} + \mathbf{K}_2\mathbf{x}^* = [\mathbf{K}_1, \mathbf{K}_2]\begin{bmatrix} s\mathbf{a}(\theta)+\mathbf{n} \\ s^*\mathbf{a}^*(\theta)+\mathbf{n}^* \end{bmatrix} \quad (8)$$

where

$$\mathbf{K}_1 = \begin{bmatrix} K_{1,1} & 0 & \cdots & 0 \\ 0 & K_{1,2} & \cdots & 0 \\ \vdots & \vdots & \ddots & \vdots \\ 0 & 0 & \cdots & K_{1,N} \end{bmatrix} \quad (9)$$

and

$$\mathbf{K}_2 = \begin{bmatrix} K_{2,1} & 0 & \cdots & 0 \\ 0 & K_{2,2} & \cdots & 0 \\ \vdots & \vdots & \ddots & \vdots \\ 0 & 0 & \cdots & K_{2,N} \end{bmatrix}. \quad (10)$$

Matrices $\mathbf{K}_1$ and $\mathbf{K}_2$ are referring to the I/Q imbalance coefficients of each parallel receiver branch. When the ideal signal snapshots in (3) are substituted with the signal snapshots including I/Q imbalance in (8), the output signal with given weights and under I/Q imbalance is now given by

$$\begin{aligned} y_{\mathrm{imb}}(\theta) &= \mathbf{w}^H(\theta_{\mathrm{d}})\mathbf{x}_{\mathrm{imb}} \\ &= \mathbf{w}^H(\theta_{\mathrm{d}})\left[\mathbf{K}_1, \mathbf{K}_2\right]\begin{bmatrix} s\mathbf{a}(\theta)+\mathbf{n} \\ s^*\mathbf{a}^*(\theta)+\mathbf{n}^* \end{bmatrix} \\ &= \mathbf{w}^H(\theta_{\mathrm{d}})\mathbf{K}_1\left(s\mathbf{a}(\theta)+\mathbf{n}\right) \\ &\quad + \mathbf{w}^H(\theta_{\mathrm{d}})\mathbf{K}_2\left(s^*\mathbf{a}^*(\theta)+\mathbf{n}^*\right). \end{aligned} \quad (11)$$

This interesting result has two important implications. On the one hand, the output is not only corrupted by the common response $\mathbf{K}_1$ but also suffers from the self interference due to complex conjugate term. Since in realistic scenarios $|K_{1,i}| \gg |K_{2,i}|\ \forall\, i$ [25] and $\left|\mathbf{w}^H(\theta_{\mathrm{d}})\mathbf{a}(\theta)\right| \gg \left|\mathbf{w}^H(\theta_{\mathrm{d}})\mathbf{a}^*(\theta)\right|$, the effect of the conjugate term is fairly small but cannot be neglected, especially with high-order modulations. In fact, this term creates a twist to the original symbols which is illustrated with numerical results in section V. On the other hand, and more importantly, if there happens to be an actual interfering signal coming from the direction θ_{int} which satisfies an equality $\mathbf{a}^*(\theta_{\mathrm{int}}) = \mathbf{a}(\theta)$, the conjugate term of this interfering signal is essentially seen by the beamformer as an additional signal coming from the desired direction. Since the interfering signal can be much stronger than the desired signal, the additional signal term can be even stronger than the desired signal and the overall performance is heavily deteriorated. It should also be noticed that I/Q imbalance indeed creates a WL transformation to the signal which

gives us a motivation for the WL beamforming developments in section II-C.

Assuming next a circular input signal s, for which $\mathbb{E}\left[s^2\right] = 0$, the power of the output signal in (11) under I/Q imbalance is then given by

$$\begin{aligned}\mathbb{E}\left[|y_{\text{imb}}(\theta)|^2\right] &= \sigma_s^2 \left|\mathbf{w}^H(\theta_\text{d})\mathbf{K}_1\mathbf{a}(\theta)\right|^2 \\ &+ \sigma_s^2 \left|\mathbf{w}^H(\theta_\text{d})\mathbf{K}_2\mathbf{a}^*(\theta)\right|^2 \\ &+ \mathbf{w}^H(\theta_\text{d})\mathbf{K}_1\mathbf{R}_\mathbf{n}\mathbf{K}_1^H\mathbf{w}(\theta_\text{d}) \\ &+ \mathbf{w}^H(\theta_\text{d})\mathbf{K}_2\mathbf{R}_\mathbf{n}^*\mathbf{K}_2^H\mathbf{w}(\theta_\text{d}) \qquad (12)\end{aligned}$$

Stemming from (12), the radiation pattern of the beamformer under I/Q imbalance can be formulated similarly to (5). Thus the radiation pattern is now given by

$$D_{\text{imb}}(\theta) = \left|\mathbf{w}^H(\theta_\text{d})\mathbf{K}_1\mathbf{a}(\theta)\right|^2 + \left|\mathbf{w}^H(\theta_\text{d})\mathbf{K}_2\mathbf{a}^*(\theta)\right|^2. \quad (13)$$

Due to the effect of I/Q imbalance, the radiation pattern is clearly corrupted and consists of two terms. Here, it is interesting to notice that in case of the ULA, $\mathbf{a}^*(\theta)$ corresponds to the *spatially mirrored steering vector* $\mathbf{a}(180^\circ - \theta)$. This creates an additional beam to the mirror direction $180^\circ - \theta$ and this beam is therefore referred to as the *mirror beam* [20]. Thus, this increases the sensitivity of the array to receive energy also from the mirror angle $180^\circ - \theta$.

C. Widely-Linear Beamforming

WL beamforming is a natural choice for mitigating the effect of I/Q imbalance, since by definition the WL structure combines both the direct signal snapshot $\mathbf{x}$ and the complex conjugate $\mathbf{x}^*$ with weights $\mathbf{w}_1$ and $\mathbf{w}_2$, respectively. This results in doubled computational complexity compared with the conventional linear beamforming but also offers doubled degrees of freedom to obtain I/Q imbalance-free output signal. The WL beamformer is depicted in Fig. 2.

In order to emphasize the general properties of the WL beamforming, a definition for the WL beamforming under perfect I/Q balance is first given by

$$\tilde{y} = \mathbf{w}_1^H\mathbf{x} + \mathbf{w}_2^H\mathbf{x}^* = \tilde{\mathbf{w}}^H\tilde{\mathbf{x}} \qquad (14)$$

where the augmented weight vector $\tilde{\mathbf{w}} = [\mathbf{w}_1^T, \mathbf{w}_2^T]^T \in \mathbb{C}^{2N\times 1}$ and the augmented signal snapshot vector $\tilde{\mathbf{x}} = [\mathbf{x}^T, \mathbf{x}^H]^T \in \mathbb{C}^{2N\times 1}$. When using the signal model in (2), the output signal of the WL beamformer can be written as

$$\begin{aligned}\tilde{y}(\theta) &= \begin{bmatrix}\mathbf{w}_1^H(\theta_\text{d}) & \mathbf{w}_2^H(\theta_\text{d})\end{bmatrix}\begin{bmatrix}s\mathbf{a}(\theta)+\mathbf{n} \\ s^*\mathbf{a}^*(\theta)+\mathbf{n}^*\end{bmatrix} \\ &= \mathbf{w}_1^H(\theta_\text{d})\left(s\mathbf{a}(\theta)+\mathbf{n}\right) + \mathbf{w}_2^H(\theta_\text{d})\left(s^*\mathbf{a}^*(\theta)+\mathbf{n}^*\right). \qquad (15)\end{aligned}$$

Here, the similarities with WL transformation in (11) due to I/Q imbalance can be seen easily, i.e. the signal itself and its complex conjugate are present. Here, however, we have more degrees of freedom due to two sets of weights to form the output signal, in general.

With circular signals and ideal I/Q balance, complex conjugate of the signal does not include any additional information for the beamforming problem (the signal itself is totally uncorrelated with its complex conjugate) and therefore WL processing does not offer any particular performance gain. However, as shown in this paper, the WL processing can offer high performance gain in the presence of RF I/Q imbalance. Now, under

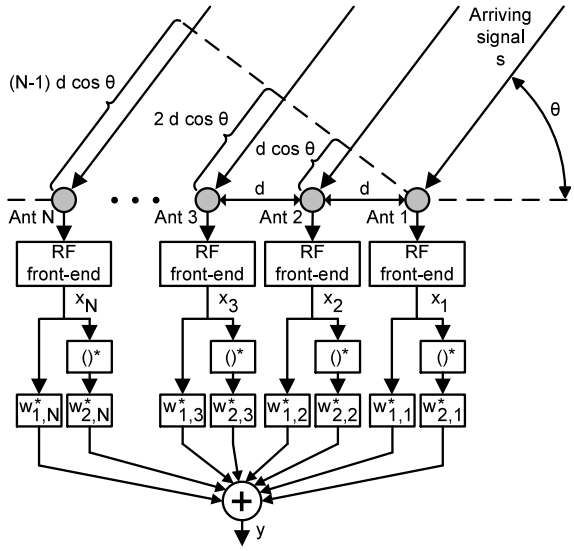

Fig. 2. The widely-linear beamformer with a uniform linear array implementation. The flow of the arriving signal is presented by arrows.

$$\tilde{y}_{\text{imb}}(\theta) = \tilde{\mathbf{w}}^H(\theta_\text{d})\tilde{\mathbf{x}}_{\text{imb}} = \begin{bmatrix}\mathbf{w}_1^H(\theta_\text{d}) & \mathbf{w}_2^H(\theta_\text{d})\end{bmatrix}\begin{bmatrix}\mathbf{K}_1 & \mathbf{K}_2 \\ \mathbf{K}_2^* & \mathbf{K}_1^*\end{bmatrix}\begin{bmatrix}s\mathbf{a}(\theta)+\mathbf{n} \\ s^*\mathbf{a}^*(\theta)+\mathbf{n}^*\end{bmatrix}$$
$$= \left(\mathbf{w}_1^H(\theta_\text{d})\mathbf{K}_1 + \mathbf{w}_2^H(\theta_\text{d})\mathbf{K}_2^*\right)\left(s\mathbf{a}(\theta)+\mathbf{n}\right) + \left(\mathbf{w}_1^H(\theta_\text{d})\mathbf{K}_2 + \mathbf{w}_2^H(\theta_\text{d})\mathbf{K}_1^*\right)\left(s^*\mathbf{a}^*(\theta)+\mathbf{n}^*\right) \qquad (16)$$

$$\begin{aligned}\mathbb{E}\left[|\tilde{y}_{\text{imb}}(\theta)|^2\right] &= \sigma_s^2\left|\mathbf{w}_1^H(\theta_\text{d})\mathbf{K}_1\mathbf{a}(\theta) + \mathbf{w}_2^H(\theta_\text{d})\mathbf{K}_2^*\mathbf{a}(\theta)\right|^2 + \sigma_s^2\left|\mathbf{w}_1^H(\theta_\text{d})\mathbf{K}_2\mathbf{a}^*(\theta) + \mathbf{w}_2^H(\theta_\text{d})\mathbf{K}_1^*\mathbf{a}^*(\theta)\right|^2 \\ &+ \mathbf{w}_1^H(\theta_\text{d})\mathbf{K}_1\mathbf{R}_\mathbf{n}\mathbf{K}_1^H\mathbf{w}_1(\theta_\text{d}) + \mathbf{w}_2^H(\theta_\text{d})\mathbf{K}_2^*\mathbf{R}_\mathbf{n}\mathbf{K}_2^T\mathbf{w}_2(\theta_\text{d}) + \mathbf{w}_1^H(\theta_\text{d})\mathbf{K}_2\mathbf{R}_\mathbf{n}^*\mathbf{K}_2^H\mathbf{w}_1(\theta_\text{d}) \\ &+ \mathbf{w}_2^H(\theta_\text{d})\mathbf{K}_1^*\mathbf{R}_\mathbf{n}^*\mathbf{K}_1^T\mathbf{w}_2(\theta_\text{d}) + \mathbf{w}_1^H(\theta_\text{d})\mathbf{K}_1\mathbf{R}_\mathbf{n}\mathbf{K}_2^T\mathbf{w}_2(\theta_\text{d}) + \mathbf{w}_2^H(\theta_\text{d})\mathbf{K}_2^*\mathbf{R}_\mathbf{n}\mathbf{K}_1^H\mathbf{w}_1(\theta_\text{d}) \\ &+ \mathbf{w}_1^H(\theta_\text{d})\mathbf{K}_2\mathbf{R}_\mathbf{n}^*\mathbf{K}_1^T\mathbf{w}_2(\theta_\text{d}) + \mathbf{w}_2^H(\theta_\text{d})\mathbf{K}_1^*\mathbf{R}_\mathbf{n}^*\mathbf{K}_2^H\mathbf{w}_1(\theta_\text{d}) \qquad (17)\end{aligned}$$

RF I/Q imbalance, the WL combiner output signal as a function of direction θ is given by (16). Further, the power of this output signal is given by (17). Based on this, the radiation pattern of the WL beamformer under I/Q imbalance is given by

$$\tilde{D}_{\text{imb}}(\theta) = \left|\mathbf{w}_1^H(\theta_\text{d})\mathbf{K}_1\mathbf{a}(\theta) + \mathbf{w}_2^H(\theta_\text{d})\mathbf{K}_2^*\mathbf{a}(\theta)\right|^2 + \left|\mathbf{w}_1^H(\theta_\text{d})\mathbf{K}_2\mathbf{a}^*(\theta) + \mathbf{w}_2^H(\theta_\text{d})\mathbf{K}_1^*\mathbf{a}^*(\theta)\right|^2. \quad (18)$$

Again, it is clear that both terms, relative to the initial steering vector $\mathbf{a}(\theta)$ and to the complex conjugate $\mathbf{a}^*(\theta)$, exist in the radiation pattern equation. The first term represents the desired response whereas the second one represents the unwanted spurious response. However, both these terms depend now on the two sets of weights, $\mathbf{w}_1$ and $\mathbf{w}_2$, and thus there are more degrees of freedom to control the beam characteristics.

In the following sections, we will use these fundamental signal models and derive RF-aware beamforming coefficients deploying e.g. the MVDR optimization criteria. Also input interference is taken explicitly into account.

III. Reference Beamforming under Known I/Q Imbalance

To clarify the capabilities of linear and WL beamformers, in terms of mitigating the effects of I/Q imbalance, a comparison to the well-known SMF under perfect I/Q balance is done next. In general, SMF is defined as a combiner with perfect phase alignment for the signals from different antenna elements. In the context of beamforming, SMF is matched to the steering vector of an antenna array. This way, SMF maximizes the total useful signal output power under the constraint $||\mathbf{w}|| = 1$ and the weights of SMF are given by

$$\mathbf{w}_{\text{SMF}}(\theta_\text{d}) = \frac{\mathbf{a}(\theta_\text{d})}{\sqrt{\mathbf{a}^H(\theta_\text{d})\mathbf{a}(\theta_\text{d})}} = \frac{\mathbf{a}(\theta_\text{d})}{\sqrt{N}}. \quad (19)$$

When combining the ideal signal snapshots $\mathbf{x}$ with these weights, the resulting output signal is given by

$$y_{\text{SMF}}(\theta) = \mathbf{w}_{\text{SMF}}^H(\theta_\text{d})\mathbf{x} = \frac{s\mathbf{a}^H(\theta_\text{d})\mathbf{a}(\theta) + \mathbf{a}^H(\theta_\text{d})\mathbf{n}}{\sqrt{N}}. \quad (20)$$

Thus, when signal is arriving from the desired direction θ_d, the output $y_{\text{SMF}}(\theta_\text{d}) = \sqrt{N}s + \mathbf{a}^H(\theta_\text{d})\mathbf{n}/\sqrt{N}$.

In order to achieve such response characteristics with the conventional linear beamformer under I/Q imbalance, the responses in (11) and (20) have to be equal. This leads to the following set of equations:

$$\begin{cases} \mathbf{w}^H\mathbf{K}_1 \;=\; \dfrac{\mathbf{a}^H(\theta_\text{d})}{\sqrt{N}} \\ \mathbf{w}^H\mathbf{K}_2 \;=\; \mathbf{0}_N \end{cases} \quad (21)$$

where $\mathbf{0}_N$ is $N \times 1$ zero vector. Since $\mathbf{K}_1$ and $\mathbf{K}_2$ are not zero, these two requirements are contradicting and therefore not reachable simultaneously. Consequently, the weights of the linear beamformer will always lead to a corrupted output signal which is a combination of the desired response (the term in (11) including $\mathbf{w}^H\mathbf{K}_1$) and spurious response (the term in (11) including $\mathbf{w}^H\mathbf{K}_2$).

In case of WL beamforming, however, the comparison between (16) and (20) shows that the optimal solution for the WL weights, in SMF sense, can be obtained with the following two requirements.

$$\begin{cases} \mathbf{w}_1^H\mathbf{K}_1 + \mathbf{w}_2^H\mathbf{K}_2^* \;=\; \dfrac{\mathbf{a}^H(\theta_\text{d})}{\sqrt{N}} \\ \mathbf{w}_1^H\mathbf{K}_2 + \mathbf{w}_2^H\mathbf{K}_1^* \;=\; \mathbf{0}_N \end{cases} \quad (22)$$

These requirements can be met simultaneously without any contradictions or trade-offs. Solving (22) for the weights yields

$$\mathbf{w}_1 = \left[-\frac{\mathbf{a}^H(\theta_\text{d})}{\sqrt{N}}\left[-\mathbf{K}_1^*\mathbf{K}_2^{-1}\mathbf{K}_1 + \mathbf{K}_2^*\right]^{-1}\mathbf{K}_1^*\mathbf{K}_2^{-1}\right]^H, \quad (23)$$

$$\mathbf{w}_2 = \left[\frac{\mathbf{a}^H(\theta_\text{d})}{\sqrt{N}}\left[-\mathbf{K}_1^*\mathbf{K}_2^{-1}\mathbf{K}_1 + \mathbf{K}_2^*\right]^{-1}\right]^H. \quad (24)$$

With these weights, the output of the WL beamformer under I/Q imbalance matches perfectly to the output of the SMF under perfect I/Q balance. However, this solution does not take possible interfering signals into account and thus is not able to steer explicit nulls towards interference sources. To overcome this problem, MVDR and WL-MVDR based solutions, which have a built-in capability for null steering towards interference sources, are studied in the next section. Thus, the above principal derivations mainly serve to pointing out the better structural capabilities of WL beamforming compared to classical linear solutions. In general, efficient interference suppression solutions are one of the biggest targets of massive MIMO deployments e.g. in cellular mobile radio systems.

IV. MVDR and WL-MVDR Beamforming under I/Q Imbalance

In the previous sections, the signal characteristics and radiation patterns of linear arrays under RF I/Q imbalance were derived for arbitrary (given) beamformer weights, while the detailed beamformer weight optimization problem was not yet addressed. In this section, we focus in detail on this weight optimization task when the desired direction θ_d and therefore also the corresponding steering vector $\mathbf{a}(\theta_\text{d})$ are known. The focus will be on the well-known MVDR beamformer (also known as Capon's beamformer [26]) concept and WL-MVDR. They are able to steer nulls towards possible interference sources without explicitly knowing directions of the interference and thus in general to improve the combiner output signal quality in different interference scenarios.

To quantify the null steering capabilities of MVDR and WL-MVDR, the interfering signals are now added explicitly to the signal model. The modified signal model (first assuming ideal I/Q balance) is given by

$$\mathbf{x} = s\mathbf{a}(\theta) + \mathbf{z} \quad (25)$$

where the total interference plus noise term $\mathbf{z}$ is given by

$$\mathbf{z} = \sum_{j=1}^{M_{\text{int}}} s_{\text{int},j}\mathbf{a}(\theta_{\text{int},j}) + \mathbf{n}. \quad (26)$$

Here, $\mathbf{z}$ consist of the interfering signals $s_{\text{int},j}$ with the corresponding steering vectors $\mathbf{a}(\theta_{\text{int},j})$, and the noise vector $\mathbf{n}$. Further, M_{int} denotes the amount of the interfering signals and s, $s_{\text{int},j}\ \forall\ j$ and elements of $\mathbf{n}$ are all assumed to be circular and mutually uncorrelated. We assume no knowledge of the interference angles or powers, nor the noise power. Now, when I/Q imbalance is included into the signal model (25), the result is given by

$$\mathbf{x}_{\text{imb}} = \mathbf{K}_1\mathbf{x} + \mathbf{K}_2\mathbf{x}^* = [\mathbf{K}_1, \mathbf{K}_2]\begin{bmatrix} s\mathbf{a}(\theta) + \mathbf{z} \\ s^*\mathbf{a}^*(\theta) + \mathbf{z}^* \end{bmatrix}. \quad (27)$$

A. Linear MVDR under I/Q Imbalance

By definition, and starting first without I/Q imbalance for reference, the conventional MVDR beamformer minimizes the total output variance

$$\mathbb{E}\left[|y|^2\right] = \mathbf{w}^H\,\mathbb{E}\left[\mathbf{x}\mathbf{x}^H\right]\mathbf{w} = \mathbf{w}^H\mathbf{R}_{\mathbf{x}}\mathbf{w} \quad (28)$$

under the constraint $\mathbf{w}^H\mathbf{a}(\theta_{\text{d}}) = 1$ [21]. Here, $\mathbf{R}_{\mathbf{x}} \in \mathbb{C}^{N\times N}$ denotes the covariance matrix of $\mathbf{x}$ and is given by

$$\begin{aligned}\mathbf{R}_{\mathbf{x}} &= \mathbb{E}\left[\mathbf{x}\mathbf{x}^H\right] \\ &= \sigma_s^2\mathbf{a}(\theta_{\text{d}})\mathbf{a}^H(\theta_{\text{d}}) + \sigma_n^2\mathbf{I}_N \\ &\quad + \sum_{j=1}^{M_{\text{int}}}\sigma_{\text{int},j}^2\mathbf{a}(\theta_{\text{int},j})\mathbf{a}^H(\theta_{\text{int},j}) \end{aligned} \quad (29)$$

where σ_s^2 denotes signal variance, σ_n^2 stands for noise variance, $\sigma_{\text{int},j}^2$ is variance of the interfering signal j and $\mathbf{I}_N$ is a unit matrix of size $N \times N$.

The minimization of the output variance leads to the built-in capability to attenuate interfering signals, i.e. MVDR is able to steer nulls towards the interference sources in the surroundings. This is of course well known [27]. The optimum solution for the minimization task above, is a weight vector given by [21]

$$\mathbf{w}_{\text{MVDR}}(\theta_{\text{d}}) = \frac{\mathbf{R}_{\mathbf{x}}^{-1}\mathbf{a}(\theta_{\text{d}})}{\mathbf{a}^H(\theta_{\text{d}})\mathbf{R}_{\mathbf{x}}^{-1}\mathbf{a}(\theta_{\text{d}})}. \quad (30)$$

In the presence of I/Q imbalance, received signal snapshots are corrupted and the covariance matrix is distorted. Stemming from (27), the covariance matrix under I/Q imbalance is given by

$$\begin{aligned}\mathbf{R}_{\mathbf{x},\text{imb}} &= \mathbb{E}\left[\mathbf{x}_{\text{imb}}{\mathbf{x}_{\text{imb}}}^H\right] \\ &= \sigma_s^2\mathbf{K}_1\mathbf{a}(\theta_{\text{d}})\mathbf{a}^H(\theta_{\text{d}})\mathbf{K}_1^H + \sigma_n^2\mathbf{K}_1\mathbf{I}_N\mathbf{K}_1^H \\ &\quad + \sum_{j=1}^{M_{\text{int}}}\sigma_{\text{int},j}^2\mathbf{K}_1\mathbf{a}(\theta_{\text{int},j})\mathbf{a}^H(\theta_{\text{int},j})\mathbf{K}_1^H \\ &\quad + \sigma_s^2\mathbf{K}_2\mathbf{a}^*(\theta_{\text{d}})\mathbf{a}^T(\theta_{\text{d}})\mathbf{K}_2^H + \sigma_n^2\mathbf{K}_2\mathbf{I}_N\mathbf{K}_2^H \\ &\quad + \sum_{j=1}^{M_{\text{int}}}\sigma_{\text{int},j}^2\mathbf{K}_2\mathbf{a}^*(\theta_{\text{int},j})\mathbf{a}^T(\theta_{\text{int},j})\mathbf{K}_2^H. \end{aligned} \quad (31)$$

Now it is clear that $\mathbf{R}_{\mathbf{x},\text{imb}}$ in (31) is a distorted version of $\mathbf{R}_{\mathbf{x}}$ in (29), on the one hand due to the multiplication of the wanted terms with $\mathbf{K}_1$ and $\mathbf{K}_1^H$ and on the other due to the new terms including $\mathbf{K}_2$ and $\mathbf{K}_2^H$. In particular, one can notice that if one of the interfering signals arrives from angle $180^\circ - \theta_{\text{d}}$, then this creates a term structurally identical to the desired steering vector since $\mathbf{a}^*(180^\circ - \theta_{\text{d}}) = \mathbf{a}(\theta_{\text{d}})$. This will greatly degrade the interference suppression capabilities like will be illustrated later.

In order to suppress the unwanted effects of the corrupted covariance matrix, the MVDR algorithm has to be modified. The algorithm should now minimize the unwanted effects of I/Q imbalance while still having unit response to the desired direction. If the I/Q imbalance coefficients $\mathbf{K}_1$ and $\mathbf{K}_2$ (i.e. g_i and $\phi_i\ \forall\ i$) are known or can be estimated in advance (state-of-the-art blind imbalance extraction methods are described e.g., in [28]), these requirements can be rewritten as modified MVDR constraints, namely

$$\begin{cases} \mathbf{w}^H\mathbf{K}_1\mathbf{a}(\theta_{\text{d}}) &= 1 \\ \mathbf{w}^H\mathbf{K}_2\mathbf{a}^*(\theta_{\text{d}}) &= 0 \end{cases}. \quad (32)$$

It should be noticed that with this method only the knowledge of the I/Q imbalance coefficients is needed but the I/Q imbalance calibration itself does not have to be done for individual receiver chains. These constraints result in weights given by

$$\mathbf{w}_{\text{MVDR,mod}}(\theta_{\text{d}}) = \mathbf{R}_{\mathbf{x},\text{imb}}^{-1}\mathbf{A}(\theta_{\text{d}})\left[\mathbf{A}^H(\theta_{\text{d}})\mathbf{R}_{\mathbf{x},\text{imb}}^{-1}\mathbf{A}(\theta_{\text{d}})\right]^{-1}\begin{bmatrix} 1 \\ 0 \end{bmatrix} \quad (33)$$

where $\mathbf{A}(\theta_{\text{d}}) = [\mathbf{K}_1\mathbf{a}(\theta_{\text{d}}), \mathbf{K}_2\mathbf{a}^*(\theta_{\text{d}})] \in \mathbb{C}^{N\times 2}$ is the modified steering vector containing the knowledge of the I/Q imbalance coefficients and $[1, 0]^T$ is a vector consisting of the wanted responses. This modification enables some attenuation of the I/Q imbalance effects, however the plain linear processing cannot fully suppress the I/Q imbalance effects due to lack of degrees of freedom noticed already in (21). Another drawback of this algorithm is that it cannot be used under perfect I/Q balance since in that case the right column of $\mathbf{A}(\theta_{\text{d}})$ is all zeros, and therefore the matrix inversion in (33) cannot be done.

B. WL-MVDR under I/Q imbalance

The WL extension of MVDR referred to as WL-MVDR offers the same flexibility as WL beamforming in general while also having the built-in null steering capability. WL-MVDR minimizes the total output variance under the augmented signal model written here first without I/Q imbalance as

$$\mathbb{E}\left[|\tilde{y}|^2\right] = \tilde{\mathbf{w}}^H\,\mathbb{E}\left[\tilde{\mathbf{x}}\tilde{\mathbf{x}}^H\right]\tilde{\mathbf{w}} = \tilde{\mathbf{w}}^H\tilde{\mathbf{R}}_{\mathbf{x}}\tilde{\mathbf{w}} \quad (34)$$

under the constraints $\mathbf{w}_1^H\mathbf{a}(\theta_{\text{d}}) = 1$ and $\mathbf{w}_2^H\mathbf{a}^*(\theta_{\text{d}}) = 0$ [14]. Again, the augmented weight vector $\tilde{\mathbf{w}} = [\mathbf{w}_1^T, \mathbf{w}_2^T]^T \in \mathbb{C}^{2N\times 1}$ and augmented signal snapshot vector $\tilde{\mathbf{x}} = [\mathbf{x}^T, \mathbf{x}^H]^T \in \mathbb{C}^{2N\times 1}$. The optimum solution for the augmented weight vector is given by

$$\tilde{\mathbf{w}}_{\text{MVDR}}(\theta_{\text{d}}) = \tilde{\mathbf{R}}_{\mathbf{x}}^{-1}\tilde{\mathbf{A}}(\theta_{\text{d}})\left[\tilde{\mathbf{A}}^H(\theta_{\text{d}})\tilde{\mathbf{R}}_{\mathbf{x}}^{-1}\tilde{\mathbf{A}}(\theta_{\text{d}})\right]^{-1}\begin{bmatrix} 1 \\ 0 \end{bmatrix} \quad (35)$$

where the augmented steering vector or matrix is equal to

$$\tilde{\mathbf{A}}(\theta_{\mathrm{d}}) = \begin{bmatrix} \mathbf{a}(\theta_{\mathrm{d}}) & \mathbf{0}_{N\times 1} \\ \mathbf{0}_{N\times 1} & \mathbf{a}^*(\theta_{\mathrm{d}}) \end{bmatrix} \tag{36}$$

and the augmented covariance matrix is given by

$$\tilde{\mathbf{R}}_{\mathbf{x}} = \begin{bmatrix} \mathbf{R}_{\mathbf{x}} & \mathbf{C}_{\mathbf{x}} \\ \mathbf{C}_{\mathbf{x}}^* & \mathbf{R}_{\mathbf{x}}^* \end{bmatrix}. \tag{37}$$

Here $\mathbf{C}_{\mathbf{x}} = \mathbb{E}\left[\mathbf{x}\mathbf{x}^T\right] \in \mathbb{C}^{N\times N}$ denotes the complementary covariance matrix of $\mathbf{x}$.

Next we take the effects of I/Q imbalance again into account. The corruption of the covariance matrix $\mathbf{R}_{\mathbf{x}}$, shown in (31), has its own contribution since it is a part of the augmented covariance matrix $\tilde{\mathbf{R}}_{\mathbf{x}}$. In addition, the complementary covariance matrix is also affected by I/Q imbalance and is given by

$$\begin{aligned} \mathbf{C}_{\mathbf{x},\mathrm{imb}} &= \mathbb{E}\left[\mathbf{x}_{\mathrm{imb}}\mathbf{x}_{\mathrm{imb}}^T\right] \\ &= \sigma_s^2\mathbf{K}_1\mathbf{a}(\theta_{\mathrm{d}})\mathbf{a}^H(\theta_{\mathrm{d}})\mathbf{K}_2^T + \sigma_n^2\mathbf{K}_1\mathbf{I}_N\mathbf{K}_2^T \\ &\quad + \sum_{j=1}^{M_{\mathrm{int}}} \sigma_{\mathrm{int},j}^2\mathbf{K}_1\mathbf{a}(\theta_{\mathrm{int},j})\mathbf{a}^H(\theta_{\mathrm{int},j})\mathbf{K}_2^T \\ &\quad + \sigma_s^2\mathbf{K}_2\mathbf{a}^*(\theta_{\mathrm{d}})\mathbf{a}^T(\theta_{\mathrm{d}})\mathbf{K}_1^T + \sigma_n^2\mathbf{K}_2\mathbf{I}_N\mathbf{K}_1^T \\ &\quad + \sum_{j=1}^{M_{\mathrm{int}}} \sigma_{\mathrm{int},j}^2\mathbf{K}_2\mathbf{a}^*(\theta_{\mathrm{int},j})\mathbf{a}^T(\theta_{\mathrm{int},j})\mathbf{K}_1^T. \end{aligned} \tag{38}$$

Here, it is easy to see that under perfect I/Q balance (when $\mathbf{K}_1 = \mathbf{I}_N$ and $\mathbf{K}_2 = \mathbf{0}_N$) $\mathbf{C}_{\mathbf{x},\mathrm{imb}}$ becomes zero stemming from the circularity assumption of the ideal signals. Again, we can notice the impact of possible interference arriving from the mirror angle $180^\circ - \theta_{\mathrm{d}}$, creating a covariance term structurally similar to the ideal signal component.

Now, it is straightforward to define the augmented covariance matrix under I/Q imbalance to be used with WL-MVDR in (35). It is simply a combination of $\mathbf{R}_{\mathbf{x},\mathrm{imb}}$ in (31) and $\mathbf{C}_{\mathbf{x},\mathrm{imb}}$ in (38) given by

$$\tilde{\mathbf{R}}_{\mathbf{x},\mathrm{imb}} = \begin{bmatrix} \mathbf{R}_{\mathbf{x},\mathrm{imb}} & \mathbf{C}_{\mathbf{x},\mathrm{imb}} \\ \mathbf{C}_{\mathbf{x},\mathrm{imb}}^* & \mathbf{R}_{\mathbf{x},\mathrm{imb}}^* \end{bmatrix}. \tag{39}$$

Then, similar to earlier discussion concerning MVDR, also WL-MVDR has to be modified in order to mitigate the effects of the corrupted covariance matrix. It can be seen from (16) already that for suppressing the effects of I/Q imbalance completely from the response, the following two constraints have to be fulfilled

$$\begin{cases} \mathbf{w}_1^H\mathbf{K}_1\mathbf{a}(\theta_{\mathrm{d}}) + \mathbf{w}_2^H\mathbf{K}_2^*\mathbf{a}(\theta_{\mathrm{d}}) &= 1 \\ \mathbf{w}_1^H\mathbf{K}_2\mathbf{a}^*(\theta_{\mathrm{d}}) + \mathbf{w}_2^H\mathbf{K}_1^*\mathbf{a}^*(\theta_{\mathrm{d}}) &= 0 \end{cases}. \tag{40}$$

When these constraints are used with WL-MVDR, the augmented steering vector, to be used in (35) instead of $\tilde{\mathbf{A}}(\theta_{\mathrm{d}})$, has to be rewritten in the form of

$$\tilde{\mathbf{A}}_{\mathrm{mod}}(\theta_{\mathrm{d}}) = \begin{bmatrix} \mathbf{K}_1\mathbf{a}(\theta_{\mathrm{d}}) & \mathbf{K}_2\mathbf{a}^*(\theta_{\mathrm{d}}) \\ \mathbf{K}_2^*\mathbf{a}(\theta_{\mathrm{d}}) & \mathbf{K}_1^*\mathbf{a}^*(\theta_{\mathrm{d}}) \end{bmatrix}. \tag{41}$$

This way, WL-MVDR suppresses all the effects of I/Q imbalance and is simultaneously able to steer nulls towards possible interfering signal sources as will be shown in the next section with numerical examples. We call this solution *RF-aware WL-MVDR beamformer.*

C. SINR Expressions

To explicitly quantify and compare the properties of the output signals with different beamforming solutions, the signal-to-interference-plus-noise ratios (SINR's) are defined and analyzed next. For general weights $\mathbf{w}(\theta_{\mathrm{d}})$ (optimized under a given optimization criterion), the SINR of the linear beamformer without I/Q imbalance can be written as

$$\mathrm{SINR}(\theta_{\mathrm{d}}) = \frac{\sigma_s^2\left|\mathbf{w}^H(\theta_{\mathrm{d}})\mathbf{a}(\theta_{\mathrm{d}})\right|^2}{\mathbf{w}^H(\theta_{\mathrm{d}})\mathbf{R}_{\mathbf{z}}\mathbf{w}(\theta_{\mathrm{d}})} \tag{42}$$

where $\mathbf{R}_{\mathbf{z}} = \mathbb{E}\left[\mathbf{z}\mathbf{z}^H\right] \in \mathbb{C}^{N\times N}$ refers to the covariance matrix of $\mathbf{z}$ in (26). If there are no interferers present, i.e. $\mathbf{z} = \mathbf{n}$, this results matches also to the classical definition of signal-to-noise ratio (SNR).

I/Q imbalance corrupts the signals and thus obviously also influences the SINR. The SINR of the linear beamformer under I/Q imbalance is given by (43) at the bottom of the page. There we have already included the conjugate signal term relative to $s^*\mathbf{a}^*(\theta)$ into the interference, stemming from the above discussion related to spurious response, in addition to all the actual interference terms contained in $\mathbf{R}_{\mathbf{z}}$ and $\mathbf{R}_{\mathbf{z}}^*$. Now it is clear that not only the useful signal power itself is changed, with respect to the $\mathbf{K}_1$, but also the interference includes a term which depends on the input signal characteristics and the mirroring effect as well as the conjugates of all the original interferers. Numerical examples will be given later.

$$\mathrm{SINR}_{\mathrm{imb}}(\theta_{\mathrm{d}}) = \frac{\sigma_s^2\left|\mathbf{w}^H(\theta_{\mathrm{d}})\mathbf{K}_1\mathbf{a}(\theta_{\mathrm{d}})\right|^2}{\sigma_s^2\left|\mathbf{w}^H(\theta_{\mathrm{d}})\mathbf{K}_2\mathbf{a}^*(\theta_{\mathrm{d}})\right|^2 + \mathbf{w}^H(\theta_{\mathrm{d}})\mathbf{K}_1\mathbf{R}_{\mathbf{z}}\mathbf{K}_1^H\mathbf{w}(\theta_{\mathrm{d}}) + \mathbf{w}^H(\theta_{\mathrm{d}})\mathbf{K}_2\mathbf{R}_{\mathbf{z}}^*\mathbf{K}_2^H\mathbf{w}(\theta_{\mathrm{d}})} \tag{43}$$

$$\begin{aligned} \widetilde{\mathrm{SINR}}_{\mathrm{imb}}(\theta_{\mathrm{d}}) = \frac{\sigma_s^2\left|\mathbf{w}_1^H(\theta_{\mathrm{d}})\mathbf{K}_1\mathbf{a}(\theta_{\mathrm{d}}) + \mathbf{w}_2^H(\theta_{\mathrm{d}})\mathbf{K}_2^*\mathbf{a}(\theta_{\mathrm{d}})\right|^2}{\sigma_s^2\left|\mathbf{w}_1^H(\theta_{\mathrm{d}})\mathbf{K}_2\mathbf{a}^*(\theta_{\mathrm{d}}) + \mathbf{w}_2^H(\theta_{\mathrm{d}})\mathbf{K}_1^*\mathbf{a}^*(\theta_{\mathrm{d}})\right|^2 + \mathbf{w}_1^H(\theta_{\mathrm{d}})\mathbf{K}_1\mathbf{R}_{\mathbf{z}}\mathbf{K}_1^H\mathbf{w}_1(\theta_{\mathrm{d}})} \\ + \mathbf{w}_2^H(\theta_{\mathrm{d}})\mathbf{K}_2^*\mathbf{R}_{\mathbf{z}}\mathbf{K}_2^T\mathbf{w}_2(\theta_{\mathrm{d}}) + \mathbf{w}_1^H(\theta_{\mathrm{d}})\mathbf{K}_2\mathbf{R}_{\mathbf{z}}^*\mathbf{K}_2^H\mathbf{w}_1(\theta_{\mathrm{d}}) + \mathbf{w}_2^H(\theta_{\mathrm{d}})\mathbf{K}_1^*\mathbf{R}_{\mathbf{z}}^*\mathbf{K}_1^T\mathbf{w}_2(\theta_{\mathrm{d}}) \\ + \mathbf{w}_1^H(\theta_{\mathrm{d}})\mathbf{K}_1\mathbf{R}_{\mathbf{z}}\mathbf{K}_2^T\mathbf{w}_2(\theta_{\mathrm{d}}) + \mathbf{w}_2^H(\theta_{\mathrm{d}})\mathbf{K}_2^*\mathbf{R}_{\mathbf{z}}\mathbf{K}_1^H\mathbf{w}_1(\theta_{\mathrm{d}}) + \mathbf{w}_1^H(\theta_{\mathrm{d}})\mathbf{K}_2\mathbf{R}_{\mathbf{z}}^*\mathbf{K}_1^T\mathbf{w}_2(\theta_{\mathrm{d}}) \\ + \mathbf{w}_2^H(\theta_{\mathrm{d}})\mathbf{K}_1^*\mathbf{R}_{\mathbf{z}}^*\mathbf{K}_2^H\mathbf{w}_1(\theta_{\mathrm{d}}) \end{aligned} \tag{44}$$

When applying then the same ideology to the output signal of the WL beamformer under I/Q imbalance, the resulting SINR is given by (44) at the bottom of the previous page. The desired signal part consists now of two terms with weights $\mathbf{w}_1$ and $\mathbf{w}_2$, respectively. In addition, the interference-plus-noise term consists of two terms relative to the signal power and several terms relative to the interference-plus-noise. We will use these expressions in the following section to quantify the performance of different beamforming solutions under I/Q imbalance.

V. Numerical Results and Examples

A. Simulation Setup

Numerical results have been acquired by extensive MATLAB simulations. In the simulations, uniform linear arrays with 8 and 50 antenna elements were used to emphasize the differences between small and massive arrays. Element spacing d for the arrays was equal to the half of the carrier signal wavelength λ. A 16-QAM waveform was generated for modeling consecutive signal snapshots of the incoming desired signal. In addition, four complex (and circular) Gaussian signals were generated for modeling interfering signals. The desired signal was chosen to be coming from the direction $\theta_{\text{d}} = 57°$, while the interfering signals were coming from the directions $\theta_{\text{int},1} = 28°$, $\theta_{\text{int},2} = 90°$, $\theta_{\text{int},3} = 180° - 57° = 123°$ and $\theta_{\text{int},4} = 151°$. All interfering signals were 3 dB stronger than the desired signal to demonstrate a challenging example scenario. Notice that the 3$^{\text{rd}}$ interference angle is indeed the mirror angle of the desired signal. On top of the desired and interfering signals, an additive white Gaussian noise floor was added for modeling the noise of the receiver components. The noise power was 10 dB lower than the power of the desired signal.

I/Q imbalance in the RF chains was implemented in two different ways; as a random unequal I/Q imbalance in receiver branches (g and ϕ were uniformly distributed in [0.85, 1.15] and [-15°, 15°], respectively), and as a systematic I/Q imbalance where the I/Q imbalance coefficients were equal in all receiver branches (g was 0.85 and ϕ was -15°). In the former case, all parallel receiver branches have their own hardware which is the most probable solution in distributed array structures. In the latter case, all receiver branches are sharing hardware resources as much as possible, such as RF local oscillator (LO). In reality, the behavior is most likely somewhere in-between, that is I/Q imbalance has common and independent subcomponents (from RX chain to another), but these two scenarios represent the two limiting cases.

B. Results under Systematic I/Q imbalance

Radiation patterns under systematic I/Q imbalance with 8 and 50 antenna elements are depicted in Fig. 3 and Fig. 4, respectively. The interfering signals coming from the directions 28°, 90° and 151° are well attenuated in all cases. However, both figures show that systematic I/Q imbalance degrades the built-in null steering capability of MVDR and RF-aware MVDR towards the interference source in the mirror direction, i.e. $\theta_{\text{int},3} = 123°$, whereas WL-MVDR and the proposed RF-aware WL-MVDR are able to attenuate this interference effectively. WL-MVDR is slightly sacrificing the desired unity response constraint (there is 1 dB attenuation to the desired direction) at the expense of attenuating the strong interference. This is a non-wanted feature, though not very significant. The best results, which match completely with the wanted radiation properties, are given by the proposed RF-aware WL-MVDR. This comes on one hand from the proper utilization of the RF impairment features and on the other hand from the doubled degree of freedom in weights. It should be also noticed that the difference between the mirror beam level and the response floor (without WL processing and resulting RF impairment suppression) is much bigger with 50 than with 8 antenna elements. This demonstrates that big arrays are much more sensitive to RF imperfections than classical small arrays, and could be a severe problem e.g. when extremely good spatial resolution is wanted.

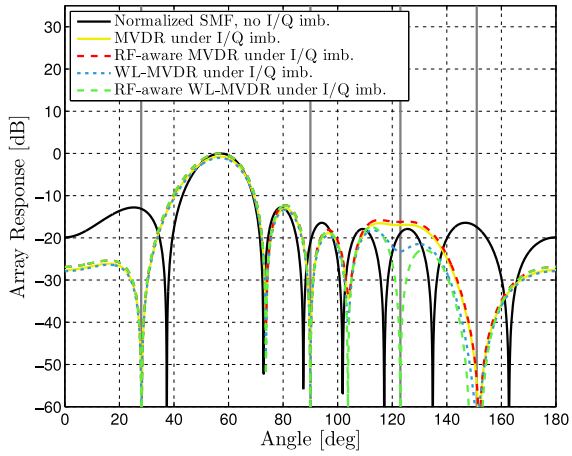

Fig. 3. Radiation patterns under systematic I/Q imbalance, 8 antenna elements. $\theta_{\text{d}} = 57°$, $\theta_{\text{int},1-4} = 28°$, 90°, 123° and 151°. Vertical gray bars denote directions of the interference sources.

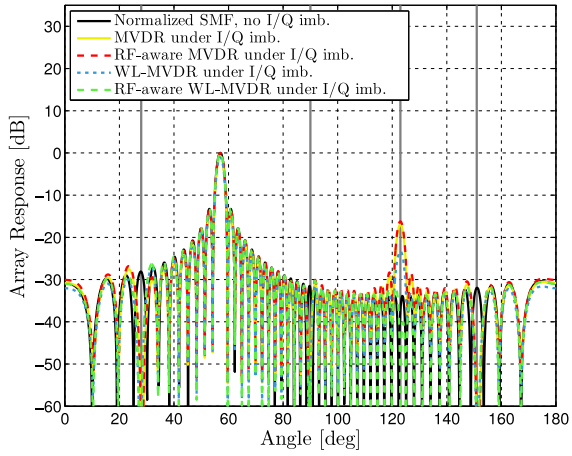

Fig. 4. Radiation patterns under systematic I/Q imbalance, 50 antenna elements. $\theta_{\text{d}} = 57°$, $\theta_{\text{int},1-4} = 28°$, 90°, 123° and 151°. Vertical gray bars denote directions of the interference sources.

A more detailed quantification of the mirror beam suppres-

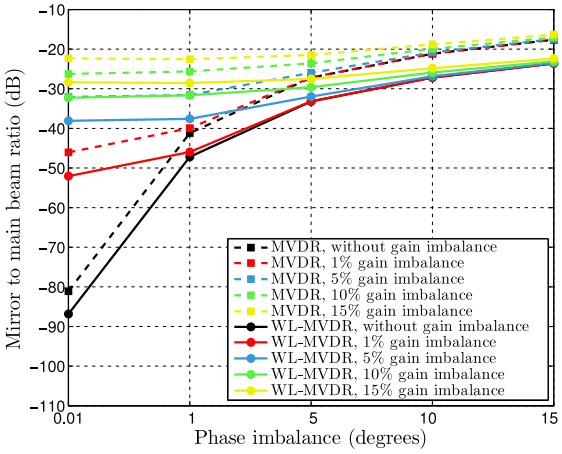

Fig. 5. The effects of the systematic gain and phase imbalances on the mirror to main beam ratio, 50 antenna elements. Linear and widely-linear MVDR beamformers.

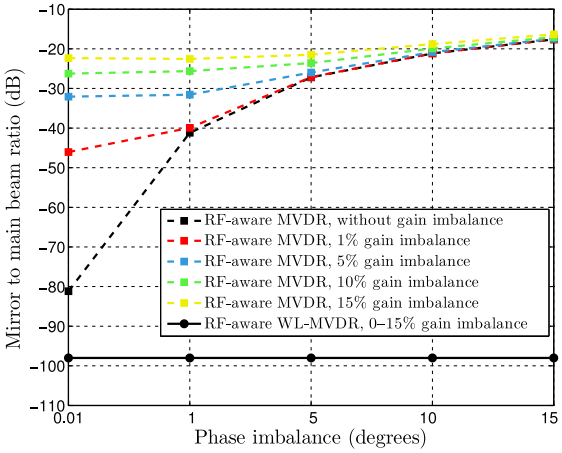

Fig. 6. The effects of the systematic gain and phase imbalances on the mirror to main beam ratio, 50 antenna elements. RF-aware linear and widely-linear MVDR beamformers.

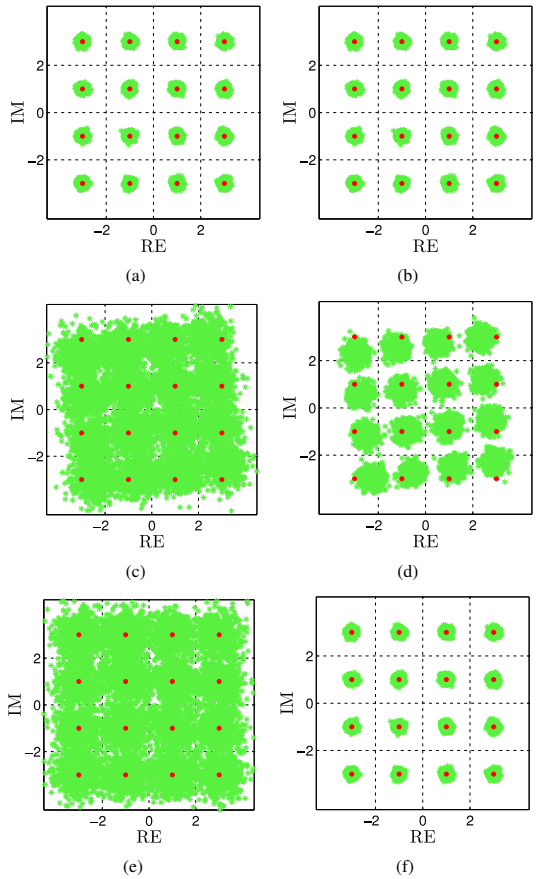

Fig. 7. Constellation diagrams with 50 antenna elements. a) MVDR under ideal I/Q balance; b) WL-MVDR under ideal I/Q balance; c) MVDR under systematic I/Q imbalance; d) WL-MVDR under systematic I/Q imbalance; e) RF-aware MVDR under systematic I/Q imbalance; and f) RF-aware WL-MVDR under systematic I/Q imbalance. The green stars depict the output signal snapshots while the red circles present ideal constellation points.

sion is given in Fig. 5 and Fig. 6. They show the mirror to main beam ratio (MMR) as a function of gain and phase imbalances with the conventional MVDR and WL-MVDR, and RF-aware MVDR and WL-MVDR, respectively. The results emphasize the ability of the normal and RF-aware WL-MVDR to steer a strong attenuation towards the interference source, even under severe I/Q imbalance, while MVDR and RF-aware MVDR are not able to do this as efficiently. In addition, results show that either the gain or phase imbalance alone is enough for creating the mirror beam to the radiation pattern, although the joint effect is naturally stronger. Further studies have also shown, that the attenuation of WL-MVDR towards the interference source is increased if the interference becomes stronger, whereas MVDR and RF-aware MVDR are lacking this flexibility. This is of course a further beneficial property of the WL processing.

The constellation diagrams of the received signal under systematic I/Q imbalance are depicted in Fig. 7. The uppermost subfigures 7(a) and 7(b) present the output signal of MVDR and WL-MVDR under perfect I/Q balance, respectively. The middle row subfigures 7(c) and 7(d) present corrupted results under I/Q imbalance with MVDR and WL-MVDR, respectively. Since I/Q imbalance is here systematic, the output signal can be interpreted as a sum of several input signals with coherent errors. There is a clear constellation twist in both diagrams, which is typical for I/Q imbalance when considering a single receiver chain [29]. Further analysis has shown that here the twist is not as strong as in the individual receiver chains because beamforming tends to compensate this twist. However, the twist cannot be removed totally since the I/Q imbalance coefficients are not known in the beamforming algorithm. In addition, WL-MVDR gives less disturbed result than MVDR since it has stronger attenuation towards the interfering signal in the mirror direction. Actually, the results of MVDR are already so noisy that sym-

Table 1. SINR values under the systematic I/Q imbalance scenario. Averaged over 500 realizations.

Beamforming method	SINR [dB] (8 antennas)	SINR [dB] (50 antennas)
MVDR	12.10	13.02
RF-aware MVDR, perfect $\mathbf{K_1}$ and $\mathbf{K_2}$ knowledge	12.10	13.02
RF-aware MVDR, estimated $\mathbf{K_1}$ and $\mathbf{K_2}$	12.10	12.98
WL-MVDR	15.90	18.54
RF-aware WL-MVDR, perfect $\mathbf{K_1}$ and $\mathbf{K_2}$ knowledge	18.70	26.98
RF-aware WL-MVDR, estimated $\mathbf{K_1}$ and $\mathbf{K_2}$	18.68	25.11
MVDR and WL-MVDR without I/Q imb.	18.70	26.98

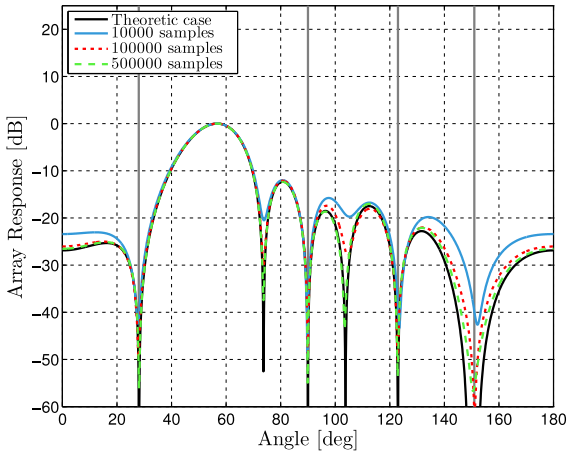

Fig. 8. The effect of the amount of signal snapshots, used for the covariance and complementary covariance matrix calculations, on radiation pattern with RF-aware WL-MVDR under systematic I/Q imbalance, 8 antenna elements. $\theta_{\mathsf{d}} = 57°$, $\theta_{int,1-4} = 28°$, $90°$, $123°$ and $151°$. Vertical gray bars denote directions of the interference sources.

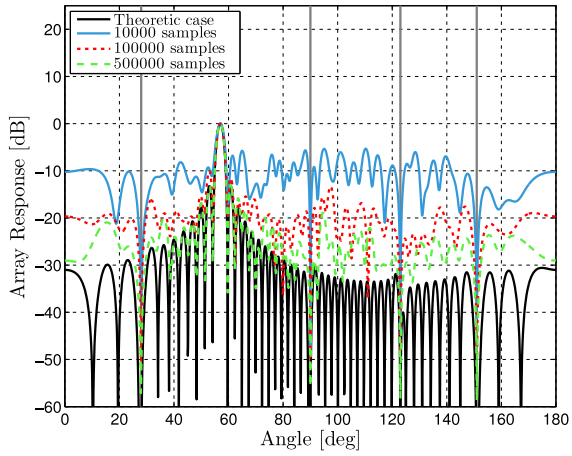

Fig. 9. The effect of the amount of signal snapshots, used for the covariance and complementary covariance matrix calculations, on radiation pattern with RF-aware WL-MVDR under systematic I/Q imbalance, 50 antenna elements. $\theta_{\mathsf{d}} = 57°$, $\theta_{\mathsf{int},1-4} = 28°$, $90°$, $123°$ and $151°$. Vertical gray bars denote directions of the interference sources.

bol detection is very difficult whereas symbols of WL-MVDR can be still detected efficiently with some simple scaling and rotation corrections. The lowermost subfigures 7(e) and 7(f) then show the output signal of RF-aware MVDR and WL-MVDR, respectively. Now, the twist is not present due to exploiting the RF impairment features properly in the combining processing. Furthermore, RF-aware WL-MVDR actually gives exactly the same signal properties as under ideal I/Q balance (subfigures 7(a) and 7(b)). RF-aware MVDR is, however, still not able to efficiently suppress the interfering signal coming from the mirror direction and therefore the overall performance is heavily degraded.

The SINR values, under systematic I/Q imbalance, are listed in Table 1. The results are well in line with the above intuitive conclusions. MVDR and RF-aware MVDR cannot fully suppress the strong interferer coming from the mirror direction and this leads to the low SINR values. Further, the WL versions do the interference suppression properly and have high SINR. In addition, when increasing the amount of the antenna elements, WL-MVDR and RF-aware WL-MVDR improve SINR significantly due to the higher processing gain whereas MVDR and RF-aware MVDR give only small improvements in SINR. Once again, RF-aware WL-MVDR outperforms other methods. Table shows also effects of practical imbalance uncertainty, which will be discussed later in subsection V-D.

The earlier derivations and previous examples all build on deploying ideal ensemble averaged covariance matrices. In practice, however, finite amount of signal snapshots are used for estimating sample covariances. This has then obviously some impact also on the radiation patterns since finite sample size results in estimation errors. Fig. 8 and Fig. 9 show the effect of the finite signal length used for RF-aware WL-MVDR covariance matrix calculations with 8 and 50 antenna elements, respectively. The results obtained with true ensemble covariances are also shown for the comparison. When using 8 antenna elements, differences between sampled and ideal cases are clear with 10 000 signal samples. Furthermore, when using 100 000 samples, results match already quite well the theoretic case and with 500 000 samples radiation pattern is almost the same as in theory. The differences are greater when using 50 antenna elements. Obviously, 10 000 signal samples are not enough for proper radiation properties. Also, the results with 100 000 and 500 000 samples are still far away from the theoretic case, but

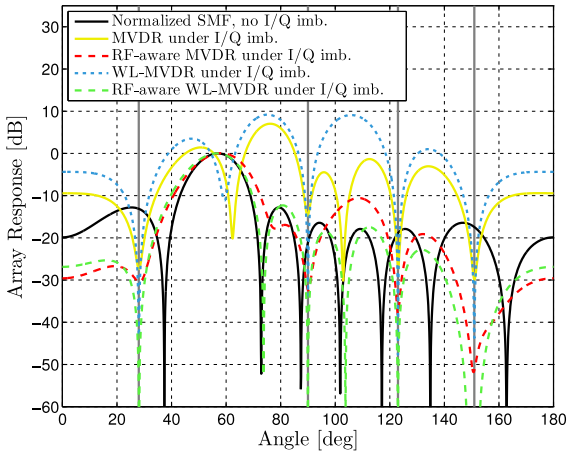

Fig. 10. Radiation patterns under random I/Q imbalance, 8 antenna elements. $\theta_{\mathrm{d}} = 57°$, $\theta_{\mathrm{int},1-4} = 28°, 90°, 123°$ and $151°$. Vertical gray bars denote directions of the interference sources.

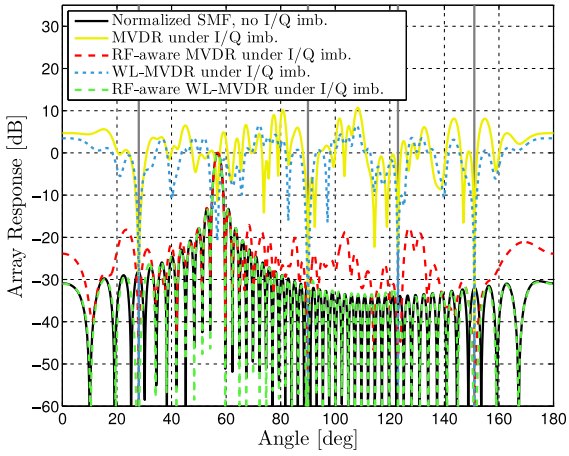

Fig. 11. Radiation patterns under random I/Q imbalance, 50 antenna elements. $\theta_{\mathrm{d}} = 57°$, $\theta_{\mathrm{int},1-4} = 28°, 90°, 123°$ and $151°$. Vertical gray bars denote directions of the interference sources.

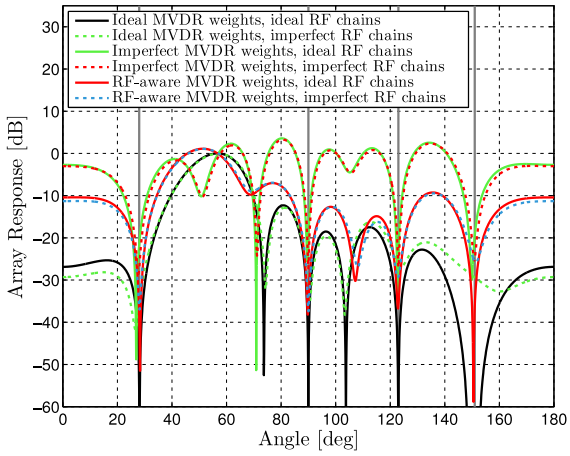

Fig. 12. The effect of random I/Q imbalance, via different factors, on the MVDR performance, 8 antenna elements. $\theta_{\mathrm{d}} = 57°$, $\theta_{\mathrm{int},1-4} = 28°, 90°, 123°$ and $151°$. Vertical gray bars denote directions of the interference sources.

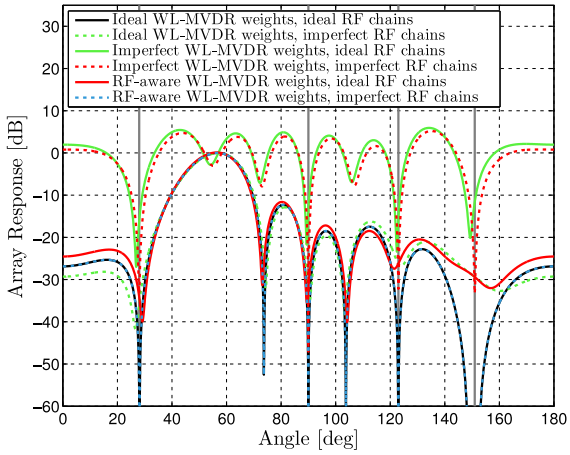

Fig. 13. The effect of random I/Q imbalance, via different factors, on the WL-MVDR performance, 8 antenna elements. $\theta_{\mathrm{d}} = 57°$, $\theta_{int,1-4} = 28°, 90°, 123°$ and $151°$. Vertical gray bars denote directions of the interference sources.

could be used in practice. As a conclusion, the more antenna elements are used, the more signal snapshots for the covariance matrix calculations are needed for attaining the wanted radiation properties.

C. Results under Random I/Q imbalance

Analysis for the beamforming performance under random I/Q imbalance is done next in Fig. 10 and Fig. 11 which show the radiation patterns with 8 and 50 antenna elements, respectively. Now, certain level of null steering towards the interference sources is in principle successful in every case. However, the algorithms without any knowledge of I/Q imbalance are not able to keep the unit response to the desired direction and neither to give a well-behaving response in general. This follows from the fact that the amplitude and phase mismatches are now unequal in different receiver chains. However, when the knowledge of I/Q imbalance features is taken properly into account with the RF-aware algorithms, they have good overall responses and simultaneously attenuate interfering signals properly. Further, RF-aware WL-MVDR again outperforms RF-aware MVDR in terms of interference attenuation and lower sidelobe levels.

The total corruption of MVDR and WL-MVDR responses under random I/Q imbalance scenario are studied further in Fig. 12 and Fig. 13 where the I/Q imbalance effects are factorized into the influences of ideal and imperfect weights and RF chains. The ideal weights, which are based on the ideal signal snapshots (under ideal I/Q balance), naturally lead to good radiation properties with both methods no matter if I/Q imbalance is as-

Table 2. SINR values under the random I/Q imbalance scenario. Averaged over 500 realizations.

Beamforming method	SINR [dB] (8 antennas)	SINR [dB] (50 antennas)
MVDR	8.65	-3.67
RF-aware MVDR, perfect $\mathbf{K_1}$ and $\mathbf{K_2}$ knowledge	15.62	26.42
RF-aware MVDR, estimated $\mathbf{K_1}$ and $\mathbf{K_2}$	15.62	25.69
WL-MVDR	4.88	-8.29
RF-aware WL-MVDR, perfect $\mathbf{K_1}$ and $\mathbf{K_2}$ knowledge	18.70	26.98
RF-aware WL-MVDR, estimated $\mathbf{K_1}$ and $\mathbf{K_2}$	18.68	25.31
MVDR and WL-MVDR without I/Q imb.	18.70	26.98

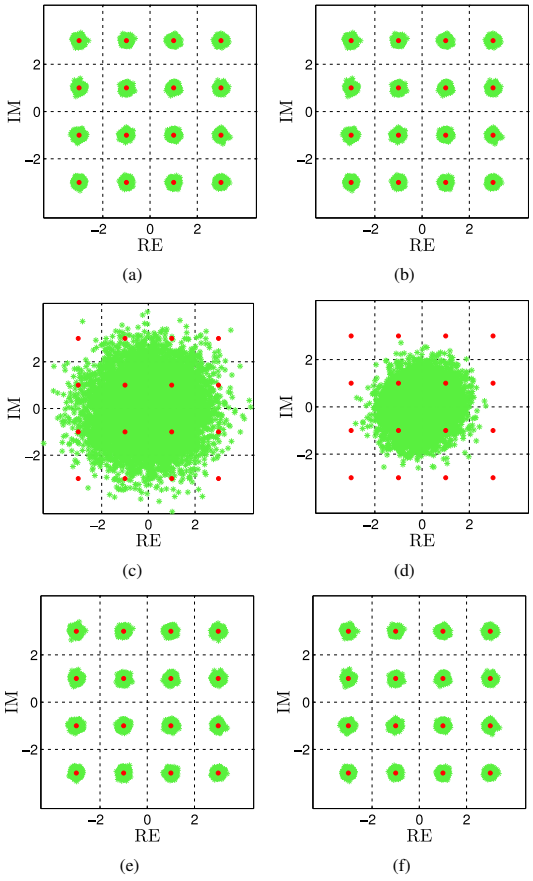

Fig. 14. Constellation diagrams with 50 antenna elements. a) MVDR under ideal I/Q balance; b) WL-MVDR under ideal I/Q balance; c) MVDR under random I/Q imbalance; d) WL-MVDR under random I/Q imbalance; e) RF-aware MVDR under random I/Q imbalance; and f) RF-aware WL-MVDR under random I/Q imbalance. The green stars depict the output signal snapshots while the red circles present ideal constellation points.

sumed to be present in equations (13) and (18) or not. However, this is mostly an artificial case since the covariance and complementary covariance matrices have to be calculated from the actual signal snapshots which also include I/Q imbalance in practice. More realistic case with imperfect weights, which are obtained with MVDR and WL-MVDR from the corrupted signal snapshots, lead to the totally corrupted response with both methods no matter if the RF chains are assumed to be ideal or not. The last cases show the radiation patterns with the modified weights, which are obtained with the RF-aware MVDR and WL-MVDR algorithms from the practical signal snapshots including I/Q imbalance. The results of RF-aware MVDR show that taking I/Q imbalance into account in the beamforming algorithm can suppress the unwanted behavior to a certain extent. However, RF-aware WL-MVDR suppresses the effects of I/Q imbalance even more effectively and outperforms RF-aware MVDR no matter whether the RF chains include I/Q imbalance or not. It should be noticed that RF-aware WL-MVDR under I/Q imbalance matches perfectly to the case under ideal I/Q balance. This comes partly from proper utilization of I/Q features and partly from the doubled degree of freedom compared to the plain linear case.

The constellation diagrams of the output signal under random I/Q imbalance are depicted in Fig. 14. The uppermost subfigures 14(a) and 14(b) present the results of MVDR and WL-MVDR under ideal I/Q balance. The subfigures 14(c) and 14(d) in the middle row, present badly corrupted results of MVDR and WL-MVDR under I/Q imbalance. Signals are attenuated heavily, since the wanted unit response to the desired direction does not hold, as can be seen e.g. from Fig. 11. This leads to the situation where the noise and interfering signals become dominant in the output signal and the desired signal is totally lost. The lowermost subfigures 14(e) and 14(f) present the results of RF-aware MVDR and WL-MVDR. Now, both methods are able to give the desired signal properties, since the unit response to the desired direction is maintained while the suppression for the interfering signals is at an adequate level.

Finally, the SINR values under random I/Q imbalance are presented in Table 2. The results confirm that RF-aware MVDR and WL-MVDR give good signal properties, while the conventional methods suffer from the desired signal suppression due to the attenuation to the desired direction. The effect is the more severe, the more antenna elements are used, and the noise and interference indeed are dominant when operating with the conventional methods and 50 antenna elements. The best method in terms of SINR is the proposed RF-aware WL-MVDR. The effects of practical imbalance uncertainty, also shown in Table 2, are discussed in the next subsection.

D. The Effects of I/Q Imbalance Uncertainty

So far in this paper, the complete knowledge of the I/Q imbalance coefficients have been assumed. However, in practice, the coefficients can not be known perfectly. In this subsection, effects of using the estimated coefficients instead of the perfect ones with the RF-aware beamforming methods are illustrated and discussed.

In general, it is well-known in the literature that I/Q imbalance estimation methods for a single receiver chain can obtain image rejection ratio (IRR) around 60 dB, see e.g. [28, 30, 31]. This means that I/Q imbalance coefficients can be estimated with accuracy having only $\pm 0.1\%$ error (relative to real value) in the gain mismatch coefficient g and simultaneously $\pm 0.1^\circ$ error in the phase mismatch coefficient ϕ. State-of-the-art blind imbalance extraction methods reaching such performance are described, e.g., in [28]. In order to model the algorithm performance with such realistic I/Q imbalance uncertainty, random estimation errors in above ranges are added to the imbalance knowledge used in the RF-aware beamforming processing.

Fig. 15 shows the results with 8 antenna elements and systematic I/Q imbalance. When compared to the results in Fig. 3, it is clear that the effects of practical imbalance uncertainty are in this case basically negligible. However, the differences become larger when more antenna elements are involved. Fig. 16 presents results with 50 antenna elements under systematic I/Q imbalance. The performance towards the main and interference directions is again very similar as in Fig. 4 but now regions between the important directions have higher ripple in the radiation patterns. The exact differences between the performances with the ideal and estimated coefficients can be found from Table 1. It supports the results in the radiation pattern figures, i.e. with 8 antenna elements, the performances with and without estimation errors are practically identical. In addition, the differences are higher when 50 antenna elements are used. RF-aware MVDR with the estimated coefficients performs (almost) equally with the conventional MVDR. However, the best practical performance is obtained with the proposed RF-aware WL-MVDR, despite of practical imbalance uncertainty, whose performance is only slightly degraded compared to the ideal case.

Fig. 17 illustrates the performance with the estimated I/Q imbalance coefficients and 8 antenna elements under random I/Q imbalance scenario. The behavior is similar as with the ideal coefficients in Fig. 10, although the exact shapes are not identical due to randomness in realizations. There are similar ripples in the "don't care" directions but both RF-aware algorithms are performing well in the main and interference directions. Fig. 18 shows the corresponding results with 50 antenna elements. Again, the response towards the important directions is good while the ripple in other directions is higher than with ideal coefficients in Fig. 11. SINR values in Table 2 confirm the results in the radiation patterns. In the absence of the mirror beam, both RF-aware methods perform very well.

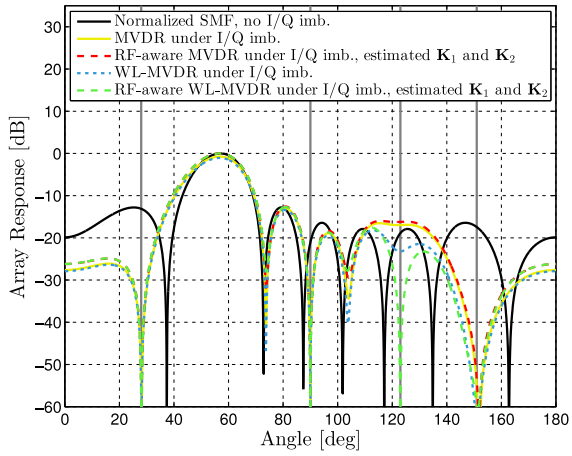

Fig. 15. Radiation patterns under systematic I/Q imbalance and with estimated I/Q imbalance coefficients, 8 antenna elements. $\theta_\mathrm{d} = 57^\circ$, $\theta_{\mathrm{int},1-4} = 28^\circ$, 90°, 123° and 151°. Vertical gray bars denote directions of the interference sources.

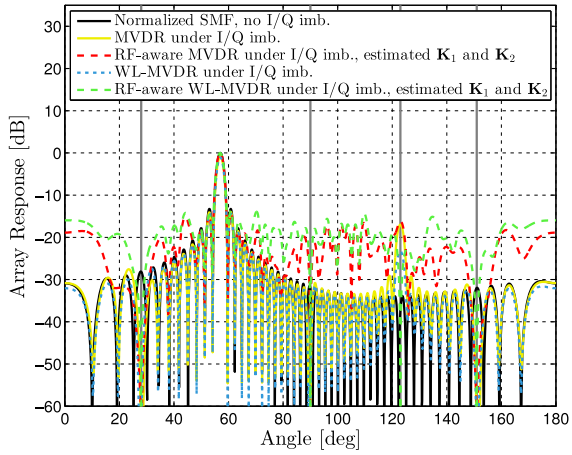

Fig. 16. Radiation patterns under systematic I/Q imbalance and with estimated I/Q imbalance coefficients, 50 antenna elements. $\theta_\mathrm{d} = 57^\circ$, $\theta_{\mathrm{int},1-4} = 28^\circ$, 90°, 123° and 151°. Vertical gray bars denote directions of the interference sources.

VI. Conclusions

In this paper, the sensitivity of massive antenna arrays to RF I/Q imbalance was studied and analyzed in the beamforming context. Also, RF-aware digital beamforming methods were developed for mitigating the unwanted effects of I/Q imbalance without calibrations in individual receiver branches. It was shown, through closed-form radiation pattern and SINR analyses, that I/Q imbalance corrupts the output signal properties as well as compromises the beamforming capabilities of the beamformer. Systematic I/Q imbalance creates an unwanted beam towards the mirror direction, while random I/Q imbalance deteriorates the spatial response totally. These effects were shown to be the stronger, the more antenna elements were used. In addition, the more antenna elements were used, the more signal snapshots were needed for sample covariance matrix calculation under I/Q imbalance in order to reach the desired behavior.

It was also shown analytically, that WL processing can mitigate the unwanted effects of I/Q imbalance completely whereas

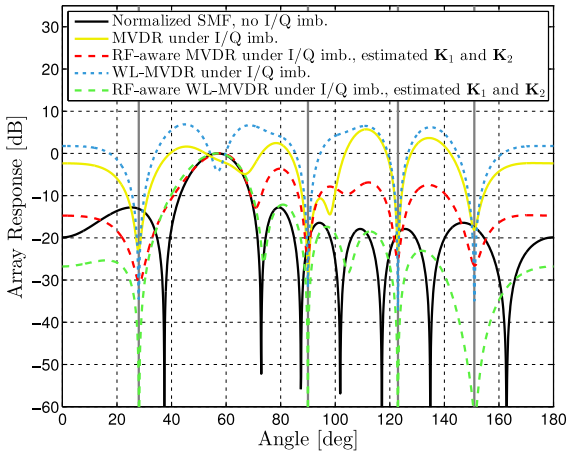

Fig. 17. Radiation patterns under random I/Q imbalance and with estimated I/Q imbalance coefficients, 8 antenna elements. $\theta_{\mathsf{d}} = 57°$, $\theta_{\mathsf{int},1-4} = 28°, 90°, 123°$ and $151°$. Vertical gray bars denote directions of the interference sources.

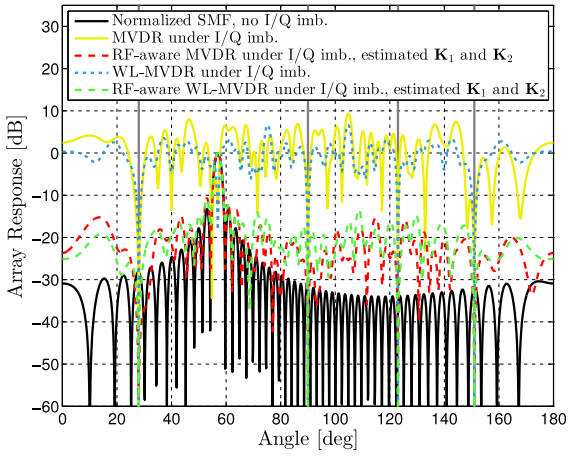

Fig. 18. Radiation patterns under random I/Q imbalance and with estimated I/Q imbalance coefficients, 50 antenna elements. $\theta_{\mathsf{d}} = 57°$, $\theta_{\mathsf{int},1-4} = 28°, 90°, 123°$ and $151°$. Vertical gray bars denote directions of the interference sources.

the conventional linear beamforming is lacking sufficient degrees of freedom. The provided numerical examples with MVDR and WL-MVDR as well as their proposed RF-aware versions exploiting the knowledge of I/Q imbalance features were supporting the analytical results. WL-MVDR outperformed MVDR, whereas the proposed RF-aware WL-MVDR (exploiting I/Q imbalance features) was the best solution for the beamforming problem, leading exactly to the desired performance. Thus, the proposed RF-aware WL-MVDR offers a robust solution for high-resolution beamforming in massive antenna arrays, despite of the presence of RF circuit imperfections. Finally, the impact of practical I/Q imbalance uncertainty was addressed, showing that the proposed RF-aware WL-MVDR beamformer can still reach close to ideal SINR performance despite of such uncertainty. Our future work will focus on explicitly extending the developments reported in this article towards wideband multicarrier waveforms and rich scattering environments.

REFERENCES

[1] Ericsson AB, "Traffic and market report," Stockholm, Sweden, Tech. Rep. 198/287 01-FGB 101 220, Jun. 2012.

[2] 3GPP Technical Specification Group Radio Access Network, "Evolved universal terrestrial radio access (E-UTRA); Physical channels and modulation," Technical Specification TS 36.211, version 11.2.0, release 11, Apr. 2013.

[3] F. Rusek, D. Persson, B. K. Lau, E. Larsson, T. Marzetta, O. Edfors, and F. Tufvesson, "Scaling up MIMO: opportunities and challenges with very large arrays," *IEEE Signal Processing Magazine*, vol. 30, no. 1, pp. 40–60, Jan. 2013.

[4] J. Hoydis, S. ten Brink, and M. Debbah, "Massive MIMO in the UL/DL of cellular networks: How many antennas do we need?" *IEEE J. Sel. Areas Commun.*, vol. 31, no. 2, pp. 160–171, Feb. 2013.

[5] S. Mirabbasi and K. Martin, "Classical and modern receiver architectures," *IEEE Commun. Mag.*, vol. 38, no. 11, pp. 132 – 139, Nov. 2000.

[6] R. M. Svitek, "SiGe BiCMOS RF ICs and components for high speed wireless data networks," Ph.D. dissertation, Virginia Polytechnic Institute and State University, Blacksburg, Virginia, Apr. 2005.

[7] P. Mak et al., "Transceiver architecture selection: Review, state-of-the-art survey and case study," *IEEE Circuits Syst. Mag.*, vol. 7, no. 2, pp. 6 –25, 2007.

[8] A. Mashmour, W. Domino, and N. Beamish, "On the direct conversion receiver – a tutorial," *Microwave J.*, vol. 44, no. 6, pp. 114–128, Jun. 2001.

[9] T. Schenk, *RF Imperfections in High-rate Wireless Systems: Impact and Digital Compensation*, 1st ed. Springer, Feb. 2008.

[10] M. Valkama and M. Renfors, "Advanced DSP for I/Q imbalance compensation in a low-IF receiver," in *Proc. IEEE ICC*, vol. 2, 2000, pp. 768 –772 vol.2.

[11] L. Anttila and M. Valkama, "On circularity of receiver front-end signals under RF impairments," *Proc. EW*, pp. 1 –8, Apr. 2011.

[12] M. Valkama, M. Renfors, and V. Koivunen, "Blind signal estimation in conjugate signal models with application to I/Q imbalance compensation," *IEEE Signal Process. Lett.*, vol. 12, no. 11, pp. 733 – 736, Nov. 2005.

[13] T. McWhorter and P. Schreier, "Widely-linear beamforming," in *Proc. ASILOMAR*, vol. 1, Nov. 2003, pp. 753 – 759 Vol.1.

[14] P. Chevalier and A. Blin, "Widely linear MVDR beamformers for the reception of an unknown signal corrupted by noncircular interferences," *IEEE Trans. Signal Process.*, vol. 55, no. 11, pp. 5323 –5336, Nov. 2007.

[15] Q. J. You, Z. Jianyun, and Z. Xin'an, "A widely-linear LMS algorithm for adaptive beamformer," in *Proc. MAPE*, Aug. 2007, pp. 1060 –1063.

[16] S. Douglas, "Widely-linear recursive least-squares algorithm for adaptive beamforming," in *Proc. IEEE ICASSP*, Apr. 2009, pp. 2041 –2044.

[17] P. Chevalier, J.-P. Delmas, and A. Oukaci, "Optimal widely linear MVDR beamforming for noncircular signals," in *Proc. IEEE ICASSP*, Apr. 2009, pp. 3573 –3576.

[18] N. Song, J. Steinwandt, L. Wang, R. C. de Lamare, and M. Haardt, "Non-data-aided adaptive beamforming algorithm based on the widely linear auxiliary vector filter," in *Proc. IEEE ICASSP*, May 2011, pp. 2636 –2639.

[19] J. Steinwandt, R. de Lamare, L. Wang, N. Song, and M. Haardt, "Widely linear adaptive beamforming algorithm based on the conjugate gradient method," in *Proc. WSA*, Feb. 2011, pp. 1 –4.

[20] A. Hakkarainen, J. Werner, and M. Valkama, "RF imperfections in antenna arrays: Response analysis and widely-linear digital beamforming," in *Proc. IEEE RWS*, Jan. 2013, pp. 187 –189.

[21] J. Litva, *Digital Beamforming in Wireless Communications*. Artech House Publishers, Aug. 1996.

[22] B. Van Veen and K. Buckley, "Beamforming: a versatile approach to spatial filtering," *IEEE ASSP Mag.*, vol. 5, no. 2, pp. 4–24, 1988.

[23] H. Matsuoka and H. Shoki, "Comparison of pre-FFT and post-FFT processing adaptive arrays for OFDM systems in the presence of co-channel interference," in *Proc. IEEE PIMRC*, vol. 2, 2003, pp. 1603–1607 vol.2.

[24] A. Abidi, "Direct-conversion radio transceivers for digital communications," in *Proc. IEEE ISSCC*, Feb. 1995, pp. 186 –187, 363–4.

[25] L. Anttila, M. Valkama, and M. Renfors, "Blind moment estimation techniques for I/Q imbalance compensation in quadrature receivers," in *Proc. IEEE PIMRC*, Sep. 2006, pp. 1 –5.

[26] J. Capon, "High-resolution frequency-wavenumber spectrum analysis," *Proc. IEEE*, vol. 57, no. 8, pp. 1408 – 1418, Aug. 1969.

[27] S. Haykin, *Adaptive Filter Theory*, 3rd ed. Prentice Hall, Dec. 1995.

[28] L. Anttila, M. Valkama, and M. Renfors, "Circularity-Based I/Q Imbalance Compensation in Wideband Direct-Conversion receivers," *IEEE Trans. Veh. Technol.*, vol. 57, no. 4, pp. 2099 –2113, Jul. 2008.
[29] J. Lee, K. Cho, and D. Yoon, "New BER expression of hierarchical m-ary phase shift keying," *ETRI J.*, vol. 29, no. 6, pp. 707–715, Dec. 2007.
[30] N. A. Moseley and C. H. Slump, "A low-complexity feed-forward I/Q imbalance compensation algorithm," in *Proc. Annual Workshop on Circuits*, Veldhoven, The Netherlands, Nov. 2006, pp. 158–164.
[31] L. Anttila, M. Valkama, and M. Renfors, "Frequency-selective I/Q mismatch calibration of wideband direct-conversion transmitters," *IEEE Trans. Circuits Syst. II: Exp. Briefs*, vol. 55, no. 4, pp. 359–363, Apr. 2008.

Aki Hakkarainen was born in Joensuu, Finland, in 1982. He received the M.Sc. (with honours) in communication electronics from Tampere University of Technology (TUT), Finland, in 2007. From 2007 to 2009, he was working as a RF design engineer with Nokia, Salo. From 2009 to 2011, he was working as a Radio system specialist with Elisa, Tampere. Currently, he is working towards a Ph.D. degree at TUT. He is a researcher and doctoral student at the Department of Electronics and Communications Engineering, TUT. His main research interests are digital signal processing methods for RF impairment mitigation, and localization issues in cognitive radios.

Janis Werner was born in Berlin, Germany, in 1986. He received his Diplom-Ingenieur degree in electrical engineering from the Dresden University of Technology (TUD), Germany in 2011. Currently he is working towards a Ph.D. degree at the Tampere University of Technology (TUT), Finland, where he is a researcher at the Department of Electronics and Communications Engineering. His main research interests are cognitive radio, localization and smart antennas.

Kapil R. Dandekar received the B.S. degree in Electrical Engineering (1997) from the University of Virginia, Charlottesville, VA; the M.S. and Ph.D. degrees in Electrical and Computer Engineering from the University of Texas at Austin (1998, 2001), Austin, TX. Beginning in 2001, he joined the faculty at Drexel University in Philadelphia, PA. He is currently an Associate Professor in Electrical and Computer Engineering at Drexel University; the Director of the Drexel Wireless Systems Laboratory (DWSL); Associate Dean for Research in the Drexel University College of Engineering.

Dandekar's research has been supported by the U.S. National Science Foundation, Army CERDEC, National Security Agency, Office of Naval Research, and private industry. Dandekar's current research interests and publications involve wireless, ultrasonic, and optical communications, reconfigurable antennas, and smart textiles. Antenna technology from DWSL has been licensed by external companies for technology commercialization. The Software Defined Communication (SDC) testbed developed by DWSL has been released for adoption by the academic and industrial research community.

Mikko Valkama was born in Pirkkala, Finland, in 1975. He received the M.Sc. and Ph.D. Degrees (both with honours) in electrical engineering (EE) from Tampere University of Technology (TUT), Finland, in 2000 and 2001, respectively. In 2002 he received the Best Ph.D. Thesis -award by the Finnish Academy of Science and Letters for his dissertation entitled Advanced I/Q signal processing for wideband receivers: Models and algorithms. In 2003, he was working as a visiting researcher with the Communications Systems and Signal Processing Institute at SDSU, San Diego, CA. Currently, he is a Full Professor and Department Vice-Head at the Department of Electronics and Communications Engineering at TUT, Finland. He has been involved in organizing conferences, like the IEEE SPAWC07 (Publications Chair) held in Helsinki, Finland. His general research interests include communications signal processing, estimation and detection techniques, signal processing algorithms for software defined flexible radios, cognitive radio, digital transmission techniques such as different variants of multicarrier modulation methods and OFDM, radio localization methods, and radio resource management for ad-hoc and mobile networks.

Publication 5

A. Hakkarainen, J. Werner, K. Dandekar, and M. Valkama, "Interference Suppression with Antenna Arrays in OFDM Systems under Transceiver I/Q Imbalance," in *Proceedings of the 9th International Conference on Cognitive Radio Oriented Wireless Networks (CROWNCOM)*, Oulu, Finland, 2–4 June 2014. DOI: 10.4108/icst.crowncom.2014.255187

Interference Suppression with Antenna Arrays in OFDM Systems under Transceiver I/Q Imbalance

Aki Hakkarainen*, Janis Werner*, Kapil Dandekar† and Mikko Valkama*
*Department of Electronics and Communications Engineering, Tampere University of Technology, Tampere, Finland
Emails: {aki.hakkarainen, janis.werner, mikko.e.valkama}@tut.fi
†Department of Electrical and Computer Engineering, Drexel University, Philadelphia, PA 19104, USA
Email: dandekar@coe.drexel.edu

***Abstract*—In this paper, we address the effects of radio frequency (RF) transceiver in-phase/quadrature-phase (I/Q) imbalance in transmission systems which are utilizing orthogonal frequency-division multiplexing (OFDM) waveforms. Special emphasis is on the analysis of external interference sources and their mitigation with receiver antenna array processing, assuming independent fading for the antenna elements. In addition, I/Q imbalance is assumed to be arbitrarily frequency selective and independent in different transceiver branches. We show that I/Q imbalance is especially harmful in the presence of strong interferers when conventional per-subcarrier processing is implemented on the receiver side. Based on these results, we propose a joint subcarrier processing where each of the subcarrier signals is combined with the signal at the image carrier. Such processing is shown to be very efficient in I/Q imbalance mitigation as well as in the total interference suppression.**

***Index Terms*—antenna arrays, in-phase/quadrature-phase (I/Q) imbalance, orthogonal frequency-division multiplexing (OFDM), uncorrelated fading**

I. Introduction

Interference suppression is a very important topic in modern radio systems. E.g. in cognitive radio systems, primary users (PU) have to be protected from the interference caused by the secondary users (SU) for preventing system failures in the primary network [1]. In addition, SUs need to suppress strong interference coming from the PUs, in order to operate reliably within the same area. Such interference protection/suppression capabilities can be obtained e.g. with antenna arrays. With antenna array processing [2], a signal can be transmitted/received by several antennas and thus the data link can be steered towards the desired direction while nulling the influence to/from the non-desired directions. Unfortunately, imperfections in radio frequency (RF) electronics can be very harmful for these functionalities, see e.g. [3], [4].

This work is supported by the Finnish Funding Agency for Technology and Innovation (Tekes) under the project "Reconfigurable Antenna-based Enhancement of Dynamic Spectrum Access Algorithms", the Industrial Research Fund of Tampere University of Technology (Tuula and Yrjö Neuvo Fund), the Academy of Finland under the project 251138 "Digitally-Enhanced RF for Cognitive Radio Devices", the Doctoral Programme of the President of Tampere University of Technology, and the Foundation of Nokia Corporation.

The work is also supported by National Science Foundation (NSF) under award number 1147838.

One of these RF imperfections is in-phase quadrature-phase (I/Q) imbalance [5] which is created in direct-conversion transceivers (DCT) [6]. It is distorting the signal properties and thus degrading the overall performance of the transmission system [5]. Despite of I/Q imbalance and other disadvantages, DCT is a very promising RF front-end implementation candidate for modern transmission systems due to the smaller size and cost than e.g. with the superheterodyne transceivers [7].

The importance of I/Q imbalance and its mitigation has risen when high data rate transmission systems, utilizing large symbol alphabets and orthogonal frequency-division multiplexing (OFDM) waveforms [8], have become more popular. A comprehensive analysis of I/Q imbalance of a single data link in OFDM systems is given in [9], [10]. Analysis is extended to consider multiple transmitter (TX) antennas in [11] whereas [12], [13] include several antennas on both TX and receiver (RX) sides. In [14] the I/Q imbalance problem is studied together with power amplifier nonlinearities whereas [15] concentrates on the joint effects of I/Q imbalance and carrier frequency offset. However, the influence of external interference sources is not included in any of these analyses.

In this paper we analyze the influence of external interference in antenna array processing under transceiver I/Q imbalance. Analysis is done at the subcarrier level in order to keep the results applicable for general OFDM systems. We do not assume any specific dependency in the I/Q imbalance parameters between transceiver branches or subcarriers, and thus the I/Q imbalance parameters can be arbitrarily frequency selective. As proposed e.g. in [9], [13], we will use joint subcarrier processing as the key element in I/Q imbalance mitigation and interference suppression under I/Q imbalance. The proposed solution is based on a data-aided processing which is implemented in the RX side only and thus does not require any additional communication between RX and TX. It will be shown that the proposed solution provides effective interference suppression in spite of severe RF imperfections.

The paper is organized as follows. Section II presents TX and RX signal models under I/Q imbalance, and describes joint subcarrier processing. In Section III, an analytical evaluation is carried out with covariance matrices, output powers and signal to interference plus noise ratios (SINRs). Section IV describes how to optimize the receiver spatial array processing

in the minimum mean square error (MMSE) sense. Numerical evaluations are given in Section V and finally, conclusions are drawn in Section VI.

Notation: Throughout this paper, vectors and matrices are written with bold characters. The superscripts $(\cdot)^T$, $(\cdot)^H$, $(\cdot)^*$ and $(\cdot)^{-1}$ represent transpose, Hermitian (conjugate) transpose, conjugate and matrix inverse, respectively. The tilde sign $\tilde{(\cdot)}$ is used to present an augmented quantity and the results obtained by the augmented processing. The statistical expectation is denoted with $\mathbb{E}[\cdot]$. A complex random variable x is called circular if $\mathbb{E}\left[x^2\right] = 0$.

II. Essential Signal Models

A. Signals with TX and RX I/Q Imbalances

In OFDM transmission, a wide transmission band is divided into several orthogonal subcarriers which carry, in general, independent data streams [8]. These individual subcarrier signals can be considered as narrowband signals which have constant (flat) propagation conditions within their own bands. Throughout the paper, the subcarrier index is marked with c and the total amount of subcarriers with C, and consequently $c \in \{-C/2, ..., -1, 1, ..., C/2\}$. The image (or mirror) carrier is defined as $c' = -c$. Additionally, we mark the baseband equivalent signal snapshot at subcarrier c as s_c and the signal at the image carrier as $s_{c'}$.

When I/Q imbalance occurs in OFDM TX, the transmitted baseband equivalent signal snapshot at subcarrier c equals [16]

$$s_{\text{Txi},c} = s_c K_{\text{Tx1},c} + s_{c'}^* K_{\text{Tx2},c}. \tag{1}$$

Here, $K_{\text{Tx1},c}$ and $K_{\text{Tx2},c}$ are the TX I/Q imbalance coefficients, again at subcarrier c, which are given by

$$K_{\text{Tx1},c} = \frac{1 + g_{\text{Tx},c} e^{j\phi_{\text{Tx},c}}}{2} \quad \text{and} \quad K_{\text{Tx2},c} = \frac{1 - g_{\text{Tx},c} e^{j\phi_{\text{Tx},c}}}{2} \tag{2}$$

where $g_{\text{Tx},c}$ and $\phi_{\text{Tx},c}$ are the gain and phase imbalance parameters, respectively [5]. Note that ideally $g_{\text{Tx},c} = 1$ and $\phi_{\text{Tx},c} = 0$ and the transmitted signal snapshot reduces to s_c. Based on (1), we can note that the transmitted signal at subcarrier c is actually consisting of the desired signal but also of the signal meant to be transmitted at the image carrier.

When the transmitted signal snapshot, affected by TX I/Q imbalance, is received by an antenna array with N antenna elements, the received baseband equivalent signal snapshots $\mathbf{r}_{\text{Txi},c} = \left[r_{\text{Txi},1,c}, r_{\text{Txi},2,c}, ..., r_{\text{Txi},N,c}\right] \in \mathbb{C}^{N\times 1}$ can be presented as

$$\mathbf{r}_{\text{Txi},c} = s_{\text{Txi},c}\mathbf{h}_c + \mathbf{z}_c = s_c K_{\text{Tx1},c}\mathbf{h}_c + s_{c'}^* K_{\text{Tx2},c}\mathbf{h}_c + \mathbf{z}_c \tag{3}$$

where a perfect synchronization between TX and RX is assumed. Firstly, $\mathbf{h}_c \in \mathbb{C}^{N\times 1}$ consists of channel responses between the TX antenna and each of the RX antennas. We don't assume any specific spatial correlation for the channel responses and thus all formulations are valid in general. In addition, throughout the paper, the channel response elements as well as the I/Q imbalance parameters are assumed to be constant within each of the narrow subcarrier bands. Secondly, $\mathbf{z}_c \in \mathbb{C}^{N\times 1}$ is the interference plus noise vector at subcarrier c and equals

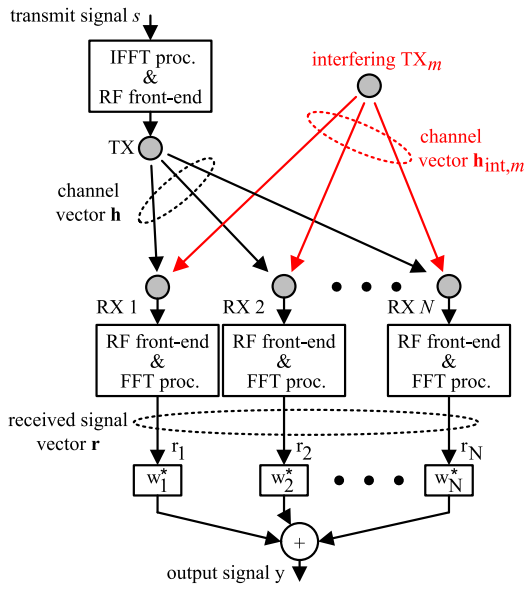

Fig. 1. A simplified illustration of considered scenario. All variables represents signals, responses, or coefficients at an arbitrary OFDM subcarrier.

$$\mathbf{z}_c = \sum_{m=1}^{M} s_{\text{int},c,m}\mathbf{h}_{\text{int},c,m} + \mathbf{n}_c. \tag{4}$$

Here, $s_{\text{int},c,m}$ and $\mathbf{h}_{\text{int},c,m} \in \mathbb{C}^{N\times 1}$ represent signal snapshot and the channel response vector of the m^{th} interfering signal, respectively. The total amount of interfering signals equals M and the noise vector $\mathbf{n}_c \in \mathbb{C}^{N\times 1}$ models the additive white Gaussian noise in the RX electronics. Noise elements in different RX branches are assumed to be complex circular and mutually uncorrelated. A complete transmission chain with an interferer is depicted in Fig. 1.

Next we consider that I/Q imbalance occurs also on the RX side. For convenience, we first define RX I/Q imbalance coefficient matrices $\left(\in \mathbb{C}^{N\times N}\right)$ given by

$$\mathbf{K}_{\text{Rx1},c} = \text{diag}(K_{\text{Rx1},1,c}, \cdots, K_{\text{Rx1},N,c}) \tag{5}$$

$$\mathbf{K}_{\text{Rx2},c} = \text{diag}(K_{\text{Rx2},1,c}, \cdots, K_{\text{Rx2},N,c}) \tag{6}$$

where the RX I/Q imbalance coefficients of the n^{th} individual RX branch are equal to [5]

$$K_{\text{Rx1},n,c} = \frac{1 + g_{\text{Rx},n,c} e^{-j\phi_{\text{Rx},n,c}}}{2} \tag{7}$$

$$K_{\text{Rx2},n,c} = \frac{1 - g_{\text{Rx},n,c} e^{j\phi_{\text{Rx},n,c}}}{2} \tag{8}$$

where $g_{\text{Rx},n,c}$ and $\phi_{\text{Rx},n,c}$ are now the gain and phase imbalance parameters of the n^{th} RX branch at subcarrier c. Then, the

received signal snapshots $\mathbf{r}_{\text{TxRxi},c} \in \mathbb{C}^{N\times 1}$ under joint TX+RX I/Q imbalance are given by

$$\begin{aligned}\mathbf{r}_{\text{TxRxi},c} &= \mathbf{K}_{\text{Rx1},c}\mathbf{r}_{\text{Txi},c} + \mathbf{K}_{\text{Rx2},c}\mathbf{r}^*_{\text{Txi},c'} \\ &= s_c\mathbf{K}_{\text{Rx},c}\tilde{\mathbf{K}}_{\text{TxA},c}\tilde{\mathbf{h}}_c + s^*_{c'}\mathbf{K}_{\text{Rx},c}\tilde{\mathbf{K}}_{\text{TxB},c}\tilde{\mathbf{h}}_c + \mathbf{K}_{\text{Rx},c}\tilde{\mathbf{z}}_c\end{aligned} \tag{9}$$

where the augmented channel response vector $\tilde{\mathbf{h}}_c = \left[\mathbf{h}_c^T, \mathbf{h}_{c'}^H\right]^T \in \mathbb{C}^{2N\times 1}$, the augmented interference plus noise vector $\tilde{\mathbf{z}}_c = \left[\mathbf{z}_c^T, \mathbf{z}_{c'}^H\right]^T \in \mathbb{C}^{2N\times 1}$ and the RX I/Q imbalance matrix $\mathbf{K}_{\text{Rx},c} = \left[\mathbf{K}_{\text{Rx1},c}, \mathbf{K}_{\text{Rx2},c}\right] \in \mathbb{C}^{N\times 2N}$. In addition, the TX I/Q imbalance matrices $\tilde{\mathbf{K}}_{\text{TxA},c}$ and $\tilde{\mathbf{K}}_{\text{TxB},c} \in \mathbb{C}^{2N\times 2N}$ are defined as

$$\tilde{\mathbf{K}}_{\text{TxA},c} = \begin{bmatrix}\mathbf{K}_{\text{Tx1},c} & \mathbf{0} \\ \mathbf{0} & \mathbf{K}^*_{\text{Tx2},c'}\end{bmatrix} \tag{10}$$

$$\tilde{\mathbf{K}}_{\text{TxB},c} = \begin{bmatrix}\mathbf{K}_{\text{Tx2},c} & \mathbf{0} \\ \mathbf{0} & \mathbf{K}^*_{\text{Tx1},c'}\end{bmatrix}. \tag{11}$$

Here $\mathbf{K}_{\text{Tx1},c} = K_{\text{Tx1},c}\mathbf{I}_N$ and $\mathbf{K}_{\text{Tx2},c} = K_{\text{Tx2},c}\mathbf{I}_N \in \mathbb{C}^{N\times N}$. This is the general form of the received signal under joint TX+RX I/Q imbalance. Throughout the paper, the special case with I/Q imbalance only in the TX can be obtained from the signal models by substituting $\mathbf{K}_{\text{Rx1},c} = \mathbf{I}$ and $\mathbf{K}_{\text{Rx2},c} = \mathbf{0}$ for all c. Similarly, the case with I/Q imbalance only in the RX is obtained by substituting $K_{\text{Tx1},c} = 1$ and $K_{\text{Tx2},c} = 0$ for all c.

B. Output Signal of A Linear Digital Combiner

Receiver array processing is usually implemented with a digital linear combiner. It processes the received signal snapshots with complex weights $\mathbf{w} = [w_1, w_2, ..., w_N]^T \in \mathbb{C}^{N\times 1}$ and the resulting output signal y can be presented in a convenient inner product format as [17]

$$y = \mathbf{w}^H\mathbf{r}. \tag{12}$$

The combiner weights can be selected/solved with blind or non-blind methods, depending on *a priori* information, under given optimization criteria.

For the case of joint TX+RX I/Q imbalance, combining results in an output signal at subcarrier c that is equal to

$$\begin{aligned}y_{\text{TxRxi},c} &= \mathbf{w}_c^H\mathbf{r}_{\text{TxRxi},c} \\ &= s_c\mathbf{w}_c^H\mathbf{K}_{\text{Rx},c}\tilde{\mathbf{K}}_{\text{TxA},c}\tilde{\mathbf{h}}_c + s^*_{c'}\mathbf{w}_c^H\mathbf{K}_{\text{Rx},c}\tilde{\mathbf{K}}_{\text{TxB},c}\tilde{\mathbf{h}}_c \\ &\quad + \mathbf{w}_c^H\mathbf{K}_{\text{Rx},c}\tilde{\mathbf{z}}_c.\end{aligned} \tag{13}$$

Here, the first term represents the contribution of the desired signal at subcarrier c. The next term consists of the non-desired signal at image carrier c' due to I/Q imbalances and can therefore be considered as a self-interference. The last term includes the effects of interfering signals and noise. Note that through $\tilde{\mathbf{z}}_c$, the output signal under joint TX+RX I/Q imbalance includes also a contribution of the interference and noise at the image carrier.

C. Joint Subcarrier Processing Through Augmented Combiner

As we saw in the previous subsection, I/Q imbalance causes signal distortion where the signals at subcarriers c and c' are mixed with each others. This gives us a motivation for a joint subcarrier processing of the distorted signal. This is obtained by combining the received signal vector $\mathbf{r_c}$ and its conjugated counterpart $\mathbf{r}^*_{c'}$ from the image carrier with two sets of weights [9], [13], say $\mathbf{w}_{1,c}$ and $\mathbf{w}_{2,c'}$. When defining the augmented weight vector as $\tilde{\mathbf{w}}_c = \left[\mathbf{w}_{1,c}^T, \mathbf{w}_{2,c'}^T\right]^T \in \mathbb{C}^{2N\times 1}$ and the augmented signal vector as $\tilde{\mathbf{r}}_c = \left[\mathbf{r}_c^T, \mathbf{r}_{c'}^H\right]^T \in \mathbb{C}^{2N\times 1}$, the output signal of the augmented digital combiner at subcarrier c can be given simply by

$$\tilde{y}_c = \tilde{\mathbf{w}}_c^H\tilde{\mathbf{r}}_c. \tag{14}$$

Note that although the output has very similar structure as in (12), there is a fundamental difference since now also the signal at the image carrier is included in the processing.

When we define an augmented signal under joint TX+RX I/Q imbalance as $\tilde{\mathbf{r}}_{\text{TxRxi},c} = \left[\mathbf{r}^T_{\text{TxRxi},c}, \mathbf{r}^H_{\text{TxRxi},c'}\right]^T$, we can present the output signal of the augmented combiner under joint TX+RX I/Q imbalance as

$$\begin{aligned}\tilde{y}_{\text{TxRxi},c} &= \tilde{\mathbf{w}}_c^H\tilde{\mathbf{r}}_{\text{TxRxi},c} \\ &= s_c\tilde{\mathbf{w}}_c^H\tilde{\mathbf{K}}_{\text{Rx},c}\tilde{\mathbf{K}}_{\text{TxA},c}\tilde{\mathbf{h}}_c + s^*_{c'}\tilde{\mathbf{w}}_c^H\tilde{\mathbf{K}}_{\text{Rx},c}\tilde{\mathbf{K}}_{\text{TxB},c}\tilde{\mathbf{h}}_c \\ &\quad + \tilde{\mathbf{w}}_c^H\tilde{\mathbf{K}}_{\text{Rx},c}\tilde{\mathbf{z}}_c.\end{aligned} \tag{15}$$

Here the augmented RX I/Q imbalance matrix $\tilde{\mathbf{K}}_{\text{Rx},c} \in \mathbb{C}^{2N\times 2N}$ is given by

$$\tilde{\mathbf{K}}_{\text{Rx},c} = \begin{bmatrix}\mathbf{K}_{\text{Rx1}c} & \mathbf{K}_{\text{Rx2}} \\ \mathbf{K}^*_{\text{Rx2}c'} & \mathbf{K}^*_{\text{Rx1}c'}\end{bmatrix}. \tag{16}$$

Clearly, the structures of (15) and (13) are very similar. However, (15) uses twice as many weights as (13) in order to process both subcarrier signals simultaneously. Naturally this yields doubled computational complexity but also gives us more degrees of freedom for obtaining the wanted signal and interference suppression properties even under I/Q imbalance.

III. Analytical Evaluation

A. Covariance Matrices

In order to evaluate the performance of the combiners, most notably combiner output SINR, we will next derive formulas for the covariance matrices of the received signals. We assume that the signals at subcarriers c and c', the interfering signals and the additive noise are all mutually uncorrelated. In addition, we assume that the interfering signals and noise are complex circular. Then the covariance matrix $\mathbf{R}_c \in \mathbb{C}^{N\times N}$ of the received signal under perfect I/Q matching is given by

$$\mathbf{R}_c = \mathbb{E}\left[\mathbf{r}_c\mathbf{r}_c^H\right] = \sigma^2_{\text{s},c}\mathbf{h}_c\mathbf{h}_c^H + \mathbf{R}_{\text{z},c} \tag{17}$$

where $\sigma^2_{\text{s},c} = \mathbb{E}\left[|s_c|^2\right]$ is the power of the desired signal at subcarrier c and the covariance matrix of the interference plus

noise equals

$$\mathbf{R}_{\mathrm{z},c} = \mathbb{E}\left[\mathbf{z}_c \mathbf{z}_c^H\right] = \sum_{m=1}^{M} \sigma_{\mathrm{int},c,m}^2 \mathbf{h}_{\mathrm{int},c,m} \mathbf{h}_{\mathrm{int},c,m}^H + \sigma_{\mathrm{n},c}^2 \mathbf{I}_N. \tag{18}$$

Here, $\sigma_{\mathrm{int},c,m}^2$ and $\sigma_{\mathrm{n},c}^2$ are the powers of the m^{th} interfering signal and noise, respectively. For future use, we also define $\tilde{\mathbf{R}}_{\mathrm{z},c} = \mathbb{E}\left[\tilde{\mathbf{z}}_c \tilde{\mathbf{z}}_c^H\right] \in \mathbb{C}^{2N \times 2N}$ as the covariance matrix for the augmented interference and noise vector. Under the aforementioned assumptions, it yields

$$\tilde{\mathbf{R}}_{\mathrm{z},c} = \begin{bmatrix} \mathbf{R}_{\mathrm{z},c} & \mathbf{0} \\ \mathbf{0} & \mathbf{R}_{\mathrm{z},c'}^* \end{bmatrix}. \tag{19}$$

When considering the effects of joint TX+RX I/Q imbalances, the covariance matrix equals

$$\begin{aligned} \mathbf{R}_{\mathrm{TxRxi},c} &= \mathbb{E}\left[\mathbf{r}_{\mathrm{TxRxi},c} \mathbf{r}_{\mathrm{TxRxi},c}^H\right] \\ &= \sigma_{\mathrm{s},c}^2 \mathbf{K}_{\mathrm{Rx},c} \tilde{\mathbf{K}}_{\mathrm{TxA},c} \tilde{\mathbf{h}}_c \tilde{\mathbf{h}}_c^H \tilde{\mathbf{K}}_{\mathrm{TxA},c}^H \mathbf{K}_{\mathrm{Rx},c}^H \\ &\quad + \sigma_{\mathrm{s},c'}^2 \mathbf{K}_{\mathrm{Rx},c} \tilde{\mathbf{K}}_{\mathrm{TxB},c} \tilde{\mathbf{h}}_c \tilde{\mathbf{h}}_c^H \tilde{\mathbf{K}}_{\mathrm{TxB},c}^H \mathbf{K}_{\mathrm{Rx},c}^H \\ &\quad + \mathbf{K}_{\mathrm{Rx},c} \tilde{\mathbf{R}}_{\mathrm{z},c} \mathbf{K}_{\mathrm{Rx},c}^H. \end{aligned} \tag{20}$$

Here, the first term represents the effect of the desired signal term at subcarrier c, whereas the second term corresponds to the self-interference from the image carrier. The last row represents the effect of the interference and noise.

The augmented signal has a slightly more complicated covariance matrix than (20). Fortunately, the covariance matrix of the augmented signal model can be in general expressed as

$$\tilde{\mathbf{R}}_c = \begin{bmatrix} \mathbf{R}_c & \mathbf{C}_c \\ \mathbf{C}_{c'}^* & \mathbf{R}_{c'}^* \end{bmatrix} \tag{21}$$

where $\tilde{\mathbf{R}}_c \in \mathbb{C}^{2N \times 2N}$ and the complementary covariance matrix $\mathbf{C}_c = \mathbb{E}\left[\mathbf{r}_c \mathbf{r}_{c'}^T\right] \in \mathbb{C}^{N \times N}$. Therefore, in order to find an expression for the covariance matrix of the augmented signal model, we need to derive the complementary covariance matrix under I/Q imbalance. With ideal RF electronics and assuming that the signals at subcarriers c and c' are complex circular and uncorrelated, the complementary covariance matrices become zero matrices. However, as shown in the previous section, I/Q imbalance creates dependencies between the signals at different subcarriers and thus results in non-circular signals, even if the signals have been originally circular. Consequently, the complementary covariance matrix of the received signal under joint TX+RX I/Q imbalance equals

$$\begin{aligned} \mathbf{C}_{\mathrm{TxRxi},c} &= \mathbb{E}\left[\mathbf{r}_{\mathrm{TxRxi},c} \mathbf{r}_{\mathrm{TxRxi},c'}^T\right] \\ &= \sigma_{\mathrm{s},c}^2 \mathbf{K}_{\mathrm{Rx},c} \tilde{\mathbf{K}}_{\mathrm{TxA},c} \tilde{\mathbf{h}}_c \tilde{\mathbf{h}}_{c'}^T \tilde{\mathbf{K}}_{\mathrm{TxB},c'}^T \mathbf{K}_{\mathrm{Rx},c'}^T \\ &\quad + \sigma_{\mathrm{s},c'}^2 \mathbf{K}_{\mathrm{Rx},c} \tilde{\mathbf{K}}_{\mathrm{TxB},c} \tilde{\mathbf{h}}_{c'} \tilde{\mathbf{h}}_{c'}^T \tilde{\mathbf{K}}_{\mathrm{TxA},c'}^T \mathbf{K}_{\mathrm{Rx},c'}^T \\ &\quad + \mathbf{K}_{\mathrm{Rx1},c} \mathbf{R}_{\mathrm{z},c} \mathbf{K}_{\mathrm{Rx2},c'}^T + \mathbf{K}_{\mathrm{Rx2},c} \mathbf{R}_{\mathrm{z},c'}^* \mathbf{K}_{\mathrm{Rx1},c'}^T. \end{aligned} \tag{22}$$

Now we obtain the covariance matrix of the augmented signal model under joint TX+RX I/Q imbalance simply by substituting (20) and (22) into (21).

B. Output Powers

The total output power of the combiner under ideal I/Q matching can be given first simply by [17]

$$\begin{aligned} \mathbb{E}\left[|y_c|^2\right] &= \mathbf{w}_c^H \mathbf{R}_c \mathbf{w}_c \\ &= \sigma_{\mathrm{s},c}^2 \left|\mathbf{w}_c^H \mathbf{h}_c\right|^2 + \sum_{m=1}^{M} \sigma_{\mathrm{int},c,m}^2 \left|\mathbf{w}_c^H \mathbf{h}_{\mathrm{int},c,m}\right|^2 \\ &\quad + \sigma_{\mathrm{n},c}^2 \mathbf{w}_c^H \mathbf{I}_N \mathbf{w}_c. \end{aligned} \tag{23}$$

The total output power depends clearly on three terms. The first term represents the contribution of the desired signal. In order to obtain good signal characteristics, the weights should be selected in such a manner that $\left|\mathbf{w}_c^H \mathbf{h}_c\right|$ is maximized. The second term consists of the contributions of the external interferers. This term should naturally be minimized and therefore $\left|\mathbf{w}_c^H \mathbf{h}_{\mathrm{int},c,m}\right|$ should be as small as possible for all m , i.e. the weights should be orthogonal with all of the interferer channel responses. Finally, the noise contributes the total output power simply through the noise power, having neither channel nor spatial dependency involved.

When substituting (20) into (23) we get the output power under joint TX+RX I/Q imbalance as

$$\begin{aligned} \mathbb{E}\left[\left|y_{\mathrm{TxRxi},c}\right|^2\right] &= \mathbf{w}_c^H \mathbf{R}_{\mathrm{TxRxi},c} \mathbf{w}_c \\ &= \sigma_{\mathrm{s},c}^2 \left|\mathbf{w}_c^H \mathbf{K}_{\mathrm{Rx},c} \tilde{\mathbf{K}}_{\mathrm{TxA},c} \tilde{\mathbf{h}}_c\right|^2 \\ &\quad + \sigma_{\mathrm{s},c'}^2 \left|\mathbf{w}_c^H \mathbf{K}_{\mathrm{Rx},c} \tilde{\mathbf{K}}_{\mathrm{TxB},c} \tilde{\mathbf{h}}_c\right|^2 \\ &\quad + \mathbf{w}_c^H \mathbf{K}_{\mathrm{Rx},c} \tilde{\mathbf{R}}_{\mathrm{z},c} \mathbf{K}_{\mathrm{Rx},c}^H \mathbf{w}_c. \end{aligned} \tag{24}$$

Again, the first term corresponds to the desired signal term whereas the second term represents the influence of the self-interference. The last term includes the contribution of the external interference and noise.

The power for the output signal of the augmented combiner is similar to (24) but the weights as well as the covariance matrix have to be replaced with their augmented counterparts. The resulting output power of the augmented signal under joint TX+RX I/Q imbalance is then given simply by

$$\begin{aligned} \mathbb{E}\left[\left|\tilde{y}_{\mathrm{TxRxi},c}\right|^2\right] &= \tilde{\mathbf{w}}_c^H \tilde{\mathbf{R}}_{\mathrm{TxRxi},c} \tilde{\mathbf{w}}_c \\ &= \sigma_{\mathrm{s},c}^2 \left|\tilde{\mathbf{w}}_c^H \tilde{\mathbf{K}}_{\mathrm{Rx},c} \tilde{\mathbf{K}}_{\mathrm{TxA},c} \tilde{\mathbf{h}}_c\right|^2 \\ &\quad + \sigma_{\mathrm{s},c'}^2 \left|\tilde{\mathbf{w}}_c^H \tilde{\mathbf{K}}_{\mathrm{Rx},c} \tilde{\mathbf{K}}_{\mathrm{TxB},c} \tilde{\mathbf{h}}_c\right|^2 \\ &\quad + \tilde{\mathbf{w}}_c^H \tilde{\mathbf{K}}_{\mathrm{Rx},c} \tilde{\mathbf{R}}_{\mathrm{z},c} \tilde{\mathbf{K}}_{\mathrm{Rx},c}^H \tilde{\mathbf{w}}_c. \end{aligned} \tag{25}$$

C. Signal to Interference and Noise Ratios

In order to evaluate the performance of the conventional and augmented combiners under I/Q imbalance, we will next formulate SINR expressions for the combiner output signals. SINRs illustrate the performance of the combiners from a practical point of view, while also offering a commonly used metric for comparisons with other studies in the literature.

SINRs are easily derived from the output signal powers in (24)-(25), since we have grouped them conveniently already in the previous subsection. As a result, SINR expression for the conventional combiner is given by (26), whereas SINR for the augmented combiner is given by (27).

$$\mathrm{SINR}_{\mathrm{TxRxi},c} = \frac{\sigma^2_{\mathrm{s},c}\left|\mathbf{w}_c^H\mathbf{K}_{\mathrm{Rx},c}\tilde{\mathbf{K}}_{\mathrm{TxA},c}\tilde{\mathbf{h}}_c\right|^2}{\left\{\sigma^2_{\mathrm{s},c'}\left|\mathbf{w}_c^H\mathbf{K}_{\mathrm{Rx},c}\tilde{\mathbf{K}}_{\mathrm{TxB},c}\tilde{\mathbf{h}}_c\right|^2 + \mathbf{w}_c^H\mathbf{K}_{\mathrm{Rx},c}\tilde{\mathbf{R}}_{\mathrm{z},c}\mathbf{K}^H_{\mathrm{Rx},c}\mathbf{w}_c\right\}} \quad (26)$$

$$\widetilde{\mathrm{SINR}}_{\mathrm{TxRxi},c} = \frac{\sigma^2_{\mathrm{s},c}\left|\tilde{\mathbf{w}}_c^H\tilde{\mathbf{K}}_{\mathrm{Rx},c}\tilde{\mathbf{K}}_{\mathrm{TxA},c}\tilde{\mathbf{h}}_c\right|^2}{\left\{\sigma^2_{\mathrm{s},c'}\left|\tilde{\mathbf{w}}_c^H\tilde{\mathbf{K}}_{\mathrm{Rx},c}\tilde{\mathbf{K}}_{\mathrm{TxB},c}\tilde{\mathbf{h}}_c\right|^2 + \tilde{\mathbf{w}}_c^H\tilde{\mathbf{K}}_{\mathrm{Rx},c}\tilde{\mathbf{R}}_{\mathrm{z},c}\tilde{\mathbf{K}}^H_{\mathrm{Rx},c}\tilde{\mathbf{w}}_c\right\}} \quad (27)$$

Notice that, through $\tilde{\mathbf{R}}_{\mathrm{z},c}$, (26) and (27) are affected by the interference and noise from the desired subcarrier but also from the image carrier. Obviously this non-desired behavior, caused by I/Q imbalance, creates additional challenges for the combiner weight selection. In the next subsection, we will discuss the weight selection problem and formulate two solution methods for the weights. We will also show that due to the doubled degrees of freedom, the augmented combiner suppresses the interference and noise more efficiently than the conventional per-subcarrier processing.

IV. Optimal MMSE Combiner

A well-known statistical method for solving stationary estimation problems is the so-called Wiener filter. It is an optimal solution in the MMSE sense [2] and the corresponding solution for the weight selection problem at hand is given by

$$\mathbf{w}_{\mathrm{MMSE},c} = \mathbf{R}_c^{-1}\mathbf{p}_c \quad (28)$$

where $\mathbf{p}_c = \mathbb{E}\left[s_c^*\mathbf{r}_c\right] \in \mathbb{C}^{N\times 1}$ is the cross-correlation vector between the desired signal and the received signal snapshots. The cross-correlation vector under joint TX+RX I/Q imbalance equals

$$\mathbf{p}_{\mathrm{TxRxi},c} = \mathbb{E}\left[s_c^*\mathbf{r}_{\mathrm{TxRxi},c}\right] = \sigma^2_{s,c}\mathbf{K}_{\mathrm{Rx},c}\tilde{\mathbf{K}}_{\mathrm{TxA},c}\tilde{\mathbf{h}}_c. \quad (29)$$

Unfortunately, the Wiener combiner is sensitive to I/Q imbalance leading to performance degradation [4]. To overcome this problem, the augmented Wiener combiner can be used since it is structurally capable of the joint subcarrier processing. The optimal solution is then given by

$$\tilde{\mathbf{w}}_{\mathrm{MMSE},c} = \tilde{\mathbf{R}}_c^{-1}\tilde{\mathbf{p}}_c \quad (30)$$

which is very similar to (28) but now all variables are given in the augmented form. The augmented cross-correlation vector $\left(\in \mathbb{C}^{2N\times 2N}\right)$ under I/Q imbalance equals now

$$\tilde{\mathbf{p}}_{\mathrm{TxRxi},c} = \mathbb{E}\left[s_c^*\tilde{\mathbf{r}}_{\mathrm{TxRxi},c}\right] = \begin{bmatrix}\sigma^2_{s,c}\mathbf{K}_{\mathrm{Rx},c}\tilde{\mathbf{K}}_{\mathrm{TxA},c}\tilde{\mathbf{h}}_c \\ \sigma^2_{s,c}\mathbf{K}^*_{\mathrm{Rx},c'}\tilde{\mathbf{K}}^*_{\mathrm{TxB},c'}\tilde{\mathbf{h}}^*_{c'}\end{bmatrix}. \quad (31)$$

Wiener combiners would result in optimal MMSE solutions, but the exact statistical information, i.e. $\mathbf{R}_c$ and $\mathbf{p}_c$, is rarely available. Fortunately, Wiener combiner can be approximated with adaptive data-aided methods [18] which adapt to the current channel conditions and RF imperfections with the help of beacons or pilot signals. One of these methods is least mean squares (LMS) [19] which converges close to Wiener solution. In addition, LMS does not require computationally complex matrix inversions and therefore leads to a solution with lower complexity than the exact Wiener solution. In order to avoid input signal power dependency, we selected to illustrate the results with normalized LMS (NLMS) [19] which can adapt to varying input powers in a more flexible way than the conventional LMS. One should note that (N)LMS is only one of the many applicable adaptive methods. E.g. if faster convergence is wanted, one could use the recursive least squares (RLS) algorithm [19] but this would also result in higher complexity and computational power.

The adaptive augmented NLMS algorithm for the augmented signal model is given by

$$\tilde{y}_c(i) = \tilde{\mathbf{w}}^H_{\mathrm{NLMS},c}(i)\tilde{\mathbf{r}}_c(i) \quad (32)$$

$$\tilde{e}_c(i) = s_c(i) - \tilde{y}_c(i) \quad (33)$$

$$\tilde{\mathbf{w}}_{\mathrm{NLMS},c}(i+1) = \tilde{\mathbf{w}}_{\mathrm{NLMS}}(i) + \tilde{\mu}\frac{\tilde{\mathbf{r}}_c(i)\tilde{e}^*_c(i)}{||\tilde{\mathbf{r}}_c(i)||^2} \quad (34)$$

where $\tilde{\mathbf{w}}_{\mathrm{NLMS},c} \in \mathbb{C}^{2N\times 1}$ denotes the augmented NLMS weights, $\tilde{e}_c$ is the estimation error and $\tilde{\mu}$ stands for the step-size coefficient. All parameters, excluding $\tilde{\mu}$, present the values on the i^{th} iteration round. The weights can be initialized e.g. with all-zeros or with *a priori* information if available. A corresponding algorithm for the conventional signal models is obtained by replacing all variables in (32)-(34), excluding s_c, with their non-augmented counterparts. In the next section we evaluate the performance of the combiners numerically.

V. Numerical Evaluations

In numerical evaluations we model a setup where one TX transmits an OFDM signal waveform which is received by an antenna array consisting of eight antenna elements. Mutually independent 16-quadrature amplitude modulation (QAM) symbols are deployed as subcarrier modulation. We also add four complex circular Gaussian waveforms to the received signals for modeling the contribution of external interference from other, non-desired, users. The transmission channels between all TX-RX antenna pairs as well as between all interferer-RX antenna pairs are independent and Rayleigh distributed. Finally, we add additive white Gaussian noise on top of the received signals for modeling the noise in the RX electronics. The noise power in all RX branches is assumed to be the same. We define the signal to noise ratio (SNR) as a ratio of the averaged received signal power (per RX antenna) and noise power. The signal to interference ratio (SIR) is defined as a ratio of the received signal power and the total received interference power.

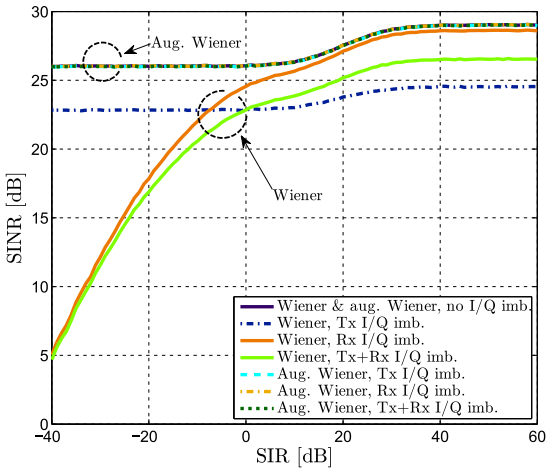

Fig. 2. SINR as a function of SIR when all four interferers have equal powers and SNR is fixed to 20 dB. The results are averaged over 10000 realizations. Note that the combiners have equal performance under perfect I/Q matching.

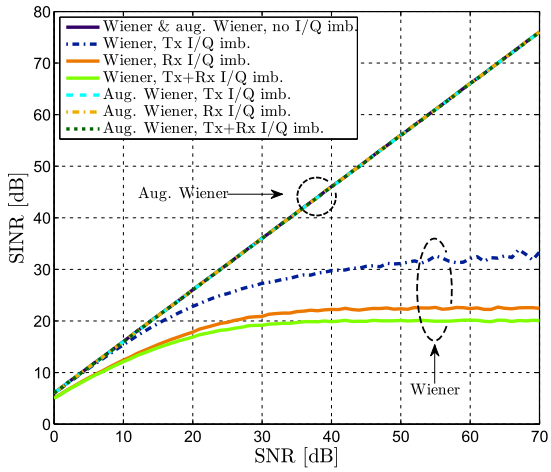

Fig. 3. SINR as a function of SNR when SIR is fixed to -20 dB. The results are averaged over 10000 realizations. Note that the combiners have equal performance under perfect I/Q matching.

For each realization, the I/Q imbalance gain coefficients $g_{\text{Tx},c}$ and $g_{\text{Rx},c,i}, i = 1, \cdots, N$, are independently selected from $\mathcal{U}(0.9, 1.1)$ whereas the phase imbalance coefficients $\phi_{\text{Tx},c}$ and $\phi_{\text{Rx},c,i}, i = 1, \cdots, N$, are independently selected from $\mathcal{U}(-10^\circ, 10^\circ)$. The I/Q imbalance parameters at different subcarriers are assumed to be independent for modeling arbitrarily frequency selective I/Q imbalance.

Fig. 2 depicts the SINR as a function of the SIR for Wiener combiners under different I/Q imbalance scenarios. We assumed four interferers with equal powers and a fixed SNR = 20 dB. Evidently, the Wiener combiner suffers from I/Q imbalances and its overall performance is degraded. With low interference levels, i.e. with the high SIRs, the impact of the noise is dominant over the impact of I/Q imbalance and TX I/Q imbalance results in the worst performance. This is well in line with the results in [20]. However, when SIR decreases, the interference becomes more dominant and the performance under either RX I/Q or joint TX+RX I/Q imbalances deteriorate heavily, becoming worse than under TX I/Q imbalance. This is a consequence from the fact that the contribution of the interference and noise depends on RX I/Q imbalance (see (26) and (27)) whereas TX I/Q imbalance affects only the self-interference. This is an essential result and should be taken into consideration when OFDM based systems utilizing antenna arrays are used in the presence of strong interferers. In contrast to the conventional per-subcarrier processing, the augmented Wiener combiner provides good performance in all imbalance cases. The overall performance is flooring at both low and high SIRs, not because of I/Q imbalances but because of the theoretical performance limits of the ideal combiners.

Fig. 3 shows the SINR as a function of SNR for Wiener combiners under different I/Q imbalance scenarios. The total received interference power level is here 20 dB higher than the desired signal power. Results show that the SINR of the conventional Wiener combiner under I/Q imbalances saturates with low noise levels and hence becomes interference limited. In addition, TX I/Q imbalance is not as harmful as RX I/Q imbalance which extends the results in [12] where a simpler I/Q imbalance scenario was used without external interferers. Intuitively, the joint TX+RX I/Q imbalance leads to the worst performance. Again, in contrast to the conventional Wiener combiner, the augmented Wiener combiner does not suffer from similar performance degradation. Based on the results, it can remove the effects of I/Q imbalance completely and thus results in good overall performance in all imbalance cases.

Finally, we analyze the performance of the practical data-aided NLMS combiners. Fig. 4 shows how the performance of NLMS algorithm is improved as a function of iteration rounds when the SNR is fixed to 20 dB and the SIR is fixed to -15 dB. The results show that NLMS indeed converges close to Wiener solutions. In addition, we can note that if RX I/Q imbalance is included in the system, the convergence is slower than in other cases. Fig. 5 depicts the performance of the augmented NLMS algorithm under the same conditions as NLMS in Fig. 4. Clearly, the performance of the augmented NLMS under I/Q imbalances is significantly better than with NLMS. In contrast to the conventional NLMS, the convergence speed is now almost independent of the I/Q imbalance scenario and consequently the convergence under RX and TX+RX I/Q imbalance is much faster than with NLMS. We have further noticed that the total interference plus noise level affects highly the convergence speed of both combiners. E.g. with SIR = ∞ and SNR = 20 dB, NLMS converges after 5000 iterations and the augmented NLMS is even faster, converging already after 150 iterations under all I/Q imbalance scenarios.

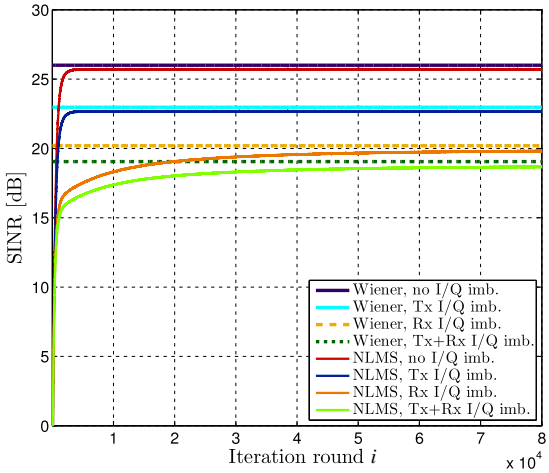

Fig. 4. Convergence of SINR with the conventional combiner. SNR is fixed to 20 dB and SIR is fixed to -15dB. The results are averaged over 500 realizations. Step-size parameter $\mu = 0.1$. Note the scale of the x-axis.

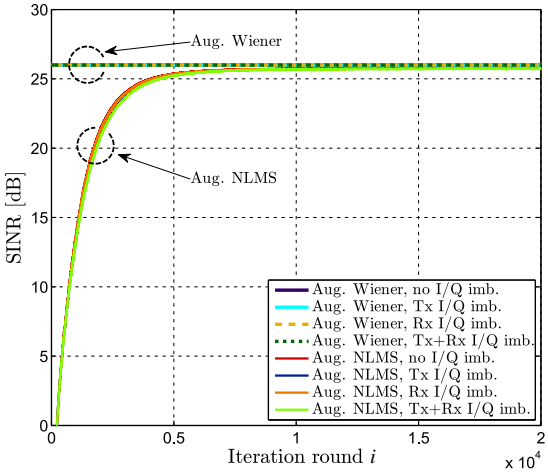

Fig. 5. Convergence of SINR with the augmented combiner. SNR is fixed to 20 dB and SIR is fixed to -15dB. The results are averaged over 500 realizations. Step-size parameter $\tilde{\mu} = 0.1$. Note the scale of the x-axis.

VI. Conclusion

In this paper, we analyzed the interference suppression with antenna arrays in OFDM systems under transceiver I/Q imbalances. We derived subcarrier level signal models for antenna array combiners in the presence of interferers and under joint TX+RX I/Q imbalances. The analytical evaluation was carrier out with covariance matrices, signal powers and SINRs. Finally, we illustrated the results numerically. All analysis assumed that the I/Q imbalance parameters and the channel responses can be arbitrarily frequency selective. In addition, we didn't assume any specific spatial correlation for the channel responses for keeping the formulations generic.

Based on the theoretical limitations of the conventional per-subcarrier processing, we proposed a joint subcarrier processing where the signal at subcarrier c is combined with the signal at the image carrier c' and across all antenna elements. Simulations showed that the conventional per-subcarrier processing results in heavy performance degradation under I/Q imbalances, especially in surroundings with high interference levels. In contrast to the per-subcarrier processing, the proposed joint subcarrier processing mitigates I/Q imbalances successfully, also in the presence of strong interferers. It removes the influence of both TX and RX I/Q imbalances and thus enables the same overall performance as if I/Q matchings were perfect.

References

[1] S. Haykin, "Cognitive radio: brain-empowered wireless communications," *IEEE J. Sel. Areas Commun.*, vol. 23, no. 2, pp. 201 – 220, Feb. 2005.

[2] H. L. V. Trees, *Detection, Estimation, and Modulation Theory, Optimum Array Processing*. John Wiley & Sons, Apr. 2004.

[3] A. Hakkarainen, J. Werner, K. Dandekar, and M. Valkama, "RF-aware widely-linear beamforming and null-steering in cognitive radio transmitters," in *Proc. CROWNCOM*, 2013, pp. 172–177.

[4] A. Hakkarainen, J. Werner, M. Renfors, K. Dandekar, and M. Valkama, "RF-Aware widely-linear MMSE beamforming," in *Proc. ISWCS*, 2013, pp. 582–586.

[5] T. Schenk, *RF Imperfections in High-rate Wireless Systems: Impact and Digital Compensation*, 1st ed. Springer, 2008.

[6] J. Cavers and M. Liao, "Adaptive compensation for imbalance and offset losses in direct conversion transceivers," *IEEE Trans. Veh. Technol.*, vol. 42, no. 4, pp. 581–588, 1993.

[7] A. Mashmour, W. Domino, and N. Beamish, "On the direct conversion receiver – a tutorial," *Microwave Journal*, vol. 44, no. 6, pp. 114–128, Jun. 2001.

[8] H. Rohling, *OFDM: Concepts for Future Communication Systems*. Springer, Mar. 2011.

[9] A. Tarighat, R. Bagheri, and A. Sayed, "Compensation schemes and performance analysis of IQ imbalances in OFDM receivers," *IEEE Trans. Signal Process.*, vol. 53, no. 8, pp. 3257–3268, 2005.

[10] A. Tarighat and A. Sayed, "Joint compensation of transmitter and receiver impairments in OFDM systems," *IEEE Trans. Wireless Commun.*, vol. 6, no. 1, pp. 240–247, 2007.

[11] B. Maham, O. Tirkkonen, and A. Hjorungnes, "Impact of transceiver I/Q imbalance on transmit diversity of beamforming OFDM systems," *IEEE Trans. Commun.*, vol. 60, no. 3, pp. 643–648, 2012.

[12] T. C. W. Schenk, E. Fledderus, and P. F. M. Smulders, "Performance impact of IQ mismatch in direct-conversion MIMO OFDM transceivers," in *Proc. IEEE RWS*, 2007, pp. 329–332.

[13] O. Ozdemir, R. Hamila, and N. Al-Dhahir, "I/Q imbalance in multiple beamforming OFDM transceivers: SINR analysis and digital baseband compensation," *IEEE Trans. Commun.*, vol. 61, no. 5, pp. 1914–1925, 2013.

[14] J. Qi and S. Aissa, "Compensation for HPA nonlinearity and I/Q imbalance in MIMO beamforming systems," in *Proc. IEEE WiMob*, 2010, pp. 78–82.

[15] D. Tandur and M. Moonen, "Compensation of RF impairments in MIMO OFDM systems," in *Proc. IEEE ICASSP*, 2008, pp. 3097–3100.

[16] ——, "Joint adaptive compensation of transmitter and receiver IQ imbalance under carrier frequency offset in OFDM-Based systems," *IEEE Trans. Signal Process.*, vol. 55, no. 11, pp. 5246–5252, 2007.

[17] J. Litva, *Digital Beamforming in Wireless Communications*. Artech House Publishers, Aug. 1996.

[18] B. Widrow et al., "Adaptive antenna systems," *Proc. IEEE*, vol. 55, no. 12, pp. 2143–2159, Dec. 1967.

[19] S. Haykin, *Adaptive Filter Theory*, 3rd ed. Prentice Hall, 1995.

[20] O. Özdemir, R. Hamila, and N. Al-Dhahir, "Exact SINR analysis of OFDM systems under joint Tx/RX I/Q imbalance," in *Proc. IEEE PIMRC*, 2013, pp. 646–650.

Publication 6

A. Hakkarainen, J. Werner, K. R. Dandekar, and M. Valkama, "Precoded Massive MU-MIMO Uplink Transmission under Transceiver I/Q Imbalance," in *Proceedings of the IEEE Global Communications Conference (GLOBECOM) Workshops*, Austin TX, USA, 8–12 Dec. 2014. DOI: 10.1109/glocomw.2014.7063451

Precoded Massive MU-MIMO Uplink Transmission under Transceiver I/Q Imbalance

Aki Hakkarainen*, Janis Werner*, Kapil R. Dandekar† and Mikko Valkama*
*Department of Electronics and Communications Engineering, Tampere University of Technology, Tampere, Finland
Email: {aki.hakkarainen, janis.werner, mikko.e.valkama}@tut.fi
†Department of Electrical and Computer Engineering, Drexel University, Philadelphia, PA, USA
Email: dandekar@coe.drexel.edu

***Abstract*—In massive multiple-input multiple-output (MIMO) systems, combined with digital array processing, the amount of the associated radio frequency (RF) front-ends is inevitably high. This paper addresses how imperfections in these RF front-ends affect the overall system performance in precoded massive multi-user MIMO (MU-MIMO) uplink transmission. In particular, we focus on transceiver in-phase/quadrature (I/Q) imbalances and their mitigation with RF-aware spatial processing. We first derive the essential distortion and interference models for OFDMA-based massive MU-MIMO uplink system under I/Q imbalances, and then propose augmented spatial post-processing to be carried out in the uplink receiver (RX) for mitigating the harmful effects efficiently. Numerical examples show that the augmented spatial RX processing clearly outperforms the conventional linear processing, and thus provides significant performance improvements with practical low-cost RF front-ends.**

***Index Terms*—antenna arrays, in-phase/quadrature (I/Q) imbalance, interference suppression, massive multi-user multiple-input multiple-output (MU-MIMO), orthogonal frequency-division multiple access (OFDMA)**

I. Introduction

Massive multiple-input multiple-output (MIMO) systems consist of tens or even hundreds of antennas [1]. Consequently, the amount of the associated radio frequency (RF) front-ends is very high, especially when emphasizing digital array processing and beamforming. In order to implement cost-effective and reasonable size massive MIMO devices in practice, the size and cost of individual RF transceivers should be low. Unfortunately, this requirement may easily result in performance degradation due to imperfections in the RF components [1], [2].

RF imperfections in massive MIMO systems have gained increasing interest recently. Our earlier work in [3] showed that RF imperfections in massive antenna arrays significantly degrade the system performance and can actually result in even bigger problems than in MIMO systems with fewer antennas. In [4], the effects of oscillator phase noise on uplink massive multiuser MIMO (MU-MIMO) systems are studied and the imperfection is shown to degrade the overall link performance. In [5], multiple aspects of the RF imperfections are provided in terms of energy efficiency as well as estimation and capacity limits in massive MIMO systems. The impact of RF imperfections is modeled in [5] as a residual additive Gaussian noise which depends only on the signal power. While such model may hold for the residual RF imperfections after the actual RF impairment processing, it does not take into account the inherent structure of distortion mechanisms of different RF imperfections.

In this paper, we consider and emphasize the structure of certain imperfections in the associated RF front-ends in massive MIMO systems. Especially, we focus on in-phase/quadrature (I/Q) imbalance and its mitigation jointly within spatial receiver (RX) post-processing without a need for separate I/Q imbalance mitigation or calibration. Starting from I/Q imbalance modeling in uplink orthogonal frequency division multiple access (OFDMA) based massive MU-MIMO systems, we show that I/Q imbalance in the RF front-ends causes signal distortion where each subcarrier signal is interfered by the signals at the image subcarrier, implying hence inter-user interference. Stemming from this phenomenon and based on the earlier I/Q imbalance studies in [6]–[9], we exploit the so-called augmented spatial post-processing at RX, now taking into account the effects of precoding in uplink transmitters (TXs). We derive the minimum mean-square error (MMSE)-optimal augmented spatial post-processing solution, and by simulating the system performance as a funtion of multiple system parameters, we show that the proposed solution outperforms the traditional per-subcarrier processing clearly and thus provides significant performance improvements without costly changes in the associated RF front-ends.

This paper is organized as follows. Section II introduces fundamental signal and system models as well as RX post-processing principles in base station (BS). In Section III, we present the RF-aware precoding method as well as the linear and augmented linear MMSE (LMMSE) post-processing solutions. In Section IV, we provide numerical examples in terms of the signal-to-interference-plus-noise ratio (SINR). Finally, the conclusions are drawn in Section V.

Notation: Vectors and matrices are written with bold characters. The superscripts $(\cdot)^T$, $(\cdot)^H$, $(\cdot)^*$ and $(\cdot)^{-1}$ represent

This work was supported by the Finnish Funding Agency for Technology and Innovation (Tekes) under the project "Reconfigurable Antenna-based Enhancement of Dynamic Spectrum Access Algorithms", the Industrial Research Fund of Tampere University of Technology (Tuula and Yrjö Neuvo Fund), the Academy of Finland under the project 251138 "Digitally-Enhanced RF for Cognitive Radio Devices", the Doctoral Programme of the President of Tampere University of Technology, and the Foundation of Nokia Corporation.

The work was also supported by National Science Foundation (NSF) under award number 1147838.

transpose, Hermitian (conjugate) transpose, complex conjugate and matrix inverse, respectively. The tilde sign $\widetilde{(\cdot)}$ is used to present an augmented quantity and the results obtained by augmented processing. We write diag $(x_{11}, x_{22}, \cdots, x_{ii})$ to denote the diagonal matrix $\mathbf{X}$ with elements x_{ii} on the main diagonal. The statistical expectation is denoted with $\mathbb{E}[\cdot]$. Finally, tr $(\cdot)$ denotes the trace of a matrix.

II. Signal and System Models

In this paper, we consider precoded spatial multiplexing in uplink OFDMA MU-MIMO transmission from an arbitrary subcarrier point of view. Our generic model comprises a single BS which serves simultaneously multiple user equipment (UEs) in each time-frequency resource. The subcarriers are indexed with $c \in \{-C/2, \ldots, -1, 1, \ldots, C/2\}$ where C is the total amount of active subcarriers. Furthermore, the image (or mirror) subcarrier is defined as $c' = -c$. With U and V we denote the number of UEs spatially multiplexed at subcarriers c and c', respectively. The corresponding UEs are indexed with $u \in \{1, \ldots, U\}$ and $v \in \{1, \ldots, V\}$. Note that depending on the frequency allocation for the UEs, u and v might refer to the same UE which is active at both subcarriers c and c'.

The BS has N RX antennas whereas UE u is equipped with M_u TX antennas. The number of parallel independent data streams of UE u at subcarrier c is denoted by Q_u. At subcarrier c, the data symbol vector $\mathbf{x}_{u,c} \in \mathbb{C}^{Q_u \times 1}$ of UE u is precoded with precoder $\mathbf{G}_{u,c} \in \mathbb{C}^{M_u \times Q_u}$ resulting in antenna signal vector $\mathbf{s}_{u,c} \in \mathbb{C}^{M_u \times 1}$. The corresponding variables at the image subcarrier c' for UE v are denoted by $\mathbf{x}_{v,c'} \in \mathbb{C}^{Q_v \times 1}$, $\mathbf{G}_{v,c'} \in \mathbb{C}^{M_v \times Q_v}$, and $\mathbf{s}_{v,c'} \in \mathbb{C}^{M_v \times 1}$. In addition to the UE signals, we include L external interferers into the model. External interferer l is assumed to have J_l TX antennas and the spatial signal snapshot vector originating from that external interferer is denoted by $\mathbf{s}_{\text{int},l,c} \in \mathbb{C}^{J_l \times 1}$. All data vectors refer to subcarrier-level (frequency-domain) quantities in the considered OFDMA radio system, i.e., prior to the inverse fast Fourier transform (IFFT) in the TXs and after the fast Fourier transform (FFT) in the RXs.

A. Joint TX+RX I/Q Imbalances in MU-MIMO Systems

Direct-conversion transceivers (DCTs) [10] are regarded as promising candidates for the radio architecture in massive MIMO systems since they do not need additional intermediate-frequency filters, in contrast to the heterodyne transceivers [10]. Consequently, the total size and cost of DCT are smaller compared to conventional solutions. Unfortunately, the imperfections in the analog RF electronics of DCT are known to result in I/Q imbalance [10], [11]. I/Q imbalance is caused by gain and phase imbalance, g and ϕ, between the I and Q branches. The roots of the phenomenon lie in the implementation inaccuracies of the associated amplifiers, filters, mixers and digital-to-analog and analog-to-digital converters.

In precoded uplink MU-MIMO transmission, the transmitted antenna signal vector of UE u at subcarrier c, assuming first perfect I/Q matching, can be written as $\mathbf{s}_{u,c} = \mathbf{G}_{u,c}\mathbf{x}_{u,c}$ [12]. However, when considering *I/Q imbalance in the TX electronics of an individual UE*, the transmitted antenna signal vector of UE u at subcarrier c becomes [9], [13]

$$\begin{aligned}\mathbf{s}_{\text{Txi},u,c} &= \mathbf{K}_{\text{Tx1},u,c}\mathbf{s}_{u,c} + \mathbf{K}_{\text{Tx2},u,c}\mathbf{s}^*_{u,c'} \\ &= \mathbf{K}_{\text{Tx1},u,c}\mathbf{G}_{u,c}\mathbf{x}_{u,c} + \mathbf{K}_{\text{Tx2},u,c}\mathbf{G}^*_{u,c'}\mathbf{x}^*_{u,c'} \end{aligned} \quad (1)$$

with the TX I/Q imbalance matrices $\mathbf{K}_{\text{Tx1},u,c} = \text{diag}(K_{\text{Tx1},1,u,c}, \cdots, K_{\text{Tx1},M_u,u,c}) \in \mathbb{C}^{M_u \times M_u}$ and $\mathbf{K}_{\text{Tx2},u,c} = \text{diag}(K_{\text{Tx2},1,u,c}, \cdots, K_{\text{Tx2},M_u,u,c}) \in \mathbb{C}^{M_u \times M_u}$. The diagonal entries of the matrices are given by $K_{\text{Tx1},m,u,c} = (1 + g_{\text{Tx},m,u,c}e^{j\phi_{\text{Tx},m,u,c}})/2$ and $K_{\text{Tx2},m,u,c} = (1 - g_{\text{Tx},m,u,c}e^{j\phi_{\text{Tx},m,u,c}})/2$ where $g_{\text{Tx},m,u,c}$ and $\phi_{\text{Tx},m,u,c}$ are the gain and phase imbalance coefficients for TX antenna branch m of user u at subcarrier c [11]. Clearly, the transmitted signal is distorted, resulting in cross-talk between subcarriers c and c'. This is a well-known phenomenon, discussed e.g. in [9], [11], [13]–[15]. In general, when the image subcarrier c' is allocated to another UE v, this results in cross-talk between UEs at mirror subcarriers.

The transmitted signal vectors propagate through the wireless channels and are then received in the RX. Consequently, the total received signal vector $\mathbf{r}_{\text{Txi},c} \in \mathbb{C}^{N \times 1}$ at subcarrier c under I/Q imbalances of UE TXs is

$$\begin{aligned}\mathbf{r}_{\text{Txi},c} = &\sum_{u=1}^{U} \mathbf{H}_{u,c}\mathbf{K}_{\text{Tx1},u,c}\mathbf{G}_{u,c}\mathbf{x}_{u,c} \\ &+ \sum_{v=1}^{V} \mathbf{H}_{v,c}\mathbf{K}_{\text{Tx2},v,c}\mathbf{G}^*_{v,c'}\mathbf{x}^*_{v,c'} + \mathbf{z}_c \end{aligned} \quad (2)$$

where we assume, for simplicity, perfect timing and frequency synchronization between the UEs and the BS. Here, $\mathbf{H}_{u,c} \in \mathbb{C}^{N \times M_u}$ and $\mathbf{H}_{v,c} \in \mathbb{C}^{N \times M_v}$ are the channel response matrices of UEs u and v, respectively, at subcarrier c. Throughout the paper, the channel response elements are assumed to be constant within each narrow subcarrier. Finally, the external interference plus noise vector $\mathbf{z}_c \in \mathbb{C}^{N \times 1}$ is given by

$$\mathbf{z}_c = \sum_{l=1}^{L} \mathbf{H}_{\text{int},l,c}\mathbf{s}_{\text{int},l,c} + \mathbf{n}_c. \quad (3)$$

Here, $\mathbf{H}_{\text{int},l,c} \in \mathbb{C}^{N \times J_l}$ is the channel response matrix of external interferer l, and $\mathbf{n}_c \in \mathbb{C}^{N \times 1}$ models the additive noise in the RX electronics. Noise elements in different RX branches are assumed to be complex, circular and mutually uncorrelated. A corresponding formulation for the external interference and noise at the image subcarrier is obtained from (3) by substituting the subcarrier index c with c'.

When taking next into account that *I/Q imbalance occurs also in the RX*, the received signal vector $\mathbf{r}_{\text{TxRxi},c} \in \mathbb{C}^{N \times 1}$ at subcarrier c under joint TX+RX I/Q imbalances is equal to

$$\begin{aligned}\mathbf{r}_{\text{TxRxi},c} &= \mathbf{K}_{\text{Rx1},c}\mathbf{r}_{\text{Txi},c} + \mathbf{K}_{\text{Rx2},c}\mathbf{r}^*_{\text{Txi},c'} \\ &= \sum_{u=1}^{U} \widetilde{\mathbf{\Psi}}_{u,c}\mathbf{G}_{u,c}\mathbf{x}_{u,c} + \sum_{v=1}^{V} \widetilde{\mathbf{\Omega}}_{v,c}\mathbf{G}^*_{v,c'}\mathbf{x}^*_{v,c'} \\ &\quad + \mathbf{K}_{\text{Rx1},c}\mathbf{z}_c + \mathbf{K}_{\text{Rx2},c}\mathbf{z}^*_{c'} \end{aligned} \quad (4)$$

where the RX I/Q imbalance matrices are given by $\mathbf{K}_{\text{Rx1},c} = \text{diag}(K_{\text{Rx1},1,c}, \cdots, K_{\text{Rx1},N,c}) \in \mathbb{C}^{N\times N}$ and $\mathbf{K}_{\text{Rx2},c} = \text{diag}(K_{\text{Rx2},1,c}, \cdots, K_{\text{Rx2},N,c}) \in \mathbb{C}^{N\times N}$. Here, the diagonal entries of the matrices are given by $K_{\text{Rx1},n,c} = (1 + g_{\text{Rx},n,c}e^{-j\phi_{\text{Rx},n,c}})/2$ and $K_{\text{Rx2},n,c} = (1 - g_{\text{Rx},n,c}e^{j\phi_{\text{Rx},n,c}})/2$. Similarly as for the TX, $g_{\text{Rx},n,c}$ and $\phi_{\text{Rx},n,c}$ denote the gain and phase imbalance coefficients of RX antenna branch n [11]. Furthermore, the total effective channel matrices, consisting of the influence of TX and RX I/Q imbalances as well as the wireless propagation channels, are given by

$$\widetilde{\mathbf{\Psi}}_{u,c} = \begin{bmatrix}\mathbf{K}_{\text{Rx1},c} & \mathbf{K}_{\text{Rx2},c}\end{bmatrix} \begin{bmatrix}\mathbf{H}_{u,c} & \mathbf{0} \\ \mathbf{0} & \mathbf{H}^*_{u,c'}\end{bmatrix} \begin{bmatrix}\mathbf{K}_{\text{Tx1},u,c} \\ \mathbf{K}^*_{\text{Tx2},u,c'}\end{bmatrix} \quad (5)$$

$$\widetilde{\mathbf{\Omega}}_{v,c} = \begin{bmatrix}\mathbf{K}_{\text{Rx1},c} & \mathbf{K}_{\text{Rx2},c}\end{bmatrix} \begin{bmatrix}\mathbf{H}_{v,c} & \mathbf{0} \\ \mathbf{0} & \mathbf{H}^*_{v,c'}\end{bmatrix} \begin{bmatrix}\mathbf{K}_{\text{Tx2},v,c} \\ \mathbf{K}^*_{\text{Tx1},v,c'}\end{bmatrix} \quad (6)$$

where $\widetilde{\mathbf{\Psi}}_{u,c} \in \mathbb{C}^{N\times M_u}$ and $\widetilde{\mathbf{\Omega}}_{v,c} \in \mathbb{C}^{N\times M_v}$. Clearly, (4) includes contribution not only from the desired subcarrier c but also from the image subcarrier c'. The signals transmitted at the image subcarrier c' leak to subcarrier c due to both TX and RX I/Q imbalances and thus we call it *inter-user interference* from the image subcarrier. In contrast to the data signals, the external interference and noise from the image subcarrier c' alias to subcarrier c only due to RX I/Q imbalance. Stemming from the special nature of I/Q imbalance, signals at other subcarriers are not affected.

Note that the special case with I/Q imbalance only in the TX (RX) is obtained from (4) by substituting $\mathbf{K}_{\text{Rx1},c} = \mathbf{I}$ and $\mathbf{K}_{\text{Rx2},c} = \mathbf{0}$ $\forall c$ ($\mathbf{K}_{\text{Tx1},u,c} = \mathbf{I}$ and $\mathbf{K}_{\text{Tx2},u,c} = \mathbf{0}$ $\forall u,c$).

B. Receiver Post-Processing in The Base Station

In MU-MIMO systems the transmitted data streams of different UEs must be eventually separated in the BS while also suppressing any harmful interference effectively. The RX post-processing is implemented by combining the received signals from the RX antennas in a selected manner. When using linear combining, the signals at subcarrier c are post-processed in the digital domain using the combiner weight matrix $\mathbf{W}_c = \left[\mathbf{w}^T_{1,1,c}, \mathbf{w}^T_{1,2,c}, \cdots, \mathbf{w}^T_{Q_U,U,c}\right]^T \in \mathbb{C}^{S\times N}$ where row vector $\mathbf{w}_{q,u,c} \in \mathbb{C}^{1\times N}$ denotes the weights for data stream q of UE u and $S = \sum_{u=1}^{U} Q_u$ is the total amount of the transmitted data streams. Then, the output signal vector $\mathbf{y}_c \in \mathbb{C}^{S\times 1}$ under perfect I/Q matching is given by

$$\mathbf{y}_c = \mathbf{W}_c\mathbf{r}_c = \sum_{u=1}^{U} \mathbf{W}_c\mathbf{H}_{u,c}\mathbf{G}_{u,c}\mathbf{x}_{u,c} + \mathbf{W}_c\mathbf{z}_c. \quad (7)$$

Since the data is processed at the subcarrier level, we call this method per-subcarrier processing. The overall MU-MIMO system with precoded spatial multiplexing is depicted in Fig. 1.

As shown in (4), I/Q imbalance distorts the received antenna signals. Consequently, the combiner output signal under joint

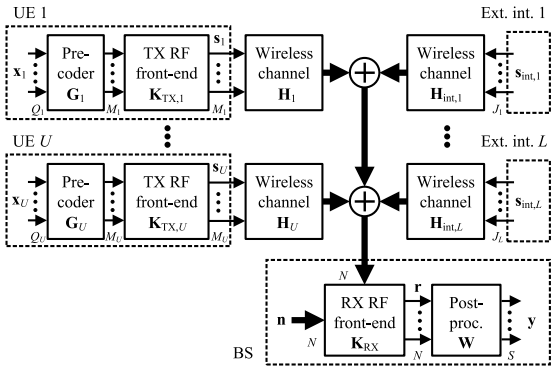

Fig. 1. Illustration of the considered uplink MU-MIMO scenario with devices being active at subcarrier c.

TX+RX I/Q imbalances becomes

$$\begin{aligned}\mathbf{y}_{\text{TxRxi},c} &= \mathbf{W}_c\mathbf{r}_{\text{TxRxi},c} \\ &= \sum_{u=1}^{U} \mathbf{W}_c\widetilde{\mathbf{\Psi}}_{u,c}\mathbf{G}_{u,c}\mathbf{x}_{u,c} + \sum_{v=1}^{V} \mathbf{W}_c\widetilde{\mathbf{\Omega}}_{v,c}\mathbf{G}^*_{v,c'}\mathbf{x}^*_{v,c'} \\ &\quad + \mathbf{W}_c\mathbf{K}_{\text{Rx1},c}\mathbf{z}_c + \mathbf{W}_c\mathbf{K}_{\text{Rx2},c}\mathbf{z}^*_{c'}. \end{aligned} \quad (8)$$

Clearly, the output signal consists of both the desired data streams as well as the interfering UE signals originating from the image subcarrier. In addition, the output signal includes external interference and noise at both subcarriers c and c'. The signal leakage naturally makes the signal separation in the RX more difficult and consequently the overall system performance is also deteriorated, as shown in Section IV.

The signal distortion, where each subcarrier signal is mixed with the signals at the image subcarrier, guides us towards joint post-processing of mirror-subcarriers [6]–[8]. When defining the augmented received signal as $\widetilde{\mathbf{r}}_c = \left[\mathbf{r}^T_c, \mathbf{r}^H_{c'}\right]^T \in \mathbb{C}^{2N\times 1}$, the augmented post-processing is of the form $\widetilde{\mathbf{y}}_c = \widetilde{\mathbf{W}}_c\widetilde{\mathbf{r}}_c$ where the augmented weight matrix $\widetilde{\mathbf{W}}_c = \left[\widetilde{\mathbf{w}}^T_{1,1,c}, \cdots, \widetilde{\mathbf{w}}^T_{Q_U,U,c}\right]^T \in \mathbb{C}^{S\times 2N}$. Now, row vector $\widetilde{\mathbf{w}}_{M_\text{U},U,c} \in \mathbb{C}^{1\times 2N}$ contains separate weights for both subcarrier signals and thus provides more degrees of freedom (DoF) in post-processing.

Under joint TX+RX I/Q imbalances, the augmented combiner output signal $\widetilde{\mathbf{y}}_{\text{TxRxi},c} \in \mathbb{C}^{S\times 1}$ is given by

$$\begin{aligned}\widetilde{\mathbf{y}}_{\text{TxRxi},c} &= \widetilde{\mathbf{W}}_c\widetilde{\mathbf{r}}_{\text{TxRxi},c} \\ &= \sum_{u=1}^{U} \widetilde{\mathbf{W}}_c\widetilde{\mathbf{\Xi}}_{u,c}\mathbf{G}_{u,c}\mathbf{x}_{u,c} + \sum_{v=1}^{V} \widetilde{\mathbf{W}}_c\widetilde{\mathbf{\Phi}}_{v,c}\mathbf{G}^*_{v,c'}\mathbf{x}^*_{v,c'} \\ &\quad + \widetilde{\mathbf{W}}_c\widetilde{\mathbf{K}}_{\text{RxA},c}\mathbf{z}_c + \widetilde{\mathbf{W}}_c\widetilde{\mathbf{K}}_{\text{RxB},c}\mathbf{z}^*_{c'}. \end{aligned} \quad (9)$$

Here, the augmented signal vector under joint TX+RX I/Q imbalances is $\widetilde{\mathbf{r}}_{\text{TxRxi},c} = \left[\mathbf{r}^T_{\text{TxRxi},c}, \mathbf{r}^H_{\text{TxRxi},c'}\right]^T \in \mathbb{C}^{2N\times 1}$ and

the total augmented effective channel matrices are given by

$$\widetilde{\mathbf{\Xi}}_{u,c} = \begin{bmatrix} \mathbf{K}_{\text{Rx1},c} & \mathbf{K}_{\text{Rx2},c} \\ \mathbf{K}^*_{\text{Rx2},c'} & \mathbf{K}^*_{\text{Rx1},c'} \end{bmatrix} \begin{bmatrix} \mathbf{H}_{u,c} & \mathbf{0} \\ \mathbf{0} & \mathbf{H}^*_{u,c'} \end{bmatrix} \begin{bmatrix} \mathbf{K}_{\text{Tx1},u,c} \\ \mathbf{K}^*_{\text{Tx2},u,c'} \end{bmatrix} \quad (10)$$

$$\widetilde{\mathbf{\Phi}}_{v,c} = \begin{bmatrix} \mathbf{K}_{\text{Rx1},c} & \mathbf{K}_{\text{Rx2},c} \\ \mathbf{K}^*_{\text{Rx2},c'} & \mathbf{K}^*_{\text{Rx1},c'} \end{bmatrix} \begin{bmatrix} \mathbf{H}_{v,c} & \mathbf{0} \\ \mathbf{0} & \mathbf{H}^*_{v,c'} \end{bmatrix} \begin{bmatrix} \mathbf{K}_{\text{Tx2},v,c} \\ \mathbf{K}^*_{\text{Tx1},v,c'} \end{bmatrix} \quad (11)$$

where $\widetilde{\mathbf{\Xi}}_{u,c} \in \mathbb{C}^{2N \times M_u}$ and $\widetilde{\mathbf{\Phi}}_{v,c} \in \mathbb{C}^{2N \times M_v}$. Finally, the augmented RX I/Q imbalance matrices, both $\in \mathbb{C}^{2N \times N}$, are

$$\widetilde{\mathbf{K}}_{\text{RxA},c} = \begin{bmatrix} \mathbf{K}_{\text{Rx1},c} \\ \mathbf{K}^*_{\text{Rx2},c'} \end{bmatrix}, \widetilde{\mathbf{K}}_{\text{RxB},c} = \begin{bmatrix} \mathbf{K}_{\text{Rx2},c} \\ \mathbf{K}^*_{\text{Rx1},c'} \end{bmatrix}. \quad (12)$$

Despite the similarities between (8) and (9), the underlying capability of the joint subcarrier processing in (9) should be kept in mind. The doubled amount of the weights naturally doubles the computational complexity of the combining process but also enables more flexible post-processing for obtaining the desired signal separation and interference suppression, even under challenging I/Q imbalances. Note that this flexibility is obtained by changing the digital combiner block alone whereas the costly RF chains and demanding FFT processing remain the same as for classical per-subcarrier processing.

III. Precoding and MMSE Post-Processing

Closed-loop type spatial multiplexing can provide significant performance improvements due to the exploitation of known channel state information (CSI) [16]. The spatial signal processing is shared between the TX and RX sides such that the desired link performance is provided. On the TX side, the precoder pre-processes and maps the data streams to the TX antennas. On the RX side, the received antenna signals are post-processed such that different data streams are properly separated while harmful interference is effectively suppressed. In this paper, we assume that perfect uplink CSI for subcarriers c and c', including also the effects of I/Q imbalance, is available for both the UEs as well as the BS. Although this assumption is over-optimistic in practice, we use it for evaluating and demonstrating the performance limits of the closed-loop spatial multiplexing under I/Q imbalance.

A. RF-Aware Precoding

One of the precoding methods is based on singular-value decomposition of the known channel matrix. The singular-value decomposition for the total effective channel matrix of UE u at subcarrier c is given by

$$\widetilde{\mathbf{\Psi}}_{u,c} = \mathbf{U}_{u,c}\mathbf{\Lambda}_{u,c}\mathbf{V}^H_{u,c} \quad (13)$$

where $\mathbf{U}_{u,c} \in \mathbb{C}^{N \times N}$ contains the left singular vectors, $\mathbf{\Lambda}_{u,c} \in \mathbb{C}^{N \times M_u}$ is a diagonal matrix including the singular values, and $\mathbf{V}_{u,c} = \left[\mathbf{v}_{1,u,c}, \mathbf{v}_{2,u,c}, \cdots, \mathbf{v}_{M_u,u,c}\right] \in \mathbb{C}^{M_u \times M_u}$ consists of the right singular vectors. The precoding matrix $\mathbf{G}_{u,c} \in \mathbb{C}^{M_u \times Q_u}$ for UE u, assuming that UE knows only the CSI of its own, at subcarrier c is then obtained as

$$\mathbf{G}_{u,c} = \left[\mathbf{v}_{1,u,c}, \mathbf{v}_{2,u,c}, \cdots, \mathbf{v}_{Q_u,u,c}\right] \quad (14)$$

i.e. the precoder consists of the first Q_u columns of $\mathbf{V}_{u,c}$ [12]. In order to fulfil maximum TX power constraint $P_{\max}$, we need to scale the precoder such that $\text{tr}\left(\mathbf{G}_{u,c}\mathbf{R}_{\text{x},u,c}\mathbf{G}^H_{u,c}\right) \leq P_{\max}$ where $\mathbf{R}_{\text{x},u,c} = \mathbb{E}\left[\mathbf{x}_{u,c}\mathbf{x}^H_{u,c}\right]$ [12]. For simplicity, we assume that the data streams of an individual UE are equal in power. Note that the precoder in (14) adapts the transmission not only to the propagation channel but also to the associated RF front-ends and is therefore called RF-aware precoder.

B. Linear and Augmented Linear MMSE Post-Processing

Spatial post-processing can be implemented in the BS with the well-known LMMSE spatial filter. With the used notation, the LMMSE filter $\mathbf{W}_{\text{LMMSE},c} \in \mathbb{C}^{S \times N}$ is equal to [17]

$$\mathbf{W}_{\text{LMMSE},c} = \left(\mathbf{H}^H_{\text{eff},c}\mathbf{R}^{-1}_{\text{int},c}\mathbf{H}_{\text{eff},c} + \mathbf{R}^{-1}_{\text{x},c}\right)^{-1}\mathbf{H}^H_{\text{eff}}\mathbf{R}^{-1}_{\text{int},c}. \quad (15)$$

Here, $\mathbf{H}_{\text{eff},c} \in \mathbb{C}^{N \times S}$ is the total effective channel matrix consisting of channel responses and precoders of all UEs. Assuming that the total effective CSI including I/Q imbalance is available at the BS, we write

$$\mathbf{H}_{\text{eff},c} = \left[\widetilde{\mathbf{\Psi}}_{1,c}\mathbf{G}_{1,c}, \widetilde{\mathbf{\Psi}}_{2,c}\mathbf{G}_{2,c}, \cdots, \widetilde{\mathbf{\Psi}}_{U,c}\mathbf{G}_{U,c}\right]. \quad (16)$$

In addition, $\mathbf{R}_{\text{x},c} \in \mathbb{C}^{S \times S}$ is the covariance matrix of all the data streams and $\mathbf{R}_{\text{int},c} \in \mathbb{C}^{N \times N}$ is the covariance matrix of the interference and noise. Under joint TX+RX I/Q imbalances $\mathbf{R}_{\text{int},c}$ includes the inter-user interference from c' as well the external interference and noise from both c and c', and is equal to

$$\begin{aligned}\mathbf{R}_{\text{int},c} = &\sum_{v=1}^{V} \sigma^2_{x,v,c'}\widetilde{\mathbf{\Omega}}_{v,c}\mathbf{G}^*_{v,c'}\mathbf{G}^T_{v,c'}\widetilde{\mathbf{\Omega}}_{v,c} \\ &+ \mathbf{K}_{\text{Rx1},c}\mathbf{R}_{\text{z},c}\mathbf{K}^H_{\text{Rx1},c} + \mathbf{K}_{\text{Rx2},c}\mathbf{R}^*_{\text{z},c'}\mathbf{K}^H_{\text{Rx2},c}. \quad (17)\end{aligned}$$

Here, $\mathbf{R}_{\text{z},c} \in \mathbb{C}^{N \times N}$ is given by

$$\mathbf{R}_{\text{z},c} = \mathbb{E}\left[\mathbf{z}_c\mathbf{z}^H_c\right] = \sum_{l=1}^{L} \sigma^2_{\text{int},l,c}\mathbf{H}_{\text{int},l,c}\mathbf{H}^H_{\text{int},l,c} + \sigma^2_{\text{n},c}\mathbf{I} \quad (18)$$

where $\sigma^2_{\text{int},l,c}$ denotes the power of the l^{th} external interferer and $\sigma^2_{\text{n},c}$ denotes the noise power, both at subcarrier c. $\mathbf{R}_{\text{z},c'}$ is obtained from (18) by substituting the subcarrier index c with c'. Note that in principle (17) can be obtained from the CSI and the precoder information of the image subcarrier UEs, and by measuring interference and noise contributions when all UEs at the given cell of the BS are momentarily silent. Finally, assuming that the data streams are independent and equal in power, we get $\mathbf{R}_{\text{x},c} = \sigma^2_{x,c}\mathbf{I}$ where $\sigma^2_{x,c}$ is the power of each data stream.

The above LMMSE spatial equalizer can be used in the RX as such. However, as discussed in Section II.B, the processing capabilities can be enhanced by processing jointly the signal at the image subcarrier. Therefore, we extend the equalizer (15) such that it can process the augmented signal $\widetilde{\mathbf{r}}_{\text{TxRxi},c}$ directly.

The augmented LMMSE equalizer $\widetilde{\mathbf{W}}_{\text{LMMSE},c} \in \mathbb{C}^{S\times 2N}$ is then given by

$$\widetilde{\mathbf{W}}_{\text{LMMSE},c} = \left(\widetilde{\mathbf{H}}_{\text{eff},c}^{H}\widetilde{\mathbf{R}}_{\text{int},c}^{-1}\widetilde{\mathbf{H}}_{\text{eff},c} + \mathbf{R}_{\text{x},c}^{-1}\right)^{-1}\widetilde{\mathbf{H}}_{\text{eff}}^{H}\widetilde{\mathbf{R}}_{\text{int},c}^{-1}. \quad (19)$$

Here, the augmented total effective channel matrix $\widetilde{\mathbf{H}}_{\text{eff},c} \in \mathbb{C}^{2N\times S}$ is obtained from (16) by substituting $\widetilde{\mathbf{\Psi}}_{u,c}$ with $\widetilde{\mathbf{\Xi}}_{u,c}$ $\forall u = 1, \cdots, U$. In addition, the augmented covariance matrix of the inter-user interference, external interference and noise is now equal to

$$\widetilde{\mathbf{R}}_{\text{int},c} = \sum_{v=1}^{V}\sigma_{x,v,c'}^{2}\widetilde{\mathbf{\Phi}}_{v,c}\mathbf{G}_{v,c'}^{*}\mathbf{G}_{v,c'}^{T}\widetilde{\mathbf{\Phi}}_{v,c} + \widetilde{\mathbf{K}}_{\text{RxA},c}\mathbf{R}_{\text{z},c}\widetilde{\mathbf{K}}_{\text{RxA},c}^{H} + \widetilde{\mathbf{K}}_{\text{RxB},c}\mathbf{R}_{\text{z},c'}^{*}\widetilde{\mathbf{K}}_{\text{RxB},c}^{H}. \quad (20)$$

The equalizer given by (19) yields the MMSE solution for the augmented linear signal model and thus offers flexible and efficient signal processing solution for I/Q imbalance mitigation as shown in the next section by numerical evaluations.

IV. Numerical Results and Analysis

A. Simulation Settings

In our simulations we consider an uplink OFDMA MU-MIMO scenario with 20 UEs that transmit simultaneously at subcarrier c towards a single BS. Additionally, 20 UEs are communicating with the BS at the image subcarrier c'. In order to illustrate a massive MIMO system, we selected the BS to be equipped with 50 antenna elements. On the UE side, each UE transmits two independent data streams in parallel and the streams are precoded for four antenna elements. At the considered subcarrier as well as at the image subcarrier, we add eight external single-antenna interferers with equal powers to the simulation setup. Furthermore, the signal-to-noise ratio (SNR) in RX branches is set to 30 dB and is here defined as the ratio between the total averaged received signal power originating from all TX branches of a single user, and the noise power. Furthermore, the data streams of the UEs are set to be equal in power. The signal-to-interference ratio (SIR) is here defined as the ratio between the total averaged received signal power of a single UE and the total received power originating from the external interferers.

The spatial channel between the BS array and TX antenna m of UE u is modeled as $\mathbf{h}_{m,u,c} = \mathcal{CN}(\mathbf{0}, \mathbf{R}_{\text{h}})$ where $\mathbf{R}_{\text{h}} = \mathbb{E}[\mathbf{h}\mathbf{h}]$ denotes the spatial covariance matrix. We set $\mathbf{R}_{\text{h}}$ according to the exponential correlation model in [5, eq. (17)] with parameters $r = 0.7$ and $\delta = 1$ for modeling highly correlated adjacent antenna elements in the RX which is a fairly common assumption in massive MIMO related work. The channels between the BS and different TX antennas of a single UE as well as between the BS and different UEs are assumed to be uncorrelated.

I/Q imbalance is defined in terms of the image rejection ratio (IRR) which is given in decibels for a single transceiver branch by $\text{IRR} = 10\log_{10}\left(|K_1|^2/|K_2|^2\right)$ [18]. Firstly, the minimum allowable IRR (IRR_{min}) is set to 25 dB which is the minimum requirement for UE TX/RX IRR in the LTE specification [19]. Secondly, we select phase imbalance coefficients $\phi_{\text{Tx},u,m,c}, \forall u, m, c$ and $\phi_{\text{Rx},c,n}, \forall n, c$ independently from $\mathcal{U}(-\alpha, \alpha)$ where α guarantees the selected IRR_{min} when the gain imbalance is set to zero. Finally, the gain imbalance coefficients $g_{\text{Tx},u,m,c}, \forall u, m, c$ and $g_{\text{Rx},c,n}, \forall n, c$ are selected independently from the conditional distribution $\mathcal{U}(g_{\text{min}}, g_{\text{max}})$ where the range edges correspond to IRR_{min} with the earlier selected ϕ. The I/Q imbalance parameters at different subcarriers are assumed to be independent for modeling arbitrarily frequency-selective I/Q imbalance. The default simulation parameters are summarized in Table I while some parameters are also varied in the evaluations.

TABLE I
Baseline simulation parameters

Parameter	Symbol	Value
RX antennas in BS	N	50
Number of UEs	U, V	20
TX antennas in UEs	M_u, M_v	4
Data streams in UEs	Q_u, Q_v	2
Number of external interferers	L_c, $L_{c'}$	8
TX antennas in external interferers	J_l	1
Signal to noise ratio	SNR	30 dB
Signal to interference ratio	SIR_c, $\text{SIR}_{c'}$	-20 dB
Minimum image rejection ratio	IRR_{min}	25 dB

The numerical analysis evaluates the SINR of an arbitrary data stream of an arbitrary UE. Due to the space limitation, the detailed SINR formulations are omitted here but they can be easily calculated based on the signal models in (8) and (9). All the results describe the performance from a single yet arbitrary subcarrier signal point of view, and are averaged over all the data streams, UEs and 1000 realizations. For each realization, the channel responses and I/Q imbalance parameters are randomly and independently generated according to the aforementioned criteria. All figures show the performance for both the LMMSE and the derived augmented LMMSE equalizers.

B. Simulation Results and Discussion

Fig. 2 visualizes the SINR as a function of the number of RX antennas. The results show clearly that the SINR is very low when $N \leq 40$. This is a consequence of the fact that the BS can not separate different data streams and external interference signals due to the lack of DoF. When increasing N, the performance improves steeply when using the augmented equalizer. The SINR improvement gets slower at around 48 antennas which coincides with $N = Q_u U + L$ and means that beyond that point the BS has already enough DoF for data stream separation and interference suppression. In contrast, the per-subcarrier processing yields slower SINR improvement when considering I/Q imbalance in the associated transceiver branches. With TX I/Q imbalance, the performance improves faster than in the other cases. Joint TX+RX imbalances cause the worst performance which suffers heavily from the signal and interference leakage from the image subcarrier. Actually, we see that in this case the LMMSE equalizer needs approximately $N = 80$ antennas to reach the performance which

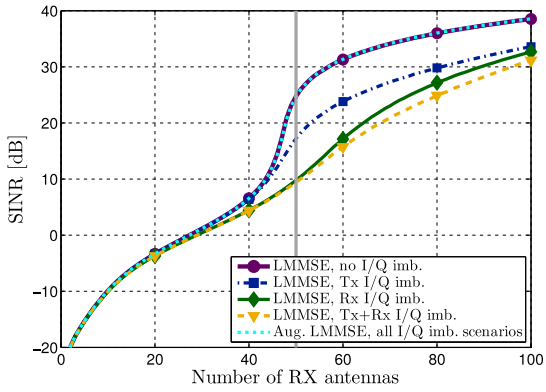

Fig. 2. Average SINR as a function of the number of RX antennas when the other parameters are fixed. The gray vertical line shows the operating point under the conditions given in Table I.

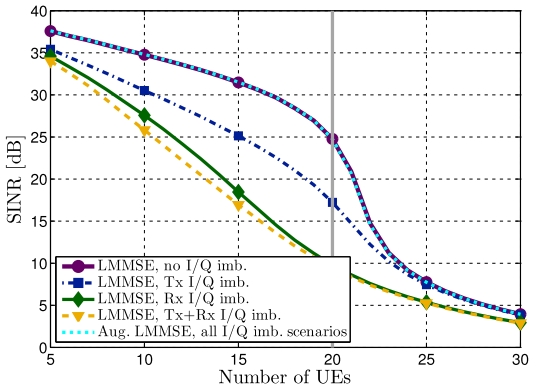

Fig. 3. Average SINR as a function of the number of UEs when the other parameters are fixed. The gray vertical line shows the operating point under the conditions given in Table I.

the augmented processing provides already with 48 antennas. This is an illustrating example of a case where a slight increase in the complexity of digital signal processing can provide big savings in the needed hardware implementation. When increasing N beyond the point where we have enough DoF, RX post-processing can use the excessive resources for noise and interference optimization and thus offer further improvements in the SINR.

Fig. 3 depicts the SINR as a function of the number of UEs. As expected, the performance is good with all the I/Q imbalance scenarios when the BS serves only few UEs. This indicates that massive amount of RX antennas makes the system more robust against I/Q imbalance if (and only if) $N \gg S$. However, with classical linear processing, the SINR deteriorates fast when adding more UEs to the system. This is obviously caused by the increased level of the inter-user interference but also by fewer DoF available for I/Q imbalance mitigation since each additional UE needs additional separation resources in the RX. Again, joint TX+RX I/Q imbalances cause the worst performance which actually degrades very quickly as a function of UEs. This is caused by the signal and interference leakage from the image subcarrier. When considering I/Q imbalance only in the TX, the SINR performance is better since the leakage of the external interference does not occur there. In contrast to the per-subcarrier processing, the derived augmented post-processing provides practically as good performance as with the ideal case and thus outperforms the per-subcarrier processing clearly. This way the overall user capacity of the BS can be increased with changes only in the associated digital signal processing. As the number of UEs goes very high, the BS can not anymore separate different data signals and consequently the performance degrades to low levels in all cases.

Fig. 4 shows the SINR as a function of the number of external interferers. Here, the total interference power is kept constant and consequently the power of individual interferers is decreased when increasing the amount of interferers. Based on the results, the SINR degrades in all cases as L increases since each additional interferer reserves additional spatial resources in the BS. The behavior of the augmented post-processing is somewhat similar to that in Fig. 3 as the total number of incoming signals is essentially swept in both figures. Additionally, the augmented LMMSE equalizer can, again, suppress the harmful effects of I/Q imbalance efficiently. In contrast to this, the performance of the classical per-subcarrier LMMSE equalizer is highly degraded even without any external interferers. This degradation is due to inter-user interference from the image subcarrier which the classical per-subcarrier processing cannot suppress efficiently. This interference is at the highest with joint TX+RX imbalances which consequently result in the worst performance.

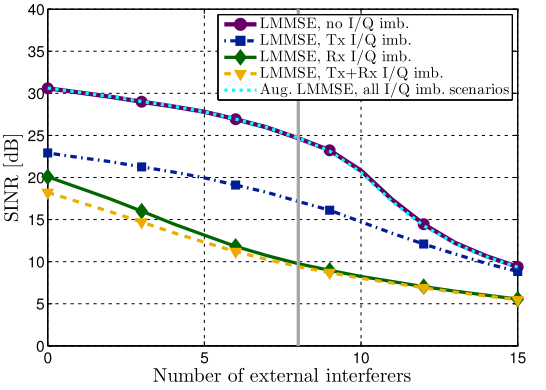

Fig. 4. Average SINR as a function of the number of external interferers when the other parameters are fixed. The gray vertical line shows the operating point under the conditions given in Table I.

Finally, Fig. 5 illustrates the SINR as a function of the minimum allowable IRR. The perfect I/Q matching as well as the augmented equalizer result in a flat SINR performance

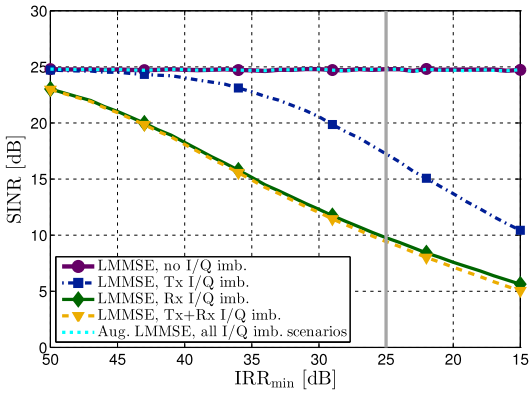

Fig. 5. Average SINR as a function of IRR when the other parameters are fixed. The gray vertical line shows the operating point under the conditions given in Table I.

over varying IRR$_{\text{min}}$. This indicates again that the augmented equalizer can mitigate the harmful effects of I/Q imbalance practically completely and thus allows lower quality for the associated RF components. The per-subcarrier processing suffers big degradations in the SINR. With TX I/Q imbalance, the performance is deteriorated by the inter-user interference from the image subcarrier. RX I/Q imbalance causes also leakage of the external interference and consequently the cases with RX and joint TX+RX imbalances provide the worst performance. Notice that the 25 dB IRR level, which is acceptable in the current LTE specification [19], causes already 8–15 dB SINR degradation.

V. Conclusion

This paper addresses precoded spatial multiplexing in massive MU-MIMO uplink transmission under imperfections in the associated RF circuits. In particular, we formulated and derived the detailed signal models in such scenario, and showed the harmful signal distortion and interference mechanism due to I/Q imbalance in the TX and RX electronics. Stemming from the distortion, where each subcarrier signal is affected also by the signals at the image subcarrier, we exploited so-called augmented spatial equalizer in the BS and derived MMSE-optimal augmented spatial receiver. There, each subcarrier signal is processed jointly with the signal at the image subcarrier, both with separate but jointly optimized sets of weights. Consequently, the available degrees of freedom are doubled while the associated RF chains remain the same as for the linear RX processing. The numerical examples showed that I/Q imbalance heavily deteriorates the performance of the classical per-subcarrier processing. Such performance degradation can be avoided by using the augmented post-processing and the results show that the augmented equalizer is able to reach the same performance as the system with perfect I/Q matchings. Thus the derived augmented spatial equalizer enables the usage of low-cost components in massive MU-MIMO devices without losses in the achievable performance.

References

[1] E. Larsson, O. Edfors, F. Tufvesson, and T. Marzetta, "Massive MIMO for next generation wireless systems," *IEEE Commun. Mag.*, vol. 52, no. 2, pp. 186–195, Feb. 2014.

[2] E. Björnson, M. Matthaiou, and M. Debbah, "Circuit-aware design of energy-efficient massive MIMO systems," in *Proc. Int. Symp. on Commun., Control, and Signal Process. (ISCCSP)*, May 2014. [Online]. Available: http://arxiv.org/abs/1403.4851

[3] A. Hakkarainen, J. Werner, K. R. Dandekar, and M. Valkama, "Widely-linear beamforming and RF impairment suppression in massive antenna arrays," *Journal of Communications and Networks*, vol. 15, no. 4, pp. 383–397, Aug. 2013.

[4] A. Pitarokoilis, S. Mohammed, and E. Larsson, "Effect of oscillator phase noise on uplink performance of large MU-MIMO systems," in *50th Annual Allerton Conference on Communication, Control, and Computing (Allerton)*, Oct. 2012, pp. 1190–1197.

[5] E. Björnson, J. Hoydis, M. Kountouris, and M. Debbah, "Massive MIMO systems with non-ideal hardware: Energy efficiency, estimation, and capacity limits," *IEEE Trans. Inf. Theory*, 2013, submitted. [Online]. Available: http://arxiv.org/abs/1307.2584

[6] A. Tarighat and A. Sayed, "MIMO OFDM receivers for systems with IQ imbalances," *IEEE Trans. Signal Process.*, vol. 53, no. 9, pp. 3583–3596, Sep. 2005.

[7] A. Tarighat, R. Bagheri, and A. Sayed, "Compensation schemes and performance analysis of IQ imbalances in OFDM receivers," *IEEE Trans. Signal Process.*, vol. 53, no. 8, pp. 3257–3268, Aug. 2005.

[8] O. Özdemir, R. Hamila, and N. Al-Dhahir, "I/Q imbalance in multiple beamforming OFDM transceivers: SINR analysis and digital baseband compensation," *IEEE Trans. Commun.*, vol. 61, no. 5, pp. 1914–1925, May 2013.

[9] A. Hakkarainen, J. Werner, K. R. Dandekar, and M. Valkama, "Analysis and augmented spatial processing for uplink OFDMA MU-MIMO receiver under transceiver I/Q imbalance and external interference," *IEEE Trans. Wireless Commun.*, 2014, submitted. [Online]. Available: http://arxiv.org/abs/1407.0524

[10] S. Mirabbasi and K. Martin, "Classical and modern receiver architectures," *IEEE Commun. Mag.*, vol. 38, no. 11, pp. 132–139, Nov. 2000.

[11] T. Schenk, *RF Imperfections in High-rate Wireless Systems: Impact and Digital Compensation*, 1st ed. Springer, 2008.

[12] D. P. Palomar and Y. Jiang, "MIMO transceiver design via majorization theory," *Foundations and Trends in Communications and Information Theory*, vol. 3, no. 4-5, pp. 331–551, 2006.

[13] D. Tandur and M. Moonen, "Joint adaptive compensation of transmitter and receiver IQ imbalance under carrier frequency offset in OFDM-based systems," *IEEE Trans. Signal Process.*, vol. 55, no. 11, pp. 5246–5252, Nov. 2007.

[14] F.-L. Luo, *Digital Front-End in Wireless Communications and Broadcasting: Circuits and Signal Processing*. Cambridge University Press, Sep. 2011.

[15] O. Özdemir, R. Hamila, and N. Al-Dhahir, "Exact SINR analysis of OFDM systems under joint Tx/RX I/Q imbalance," in *Proc. IEEE PIMRC*, 2013, pp. 646–650.

[16] H. Sampath, P. Stoica, and A. Paulraj, "Generalized linear precoder and decoder design for MIMO channels using the weighted MMSE criterion," *IEEE Trans. Commun.*, vol. 49, no. 12, pp. 2198–2206, Dec. 2001.

[17] S. Bittner, W. Rave, and G. Fettweis, "Phase noise suppression in OFDM with spatial multiplexing," in *Proc. IEEE VTC-Spring*, Apr. 2007, pp. 1826–1830.

[18] L. Anttila, M. Valkama, and M. Renfors, "Circularity-based I/Q imbalance compensation in wideband direct-conversion receivers," *IEEE Trans. Veh. Technol.*, vol. 57, no. 4, pp. 2099 –2113, Jul. 2008.

[19] *Evolved Universal Terrestrial Radio Access (E-UTRA); User Equipment (UE) radio transmission and reception*, The 3rd Generation Partnership Project (3GPP), Techical Specification 36.101 v. 11.8.0, Mar. 2014.

Publication 7

A. Hakkarainen, J. Werner, M. Renfors, K. R. Dandekar, and M. Valkama, "Transceiver I/Q Imbalance and Widely-Linear Spatial Processing in Large Antenna Systems," in *Proceedings of the 12th International Symposium on Wireless Communication Systems (ISWCS)*, Brussels, Belgium, 25–28 Aug. 2015. DOI: 10.1109/ISWCS.2015.7454428

Transceiver I/Q Imbalance and Widely-Linear Spatial Processing in Large Antenna Systems

Aki Hakkarainen*, Janis Werner*, Markku Renfors*, Kapil R. Dandekar† and Mikko Valkama*
*Department of Electronics and Communications Engineering, Tampere University of Technology, Tampere, Finland
†Department of Electrical and Computer Engineering, Drexel University, Philadelphia, PA, USA
Emails: {aki.hakkarainen, janis.werner, markku.renfors, mikko.e.valkama}@tut.fi, dandekar@coe.drexel.edu

***Abstract*—In order to keep the total device costs low, large antenna systems require affordable radio frequency (RF) electronics. Unfortunately, this requirement results in RF impairments and may thus cause performance degradations. In this paper, we show how one of these impairments, namely in-phase/quadrature (I/Q) imbalance, distorts the received signals in an uplink multiuser multiple-input multiple-output (MU-MIMO) system where multiple users are spatially multiplexed into the same time-frequency resource. In addition, we present three receiver (RX) post-processing methods and analyze their performance with different multicarrier scenarios under transceiver I/Q imbalances. The results clearly show that the simple maximum ratio combining (MRC) based RX processing suffers heavily from the presence of multiple spatially multiplexed users, especially in case of I/Q imbalances, and cannot necessarily provide sufficient performance even with the number of RX antennas approaching infinity. In contrast, the linear minimum mean-square error (LMMSE) processing offers more flexible and efficient operation characteristics but is also shown to suffer from performance degradations due to I/Q imbalances. To overcome this problem, we formulate a widely-linear (WL) variant of the MMSE method, called WL-MMSE, which provides good performance also under I/Q imbalances in different multiple access scenarios, and is thus a good candidate for future software defined radios where flexibility is a key concern.**

***Index Terms*—in-phase/quadrature (I/Q) imbalance, large antenna systems, multiuser multiple-input multiple-output (MU-MIMO), widely-linear (WL) processing**

I. Introduction

Large antenna systems, also known as massive multiple-input multiple-output (MIMO), are considered to have an order of magnitude more base station (BS) antennas than active user equipment (UEs) on a given time-frequency resource [1]–[3]. The vast amount of BS antennas demands low-cost and low-power radio frequency (RF) electronics in order to keep the total costs and dissipated power in control. This, in turn, can cause quality degradations in the associated RF circuitry and consequently the overall performance is deteriorated [2].

One of the most severe RF impairments is the so-called in-phase/quadrature (I/Q) imbalance which occurs in direct-conversion transceivers [4]. The roots of I/Q imbalance are twofold. On the one hand, nonideal mixers cause phase imbalance between the I and Q branches. On the other hand, imperfect responses of amplifiers, filters, analog-to-digital and digital-to-analog converters result in gain imbalance between the I and Q branches [4]. The resulting signal distortion is well known to cause inter-carrier interference in multicarrier systems and thus to degrade the obtainable performance [5]. In multiuser MIMO (MU-MIMO) systems, where multiple UEs are spatially multiplexed into the same time-frequence resource, the influence of I/Q imbalances is even more complex since there the imbalances generate also inter-user interference between the UEs at mirror or image subcarrier pairs [6].

In the literature many methods for I/Q imbalance mitigation are proposed. Stemming from the inter-carrier interference, the so-called augmented or widely-linear (WL) methods where each mirror subcarrier pair is processed jointly have gained lots of attention, see e.g. [7], [8]. However, these studies do not address the influence of spatially multiplexed UEs or possible external interferers and are therefore not directly applicable to MU-MIMO communications or interference-limited systems, such as mobile cellular radio with frequency reuse one.

In this paper, we focus on a very flexible system model where UEs are spatially multiplexed into the same time-frequency resource and thus operate in a challenging radio environment. In addition, we include external interferers to our models in order to model a heterogeneous network framework where users of different radio networks are all operating simultaneously at the same frequencies. We derive a signal model for the received uplink spatial signal vector and show explicitly how I/Q imbalances in the UE transmitters (TXs) and BS receiver (RX) distort the signals. Furthermore, we show with extensive computer simulations how three RX post-processing methods, namely maximum ratio combining (MRC), linear minimum mean-square error (LMMSE) spatial filter and its WL variant called WL-MMSE, handle the challenging data stream separation task with MU-MIMO transmission and under I/Q imbalances. The results clearly show that the simple MRC based spatial RX processing suffers heavily from the presence of multiple spatially multiplexed users, especially in case of I/Q imbalances, and cannot necessarily provide sufficient performance even with the number of RX antennas approaching infinity. The LMMSE based spatial processing, on the other hand, offers more flexible and efficient operation characteristics but is also shown to suffer from performance degradations due to I/Q imbalances. Finally, the WL-LMMSE based spatial processing approach results in clearly the best signal-to-interference-plus-noise ratio (SINR) performance in all considered scenarios, despite of the associated TX and RX I/Q imbalances.

This paper is organized as follows. Section II presents a generic signal and system formulation for MU-MIMO transmission under I/Q imbalances. Then, spatial RX processing methods are introduced in Section III. Section IV evaluates the system performance numerically and finally, we summarize the paper in Section V.

Notation: Vectors and matrices are written with bold characters. The superscripts $(\cdot)^{\mathrm{T}}$, $(\cdot)^{\mathrm{H}}$, $(\cdot)^*$ and $(\cdot)^{-1}$ represent transpose, Hermitian (conjugate) transpose, complex conjugate and matrix inverse, respectively. The tilde sign $\widetilde{(\cdot)}$ is used for denoting WL quantities and the results obtained by WL processing. We write

This work was supported by the Finnish Funding Agency for Technology and Innovation (Tekes) under the project "WiFiUS: Future Small-Cell Networks using Reconfigurable Antennas", the Academy of Finland under the projects 251138, 284694 and 288670, and the Doctoral Programme of the President of Tampere University of Technology.

The work was also supported by National Science Foundation (NSF) under award number CNS 1457306.

$\text{diag}(x_{11}, x_{22}, \cdots, x_{ii}, \cdots)$ to denote a diagonal matrix $\mathbf{X}$ with elements x_{ii} on the main diagonal. The statistical expectation is denoted with $\mathbb{E}[\cdot]$.

II. Signal and System Formulation

We examine an orthogonal frequency division multiplexing (OFDM) / orthogonal frequency division multiple access (OFDMA) MU-MIMO system scenario where multiple UEs are spatially multiplexed into the same time-frequency resource, as depicted in Fig.1. The subcarriers are indexed with $c \in \{-C/2, \ldots, -1, 1, \ldots, C/2\}$ where C is the total number of subcarriers. Since OFDM and OFDMA are based on independent subcarrier signals, all analysis is here done for an arbitrary subcarrier c whose mirror subcarrier is denoted by $c' = -c$. The number of UEs at subcarriers c and c' is denoted by U and V, respectively. Furthermore, a single UE at subcarrier c is indexed by u and at c' by v. In OFDM case, the same set of UEs use both subcarriers c and c'. In OFDMA case, in turn, the sets of UEs at subcarriers c and c' are different and the users are thus multiplexed also in the frequency domain. We denote the number of the RX antennas in the BS by N and the number of TX antennas of UE u by M_u. Furthermore, the number of the independent data streams of UE u at subcarrier c is given by $Q_{u,c}$ and the transmitted data vector is equal to $\mathbf{x}_{u,c} \in \mathbb{C}^{Q_u \times 1}$. Consequently, the total number of transmitted data streams at subcarrier c is equal to $S = \sum_{u=1}^{U} Q_u$. The transmitted antenna signal vector of UE u is given by $\mathbf{s}_{u,c} = \mathbf{G}_{u,c}\mathbf{x}_{u,c} \in \mathbb{C}^{M_u \times 1}$ where $\mathbf{G}_{u,c} \in \mathbb{C}^{M_u \times Q_u}$ denotes the spatial precoder matrix. In order to describe the radio environment flexibly we also include L external interferers to our models. External interferer l has J_l antennas and its transmitted antenna signal vector at subcarrier c is denoted by $\mathbf{s}_{\text{int},l,c} \in \mathbb{C}^{J_l \times 1}$. Throughout the paper, all data vectors refer to frequency domain quantities, i.e., prior to the inverse fast Fourier transform in the UEs and after the fast Fourier transform in the BS.

In uplink transmission, each UE transmits its own precoded data streams towards the BS. The transmitted antenna signal vector of UE u at subcarrier c under TX I/Q imbalance can be modeled as [6], [9]

$$\mathbf{s}_{\text{Txi},u,c} = \mathbf{K}_{\text{Tx1},u,c}\mathbf{G}_{u,c}\mathbf{x}_{u,c} + \mathbf{K}_{\text{Tx2},u,c}\mathbf{G}^*_{u,c'}\mathbf{x}^*_{u,c'}. \quad (1)$$

Here $\mathbf{K}_{\text{Tx1},u,c} = \text{diag}(K_{\text{Tx1},1,u,c}, \cdots, K_{\text{Tx1},M_u,u,c}) \in \mathbb{C}^{M_u \times M_u}$ and $\mathbf{K}_{\text{Tx2},u,c} = \text{diag}(K_{\text{Tx2},1,u,c}, \cdots, K_{\text{Tx2},M_u,u,c}) \in \mathbb{C}^{M_u \times M_u}$ denote the diagonal TX I/Q imbalance matrices. The matrix entries for TX antenna m of UE u at subcarrier c are given by $K_{\text{Tx1},m,u,c} = (1 + g_{\text{Tx},m,u,c}e^{j\phi_{\text{Tx},m,u,c}})/2$ and $K_{\text{Tx2},m,u,c} = (1 - g_{\text{Tx},m,u,c}e^{j\phi_{\text{Tx},m,u,c}})/2$ where the gain and phase imbalance coefficients are equal to $g_{\text{Tx},m,u,c}$ and $\phi_{\text{Tx},m,u,c}$, respectively [5]. Based on (1), TX I/Q imbalance causes cross-talk between the mirror subcarrier signals of an individual UE. This model holds as such for a scenario where subcarriers c and c' are both allocated to UE u. Notice, however, that if subcarrier c' is not allocated to UE u, the resulting transmitted signal at subcarrier c consists only of the first term in (1). However, when subcarrier c' is allocated, through the OFDMA principle, to another UE v which also suffers from TX I/Q imbalance, the corresponding transmitted signal of UE v at subcarrier c is equal to $\mathbf{s}_{\text{Txi},v,c} = \mathbf{K}_{\text{Tx2},v,c}\mathbf{G}^*_{v,c'}\mathbf{x}^*_{v,c'}$. For notational convenience we use the latter more general case in our models. The special case where subcarriers c and c' are both allocated for the same set of UEs is obtained from the models by substituting $V = U$ and $v = u$.

The transmitted UE signals propagate then through wireless channels and are eventually received in the BS. The received signal

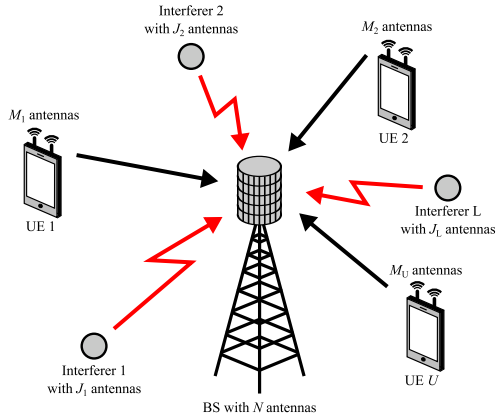

Fig. 1: The considered uplink MU-MIMO scenario with all devices being active at subcarrier c. The BS antenna array is here drawn as a cylindrical array but the signal model is not restricted to any specific array structure.

vector $\mathbf{r}_{\text{TxRx},c} \in \mathbb{C}^{N \times 1}$ under the influence of TX as well as RX I/Q imbalances is then equal to

$$\mathbf{r}_{\text{TxRxi},c} = \sum_{u=1}^{U} \widetilde{\mathbf{\Psi}}_{u,c}\mathbf{G}_{u,c}\mathbf{x}_{u,c} + \sum_{v=1}^{V} \widetilde{\mathbf{\Omega}}_{v,c}\mathbf{G}^*_{v,c'}\mathbf{x}^*_{v,c'} + \mathbf{K}_{\text{Rx1},c}\mathbf{z}_c + \mathbf{K}_{\text{Rx2},c}\mathbf{z}^*_{c'} \quad (2)$$

where we assume perfect time and frequency synchronization between the UEs and the BS. Furthermore, $\mathbf{K}_{\text{Rx1},c} = \text{diag}(K_{\text{Rx1},1,c}, \cdots, K_{\text{Rx1},N,c}) \in \mathbb{C}^{N \times N}$ and $\mathbf{K}_{\text{Rx2},c} = \text{diag}(K_{\text{Rx2},1,c}, \cdots, K_{\text{Rx2},N,c}) \in \mathbb{C}^{N \times N}$ denote the diagonal RX I/Q imbalance matrices where the entries for RX antenna n are given by $K_{\text{Rx1},n,c} = (1 + g_{\text{Rx},n,c}e^{-j\phi_{\text{Rx},n,c}})/2$ and $K_{\text{Rx2},n,c} = (1 - g_{\text{Rx},n,c}e^{j\phi_{\text{Rx},n,c}})/2$. Here the RX gain and phase imbalance coefficients are equal to $g_{\text{Rx},n,c}$ and $\phi_{\text{Rx},n,c}$, respectively [5]. The effective channel matrices, $\widetilde{\mathbf{\Psi}}_{u,c} \in \mathbb{C}^{N \times M_u}$ and $\widetilde{\mathbf{\Omega}}_{v,c} \in \mathbb{C}^{N \times M_v}$ including the effects of the wireless channels as well as TX and RX I/Q imbalances are given by

$$\begin{aligned} \widetilde{\mathbf{\Psi}}_{u,c} &= \begin{bmatrix} \mathbf{K}_{\text{Rx1},c} & \mathbf{K}_{\text{Rx2},c} \end{bmatrix} \begin{bmatrix} \mathbf{H}_{u,c} & \mathbf{0} \\ \mathbf{0} & \mathbf{H}^*_{u,c'} \end{bmatrix} \begin{bmatrix} \mathbf{K}_{\text{Tx1},u,c} \\ \mathbf{K}^*_{\text{Tx2},u,c'} \end{bmatrix}, \\ \widetilde{\mathbf{\Omega}}_{v,c} &= \begin{bmatrix} \mathbf{K}_{\text{Rx1},c} & \mathbf{K}_{\text{Rx2},c} \end{bmatrix} \begin{bmatrix} \mathbf{H}_{v,c} & \mathbf{0} \\ \mathbf{0} & \mathbf{H}^*_{v,c'} \end{bmatrix} \begin{bmatrix} \mathbf{K}_{\text{Tx2},v,c} \\ \mathbf{K}^*_{\text{Tx1},v,c'} \end{bmatrix} \end{aligned} \quad (3)$$

where $\mathbf{H}_{u,c} \in \mathbb{C}^{N \times M_u}$ and $\mathbf{H}_{v,c} \in \mathbb{C}^{N \times M_v}$ represent the wireless channel matrices of UEs u and v, respectively. Finally, the interference and noise vector $\mathbf{z}_c \in \mathbb{C}^{N \times 1}$ equals

$$\mathbf{z}_c = \sum_{l=1}^{L} \mathbf{H}_{\text{int},l,c}\mathbf{s}_{\text{int},l,c} + \mathbf{n}_c \quad (4)$$

where $\mathbf{H}_{\text{int},l,c} \in \mathbb{C}^{N \times J_l}$ denotes the wireless channel of external interferer l. Additionally, $\mathbf{n}_c \in \mathbb{C}^{N \times 1}$ denotes additive white Gaussian noise in the RX electronics. As visible in (2), transceiver I/Q imbalances cause inter-user interference between the users in mirror subcarrier pairs. In addition, also the external interference and noise from the mirror subcarrier leak to subcarrier c.

The special case with I/Q imbalance occurring only in the TX (RX) side is obtained from (2) by substituting $\mathbf{K}_{\text{Rx1},c} = \mathbf{I}$ and $\mathbf{K}_{\text{Rx2},c} = \mathbf{0}$ $\forall c$ ($\mathbf{K}_{\text{Tx1},u,c} = \mathbf{I}$ and $\mathbf{K}_{\text{Tx2},u,c} = \mathbf{0}$ $\forall u,c$).

III. Spatial RX Processing

In uplink MU-MIMO the BS exploits its multiple RX antennas for spatial processing. This means that data streams originating

from different UEs can be reliably separated even when they are transmitted over the same time-frequency resource [10]. Furthermore, one of the promising prospects of massive MIMO or large-antenna system in general is that simple RX spatial processing, even classical MRC, can potentially be adopted [11]. In general, the combiner's output signal vector $\mathbf{y}_{\text{TxRxi},c} \in \mathbb{C}^{S\times 1}$ under TX and RX I/Q imbalances is

$$\begin{aligned}\mathbf{y}_{\text{TxRxi},c} &= \mathbf{W}_c^{\text{H}}\mathbf{r}_{\text{TxRxi},c} \\ &= \sum_{u=1}^{U}\mathbf{W}_c^{\text{H}}\widetilde{\mathbf{\Psi}}_{u,c}\mathbf{G}_{u,c}\mathbf{x}_{u,c} + \sum_{v=1}^{V}\mathbf{W}_c^{\text{H}}\widetilde{\mathbf{\Omega}}_{v,c}\mathbf{G}^*_{v,c'}\mathbf{x}^*_{v,c'} \\ &\quad + \mathbf{W}_c^{\text{H}}\mathbf{K}_{\text{Rx1},c}\mathbf{z}_c + \mathbf{W}_c^{\text{H}}\mathbf{K}_{\text{Rx2},c}\mathbf{z}^*_{c'} \end{aligned} \quad (5)$$

where $\mathbf{W}_c \in \mathbb{C}^{S\times N}$ denotes the combiner weight matrix at subcarrier c [6]. In the following subsections we present different methods to select the weight matrix in large antenna systems under I/Q imbalance. The selection methods differ especially in complexity and performance.

A. MRC Approach

Commonly used argumentation with large antenna systems is that the spatial separation should be implemented in a very simple way due to the massive amount of RX antennas, see e.g. [2]. Due to this reason MRC is considered to be one of the most promising solutions for large scale processing, primarily due to its simplicity. In general, the MRC weight matrix of UE u is given simply as $\mathbf{W}_{\text{MRC},u,c} = \mathbf{H}_{u,c}\mathbf{G}_{u,c} \in \mathbb{C}^{N\times Q_u}$ [12]. However, under I/Q imbalances we need to take also the influence of TX I/Q imbalance of UE u and RX I/Q imbalance in the BS into account and thus the weight matrix of UE u becomes equal to

$$\mathbf{W}_{\text{MRC},u,c} = \widetilde{\mathbf{\Psi}}_{u,c}\mathbf{G}_{u,c}. \quad (6)$$

When stacking the weight matrices of individual UEs at subcarrier c into a total weight matrix we get $\mathbf{W}_{\text{MRC},c} = [\mathbf{W}_{\text{MRC},1,c}, \cdots, \mathbf{W}_{\text{MRC},U,c}] \in \mathbb{C}^{N\times S}$ to be adopted in (5). The MRC approach is clearly very simple but it has also its built-in limitations. MRC cannot exploit any information, other than the individual direct channel matrix $\widetilde{\mathbf{\Psi}}_{u,c}$, and is therefore vulnerable especially in noisy conditions with multiple signal sources. Notice that as the channel state information is in practice anyway obtained from uplink pilot or reference signals, it is indeed the *effective direct spatial channel matrix* that is used to form the MRC spatial filter, as given in (6). We use the MRC method as a benchmark in Section IV with numerical illustrations.

B. LMMSE Processing

In order to perform reliable data stream detection in MU-MIMO, the RX should be able to operate also in conditions with multiple active signal sources. One way to do this is the so-called Wiener or LMMSE processing. It optimizes the weights in such a way that the mean-square error between the spatially filtered received signal and the desired transmitted signal is minimized [13]. This approach implicitly suppresses the influence of any unwanted interference and noise, and therefore enables good separation capabilities also in challenging MU-MIMO schemes. The overall weight matrix for data streams from all UEs is equal to $\mathbf{W}_{\text{LMMSE},c} = [\mathbf{W}_{\text{LMMSE},1,c}, \cdots, \mathbf{W}_{\text{LMMSE},U,c}] \in \mathbb{C}^{N\times S}$ and can be directly substituted into (5). Under TX and RX I/Q imbalances the weight matrix $\mathbf{W}_{\text{LMMSE},u,c} \in \mathbb{C}^{N\times Q_u}$ for UE u is of the form

$$\mathbf{W}_{\text{LMMSE},u,c} = \mathbf{R}_{\text{r},c}^{-1}\mathbf{V}_{u,c} \quad (7)$$

where $\mathbf{R}_{\text{r},c} = \mathbb{E}[\mathbf{r}_{\text{TxRxi},c}\mathbf{r}_{\text{TxRxi},c}^{\text{H}}] \in \mathbb{C}^{N\times N}$ is the covariance matrix of the received signals and $\mathbf{V}_{u,c} \in \mathbb{C}^{N\times Q_u}$ denotes the cross-correlation matrix between the received signal vector and the transmitted signal of UE u [13]. The column of $\mathbf{V}_{u,c}$ for data stream q is given by

$$\mathbf{v}_{q,u,c} = \mathbb{E}[\mathbf{r}_{\text{TxRxi},c}x^*_{q,u,c}] = \sigma^2_{q,u,c}\widetilde{\mathbf{\Psi}}_{u,c}\mathbf{G}_{u,c}\mathbf{e}_q \quad (8)$$

where $x_{q,u,c}$ is the q^{th} element of $\mathbf{x}_{u,c}$, $\sigma^2_{q,u,c}$ is its power, and $\mathbf{e}_q$ is a vector whose q^{th} element is one and the rest are zeros. Notice that, again, the RX is deploying, explicitly or implicitly, the knowledge of *effective spatial channels* along with the associated interference and noise covariances.

C. Augmented Signal Model and WL-MMSE Processing

LMMSE processing is an effective tool in MU-MIMO BSs. However, it cannot structurally handle the inter-carrier interference and the corresponding inter-user interference caused by I/Q imbalances in the transceiver electronics. The nature of the signal distortion leads towards WL or augmented signal processing where the received signals at subcarriers c and c' are processed jointly [6]–[8]. In order to model such a method, we define an augmented received signal vector $\widetilde{\mathbf{r}}_c = [\mathbf{r}_c^{\text{T}}, \mathbf{r}_{c'}^{\text{H}}]^{\text{T}} \in \mathbb{C}^{2N\times 1}$. Then the output signal of the WL combiner is obtained simply by $\widetilde{\mathbf{y}}_c = \widetilde{\mathbf{W}}_c^{\text{H}}\widetilde{\mathbf{r}}_c \in \mathbb{C}^{S\times 1}$ where $\widetilde{\mathbf{W}}_c = [\widetilde{\mathbf{W}}_{1,c}, \cdots, \widetilde{\mathbf{W}}_{U,c}] \in \mathbb{C}^{2N\times S}$ denotes the total WL weight matrix. Here $\widetilde{\mathbf{W}}_{u,c} \in \mathbb{C}^{2N\times Q_u}$ represents the WL weight matrix of UE u. When substituting the signal model in (2) into the principle of WL processing we get

$$\begin{aligned}\widetilde{\mathbf{y}}_{\text{TxRxi},c} &= \widetilde{\mathbf{W}}_c^{\text{H}}\widetilde{\mathbf{r}}_{\text{TxRxi},c} \\ &= \sum_{u=1}^{U}\widetilde{\mathbf{W}}_c^{\text{H}}\widetilde{\mathbf{\Xi}}_{u,c}\mathbf{G}_{u,c}\mathbf{x}_{u,c} + \sum_{v=1}^{V}\widetilde{\mathbf{W}}_c^{\text{H}}\widetilde{\mathbf{\Phi}}_{v,c}\mathbf{G}^*_{v,c'}\mathbf{x}^*_{v,c'} \\ &\quad + \widetilde{\mathbf{W}}_c^{\text{H}}\widetilde{\mathbf{K}}_{\text{RxA},c}\mathbf{z}_c + \widetilde{\mathbf{W}}_c^{\text{H}}\widetilde{\mathbf{K}}_{\text{RxB},c}\mathbf{z}^*_{c'} \end{aligned} \quad (9)$$

where the effective WL channel matrices $\widetilde{\mathbf{\Xi}}_{u,c} \in \mathbb{C}^{2N\times M_u}$ and $\widetilde{\mathbf{\Phi}}_{v,c} \in \mathbb{C}^{2N\times M_v}$ are given by

$$\begin{aligned}\widetilde{\mathbf{\Xi}}_{u,c} &= \begin{bmatrix}\mathbf{K}_{\text{Rx1},c} & \mathbf{K}_{\text{Rx2},c}\\ \mathbf{K}^*_{\text{Rx2},c'} & \mathbf{K}^*_{\text{Rx1},c'}\end{bmatrix}\begin{bmatrix}\mathbf{H}_{u,c} & \mathbf{0}\\ \mathbf{0} & \mathbf{H}^*_{u,c'}\end{bmatrix}\begin{bmatrix}\mathbf{K}_{\text{Tx1},u,c}\\ \mathbf{K}^*_{\text{Tx2},u,c'}\end{bmatrix}, \\ \widetilde{\mathbf{\Phi}}_{v,c} &= \begin{bmatrix}\mathbf{K}_{\text{Rx1},c} & \mathbf{K}_{\text{Rx2},c}\\ \mathbf{K}^*_{\text{Rx2},c'} & \mathbf{K}^*_{\text{Rx1},c'}\end{bmatrix}\begin{bmatrix}\mathbf{H}_{v,c} & \mathbf{0}\\ \mathbf{0} & \mathbf{H}^*_{v,c'}\end{bmatrix}\begin{bmatrix}\mathbf{K}_{\text{Tx2},v,c}\\ \mathbf{K}^*_{\text{Tx1},v,c'}\end{bmatrix}. \end{aligned} \quad (10)$$

In addition, $\widetilde{\mathbf{K}}_{\text{RxA},c} = [\mathbf{K}^{\text{T}}_{\text{Rx1},c}, \mathbf{K}^{\text{H}}_{\text{Rx2},c'}]^{\text{T}} \in \mathbb{C}^{2N\times N}$ and $\widetilde{\mathbf{K}}_{\text{RxB},c} = [\mathbf{K}^{\text{T}}_{\text{Rx2},c}, \mathbf{K}^{\text{H}}_{\text{Rx1},c'}]^{\text{T}} \in \mathbb{C}^{2N\times N}$ denote the augmented RX I/Q imbalance matrices.

Stemming from the above models and processing principles, and the target of MSE minimization, we next formulate the WL-MMSE combiner (originally proposed in [14] for processing non-circular signals) which is able to suppress the co-channel interference as well as the inter-carrier and inter-user interference effectively in the presence of all involved I/Q imbalances. The WL weight matrix for the data streams of UE u is equal to

$$\widetilde{\mathbf{W}}_{\text{WL-MMSE},u,c} = \widetilde{\mathbf{R}}_{\text{r},c}^{-1}\widetilde{\mathbf{V}}_{u,c} \quad (11)$$

where $\widetilde{\mathbf{R}}_{\text{r},c} = \mathbb{E}[\widetilde{\mathbf{r}}_{\text{TxRxi},c}\widetilde{\mathbf{r}}^{\text{H}}_{\text{TxRxi},c}] \in \mathbb{C}^{2N\times 2N}$ is the covariance matrix of the augmented received signal. In addition, the columns of the cross-correlation matrix $\widetilde{\mathbf{V}}_{u,c} \in \mathbb{C}^{2N\times Q_u}$ are of the form

$$\widetilde{\mathbf{v}}_{q,u,c} = \mathbb{E}[\widetilde{\mathbf{r}}_{\text{TxRxi},c}x^*_{q,u,c}] = \sigma^2_{q,u,c}\widetilde{\mathbf{\Xi}}_{u,c}\mathbf{G}_{u,c}\mathbf{e}_q. \quad (12)$$

The above WL-MMSE RX utilizes effective spatial channels of all multiplexed UEs at both subcarriers c and c', together with the associated interference and noise covariances, where also the I/Q imbalance characteristics are implicitly built in. Note that whereas WL-MMSE increases the computational complexity of

TABLE I: Basic simulation parameters

Parameter	Symbol	Simulation scenario 1	Simulation scenario 2
Frequency multiplexing	-	Yes	No
Spatially multiplexed UEs	$U, (V)$	$U = 5$, $V = 5$	$U = 5$
TX antennas in UEs	$M_u, (M_v)$	1	
UE data streams	$Q_u, (Q_v)$	1	
RX antennas in BS	N	100	
Signal to noise ratio [dB]	SNR	20	
Fluctuation in UE powers [dB]	-	± 3	
Image rejection ratio [dB]	IRR	20	

the combiner block, demanding FFT processing remain the same as with LMMSE.

In the next section we provide an extensive numerical performance analysis for the linear and WL processing methods presented above. In particular, we focus on their operation capabilities in a challenging MU-MIMO environment and under transceiver I/Q imbalances.

IV. Numerical Performance Analysis

A. Simulation Setup and Scenarios

In the simulations we consider an uplink MU-MIMO multi-carrier scenario whose parameters are presented in Table I. We analyze two simulation scenarios with both common and different parameters. The common parameters are as follows. Subcarrier c has $U = 5$ single-antenna UEs transmitting simultaneously towards a single BS. We set the number of RX antennas in the BS to $N = 100$ for modeling a large antenna system. Thereby, N is an order of magnitude larger than U which is a commonly used assumption to describe large antenna and massive MIMO systems [1]–[3]. We define the signal-to-noise ratio (SNR) as the ratio between the average received signal power of a single UE and the noise power in the RX electronics and set SNR = 20 dB.

The propagation channels between all UEs and BS RX antennas as well as between subcarriers are independent and Rayleigh distributed. On top of that, we include a uniformly distributed fluctuation from a range of ± 3 dB to $\sigma^2_{u,c}\ \forall u,c$ in order to model differences in the uplink power control between the UEs. I/Q imbalance is defined in terms of the image rejection ratio (IRR) given in decibels for a single transceiver branch by $\text{IRR} = 10\log_{10}(|K_1|^2/|K_2|^2)$. We set IRR = 20 dB in all transceiver branches. However, we do include randomness to the I/Q imbalance, both across different antenna branches of a single device as well as across different devices, through the phase and gain imbalance coefficients. At first, we draw $\phi_{\text{Tx},u,m,c}, \forall u, m, c$ and $\phi_{\text{Rx},c,n}, \forall n, c$ independently from $\mathcal{U}(-\alpha, \alpha)$ where α guarantees $\text{IRR} = 20$ dB if the gain imbalance coefficients were equal to one. Then, $g_{\text{Tx},u,m,c}, \forall u, m, c$ and $g_{\text{Rx},n,c}, \forall n, c$ are set in such a way that the resulting $\text{IRR} = 20$ dB with the earlier selected phase imbalance coefficients. The I/Q imbalance parameters at different subcarriers are also assumed to be independent. Finally, in order to clearly illustrate the influence of different scenarios, we set the number of external interferers to $L = 0$.

The scenarios differ in the subcarrier allocation. In scenario 1 we consider an OFDMA system where frequency multiplexing is involved, i.e. subcarriers c and c' have different sets of UEs. In this case, we set the number of UEs at the mirror subcarrier to $V = 5$. In contrast, in scenario 2 we assume an OFDM scheme, i.e., an individual UE u where $u = 1, ..., U$ operates on subcarriers c and c'. This means that the second term in (2) is replaced with $\sum_{u=1}^{U} \widetilde{\mathbf{\Omega}}_{u,c} \mathbf{G}^*_{u,c'} \mathbf{x}^*_{u,c'}$. Although a single UE operates on both subcarriers c and c', we assume uncorrelated fading between the mirror subcarriers since, practically, only very closely located subcarriers have significant fading correlation.

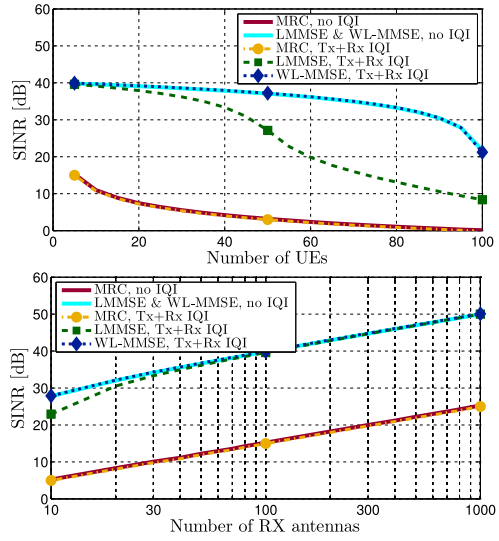

Fig. 2: Scenario 1: frequency multiplexing (OFDMA). The SINR as a function of U (top) and N (bottom) with other parameters as given in Table I. Note the logarithmic x-axis in the lower graph.

All figures discussed in the following illustrate the combiner's output SINR at an arbitrary subcarrier c. The numerator of the SINR is the signal power of a single UE u, i.e. the power of one combiner output element of the first sum in (5) and (9), whereas the denominator includes the total power of the other UEs and noise at subcarrier c as well as the inter-carrier and inter-user interference from the mirror subcarrier due to I/Q imbalance. The SINRs are averaged over all UEs and 1000 independent realizations. For each realization the UE powers, channels and I/Q imbalance coefficients are independently drawn according to the distributions above.

B. Results and Discussion

Scenario 1: Fig. 2 illustrates the average SINR as a function of the number of UEs (top) and the number of RX antennas (bottom) for scenario 1. We notice that the performance of MRC is much worse than that of the MMSE approaches. This is due to the fact that the MRC method is very vulnerable to any interference which, in this case, means the transmissions from multiple spatially multiplexed UEs. The SINR of MRC increases when either the number of UEs decreases or the number of RX antennas increases. We can also see that the SINR of MRC is dominated by the inter-user interference, no matter if the system is under I/Q imbalance or not. In contrast to MRC, the LMMSE combiner provides good results also in a MU-MIMO environment due to its built-in capability for inter-user interference suppression. However, it cannot effectively suppress the inter-carrier interference which is caused by I/Q imbalance. This is especially visible in the upper graph where the increasing number of UEs at subcarriers c and c' increases the inter-carrier-interference and decreases the degrees of freedom of LMMSE. On the contrary to the linear processing methods, the WL-MMSE combiner can suppress the inter-user as well as the inter-carrier interference very efficiently, due to its built-in capability to process signals at c and c' jointly. Consequently, it provides the best performance and, in fact, yields the same SINR as a system under ideal I/Q matching, even when operating under TX+RX I/Q imbalances.

Scenario 2: The results for scenario 2 are presented in Fig. 3. The SINRs of all combiners under perfect I/Q matching, i.e., no I/Q imbalance, are basically identical to their SINRs in scenario 1.

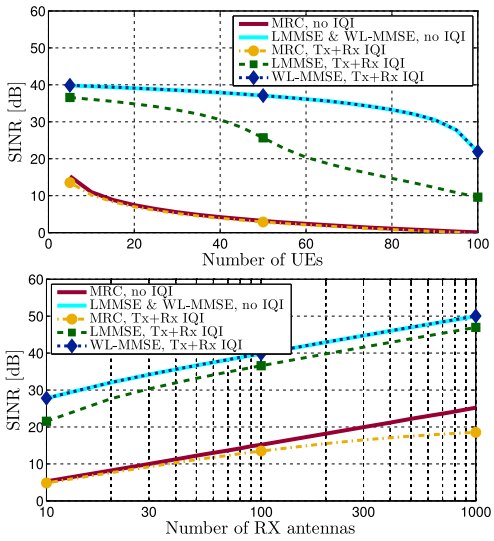

Fig. 3: Scenario 2: no frequency multiplexing (OFDM). The SINR as a function of U (top) and N (bottom) with other parameters as given in Table I. Note the logarithmic x-axis in the lower graph.

Thus we conclude that systems without I/Q imbalances are not sensitive to different subcarrier allocation schemes. However, we do observe big differences under the influence of I/Q imbalances. First of all, the SINR of MRC does not anymore improve with a slope equal to $10\log_{10}(N)$. This is caused by the following fact. The weights of MRC are matched, as shown in (6), to the effective channel $\widetilde{\mathbf{\Psi}}_{u,c}$ which is dominated by the term $\mathbf{K}_{\text{Rx1},c}\mathbf{H}_{u,c}K_{\text{Tx1},u,c}$ as visible in (3). Since the inter-carrier-interference from the same UE, caused already by UE TX I/Q imbalance, propagates through the effective channel $\widetilde{\mathbf{\Omega}}_{u,c}$ which in this scenario includes a term $\mathbf{K}_{\text{Rx1},c}\mathbf{H}_{u,c}K_{\text{Tx2},u,c}$, the only difference comes from different scaling factors $K_{\text{Tx1},u,c}$ and $K_{\text{Tx2},u,c}$. This means that the spatial propagation channels of the desired data stream and the inter-carrier interference from the same UE are very similar from the BS perspective and consequently the SINR is restricted to $10\log_{10}(|K_{\text{Tx},1}|^2/|K_{\text{Tx},2}|^2)$. This is exactly the same as the TX IRR, i.e. *the SINR of MRC is limited to the TX IRR in scenario 2*. In contrast to MRC, LMMSE is again able to provide fairly good SINRs. However, the performance of LMMSE is also deteriorated when compared to scenario 1. Also this is caused by the limited capabilities to suppress the inter-carrier-interference from the same UE, because of the high similarity of the effective spatial channels between the direct linear term and the inter-carrier interference. In this case, however, the weights are given by (7) which is more flexible than the MRC approach. Thus the SINR degradation of LMMSE is much less severe compared to what we observed for MRC. The results also indicate that *MRC as well as LMMSE are sensitive to subcarrier allocation schemes when operating under TX+RX I/Q imbalances*. In contrast, the WL-MMSE processing under I/Q imbalance provides, again, the same performance as a system under perfect I/Q matching. In fact, this is a property which WL-MMSE provides for an arbitrary number of users and RX antennas. Based on the results above, we summarize that WL-MMSE improves the performance considerably when compared to the presented linear methods. It also removes the need for separate I/Q imbalance mitigation and thus simplifies the overall RX structure. As a consequence, WL processing becomes a highly attractive solution for future large antenna systems, with lower-cost RF transceivers, potentially also incorporating software defined radio technologies where the radio interface must support multiple radio technologies on the one hand and must be flexibly controllable, on the other hand.

V. Conclusion

In this paper we have analyzed the influence of TX and RX I/Q imbalances in uplink MU-MIMO transmission with large antenna systems. First, we derived models for both the received antenna signal vector in the BS as well as the corresponding output signal after the BS spatial filter. We also presented three spatial RX processing schemes, namely MRC, LMMSE and WL-MMSE. Using numerical examples, we illustrated that the performance of the MRC method is heavily limited in a MU-MIMO environment where multiple UEs are simultaneously active in the same time-frequency resource. The poor performance was emphasized even more under I/Q imbalances. In fact, it was shown that the SINR of MRC is restricted to the TX IRR in the classical OFDM case without user multiplexing in the frequency domain. The LMMSE method, in turn, can more efficiently suppress the interference from multiple signal sources, and it was shown to operate relatively efficiently and reliably also in challenging MU-MIMO conditions. However, we observed that it cannot effectively suppress the inter-carrier-interference caused by I/Q imbalances which results in severe performance degradation. To overcome this limitation, we formulated the WL-MMSE approach where the mirror-subcarrier signals and all associated spatially multiplexed UEs are processed together. Under TX+RX I/Q imbalances, the WL-MMSE method provides consistently the best performance among the methods under comparison and, in fact, yields equal performance as a system under ideal I/Q matching.

References

[1] J. Hoydis, S. ten Brink, and M. Debbah, "Massive MIMO in the UL/DL of cellular networks: How many antennas do we need?" *IEEE J. Sel. Areas Commun.*, vol. 31, no. 2, pp. 160–171, Feb. 2013.

[2] E. Larsson, O. Edfors, F. Tufvesson, and T. Marzetta, "Massive MIMO for next generation wireless systems," *IEEE Commun. Mag.*, vol. 52, no. 2, pp. 186–195, Feb. 2014.

[3] E. Björnson, E. G. Larsson, and M. Debbah, "Massive MIMO for Maximal Spectral Efficiency: How Many Users and Pilots Should Be Allocated?" *IEEE Trans. Wireless Commun.*, 2014, submitted. [Online]. Available: http://arxiv.org/abs/1412.7102

[4] S. Mirabbasi and K. Martin, "Classical and modern receiver architectures," *IEEE Commun. Mag.*, vol. 38, no. 11, pp. 132–139, Nov. 2000.

[5] T. Schenk, *RF Imperfections in High-rate Wireless Systems: Impact and Digital Compensation*, 1st ed. Springer, 2008.

[6] A. Hakkarainen, J. Werner, K. R. Dandekar, and M. Valkama, "Precoded massive MU-MIMO uplink transmission under transceiver I/Q imbalance," in *Proc. IEEE GLOBECOM Workshops*, Dec. 2014, pp. 405–411.

[7] A. Tarighat, R. Bagheri, and A. Sayed, "Compensation schemes and performance analysis of IQ imbalances in OFDM receivers," *IEEE Trans. Signal Process.*, vol. 53, no. 8, pp. 3257–3268, Aug. 2005.

[8] Ö. Özdemir, R. Hamila, and N. Al-Dhahir, "I/Q imbalance in multiple beamforming OFDM transceivers: SINR analysis and digital baseband compensation," *IEEE Trans. Commun.*, vol. 61, no. 5, pp. 1914–1925, May 2013.

[9] D. Tandur and M. Moonen, "Joint adaptive compensation of transmitter and receiver IQ imbalance under carrier frequency offset in OFDM-based systems," *IEEE Trans. Signal Process.*, vol. 55, no. 11, pp. 5246–5252, Nov. 2007.

[10] D. Gesbert, M. Kountouris, R. Heath, C.-B. Chae, and T. Salzer, "Shifting the MIMO paradigm," *IEEE Signal Process. Mag.*, vol. 24, no. 5, pp. 36–46, Sep. 2007.

[11] H. Q. Ngo, E. Larsson, and T. Marzetta, "Energy and Spectral Efficiency of Very Large Multiuser MIMO Systems," *IEEE Trans. Commun.*, vol. 61, no. 4, pp. 1436–1449, Apr. 2013.

[12] M. Kang and M.-S. Alouini, "Largest eigenvalue of complex Wishart matrices and performance analysis of MIMO MRC systems," *IEEE J. Sel. Areas Commun.*, vol. 21, no. 3, pp. 418–426, Apr. 2003.

[13] B. Widrow, P. Mantey, L. Griffiths, and B. Goode, "Adaptive antenna systems," *Proc. IEEE*, vol. 55, no. 12, pp. 2143–2159, Dec. 1967.

[14] B. Picinbono and P. Chevalier, "Widely linear estimation with complex data," *IEEE Trans. on Signal Process.*, vol. 43, no. 8, pp. 2030–2033, Aug. 1995.

Publication 8

A. Hakkarainen, J. Werner, K. R. Dandekar, and M. Valkama, "Analysis of Augmented Spatial Processing for Uplink OFDMA MU-MIMO Receiver with Transceiver I/Q Imbalance and External Interference," in *IEEE Transactions on Wireless Communications*, vol. 15, no. 5, pp. 3422–3439, May 2016. DOI: 10.1109/TWC.2016.2521382

Analysis and Augmented Spatial Processing for Uplink OFDMA MU-MIMO Receiver with Transceiver I/Q Imbalance and External Interference

Aki Hakkarainen, *Student Member, IEEE*, Janis Werner,
Kapil R. Dandekar, *Senior Member, IEEE*, and Mikko Valkama, *Senior Member, IEEE*

***Abstract*—This paper addresses receiver (RX) signal processing in multiuser multiple-input multiple-output (MU-MIMO) systems. We focus on uplink orthogonal frequency-division multiple access (OFDMA)-based MU-MIMO communications under in-phase/quadrature (I/Q) imbalance in the associated radio frequency electronics. It is shown in the existing literature that transceiver I/Q imbalances cause cross-talk of mirror-subcarriers in OFDM systems. As opposed to typically reported single-user studies, we extend the studies to OFDMA-based MU-MIMO communications, with simultaneous user multiplexing in both frequency and spatial domains, and incorporate also external interference from multiple sources at RX input, for modeling challenging conditions in increasingly popular heterogeneous networks. In the signal processing developments, we exploit the augmented subcarrier processing, which processes each subcarrier jointly with its counterpart at the image subcarrier, and jointly across all RX antennas. Furthermore, we derive an optimal augmented linear RX in terms of minimizing the mean-squared error. The novel approach integrates the I/Q imbalance mitigation, external interference suppression and data stream separation of multiple UEs into a single processing stage, thus avoiding separate transceiver calibration. Extensive analysis and numerical results show the signal-to-interference-plus-noise ratio (SINR) and symbol-error rate (SER) behavior of an arbitrary data stream after RX spatial processing as a function of different system and impairment parameters. Based on the results, the performance of the conventional per-subcarrier processing is heavily limited under transceiver I/Q imbalances, and is particularly sensitive to external interferers, whereas the proposed augmented subcarrier processing provides a high-performance signal processing solution being able to detect the signals of different users as well as suppress the external interference efficiently. Finally, we also extend the studies to massive MIMO framework, with very large antenna systems. It is shown that, despite the huge number of RX antennas, the conventional linear processing methods still suffer heavily from I/Q imbalances while the augmented approach does not have such limitations.**

***Index Terms*—External interference, heterogeneous networks, I/Q imbalance, interference suppression, massive MIMO, multiuser MIMO, OFDMA.**

This work was supported in part by the Finnish Funding Agency for Technology and Innovation (Tekes) under the projects Recongurable Antenna-based Enhancement of Dynamic Spectrum Access Algorithms and Future Uncoordinated Small-Cell Networks Using Recongurable Antennas, in part by the Industrial Research Fund of Tampere University of Technology, in part by the Academy of Finland under the projects 251138, 284694 and 288670, in part by the Doctoral Programme of the President of Tampere University of Technology, in part by the Foundation of Nokia Corporation, and also in part by the National Science Foundation (NSF) under Grant CNS-1457306. Preliminary work addressing a limited subset of initial results was presented at the IEEE Global Communications Conference (GLOBECOM), Austin, TX, USA, December 2014 [1], and at International Symposium on Wireless Communication Systems (ISWCS), Brussels, Belgium, August 2015 [2].

A. Hakkarainen, J. Werner, and M. Valkama are with the Department of Electronics and Communications Engineering, Tampere University of Technology, Tampere 33720, Finland (e-mail: aki.hakkarainen@tut.fi janis.werner@tut.fi; mikko.e.valkama@tut.fi).

K. R. Dandekar is with the Department of Electrical and Computer Engineering, Drexel University, Philadelphia, PA 19104 USA (e-mail: dandekar@coe.drexel.edu).

I. Introduction

Modern communication systems need to support the ever-increasing user needs of faster data connections and cheaper devices. This has resulted, e.g., in adopting larger and more complicated symbol alphabets which are, unfortunately, also more vulnerable to various signal distortions than conventional solutions. In addition, the user equipment (UE), including also the analog radio frequency (RF) circuitry, should be implemented with very low costs and silicon area. These things, among other requirements of maximum performance, low power, small size etc., have resulted in a situation where the RF imperfections and their mitigation methods by cost-efficient digital signal processing have become very important aspects in system design. One of these RF imperfections is the so-called in-phase/quadrature (I/Q) imbalance which occurs in direct-conversion transceivers [3]. Physically, when the baseband signal is up-converted in the transmitters (TXs) or when the RF signal is down-converted in the receivers (RXs), the signals in the I and Q branches have slight differences in their amplitude and phase responses, e.g., due to manufacturing tolerances. This leads to imbalance between the I and Q signals and thus distorts the overall signal waveforms [4].

I/Q imbalance effects and mitigation are widely studied for orthogonal frequency division multiplexing (OFDM) waveforms. In [5]–[10], I/Q imbalance in single-input single-output (SISO) OFDM systems is studied comprehensively. The SISO approach is extended to cover multiple TX antennas in [11], [12] while [4], [13]–[16] consider multiple antennas on both TX and RX sides, resulting in full multiple-input multiple-output (MIMO) communications in single-user context (i.e., SU-MIMO). The joint effects of I/Q imbalance and power amplifier nonlinearities are studied in [17] whereas [18] focuses on I/Q imbalance with carrier frequency offset and [19], [20] consider I/Q imbalance with phase noise, all again in single-user context. Based on the studies listed above, the so-called augmented subcarrier processing for I/Q imbalance mitigation in OFDM systems has been proposed in [5], [6], [10], [13], [14], [16], [21], [22]. Therein, each subcarrier signal is processed jointly

with the corresponding signal at the image, or mirror, subcarrier. This approach is very close to widely-linear processing [23] where the signal and its complex conjugate are processed jointly. The widely-linear processing is originally proposed for processing non-circular signals, see e.g. [23]–[25], and also for time-domain I/Q imbalance mitigation, see e.g. [26], [27], since I/Q imbalance results in non-circular signals even with originally circular signals.

Although the single-user OFDM studies listed above concentrate on the I/Q imbalance challenges and their mitigation methods, they do not address multiuser MIMO (MU-MIMO) [28] aspects, i.e., having multiple UEs transmitting simultaneously at a given subcarrier. Furthermore, the above works do not address UE multiplexing in frequency domain, through orthogonal frequency division multiple access (OFDMA) principle, either. UE multiplexing through single-carrier frequency-division multiple access (SC-FDMA) together with joint TX+RX I/Q imbalances is studied in [21], [29] while TX I/Q imbalance with SC-FDMA and OFDMA is studied in [22]. However, these studies consider a case where each subcarrier is allocated only to a single single-antenna UE which transmits towards a single-antenna BS. Furthermore, none of the studies listed above take the influence of possible external interferers into account. Some of the studies also make somewhat limited assumptions of equal I/Q imbalance coefficients between different subcarriers and/or transceiver branches. Our earlier study in [30] focused on the external interference suppression with antenna array processing in OFDM systems but the study was limited only to the single-user single-input multiple-output (SU-SIMO) scenario. The rather limited SU-SISO and SU-MIMO schemes are considerable simpler than the full MU-MIMO transmission from the viewpoints of the signal models and associated signal processing algorithms. Therefore, in this paper, we extend the existing results towards more generic MU-MIMO systems, incorporating also the large antenna system or massive MIMO [31]–[33] aspects, receiving increasing interest currently. In particular, *the main contributions of this paper are the following*:

- In the analysis and mitigation, we focus on a generic uplink MU-MIMO OFDMA system under transceiver I/Q imbalances. This means that *multiple UEs transmit simultaneously towards the BS at each of the available subcarriers*, and that further UE multiplexing takes place simultaneously in the frequency domain. Such a multiple-access scheme is already adopted to IEEE802.16 Broadband Wireless Metropolitan Area Networks (WiMAX) advanced air interface specification [34] and has been considered to be a potential air interface technology for the future wireless local area network (WLAN) implementations within the IEEE 802.11ax/HEW framework [35], [36]. In addition, the considered model can be easily applied to other multicarrier systems such as 3GPP long term evolution (LTE) and LTE-Advanced which, in terms of uplink, are based on SC-FDMA waveform.
- We also include the effects of external interferers into the analysis and show how antenna array processing can be efficiently used to suppress the external interference having a given spatial response, in spite of I/Q imbalances. This kind of external interferers may exist, e.g., in increasingly popular heterogeneous networks where the UEs at the cell-edge of a macro cell, and consequently with considerably high TX power levels, severely interfere with the reception in a co-channel neighboring femto-cell BS.
- We formulate our analysis in a generic and flexible way by allowing arbitrary system parameters. This approach allows us to use frequency-selective and transceiver branch-dependent I/Q imbalance parameters in the analysis and signal processing.
- The developed augmented subcarrier processing introduces a novel combining approach which can jointly separate all spatially multiplexed UE data streams from each others as well as mitigate the effects of I/Q imbalances and external interference, thus avoiding separate transceiver calibration.
- We also extend the studies to massive MIMO framework, i.e., to cases where the number of RX antennas is an order of magnitude higher than the number of spatially multiplexed users, and show the sensitivity of such systems to transceiver I/Q imbalances with different RX spatial processing schemes.
- Finally, we provide an extensive set of numerical experiments which illustrate explicitly the influence of different system parameters under the inevitable RF imperfections.

With these considerations we can provide valuable insight for future MU-MIMO OFDMA system designers as well as a fundamental starting point for future research. One of the central technical findings is that the performance of conventional per-subcarrier spatial processing is heavily limited under transceiver I/Q imbalances, and is particularly sensitive to external interferers, whereas the proposed augmented spatial subcarrier processing provides a robust and high-performance RX signal processing solution being able to detect the data streams of different users as well as suppress the effects of the external interference in a highly efficient manner, in spite of transceiver I/Q imbalances. Another central finding is that massive MIMO systems can, indeed, be sensitive to RF chain I/Q imbalances, in spite of high processing gain stemming from the massive number of antenna units. This is an outcome that more simplified modeling based studies reported, e.g., in [37], [38], have not clearly reported.

The rest of the paper is organized as follows. Section II presents the fundamental MU-MIMO OFDMA signal and system models under transceiver I/Q imbalances. Linear minimum mean-square error (LMMSE) and augmented LMMSE RXs are derived in Section III along with output signal-to-interference-plus-noise ratio (SINR) and computational complexity analyses. Section IV gives extensive numerical evaluations and illustrations as a function of numerous system parameters. Finally, we conclude the paper in Section V.

Notation: Throughout this paper, vectors and matrices are written with bold characters. The superscripts $(\cdot)^{\mathrm{T}}$, $(\cdot)^{\mathrm{H}}$, $(\cdot)^{*}$ and $(\cdot)^{-1}$ represent transpose, Hermitian (conjugate) transpose, complex conjugate and matrix inverse, respectively. The tilde sign $\tilde{(\cdot)}$ is used to present an augmented quantity and the results obtained by the augmented processing. We write $\mathrm{diag}\left(x_{11}, x_{22}, \cdots, x_{ii}, \cdots\right)$ to denote a diagonal matrix $\mathbf{X}$

that is composed of the entries x_{ii} on the main diagonal. The natural basis vector, where the q^{th} entry is equal to one and the rest are zeros, is denoted as $\mathbf{e}_q$. The statistical expectation is denoted with $\mathbb{E}[\cdot]$. A complex random variable x is called circular if $\mathbb{E}[x^2] = 0$.

II. Fundamental Signal and System Models

OFDM and OFDMA systems are based on multicarrier transmission where the parallel subcarriers are modulated and deployed independently and where users can be flexibly multiplexed in both frequency and spatial domains. On the TX side, multiple parallel frequency domain data streams are jointly converted to time domain through the inverse fast Fourier transform (IFFT). On the RX side, the received time domain signal is then converted back to frequency domain data streams through the fast Fourier transform (FFT). Since the essential data exist at the subcarrier level, we analyze an uplink OFDMA MU-MIMO system from an arbitrary subcarrier point of view. The generic uplink system model comprises a single BS which serves multiple UEs simultaneously at each subcarrier. The subcarriers are indexed with $c \in \{-C/2, \ldots, -1, 1, \ldots, C/2\}$ where C is the total number of active subcarriers. Additionally, the image (or mirror) subcarrier is defined as $c' = -c$. The number of UEs spatially multiplexed at subcarrier c is denoted with U while the corresponding number at subcarrier c' is V. Correspondingly, the users are indexed by $u \in \{1, \ldots, U\}$ and $v \in \{1, \ldots, V\}$. Note that depending on the subcarrier allocation for the UEs, u and v might sometimes refer to the same UE if it is transmitting at both subcarriers c and c'. The BS has N RX antennas whereas UE u is equipped with M_u TX antennas. In addition, the effect of L external interferers is included to the model and external interferer l is assumed to have J_l TX antennas. The scenario under consideration is illustrated in Fig. 1.

We denote the transmitted baseband equivalent spatial signal vector of user u at subcarrier c by $\mathbf{s}_{u,c} = \mathbf{G}_{u,c}\mathbf{x}_{u,c} \in \mathbb{C}^{M_u \times 1}$. Here, $\mathbf{x}_{u,c} \in \mathbb{C}^{Q_{u,c} \times 1}$ denotes the parallel transmitted data streams of UE u at subcarrier c and $Q_{u,c}$ is the number of these streams. In addition, $\mathbf{G}_{u,c} \in \mathbb{C}^{M_u \times Q_{u,c}}$ denotes the precoder matrix which maps the actual data snapshots to TX antennas. Similarly, the transmitted baseband equivalent signal snapshot vector of user v at the image subcarrier c' is given by $\mathbf{s}_{v,c'} = \mathbf{G}_{v,c'}\mathbf{x}_{v,c'} \in \mathbb{C}^{M_v \times 1}$. Finally, $s_{\text{int},l,c} \in \mathbb{C}^{J_l \times 1}$ denotes the signal snapshot vector originating from the l^{th} external interferer at subcarrier c. Throughout this paper, we assume that in all associated devices each antenna is connected to a separate transceiver chain. All signal vectors refer to subcarrier-level (frequency-domain) quantities in the considered OFDMA radio system, i.e., before IFFT in the TXs and after FFT in the RXs. The most essential variables used throughout the paper are listed in Table I.

A. TX and RX I/Q Imbalance Characteristics

The imperfections in the analog electronics of direct-conversion transceivers create I/Q imbalance [3]. On the one hand, the gain imbalance g is created by unequal gains or attenuations between the I and Q branches in amplifiers, filters, mixers and digital-to-analog and analog-to-digital converters. On the other hand, the phase imbalance ϕ occurs mainly due to the imperfections in mixers and phase shifters, as well as due to phase response differences of the branch filters. In general, both the gain and phase imbalance are *frequency-dependent* already within a few MHz processing bandwidths [39], [40], and thus need to be modeled accordingly.

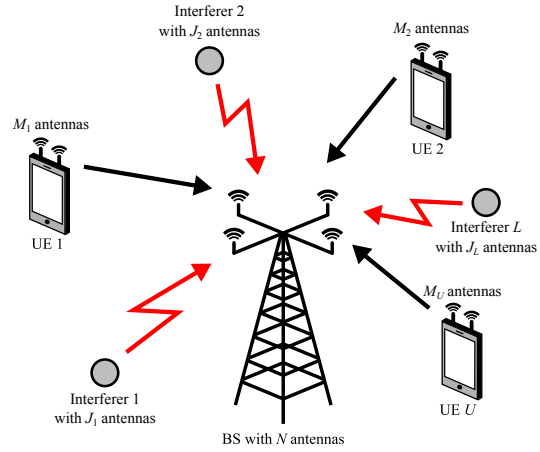

Fig. 1: A general MU-MIMO uplink scenario with a single base station, U mobile users and L external interferers, all being simultaneously active at subcarrier c. The base station is equipped with N RX antennas whereas UE u has M_u and interferer l has J_l TX antennas. Further user multiplexing takes place in the frequency domain, through the OFDMA principle.

For notational convenience, we first define TX I/Q imbalance parameters for a single TX antenna branch m of user u at subcarrier c. They are equal to $K_{\text{Tx1},m,u,c} = (1 + g_{\text{Tx},m,u,c}e^{j\phi_{\text{Tx},m,u,c}})/2$ and $K_{\text{Tx2},m,u,c} = (1 - g_{\text{Tx},m,u,c}e^{j\phi_{\text{Tx},m,u,c}})/2$ where $g_{\text{Tx},m,u,c}$ and $\phi_{\text{Tx},m,u,c}$ are the gain and phase imbalance coefficients for TX antenna branch m of user u at subcarrier c, respectively [4]. Since the UE has M_u antennas and associated TX branches, we stack the I/Q imbalance parameters of different TX branches into diagonal matrices. Consequently, the TX I/Q imbalance matrices $\mathbf{K}_{\text{Tx1},u,c}$ and $\mathbf{K}_{\text{Tx2},u,c}$, both $\in \mathbb{C}^{M_u \times M_u}$, are given by

$$\begin{aligned} \mathbf{K}_{\text{Tx1},u,c} &= \text{diag}(K_{\text{Tx1},1,u,c}, \cdots, K_{\text{Tx1},M_u,u,c}), \\ \mathbf{K}_{\text{Tx2},u,c} &= \text{diag}(K_{\text{Tx2},1,u,c}, \cdots, K_{\text{Tx2},M_u,u,c}). \end{aligned} \tag{1}$$

Similarly, the I/Q imbalance characteristics for a single RX antenna branch n at subcarrier c are equal to $K_{\text{Rx1},n,c} = (1+g_{\text{Rx},n,c}e^{-j\phi_{\text{Rx},n,c}})/2$ and $K_{\text{Rx2},n,c} = (1-g_{\text{Rx},n,c}e^{j\phi_{\text{Rx},n,c}})/2$ where $g_{\text{Rx},n,c}$ and $\phi_{\text{Rx},n,c}$ denote the gain and phase imbalance coefficients of RX antenna branch n [4]. We stack also the RX I/Q imbalance parameters into diagonal matrices, resulting in the RX I/Q imbalance matrices $\mathbf{K}_{\text{Rx1},c}$ and $\mathbf{K}_{\text{Rx2},c}$, both $\in \mathbb{C}^{N \times N}$, given by

$$\begin{aligned} \mathbf{K}_{\text{Rx1},c} &= \text{diag}(K_{\text{Rx1},1,c}, \cdots, K_{\text{Rx1},N,c}), \\ \mathbf{K}_{\text{Rx2},c} &= \text{diag}(K_{\text{Rx2},1,c}, \cdots, K_{\text{Rx2},N,c}). \end{aligned} \tag{2}$$

These matrices are used in the modeling and analysis of the total effects of TX and RX imbalances in the considered

TABLE I: Most important variables used throughout the paper

Variable	Dimensions	Definition
$\sigma^2_{n,c}$	scalar	Noise power at subcarrier c
$\sigma^2_{x,u,c}$, $\sigma^2_{x,v,c'}$	scalars	Power of a single data stream of UE u at subcarrier c and of UE v at subcarrier c'
J_l	scalar	Number of TX antennas of external interferer l
L	scalar	Number of external interferers
M_u	scalar	Number of TX antennas of UE u
N	scalar	Number of BS RX antennas
$Q_{u,c}$, $Q_{v,c'}$	scalars	Number of parallel transmitted data streams by UE u at subcarrier c and by UE v at subcarrier c'
S	scalar	Total number of all transmitted data streams from all UEs at subcarrier c, i.e., $S = \sum_{u=1}^{U} Q_{u,c}$
U, V	scalars	Number of spatially multiplexed UEs at subcarriers c and c'
c	scalar	Subcarrier index
c'	scalar	Image subcarrier index
u, v	scalars	UE indeces for subcarriers c and c'
$\widetilde{\mathbf{\Psi}}_{u,c}$, $\widetilde{\mathbf{\Omega}}_{u,c}$	$N \times M_u$	Total effective channel matrices including the joint effects of TX+RX I/Q imb. as well as the wireless channel
$\mathbf{G}_{u,c}$, $\mathbf{G}_{v,c'}$	$M_u \times Q_{u,c}$, $M_v \times Q_{v,c'}$	Precoder matrices for UE u at subcarrier c and for UE v at subcarrier c'
$\mathbf{H}_{u,c}$, $\mathbf{H}_{u,c'}$	$N \times M_u$	Channel response matrices of UE u at subcarriers c and c'
$\mathbf{K}_{\text{Rx1},c}$, $\mathbf{K}_{\text{Rx2},c}$	$N \times N$	Diagonal RX I/Q imbalance matrices of BS at subcarrier c
$\widetilde{\mathbf{K}}_{\text{RxA},c}$, $\widetilde{\mathbf{K}}_{\text{RxB},c}$	$2N \times N$	Augmented RX I/Q imbalance matrices at subcarrier c
$\mathbf{K}_{\text{Tx1},u,c}$, $\mathbf{K}_{\text{Tx2},u,c}$	$M_u \times M_u$	Diagonal TX I/Q imbalance matrices of UE u at subcarrier c
$\widetilde{\mathbf{R}}_{\text{TxRxi},c}$	$2N \times 2N$	Covariance matrix of the augmented received signal vector under joint TX+RX I/Q imbalances at subcarrier c
$\mathbf{R}_{z,c}$, $\mathbf{R}_{z,c'}$	$N \times N$	Covariance matrices of external interference and noise at subcarriers c and c'
$\mathbf{W}_c$, $\widetilde{\mathbf{W}}_c$	$N \times S$, $2N \times S$	Combiner weighting matrices at subcarrier c
$\mathbf{n}_c$	$N \times 1$	Additive noise in the RX electronics at subcarrier c
$\mathbf{s}_{\text{int},l,c}$	$J_l \times 1$	Transmitted baseband equivalent spatial signal vector of interferer l at subcarrier c
$\mathbf{s}_{u,c}$, $\mathbf{s}_{v,c'}$	$M_u \times 1$, $M_v \times 1$	Transmitted baseband equivalent spatial signal vector of UE u at subcarrier c and of UE v at subcarrier c'
$\mathbf{r}_{\text{TxRxi},c}$, $\widetilde{\mathbf{r}}_{\text{TxRxi},c}$	$N \times 1$, $2N \times 1$	Received signal vectors under joint TX+RX I/Q imbalances at subcarrier c
$\mathbf{v}_{\text{TxRxi},q,u,c}$, $\widetilde{\mathbf{v}}_{\text{TxRxi},q,u,c}$	$N \times 1$, $2N \times 1$	Cross-correlation vectors between the received signal vector and data stream q of UE u at subcarrier c
$\mathbf{x}_{u,c}$, $\mathbf{x}_{v,c'}$	$Q_{u,c} \times 1$, $Q_{v,c'} \times 1$	Transmitted data stream vectors of UE u at subcarrier c and of UE v at subcarrier c'
$\mathbf{y}_{\text{TxRxi},c}$, $\widetilde{\mathbf{y}}_{\text{TxRxi},c}$	$S \times 1$	Output signal vectors of the combiners under joint TX+RX I/Q imbalances at subcarrier c
$\mathbf{z}_c$, $\mathbf{z}_{c'}$	$N \times 1$	Sum of external interference and additive noise vectors at subcarriers c and c'

The tilde sign $\tilde{(\cdot)}$ refers to augmented quantities and the results obtained by the augmented processing.

MU-MIMO system. The above characterization allows setting the I/Q imbalance parameters freely and independently, not only between different UEs but also between different antenna branches of a single device. In addition, we assume that I/Q imbalance is frequency selective, i.e., I/Q imbalance parameters at different subcarriers are different. However, all derived expressions are valid also for the case where the I/Q imbalance parameters are equal in all transceivers, transceiver branches and/or subcarriers.

B. Uplink MU-MIMO Transmission under I/Q Imbalance

The transmitted baseband equivalent signal snapshot vector of user u at subcarrier c under TX I/Q imbalance can be now written with the help of the TX I/Q imbalance matrices directly as [18]

$$\begin{aligned}\mathbf{s}_{\text{Txi},u,c} &= \mathbf{K}_{\text{Tx1},u,c}\mathbf{s}_{u,c} + \mathbf{K}_{\text{Tx2},u,c}\mathbf{s}^*_{u,c'} \\ &= \mathbf{K}_{\text{Tx1},u,c}\mathbf{G}_{u,c}\mathbf{x}_{u,c} + \mathbf{K}_{\text{Tx2},u,c}\mathbf{G}^*_{u,c'}\mathbf{x}^*_{u,c'}.\end{aligned} \tag{3}$$

Clearly, the structure of the transmitted signal is distorted, resulting in general in cross-talk between image-subcarriers c and c'. This is already a well-established phenomenon in the existing literature, see e.g. [4], [7], [18], [40]. Notice, however, that if the image subcarrier c' is not allocated for UE u there is no cross-talk between the subcarriers of an individual UE and the resulting transmitted signal at subcarrier c consists only of the scaled version of $\mathbf{s}_{u,c}$. However, when subcarrier c' is allocated to another UE v, through the OFDMA principle, the corresponding emitted signal snapshot vector at subcarrier c is of the form $\mathbf{s}_{\text{Txi},v,c} = \mathbf{K}_{\text{Tx2},v,c}\mathbf{s}^*_{v,c'} = \mathbf{K}_{\text{Tx2},v,c}\mathbf{G}^*_{v,c'}\mathbf{x}^*_{v,c'}$. Then, when interpreted from RX perspective, this implies *cross-talk or interference between UEs*. This issue is not addressed or taken into account in the existing literature [6]–[8], [10]–[12], [14]–[16], [18]. The corresponding transmitted signal vectors at the image subcarrier c' are given by $\mathbf{s}_{\text{Txi},u,c'} = \mathbf{K}_{\text{Tx1},u,c'}\mathbf{G}_{u,c'}\mathbf{x}_{u,c'} + \mathbf{K}_{\text{Tx2},u,c'}\mathbf{G}^*_{u,c}\mathbf{x}^*_{u,c}$ and $\mathbf{s}_{\text{Txi},v,c'} = \mathbf{K}_{\text{Tx1},v,c'}\mathbf{G}_{v,c'}\mathbf{x}_{v,c'} + \mathbf{K}_{\text{Tx2},v,c'}\mathbf{G}^*_{v,c}\mathbf{s}^*_{v,c}$.

The signals from spatially and frequency multiplexed UEs propagate through wireless channels and are finally received by the BS equipped with N antennas. When *I/Q imbalance occurs also in the parallel RX branches of the BS*, the received signal snapshot vector $\mathbf{r}_{\text{TxRxi},c} \in \mathbb{C}^{N\times 1}$ at subcarrier c, under joint TX+RX I/Q imbalances can be expressed as

$$\begin{aligned}\mathbf{r}_{\text{TxRxi},c} &= \mathbf{K}_{\text{Rx1},c}\mathbf{r}_{\text{Txi},c} + \mathbf{K}_{\text{Rx2},c}\mathbf{r}^*_{\text{Txi},c'} \\ &= \sum_{u=1}^{U}\widetilde{\mathbf{\Psi}}_{u,c}\mathbf{G}_{u,c}\mathbf{x}_{u,c} + \sum_{v=1}^{V}\widetilde{\mathbf{\Omega}}_{v,c}\mathbf{G}^*_{v,c'}\mathbf{x}^*_{v,c'} \\ &\quad + \mathbf{K}_{\text{Rx1},c}\mathbf{z}_c + \mathbf{K}_{\text{Rx2},c}\mathbf{z}^*_{c'}\end{aligned} \tag{4}$$

where perfect time and frequency synchronization between the UEs and BS is assumed for simplicity. Here, $\widetilde{\mathbf{\Psi}}_{u,c} \in \mathbb{C}^{N\times M_u}$ and $\widetilde{\mathbf{\Omega}}_{v,c} \in \mathbb{C}^{N\times M_v}$ denote the total effective linear channels of UE u and v including the joint effects of TX and RX I/Q imbalances as well as the wireless propagation channels. The matrices are given by

$$\begin{aligned}\widetilde{\mathbf{\Psi}}_{u,c} &= \begin{bmatrix}\mathbf{K}_{\text{Rx1},c} & \mathbf{K}_{\text{Rx2},c}\end{bmatrix}\begin{bmatrix}\mathbf{H}_{u,c} & \mathbf{0} \\ \mathbf{0} & \mathbf{H}^*_{u,c'}\end{bmatrix}\begin{bmatrix}\mathbf{K}_{\text{Tx1},u,c} \\ \mathbf{K}^*_{\text{Tx2},u,c'}\end{bmatrix}, \\ \widetilde{\mathbf{\Omega}}_{v,c} &= \begin{bmatrix}\mathbf{K}_{\text{Rx1},c} & \mathbf{K}_{\text{Rx2},c}\end{bmatrix}\begin{bmatrix}\mathbf{H}_{v,c} & \mathbf{0} \\ \mathbf{0} & \mathbf{H}^*_{v,c'}\end{bmatrix}\begin{bmatrix}\mathbf{K}_{\text{Tx2},v,c} \\ \mathbf{K}^*_{\text{Tx1},v,c'}\end{bmatrix}\end{aligned} \tag{5}$$

where $\mathbf{H}_{u,c} \in \mathbb{C}^{N \times M_u}$ and $\mathbf{H}_{v,c} \in \mathbb{C}^{N \times M_v}$ are the channel response matrices of user u and v at subcarrier c, respectively, and again c' denotes the image subcarrier. Throughout the paper, the channel response elements are assumed to be constants within each narrow subcarrier. Additionally, the external interference plus noise vector $\mathbf{z}_c \in \mathbb{C}^{N \times 1}$ at RX input is given by

$$\mathbf{z}_c = \sum_{l=1}^{L} \mathbf{H}_{\text{int},l,c} \mathbf{s}_{\text{int},l,c} + \mathbf{n}_c \tag{6}$$

where $\mathbf{H}_{\text{int},l,c} \in \mathbb{C}^{N \times J_l}$ represents the channel response matrix of the l^{th} interferer at subcarrier c. Since the interferers are generally not synchronized with the BS and since we are not limiting the study to any specific interference waveform, $\mathbf{s}_{\text{int},l,c}$ is basically the result of the sampled interference signal at the desired subcarrier after the RX FFT processing. In practice, the interfering signals themselves can be modeled, e.g., with complex Gaussian signals but it should be noted that in any case, the contribution of each interferer has a strong spatial response through channel $\mathbf{H}_{\text{int},l,c}$. The noise vector $\mathbf{n}_c \in \mathbb{C}^{N \times 1}$ models the additive noise in the RX electronics. Noise elements in different RX branches, without I/Q imbalances, are assumed to be complex circular and mutually uncorrelated. A corresponding formulation for $\mathbf{z}_{c'}$, i.e., the external interference and noise at the image subcarrier, is obtained from (6) by substituting the subcarrier index c with c'.

The model in (4) explicitly describes how the received signal is structured in OFDMA MU-MIMO systems under transceiver I/Q imbalances. Unlike in SU-MIMO systems, the received signal in (4) includes substantial inter-user interference from the other spatially multiplexed UEs at subcarrier c. Furthermore, we note that the signal includes contribution not only from subcarrier c but also from the image subcarrier c'. The UE signals transmitted at the image subcarrier leak to the considered subcarrier due to both TX and RX I/Q imbalances and consequently we call it inter-user interference from the image subcarrier. In contrast to UE signals, the external interference and noise alias to subcarrier c only due to RX I/Q imbalance. The overall spectral structure of the received signal is illustrated in Fig. 2.

In practice, a subcarrier with very high interference levels could be left unused for data transmission if there are subcarriers with better conditions available. However, due to RX I/Q imbalance, the strong external interference from the image subcarrier aliases on top of the desired signal, even if the image subcarrier is not used for data transmission at all. This is unavoidable, since the analog electronics in transceivers are never ideal in practice. The overall scale of the signal distortion is naturally determined by the I/Q imbalance parameters, and the overall severity depends on the sensitivity of the application under consideration. Furthermore, the primary target of separating the multiplexed streams of different UEs at subcarrier c, under the external interference and transceiver I/Q imbalances is a key concern. This will be elaborated in the forthcoming sections where RX spatial processing is taken into account.

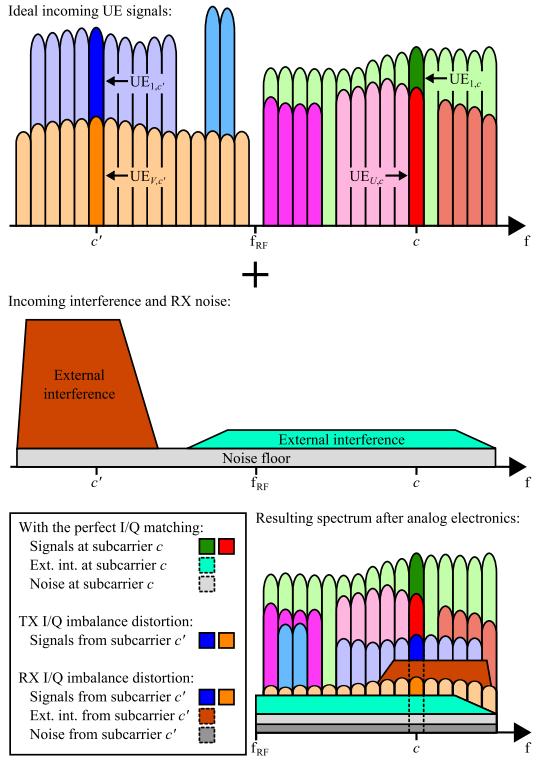

Fig. 2: Illustration of the spectral components of the received signal under I/Q imbalances. The signals at the image subcarrier alias due to the both TX and RX I/Q imbalances whereas the external interference and noise are affected only by RX I/Q imbalance.

Note that (4) expresses the received signal under joint TX+RX I/Q imbalances in a generic form. Throughout the paper, the special case with I/Q imbalance only in the TXs is obtained from the signal models by substituting $\mathbf{K}_{\text{Rx1},c} = \mathbf{I}$ and $\mathbf{K}_{\text{Rx2},c} = \mathbf{0}$ for all c. Similarly, the case with I/Q imbalance only in the RX is obtained by substituting $\mathbf{K}_{\text{Tx1},i,j} = \mathbf{I}$ and $\mathbf{K}_{\text{Tx2},i,j} = \mathbf{0}$ for all $i \in \{u, v\}$ and $j \in \{c, c'\}$.

C. Spatial Post-Processing with Digital Combiners

Multiple RX antennas enable flexible combining of the antenna signals for obtaining the desired system performance. Usually, the combining process is implemented by digital signal processing due to its high computational power, reconfigurability and small physical size. Generally speaking, a digital linear combiner processes the received signal snapshots with complex weights $\mathbf{w} = [w_1, w_2, ..., w_N]^{\text{T}} \in \mathbb{C}^{N \times 1}$ yielding an output signal $y = \mathbf{w}^{\text{H}}\mathbf{r}$ [41]. When applying this method to MU-MIMO systems utilizing OFDMA waveforms, each of $Q_{u,c}$ transmitted data streams of each U UEs at subcarrier c needs an individual weight vector $\mathbf{w}_{q,u,c}$ for separating data streams from each others in the RX. In general, the weights can be selected with blind or non-blind methods, depending on *a priori* information, under a given optimization criteria. The basic approach is, however, to combine the received signals

from different RX branches coherently while trying to minimize the effect of the non-desired interference and noise. Since this classical processing is done at the subcarrier level, we call it per-subcarrier combiner.

When stacking the weight vectors of individual data streams into a matrix, we get the complete weight matrix $\mathbf{W}_c = [\mathbf{w}_{1,1,c}, \cdots, \mathbf{w}_{Q_U,U,c}] \in \mathbb{C}^{N\times S}$ where $S = \sum_{u=1}^{\mathrm{U}} Q_{u,c}$ is the total number of the transmitted data streams at subcarrier c. Under joint TX+RX I/Q imbalances, based on (4), the output signal vector $\mathbf{y}_{\mathrm{TxRxi},c} \in \mathbb{C}^{S\times 1}$ reads

$$\begin{aligned}\mathbf{y}_{\mathrm{TxRxi},c} &= \mathbf{W}_c^{\mathrm{H}}\mathbf{r}_{\mathrm{TxRxi},c} \\ &= \sum_{u=1}^{U}\mathbf{W}_c^{\mathrm{H}}\widetilde{\mathbf{\Psi}}_{u,c}\mathbf{G}_{u,c}\mathbf{x}_{u,c} + \sum_{v=1}^{V}\mathbf{W}_c^{\mathrm{H}}\widetilde{\mathbf{\Omega}}_{v,c}\mathbf{G}^*_{v,c'}\mathbf{x}^*_{v,c'} \\ &\quad + \mathbf{W}_c^{\mathrm{H}}\mathbf{K}_{\mathrm{Rx1},c}\mathbf{z}_c + \mathbf{W}_c^{\mathrm{H}}\mathbf{K}_{\mathrm{Rx2},c}\mathbf{z}^*_{c'}. \end{aligned} \tag{7}$$

The entries of the output signal vector $\mathbf{y}_{\mathrm{TxRxi},c}$ represent the data streams originating from different UEs and are thus forwarded to further signal processing stages such as decoding. As visible in (7), all signal terms are multiplied with the same weighting matrix. The first term contains the data streams of all U desired UEs, which are to be separated by the spatial processing, while at the same time suppressing the effects of the other terms as much as possible. The second term is due to the inter-user interference from the mirror UEs in the OFDMA framework while the third and fourth terms are due to the external interference and noise. Notice that the external interference contributes to the combiner output through direct co-channel coexistence as well as due to image subcarrier leakage. The above is clearly a challenge when optimizing the combiner weights and it becomes even more difficult when the number of multiplexed UEs and external interferers is increased.

Since transceiver I/Q imbalances cause both inter-user interference and external interference through image subcarrier leakage, classical per-subcarrier spatial processing can easily run out of degrees of freedom to suppress all of them sufficiently. To alleviate this and enhance the interference suppression capabilities, we next augment the spatial combiner operating principle to process each subcarrier along with its image subcarrier jointly. This means augmented processing where the signals from both subcarriers c and c' are combined with two separate sets of weights as illustrated in Fig. 3. The approach has been shown to be efficient for I/Q imbalance mitigation in SU-MIMO communication with OFDM waveforms [13], [14], [16]. In this paper, we extend the augmented combiner to operate in the considerably more challenging MU-MIMO OFDMA scheme including also the influence of the external interference.

We denote the weight sets of the augmented combiner for transmitted data stream q of user u at subcarriers c and c' by $\mathbf{w}_{\mathrm{A},q,u,c} \in \mathbb{C}^{N\times 1}$ and $\mathbf{w}_{\mathrm{B},q,u,c'} \in \mathbb{C}^{N\times 1}$, and stack them into the augmented weight vector $\widetilde{\mathbf{w}}_{q,u,c} = [\mathbf{w}^{\mathrm{T}}_{\mathrm{A},q,u,c}, \mathbf{w}^{\mathrm{T}}_{\mathrm{B},q,u,c'}]^{\mathrm{T}} \in \mathbb{C}^{2N\times 1}$. Then, similarly as for the per-subcarrier processing, the weights of individual data streams are stacked, resulting in the complete augmented weight matrix given by $\widetilde{\mathbf{W}}_c = [\widetilde{\mathbf{w}}_{1,1,c}, \cdots, \widetilde{\mathbf{w}}_{Q_U,U,c}] \in \mathbb{C}^{2N\times S}$. After

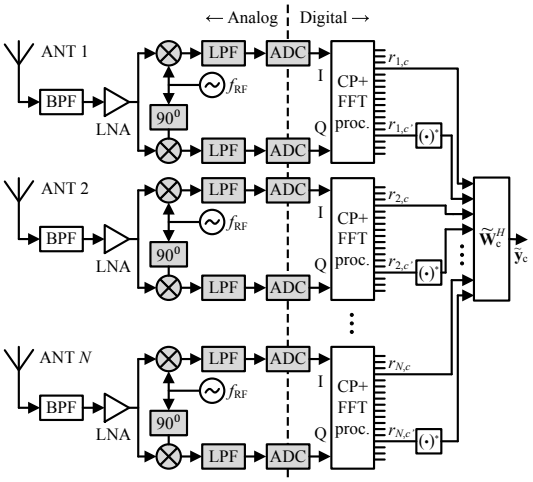

Fig. 3: The augmented RX combining in MU-MIMO systems utilizing OFDMA waveforms. The blocks with gray shading represent the main sources of I/Q imbalance in RX.

defining the augmented signal vector under joint TX+RX I/Q imbalances as $\widetilde{\mathbf{r}}_{\mathrm{TxRxi},c} = [\mathbf{r}^{\mathrm{T}}_{\mathrm{TxRxi},c}, \mathbf{r}^{\mathrm{H}}_{\mathrm{TxRxi},c'}]^{\mathrm{T}} \in \mathbb{C}^{2N\times 1}$ where $\mathbf{r}_{\mathrm{TxRxi},c}$ is as given in (4), the output signal of the augmented combiner under joint TX+RX I/Q imbalances becomes

$$\begin{aligned}\widetilde{\mathbf{y}}_{\mathrm{TxRxi},c} &= \widetilde{\mathbf{W}}_c^{\mathrm{H}}\widetilde{\mathbf{r}}_{\mathrm{TxRxi},c} \\ &= \sum_{u=1}^{U}\widetilde{\mathbf{W}}_c^{\mathrm{H}}\widetilde{\mathbf{\Xi}}_{u,c}\mathbf{G}_{u,c}\mathbf{x}_{u,c} + \sum_{v=1}^{V}\widetilde{\mathbf{W}}_c^{\mathrm{H}}\widetilde{\mathbf{\Phi}}_{v,c}\mathbf{G}^*_{v,c'}\mathbf{x}^*_{v,c'} \\ &\quad + \widetilde{\mathbf{W}}_c^{\mathrm{H}}\widetilde{\mathbf{K}}_{\mathrm{RxA},c}\mathbf{z}_c + \widetilde{\mathbf{W}}_c^{\mathrm{H}}\widetilde{\mathbf{K}}_{\mathrm{RxB},c}\mathbf{z}^*_{c'} \end{aligned} \tag{8}$$

where the effective augmented channel matrices $\widetilde{\mathbf{\Xi}}_{u,c} \in \mathbb{C}^{2N\times M_u}$ and $\widetilde{\mathbf{\Phi}}_{v,c} \in \mathbb{C}^{2N\times M_v}$ are equal to

$$\begin{aligned}\widetilde{\mathbf{\Xi}}_{u,c} &= \begin{bmatrix}\mathbf{K}_{\mathrm{Rx1},c} & \mathbf{K}_{\mathrm{Rx2},c}\\ \mathbf{K}^*_{\mathrm{Rx2},c'} & \mathbf{K}^*_{\mathrm{Rx1},c'}\end{bmatrix}\begin{bmatrix}\mathbf{H}_{u,c} & \mathbf{0}\\ \mathbf{0} & \mathbf{H}^*_{u,c'}\end{bmatrix}\begin{bmatrix}\mathbf{K}_{\mathrm{Tx1},u,c}\\ \mathbf{K}^*_{\mathrm{Tx2},u,c'}\end{bmatrix}, \\ \widetilde{\mathbf{\Phi}}_{v,c} &= \begin{bmatrix}\mathbf{K}_{\mathrm{Rx1},c} & \mathbf{K}_{\mathrm{Rx2},c}\\ \mathbf{K}^*_{\mathrm{Rx2},c'} & \mathbf{K}^*_{\mathrm{Rx1},c'}\end{bmatrix}\begin{bmatrix}\mathbf{H}_{v,c} & \mathbf{0}\\ \mathbf{0} & \mathbf{H}^*_{v,c'}\end{bmatrix}\begin{bmatrix}\mathbf{K}_{\mathrm{Tx2},v,c}\\ \mathbf{K}^*_{\mathrm{Tx1},v,c'}\end{bmatrix}. \end{aligned} \tag{9}$$

Moreover, the augmented RX I/Q imbalance matrices $\widetilde{\mathbf{K}}_{\mathrm{RxA},c}$ and $\widetilde{\mathbf{K}}_{\mathrm{RxA},c}$, both $\in \mathbb{C}^{2N\times N}$, are equal to

$$\widetilde{\mathbf{K}}_{\mathrm{RxA},c} = \begin{bmatrix}\mathbf{K}_{\mathrm{Rx1},c}\\ \mathbf{K}^*_{\mathrm{Rx2},c'}\end{bmatrix}, \quad \widetilde{\mathbf{K}}_{\mathrm{RxB},c} = \begin{bmatrix}\mathbf{K}_{\mathrm{Rx2},c}\\ \mathbf{K}^*_{\mathrm{Rx1},c'}\end{bmatrix}. \tag{10}$$

Clearly, the output signal structures of the conventional and augmented combiners are very similar. However, the underlying difference is that (8) adopts twice as many weights as (7) for processing signals at subcarriers c and c' jointly. Naturally, this doubles the computational complexity of the combining process but also gives us more degrees of freedom for obtaining the desired signal separation and interference suppression, even under challenging I/Q imbalances. Note that this flexibility is achieved by modifying the combiner block only whereas the costly RF chains and demanding FFT processing remain the same as in per-subcarrier processing. Notice also that various

kinds of special cases, e.g., TX I/Q imbalances only or RX I/Q imbalances only, are naturally obtained as corresponding special cases of (8)–(10) by proper substitutions.

III. LMMSE and Augmented LMMSE Receivers and Output SINRs

In this section, we derive the MMSE optimal linear and augmented combiners under TX+RX I/Q imbalances. In addition, we seek to characterize the output performance of the spatial combiners in terms of the combiner output SINR. Finally, we show how much the computational complexity of the whole digital signal processing chain is increased when using the augmented method instead of the more ordinary linear counterpart.

A. Received Signal Covariance Matrix

First, to support the upcoming RX derivations and SINR expressions, we derive an expression for the covariance matrix of the augmented received signal vector under joint TX+RX I/Q imbalances. We assume that the data streams of different UEs, the data streams at subcarriers c and c' (with perfect I/Q matchings), the interfering signals and the additive noise are all mutually uncorrelated. In addition, we assume that the external interference as well as noise at RX input are complex circular. Finally, we assume that all TX data streams of an individual UE u have equal powers before the TX stream-to-antenna mapping with precoder $\mathbf{G}_{u,c}$.

Under the assumptions above, the covariance matrix $\widetilde{\mathbf{R}}_{\text{TxRxi},c} \in \mathbb{C}^{2N\times 2N}$ of the *augmented signal model* under joint TX+RX I/Q imbalances can be expressed as

$$\begin{aligned}\widetilde{\mathbf{R}}_{\text{TxRxi},c} &= \mathbb{E}\left[\widetilde{\mathbf{r}}_{\text{TxRxi},c}\widetilde{\mathbf{r}}^{\text{H}}_{\text{TxRxi},c}\right] \\ &= \sum_{u=1}^{U}\sigma^2_{\text{x},u,c}\widetilde{\mathbf{\Xi}}_{u,c}\mathbf{G}_{u,c}\mathbf{G}^{\text{H}}_{u,c}\widetilde{\mathbf{\Xi}}^{\text{H}}_{u,c} \\ &\quad + \sum_{v=1}^{V}\sigma^2_{\text{x},v,c'}\widetilde{\mathbf{\Phi}}_{v,c}\mathbf{G}^{*}_{v,c'}\mathbf{G}^{\text{T}}_{v,c'}\widetilde{\mathbf{\Phi}}^{\text{H}}_{v,c} \\ &\quad + \widetilde{\mathbf{K}}_{\text{RxA},c}\mathbf{R}_{\text{z},c}\widetilde{\mathbf{K}}^{\text{H}}_{\text{RxA},c} + \widetilde{\mathbf{K}}_{\text{RxB},c}\mathbf{R}^{*}_{\text{z},c'}\widetilde{\mathbf{K}}^{\text{H}}_{\text{RxB},c}\end{aligned} \tag{11}$$

where $\sigma^2_{\text{x},u,c} = \mathbb{E}[|x_{u,c}|^2]$ denotes the power of an individual data stream of user u at subcarrier c. In addition, the covariance matrix of the external interference plus noise, $\mathbf{R}_{\text{z},c} \in \mathbb{C}^{N\times N}$, equals

$$\mathbf{R}_{\text{z},c} = \mathbb{E}\left[\mathbf{z}_c\mathbf{z}^{\text{H}}_c\right] = \sum_{l=1}^{L}\sigma^2_{\text{int},l,c}\mathbf{H}_{\text{int},l,c}\mathbf{H}^{\text{H}}_{\text{int},l,c} + \sigma^2_{\text{n},c}\mathbf{I} \tag{12}$$

where $\sigma^2_{\text{int},l,c}$ denotes the power of the l^{th} external interferer and $\sigma^2_{\text{n},c}$ denotes the noise power, both at subcarrier c. In general, the covariance matrix of the received signal has a very intuitive structure since it depends directly on the stream powers, channel matrices, and the external interference and noise. This kind of covariance structure is, in principle, well-known in the literature. However, I/Q imbalances cause signal leakage from the image subcarrier and thus generate additional terms to the covariance matrix, i.e., the second and fourth terms in (11). In addition, the propagation responses are modified from pure wireless channels to total effective channels including also the effects of the TX and RX electronics. The practical consequences of this kind of distortion will be quantified next in Section III.B. Notice that as a special case, the covariance matrix for the linear (non-augmented) signal model in (4) is given as the first quadrant of (11).

B. Signal-to-Interference-plus-Noise Ratio (SINR)

Next, we quantify the performance of the augmented combiner output signal under I/Q imbalances in terms of *the instantaneous SINR for an arbitrary data stream q originating from an arbitrary UE u*. In general, the total output power of an arbitrary data stream q of UE u is equal to

$$\widetilde{P}_{q,u,c} = \mathbb{E}\left[\left|\widetilde{y}_{\text{TxRxi},q,u,c}\right|^2\right] = \widetilde{\mathbf{w}}^{\text{H}}_{q,u,c}\widetilde{\mathbf{R}}_{\text{TxRxi},c}\widetilde{\mathbf{w}}_{q,u,c} \tag{13}$$

where, $\widetilde{\mathbf{w}}_{q,u,c}$ refers to the augmented combiner weight vector corresponding to data stream q of UE u at subcarrier c and is easily obtained by selecting the corresponding column from the weight matrix $\widetilde{\mathbf{W}}_c$. In order to express the SINR for this arbitrary data stream, we split the combiner output power in (13) to useful signal and interference/noise terms as follows:

$$\widetilde{P}_{q,u,c} = \widetilde{P}_{x,q,u,c} + \widetilde{P}_{\text{ISI},q,u,c} + \widetilde{P}_{\text{IUI},u,c} + \widetilde{P}_{\text{IUI},c'} + \widetilde{P}_{\text{z},c} + \widetilde{P}_{\text{z},c'}. \tag{14}$$

Here, $\widetilde{P}_{x,q,u,c}$ denotes the output power of the desired data stream q and $\widetilde{P}_{\text{ISI},q,u,c}$ represents the effect of the inter-stream interference originating from the other streams of the same UE u. These terms are both originating from UE u, but they are separated because when examining the received signal from an individual but arbitrary stream q of UE u perspective, the other streams of the same UE are also treated as interference. In addition, $\widetilde{P}_{\text{IUI},u,c}$ and $\widetilde{P}_{\text{IUI},c'}$ represent the inter-user interference from subcarriers c and c', respectively. Finally, $\widetilde{P}_{\text{z},c}$ and $\widetilde{P}_{\text{z},c'}$ denote the output powers of the external interference and noise originating from subcarriers c and c', respectively. The detailed derivations for these power terms are given in Appendix A. Then for the augmented signal model, *the instantaneous SINR of a single received data stream under joint TX+RX I/Q imbalances* can be expressed straightforwardly by

$$\widetilde{\text{SINR}}_{\text{TxRxi},q,u,c} = \frac{\widetilde{P}_{x,q,u,c}}{\widetilde{P}_{\text{ISI},q,u,c} + \widetilde{P}_{\text{IUI},u,c} + \widetilde{P}_{\text{IUI},c'} + \widetilde{P}_{\text{z},c} + \widetilde{P}_{\text{z},c'}}. \tag{15}$$

Note that this per-data-stream SINR includes the effects of the RX spatial processing with given, yet arbitrary, combiner weights, while the actual derivation of the linear and augmented linear MMSE optimum coefficients is provided in the next subsection. Furthermore, it should be noted that the SINR averaged over the channel fading distribution is, in general, given by $\overline{\text{SINR}}_{\text{TxRxi},q,u,c} = \mathbb{E}_{\mathbf{h}}[\widetilde{\text{SINR}}_{\text{TxRxi},q,u,c}]$ where $\mathbb{E}_{\mathbf{h}}[\cdot]$ denotes statistical expectation over all associated channel fading variables and $\mathbf{h}$ is composed of all non-zero elements in $\mathbf{H}_{u,c}$, $\mathbf{H}_{u,c'}$, $\mathbf{H}_{v,c}$, $\mathbf{H}_{v,c'}$, $\mathbf{H}_{\text{int},l,c}$, $\mathbf{H}_{\text{int},l,c'}$, $\forall u, v, l$. When expanding the power terms in (15), given in Appendix A, it becomes evident that deriving an exact closed-form expression for the

SINR averaged over the fading variables in the considered MU-MIMO scenario is infeasible due to the intractable algebraic representation, unlike in the more simple SU-SISO OFDM scheme [8], [10], in the SU-MISO OFDM scheme [16], or in MU-SISO SC-FDMA schemes [29], [42] with only one active UE at each subcarrier. Thus, in Section IV, we provide comprehensive numerical results where the above SINR expression is numerically averaged across all fading variables through Monte-Carlo simulations.

In general, the inter-stream and inter-user interferences as well as the external interference, all at subcarrier c, are unavoidable in the RX antennas of the considered OFDMA MU-MIMO systems but their effects on the output signal can be suppressed to some extent through antenna array processing. Based on (15), I/Q imbalances in general cause substantial SINR degradation due to signal leakage from the image subcarrier, i.e., the performance is deteriorated also by the inter-user interference and external interferences from the image subcarrier. Such a phenomenon obviously limits the overall performance and sets additional requirements for the combiner weight optimization task which will be considered in the next subsection. We emphasize that the existing works in the literature, such as [4]–[18], [22], [29], [42], have not considered the effects of the external interference and spatially multiplexed UEs causing inter-user interference.

The corresponding power and SINR expressions for the more conventional per-subcarrier combiner are obtained from (13)–(15) and (27)–(32) by substituting the augmented quantities by their linear counterparts but are not shown explicitly due to space constraints. Furthermore, the special case with I/Q imbalance only in the TXs is obtained from all expressions by substituting $\mathbf{K}_{\text{Rx1},c} = \mathbf{I}$ and $\mathbf{K}_{\text{Rx2},c} = \mathbf{0}$ for all c. Similarly, the case with I/Q imbalance only in the RX is obtained by substituting $\mathbf{K}_{\text{Tx1},i,j} = \mathbf{I}$ and $\mathbf{K}_{\text{Tx2},i,j} = \mathbf{0}$ for all $i \in \{u, v\}$ and $j \in \{c, c'\}$. We will illustrate and discuss the influence of different I/Q imbalance scenarios on the practical SINR performance in more detail in Section IV.

C. Linear and Augmented Linear MMSE Combiners

The above SINR expression is in principle valid for any possible combiner coefficients, while the optimization of the combiner coefficients is addressed next. A well-known statistical method for solving stationary estimation problems is the so-called Wiener filter which yields the optimal linear solution in the MMSE sense [43]. We have shown in [30] that the Wiener filter approach, when generalized to augmented or widely-linear processing, can be successfully used for the channel and hardware characteristic estimation problem under I/Q imbalance in SU-SIMO systems. Here this simple and intuitive approach is extended to cover the weight selection problem in the considered MU-MIMO OFDMA systems whereas other weight optimization methods could be used as well.

We first define the ordinary Wiener filter or LMMSE weights for signal model (4), i.e., under joint TX+RX I/Q imbalances. The weights are of the form

$$\mathbf{W}_{\text{TxRxi},c}^{\text{LMMSE}} = \mathbf{R}_{\text{TxRxi},c}^{-1}\mathbf{V}_{\text{TxRxi},c} \tag{16}$$

where $\mathbf{R}_{\text{TxRxi},c} = \mathbb{E}[\mathbf{r}_{\text{TxRxi},c}\mathbf{r}_{\text{TxRxi},c}^{\text{H}}] \in \mathbb{C}^{N\times N}$ denotes the covariance matrix of the received signal and is equal to top-left quadrant of $\widetilde{\mathbf{R}}_{\text{TxRxi},c}$ in (11). In addition, $\mathbf{V}_{\text{TxRxi},c} = [\mathbf{v}_{\text{TxRxi},1,1,c}, \cdots, \mathbf{v}_{\text{TxRxi},Q_U,U,c}] \in \mathbb{C}^{N\times S}$ is a matrix consisting of the cross-correlation vectors between the received signal snapshots and transmitted data streams. Under joint TX+RX I/Q imbalances the cross-correlation vector, related to data stream q of user u, is easily shown to read

$$\mathbf{v}_{\text{TxRxi},q,u,c} = \mathbb{E}\left[\mathbf{r}_{\text{TxRxi},c}x_{q,u,c}^{*}\right] = \sigma_{x,u,c}^{2}\widetilde{\mathbf{\Psi}}_{u,c}\mathbf{G}_{u,c}\mathbf{e}_q. \tag{17}$$

Now, the combiner weight vector related to data stream q of UE u at subcarrier c is equal to

$$\mathbf{w}_{\text{TxRxi},q,u,c}^{\text{LMMSE}} = \mathbf{R}_{\text{TxRxi},c}^{-1}\mathbf{v}_{\text{TxRxi},q,u,c}. \tag{18}$$

Notice that if I/Q imbalances are set to zero, (18) reduces to the classical Wiener filter as expected.

We next proceed to the augmented combiner coefficient optimization in the MMSE sense, referred to as augmented LMMSE or augmented Wiener filter in the following. The weight optimization problem under joint TX+RX imbalances corresponds to solving the augmented weights as

$$\widetilde{\mathbf{W}}_{\text{TxRxi},c}^{\text{LMMSE}} = \widetilde{\mathbf{R}}_{\text{TxRxi},c}^{-1}\widetilde{\mathbf{V}}_{\text{TxRxi},c} \tag{19}$$

where $\widetilde{\mathbf{R}}_{\text{TxRxi},c}$ is given in (11) and $\widetilde{\mathbf{V}}_{\text{TxRxi},c} = [\widetilde{\mathbf{v}}_{\text{TxRxi},1,1,c}, \cdots, \widetilde{\mathbf{v}}_{\text{TxRxi},Q_U,U,c}] \in \mathbb{C}^{2N\times S}$ is the cross-correlation matrix. There, the column vector related to data stream q of UE u at subcarrier c reads

$$\begin{aligned}\widetilde{\mathbf{v}}_{\text{TxRxi},q,u,c} &= \mathbb{E}\left[\widetilde{\mathbf{r}}_{\text{TxRxi},c}x_{q,u,c}^{*}\right] \\ &= \begin{bmatrix}\sigma_{x,u,c}^{2}\widetilde{\mathbf{\Psi}}_{u,c}\mathbf{G}_{u,c}\mathbf{e}_q \\ \sigma_{x,u,c}^{2}\widetilde{\mathbf{\Omega}}_{u,c'}^{*}\mathbf{G}_{u,c}\mathbf{e}_q\end{bmatrix} \\ &= \sigma_{x,u,c}^{2}\widetilde{\mathbf{\Xi}}_{u,c}\mathbf{G}_{u,c}\mathbf{e}_q\end{aligned} \tag{20}$$

and the augmented weight vector related to the same data stream becomes consequently equal to

$$\widetilde{\mathbf{w}}_{q,u,c}^{\text{LMMSE}} = \widetilde{\mathbf{R}}_{\text{TxRxi},c}^{-1}\widetilde{\mathbf{v}}_{\text{TxRxi},q,u,c}. \tag{21}$$

This kind of processing methods, which can efficiently suppress not only the classical mirror-subcarrier crosstalk within a single UE but more generally the inter-user interference inside a subcarrier and between mirror-subcarriers, as well as the external interference and noise, in spite of substantial I/Q imbalances in multi-antenna TXs and RXs, will play a big role in MU-MIMO networks especially in interference-limited conditions. Moreover, the derived augmented combiner can provide good performance also under reasonable levels of carrier frequency offsets (CFOs) and timing offsets, under the following assumptions. In practical systems the maximum CFO between the UEs and the BS is typically relatively small. E.g., it is said in the LTE/LTE-Advanced specifications [44], [45] that *"the UE modulated carrier frequency shall be accurate within* ± 0.1 PPM *observed over a period of one time slot* (0.5 ms) *compared to the carrier frequency received from the E-UTRA Node B."* With 2 GHz carrier frequency, as a concrete example, this would mean a CFO equal to maximum of $\pm$ 200 Hz which is very small relative to 15 kHz subcarrier

spacing (maximum of 1.3%). Therefore, the resulting inter-carrier interference and inter-user interference are also very small. Also, the simplest approximation of the CFO effects is that small CFOs map only to common phase error per UE and per OFDMA symbol being thus a part of the effective wireless channel, and is properly handled and processed as long as the system supports regular reference signals for channel estimation. If further assuming that the timing offsets are within the cyclic prefix length for all spatially multiplexed UEs, also these offsets simply map to being part of the effective frequency selective fading channels which are structurally processed in the proposed augmented combiner. We also emphasize that there are no explicit constraints related to synchronization of the co-channel interference signals, as they are treated in the modeling and analysis as arbitrary waveforms.

As will be illustrated by the numerical results in Section IV, the formulated augmented Wiener combiner has the structural capability to achieve substantially better performance compared to more classical per-subcarrier processing, assuming that the needed correlations devised above are available. In practice, the Wiener solutions can be well approximated by various adaptive estimation methods based on known training or reference signals [46]. In the next subsection, we shortly address how the selection of the weight estimation algorithm influences the overall computational complexity and achievable performance in the considered MU-MIMO scenario.

D. Spatial Processing Computational Complexity Aspects

In this subsection we focus on computing complexity aspects of the developed RX processing scheme with joint channel equalization, data stream separation and I/Q imbalance mitigation. In particular, we present the computational complexities of the three main digital signal processing blocks in the MIMO BS, namely the FFT processing, weight estimation and digital combining. All the computational complexities are here given in *real-valued* arithmetic operations (additions and multiplications) called floating point operations (flops) unless otherwise stated.

1) FFT processing: In OFDMA RXs FFT processing takes down-converted and digitized received signals as an input and converts them to subcarrier level observations. The computational complexity of C-point FFT with the current state-of-the-art split-radix implementation is given by [47]

$$\begin{aligned}\Theta_{\text{FFT}} = &\frac{34}{9}C\log_2 C - \frac{124}{27}C - 2\log_2 C \\ &- \frac{2}{9}\left(-1\right)^{\log_2 C}\log_2 C + \frac{16}{27}\left(-1\right)^{\log_2 C} + 8.\end{aligned} \tag{22}$$

This is the overall complexity of the whole FFT block in a single RX branch and thus the result in (22) can be divided by C if one seeks to quantify the computational load from a single subcarrier perspective.

2) Weight estimation: After the FFT processing, the receiving BS must estimate the combining weights. While the previous subsection presented the LMMSE and augmented LMMSE optimum combiner solutions, they can in practice be well estimated or approximated using reference signals together with adaptive filtering algorithms [46], [48]. Here, we shortly address the computational complexities of two elementary adaptive algorithms, namely the least mean squares (LMS) and recursive least squares (RLS), while various alternative algorithms can also be adopted in practice. In order to easily compare the computational burden between the linear per-subcarrier and the augmented subcarrier processing methods, we define N_{in} to denote the number of parallel input samples of the estimation algorithm. For the linear per-subcarrier processing $N_{\text{in}} = N$ whereas for the augmented combiner $N_{\text{in}} = 2N$ due to joint processing of signals from subcarriers c and $c^{'}$ as visible in Fig. 3.

The well-known form of the LMS algorithm, described in detail in [48, p. 238], requires $2N_{\text{in}} + 1$ complex-valued multiplications and $2N_{\text{in}}$ complex-valued additions per iteration round. Thus, the resulting per-data-stream complexity of LMS at a single subcarrier is given by

$$\Theta_{\text{LMS},c} = 16N_{\text{in}} + 6. \tag{23}$$

Correspondingly, a straightforward RLS implementation, equal to the one in [48, p. 442], requires $4N_{\text{in}}^2 + 3N_{\text{in}}$ complex-valued multiplications, $3N_{\text{in}}^2 + N$ complex-valued additions and $2N_{\text{in}}^2$ real-valued multiplications per iteration round. Consequently, the per-data-stream complexity of RLS at a single subcarrier is equal to

$$\Theta_{\text{RLS},c} = 32N_{\text{in}}^2 + 20N_{\text{in}}. \tag{24}$$

The computational complexity of RLS is clearly higher than that of LMS. Furthermore, with large N the ratio of the complexity between the augmented processing and the linear per-subcarrier processing is two for LMS and four for RLS.

3) Digital combining: When the weights have been estimated, the BS adjusts the amplitudes and phases of the signals in different antennas branches and finally adds up all the antenna signals. These operations cause N_{in} complex-valued multiplications and $N_{\text{in}} - 1$ complex-valued additions which results in the total per-data-stream computational complexity given by

$$\Theta_{\text{combining},c} = 8N_{\text{in}} - 2. \tag{25}$$

Note that also here the complexity of the augmented processing is practically doubled when compared to that of the ordinary per-subcarrier processing.

4) Overall Complexity and Discussion: The signal path from the ADC outputs to the combiner output includes the FFTs, weight estimation and digital combining. Whereas the FFT processing is carried out only once for a given signal block in every RX branch, the weight estimation and combining are done separately for each data stream but jointly for all RX branches. The ratios between the overall complexities of the augmented processing and the linear per-subcarrier processing are presented in Table IIa when the weights of an arbitrary stream are estimated with the LMS principle, and similarly in Table IIb with the RLS approach. The results show that with LMS, the augmented processing requires 33%–98% more computational effort than the per-subcarrier processing. The corresponding results of RLS show an increase equal to 121%–298%. Interestingly, these results clearly indicate that the augmented processing is not necessarily doubling the overall

TABLE II: The ratio of the computational complexities between the augmented subcarrier processing and the linear per-subcarrier processing as a function of the number of RX antennas N and the number of data streams S. Comparison includes FFT processing, weight estimation with the given algorithm as well as digital combining.

(a) Weights solved by the augmented/linear LMS.

N	S	FFT size				
		64	256	1024	2048	8192
1	1	1.52	1.45	1.39	1.37	1.33
10	5	1.86	1.81	1.77	1.75	1.72
20	10	1.92	1.90	1.87	1.86	1.84
100	50	1.98	1.98	1.97	1.97	1.96

(b) Weights solved by the augmented/linear RLS.

N	S	FFT size				
		64	256	1024	2048	8192
1	1	2.63	2.48	2.36	2.31	2.21
10	5	3.81	3.80	3.79	3.78	3.77
20	10	3.91	3.91	3.90	3.90	3.90
100	50	3.98	3.98	3.98	3.98	3.98

complexity, as often misleadingly stated, but the increase is highly dependent on the considered scenario. In particular, the less RX antennas are involved and the less data streams need to be separated, the closer is the complexity of the augmented processing to that of the per-subcarrier processing. Moreover, when increasing the number of subcarriers, the influence of the computationally heavy FFT processing is emphasized and thus the difference between the augmented and linear processing methods decreases.

The results and discussion above are based on the conventional implementations of the adaptive algorithms. More advanced versions of the algorithms, such as the normalized LMS [48, p. 324], would naturally change the exact results. However, our intention here is to highlight that the increase in the computational complexity of the augmented subcarrier processing can vary from only a few tens of percents to several hundreds of percents when compared to the conventional linear processing. Consequently, the selection between the augmented and conventional processing needs always careful consideration and is eventually a trade-off between the complexity and performance.

IV. Numerical Evaluations, Illustrations and Analysis

A. Simulation Setup

In the numerical evaluations we consider an uplink OFDMA MU-MIMO scenario with $U = 5$ UEs transmitting towards a single BS, all being active at the considered subcarrier c simultaneously. In addition, there are $V = 5$ other UEs which communicate with the BS at the corresponding image subcarrier c'. The BS is equipped with an antenna array consisting of $N = 20$ antenna elements. Furthermore, each UE has $M_u = M_v = 2$ TX antennas, illustrating a typical UE level capability in modern communications systems. Due to the rather low TX antenna number, each UE transmits only $Q_{u,c} = Q_{v,c'} = 2$ data streams at each subcarrier and for simplicity the precoding is selected to be a simple one-to-one mapping between the data streams and TX antennas. The input signal-to-noise ratio (SNR) in the individual RX branches is equal to 20 dB. Here, we define the SNR as the ratio between the total averaged received signal power originating from all TX data streams of a single user, and the noise power. The transmitted data streams are independent and the total TX power of a single UE is equally shared between its TX branches and data streams. We do realize that the chosen scenario in terms of the number of spatially multiplexed UEs and the number of BS antennas is something that is not necessarily yet feasible in today's systems. However, our intention is to push the capabilities of spatial multiplexing beyond the current systems and to understand, in particular, the sensitivity and limitations imposed by RF circuit imperfections in bigger and bigger antenna array deployments at the advent of massive MIMO [31]–[33], with a high number of spatially multiplexed UEs. The above basic scenario, in terms of, e.g., the SNR level and the number of BS antennas, is also varied in the evaluations.

At the desired subcarrier as well as at the image subcarrier, we also consider $L_c = L_{c'} = 8$ external single-antenna interferers with equal powers in the simulation setup. The signal-to-interference ratio (SIR) is defined as the ratio between the total averaged received signal power originating from all TX branches of a single user, and the total received power originating from all external interferers. Note that if the number of the interferers is increased, the power of each individual interferer is decreased in order to obtain the same total SIR. The transmission channels between all TX-RX antenna pairs as well as between all interferer-RX antenna pairs are independent and Rayleigh distributed.

I/Q imbalance is defined in terms of the image rejection ratio (IRR) given in decibels for a single transceiver branch by IRR $= 10\log_{10}(|K_1|^2/|K_2|^2)$ [27]. Firstly, the minimum allowable IRR (IRR_{min}) is set to 25 dB which can be considered to be a typical value for the radio front-end in mobile UEs, as defined, e.g., in 3GPP LTE/LTE-Advanced UE specifications [44]. Secondly, we draw phase imbalance coefficients $\phi_{\text{Tx},u,m,c}, \forall u, m, c$ and $\phi_{\text{Rx},c,n}, \forall n, c$ independently from $\mathcal{U}(-\alpha, \alpha)$ where α guarantees the selected IRR_{min} if the gain imbalance was set to zero. Finally, the gain imbalance coefficients $g_{\text{Tx},u,m,c}, \forall u, m, c$ and $g_{\text{Rx},c,n}, \forall n, c$ are selected independently from the conditional distribution $\mathcal{U}(g_{\text{min}}, g_{\text{max}})$ where the range edges correspond to IRR_{min} with the earlier selected ϕ. The I/Q imbalance parameters at different subcarriers are assumed to be independent for modeling arbitrarily frequency selective I/Q imbalance. The basic simulation parameters are summarized in Table III while many of the parameters are also systematically varied in the evaluations.

All results describe the performance from a single yet arbitrary subcarrier point of view due to the subcarrier-dependent data streams in the OFDMA systems. In order to illustrate the obtainable performance on average, the results are averaged over all data streams, UEs and 2000 realizations of the I/Q imbalance parameters and the underlying complex fading variables. For each realization, the channel matrices and I/Q imbalance parameters are randomly and independently generated according to the aforementioned criteria. All evaluations

TABLE III: Basic simulation parameters

Parameter	Symbol	Value
RX antennas	N	20
Number of UEs	U, V	5
TX antennas in UEs	M_u, M_v	2
Data streams in UEs	$Q_{u,c}$, $Q_{v,c'}$	2
Number of external interferers	L_c, $L_{c'}$	8
TX antennas in ext. interferers	J_l	1
Signal to noise ratio	SNR	20 dB
Signal to interference ratio	SIR_c, $\text{SIR}_{c'}$	-20 dB
Minimum image rejection ratio	IRR_{min}	25 dB

are carrier out for both the linear and the augmented linear MMSE RXs. Furthermore, both SINRs and symbol-error rates (SERs) are evaluated.

B. SINR and SER Simulation Results and Analysis

1) SINR as a function of the SIR: The SINR as a function of the SIR is depicted in Fig. 4. Here the power of the external interference is swept at both the desired subcarrier and the image subcarrier while the useful signal powers are kept equal and constant at both subcarriers. First of all, we notice saturation of the performance with high and low SIRs, even with perfect I/Q matching. In the *high SIR region*, the combiners can suppress the inter-user interference effectively and the influence of the external interference is very small. Therefore, the ceiling effect is mainly caused by the additive noise and the spatially multiplexed streams of different UEs. The resulting SINR is actually better than the input SNR since the effect of the noise can be decreased with the antenna array processing, as in the noise limited case, $N = 20$ RX antennas provide extra degrees of freedom relative to separating 5×2 = 10 overall streams at the considered subcarrier. Under I/Q imbalances, on the other hand, the performance is limited due to the signal leakage from the image subcarrier UEs. Clearly, TX and RX I/Q imbalances are equally deteriorating the overall performance in high SIR region. The worst SINR is, in turn, seen with joint TX+RX I/Q imbalances which result in an approximately 2.6 dB worse SINR compared to the perfect I/Q matching case.

When the *SIR decreases*, the external interference gets stronger and starts to dominate the received signal. Consequently, the combiners put structurally more effort into the external interference suppression. This is done through the spatial response of the interferers, i.e., the RXs effectively generate nulls to their responses such that the external interference coming through the spatial channels is suppressed efficiently. Actually, the SINR saturation visible in the *low SIR region* tells us that a state, where practically all effects of the external interference are suppressed, can be found in each of the cases. However, this kind of interference suppression takes lots of resources. Consequently, the resulting SINR is decreased since the combiners cannot provide as high UE stream separation and noise suppression as with higher SIRs. This is especially visible with the per-subcarrier Wiener combiner under RX and TX+RX I/Q imbalances. In those cases the combiner must mitigate not only the interference from the subcarrier c but also from the mirror subcarrier c' and therefore the combiner easily runs out of degrees of freedom. Under TX I/Q imbalance the situation is easier since the external interference does not leak to subcarrier c. The SINR degradation is then caused purely by the mirroring effect on the TX side which causes inter-user interference between the UEs at the mirror subcarriers. The augmented combiner, in turn, provides the same performance under all I/Q imbalance scenarios as the per-subcarrier combiner with ideal I/Q matching. In these cases the influence of the external interference and the inter-user interference as well can be suppressed very efficiently while still providing a slight array processing gain (the original SNR is 20 dB). We conclude that, in general, and as obvious in Fig. 4, the augmented combiner can provide substantial enhancement in the output SINR, especially under high levels of the external interference.

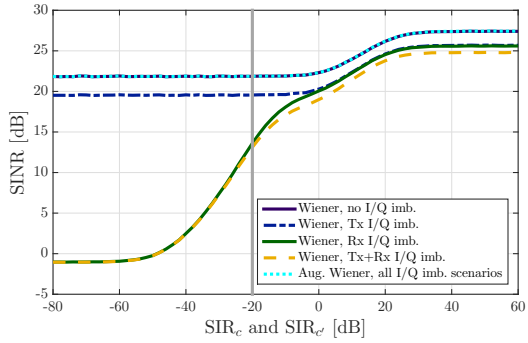

Fig. 4: Average SINR as a function of the SIR at both the desired subcarrier and the image subcarrier when the other parameters are fixed. The gray vertical line shows the operating point under the basic conditions given in Table III.

2) SINR as a function of the $\text{SIR}_{c'}$: The leakage of the external interference at the image subcarrier is further illustrated in Fig. 5. It shows the SINR when the SIR at the image subcarrier is swept while the SIR at the desired subcarrier is fixed to -20 dB. Based on the results, the augmented combiner has a flat and robust response over all $\text{SIR}_{c'}$ values and with all I/Q imbalance scenarios. This means that it can suppress the effect of the signal leakage very efficiently and thus provides good performance in all conditions. Also the per-subcarrier processing under TX I/Q imbalance only yields a flat response which has 2.3 dB lower SINR level than with the augmented combiner. This difference is purely caused by the inter-user interference from the image subcarrier since the external interference and noise at the image subcarrier are not affected by TX I/Q imbalance. The response of the ordinary Wiener combiner is not flat when considering I/Q imbalance in the RX side. In that case, the SINR drops drastically as $\text{SIR}_{c'}$ decreases. When comparing Figs. 4 and 5 with each other, we notice that actually the interference leakage is the main reason for performance degradation with high external interference levels since in those cases the resulting SINRs are almost the same in both figures. Also now, the combiner puts most of its structural resources to interference suppression and reaches saturation of the SINR. However, it simultaneously sacrifices lots of the data stream separation and noise suppression capabilities

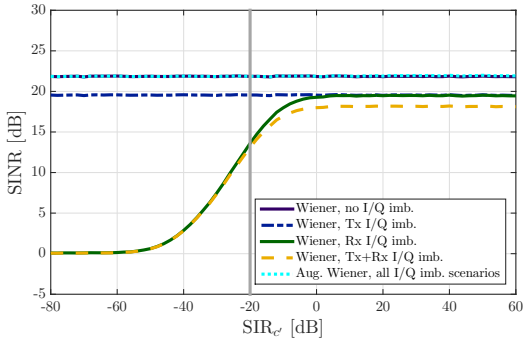

Fig. 5: Average SINR as a function of the SIR at the image subcarrier when the other parameters are fixed. The gray vertical line shows the operating point under the basic conditions given in Table III.

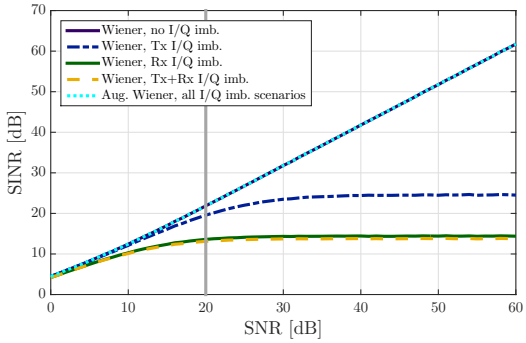

Fig. 6: Average SINR as a function of the SNR when the other parameters are fixed. The gray vertical line shows the operating point under the basic conditions given in Table III.

and consequently the resulting SINR level is fairly low. The results clearly indicate that the overall SINR performance of the ordinary per-subcarrier Wiener combiner is heavily deteriorated by the strong external interference at the image subcarrier, even if the contribution of the external interference at the considered subcarrier can be efficiently suppressed.

3) SINR as a function of the SNR: Fig. 6 visualizes the SINR as a function of the input SNR. The performance saturates under I/Q imbalances and the worst performance with the Wiener combiner is obtained if I/Q imbalance occurs in the RX electronics. The ceiling effect, due to the unavoidable signal leakage from the image subcarrier, is very strong and the SINR saturates at around 25 dB SNR with RX and TX+RX imbalance scenarios and at around 35 dB SNR with TX I/Q imbalance. At these points, the external interference and inter-user interference, both from subcarriers c and c', fully dominate the SINR behavior and the contribution of the noise is practically negligible. Again, the augmented combiner outperforms the conventional one clearly and results in a linear growth of the SINR against input SNR. The results in Fig. 6 also extend the work related to the SU-SIMO scenario in [30] and show somewhat similar behavior in both cases.

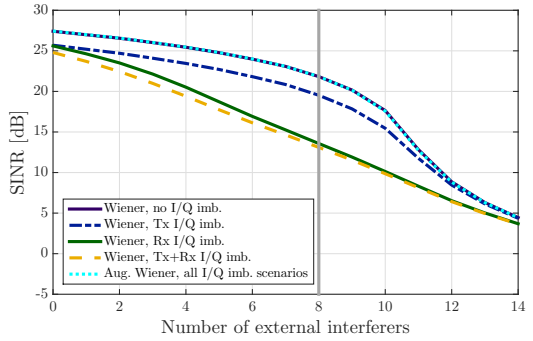

Fig. 7: Average SINR as a function of the number of external interferers L when the other parameters are fixed. The gray vertical line shows the operating point under the basic conditions given in Table III.

4) SINR as a function of L: The effect of increasing the number of external interferers is depicted in Fig. 7. With the simulation parameters given in Table III, there are $M_u U + J_l L = 18$ incoming signals at the desired subcarrier as well as at the image subcarrier. In theory, the linear combiners are able to separate $N = 20$ signals as long as all the signal sources have separable spatial characteristics, i.e., their channel responses are not fully correlated. Thus the number of single-antenna interferers could be even increased to $L = 10$, resulting in 20 incoming signals in total, without losing the ability for signal separation in theory. However, based on the figure, the SINR decreases as the number of interferers increases, even for less than $L = 10$ external interferers. This is natural as optimizing the MSE at the combiner output, corresponds to finding a proper compromise between coherent combining of the desired signal as well as suppressing the inter-stream, inter-user and external interference as well as noise, and all of their mirror images. Thus, when the number of signals increases, the optimization task becomes increasingly difficult. The best SINR is provided by the augmented combiner under any I/Q imbalance scenario whereas the per-subcarrier Wiener processing under RX and TX+RX I/Q imbalances turns out to have the worst SINRs. This is again caused by the interference leakage from the image subcarrier and is now emphasized since the number of the interferers is swept at both subcarriers. When the number of interferers exceeds 10, also the augmented combiner runs out of degrees of freedom in interference suppression and consequently the SINRs of all scenarios drop steeply towards lower levels.

5) SINR as a function of the IRR$_{\text{min}}$: Fig. 8 shows the SINR performance when the minimum allowable IRR is varied. The augmented combiner produces a flat response for all IRR$_{\text{min}}$ values, meaning that the effects of I/Q imbalances are mitigated completely even for low IRRs. The performance of the ordinary per-subcarrier processing under TX I/Q imbalance is deteriorated by the inter-user interference from the image subcarrier and therefore the SINR degrades fairly slowly as IRR$_{\text{min}}$ decreases. In contrast, the SINR under RX I/Q imbalance is heavily degraded, again due to the increasing external interference leakage from the image subcarrier. It is

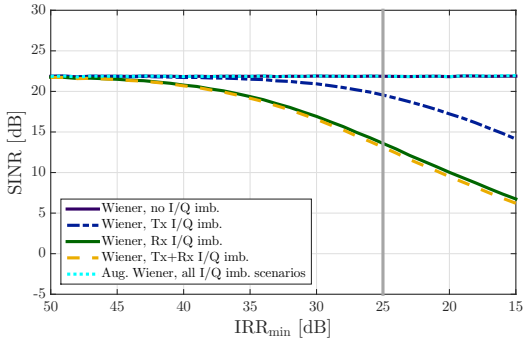

Fig. 8: Average SINR as a function of the IRR$_{\text{min}}$ when the other parameters are fixed. The gray vertical line shows the operating point under the basic conditions given in Table III.

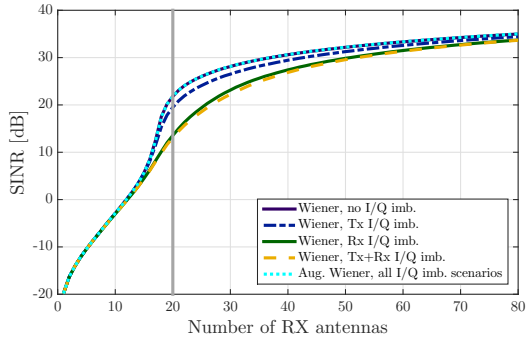

Fig. 9: Average SINR as a function of the number of RX antennas N when the other parameters are fixed. The gray vertical line shows the operating point under the basic conditions given in Table III.

worth noting that under RX or TX+RX I/Q imbalances and even with very moderate values of IRR$_{\text{min}}$ the SINR is degraded by several decibels. Even with IRR$_{\text{min}}$ $= 35$ dB, which is already a challenging number to achieve systematically, the per-subcarrier Wiener processing is some 2.5 dB below the SINR of the augmented Wiener combiner.

6) SINR as a function of N: Fig. 9 illustrates the SINR as a function of the number of RX antennas. Although modern communications systems usually support at most 4–8 antennas to be used in the BSs, this figure shows the capability of antenna array processing and thus gives an important insight also for the behavior towards emerging massive MIMO systems under I/Q imbalances, see e.g. [49]. Based on the results with varying number of RX antennas, the performance is really poor when the number of RX antennas is around 12 or less due to too little degrees of freedom to spatially separate the signals. Beyond that point, the RX starts to be able to separate different signals and the SINR of the augmented combiner grows very steeply as N increases. Also the per-subcarrier Wiener processing under TX I/Q imbalance only gets a similar performance boost. The both curves start to saturate after the point where the number of antennas matches with the number of incoming signals which is in this case equal to $M_u U + J_l L = 18$. In contrast to these curves, RX and TX+RX I/Q imbalances cause slower increase in the resulting SINR and their saturation starts later, around the point $N = 28$. That point coincides with $N = M_u U + 2J_l L$ which means that at this point the per-subcarrier Wiener processing is finally able to separate the signals from the desired subcarrier and strong interferers at both subcarriers from each others. Thus it is able to provide the same SINR as the augmented combiner has already with $N = 20$ antennas. As the number of antennas becomes very high, both combiners perform well under all I/Q imbalance scenarios. Additionally, the SINR increases only slightly when adding RX antennas to the BS side. This is a consequence of the situation where both combiners have more than enough spatial resources and they can use the extra degrees of freedom purely for noise optimization and interference suppression purposes.

7) SER as a function of SNR: In order to evaluate the performance of the augmented Wiener combiner with respect

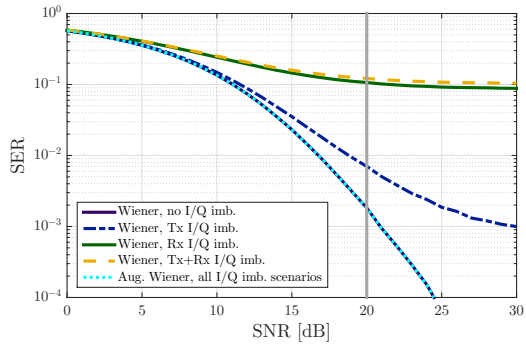

Fig. 10: Average uncoded SER as a function of the SNR when the other parameters are fixed and 16-QAM signal constellation is used. The gray vertical line shows the operating point under the basic conditions given in Table III.

to another commonly used metric we next provide the uncoded SER performance as a function of the SNR in Fig. 10. Here, we use 16-QAM signal constellation and all SERs are averaged over all data streams of all UEs and over 20000 realizations of the I/Q imbalance parameters and the underlying complex fading variables. We notice that the SER decreases as the SNR increases in all cases, which is of course natural. Additionally, we see that RX I/Q imbalance with the per-subcarrier combiner causes the SER to saturate to high levels. This was also expected based on the SINR results given in Fig. 6. Note that the exact level of the saturation might vary due to different antenna setups, I/Q imbalance parameters, signal constellations, channel models etc. Similar to RX I/Q imbalance only, saturation of the SER is visible also with joint TX+RX I/Q imbalances, again with the per-subcarrier combiner. The level of the saturation is even slightly higher than with RX I/Q imbalance only. When considering I/Q imbalance only on the TX side, the SER performance is much better than under RX and TX+RX I/Q imbalances. In addition, such a strong SER saturation is not visible under TX I/Q imbalance. The augmented combiner, in turn, provides the same SER as a system under ideal I/Q matching and consequently, no performance degradation is

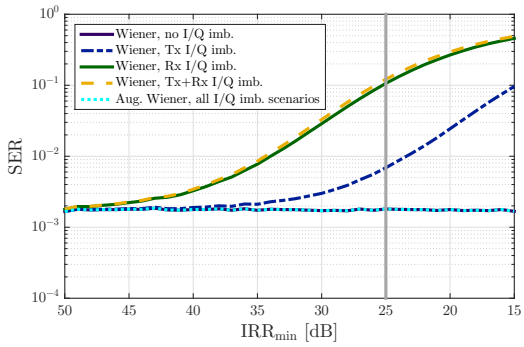

Fig. 11: Average uncoded SER as a function of the IRR$_{\text{min}}$ when the other parameters are fixed and 16-QAM signal constellation is used. The gray vertical line shows the operating point under the basic conditions given in Table III.

seen due to any I/Q imbalance. Note that this is a significant difference to the per-subcarrier combiner which suffers heavily from the signal distortion.

8) SER as a function of IRR$_{\text{min}}$: The performance evaluation is continued in Fig. 11 where the SER is depicted as a function of the IRR$_{\text{min}}$. As seen already in the SINR evaluations in Fig. 8, the performance degrades as the IRR$_{\text{min}}$ decreases. The SER evaluations clearly indicate that the augmented combiner structure can very effectively suppress the effects of I/Q imbalance and thus provides new possibilities, e.g., in terms of cheaper RF components or more robust operation. In contrast, the SER of the conventional per-subcarrier combiner is highly deteriorated by I/Q imbalances and consequently, the system performance is degraded.

C. Further Aspects in Massive MIMO Framework

In order to get the massive MIMO concept into reality, research and profound understanding are needed regarding the associated RF imperfections [32], [33]. It is indicated in some studies in the existing literature that massive MIMO systems are robust to RF imperfections or the effect of the imperfections is very small, see e.g. [37], [38]. This statement may hold for simple cases where the effect of RF impairments is modeled as additive uncorrelated Gaussian noise. However, in general, RF impairments distort the transmitted and received signals in a more complicated manner and the resulting signal distortion is dependent, e.g., on the signal power and subcarrier allocation scheme, and consequently the results with simplified distortion models may not be precise or valid anymore.

In this subsection, we specifically focus on practical aspects of I/Q imbalances in massive MIMO deployments, building on our earlier signal and system modeling, and consider two specific scenarios. Toward this end, we modify the system scenario and parameterization compared to what we had in the previous subsection. In particular, we increase the number of RX antennas considerably, being eventually an order of magnitude higher than the number of spatially multiplexed UEs at each subcarrier which is a typical assumption in massive MIMO systems [31], [32], [38]. As also in the previous

TABLE IV: Basic simulation parameters for massive MIMO setup.

Parameter	Symbol	Value
RX antennas	N	100
Number of UEs	U	5
TX antennas in UEs	M_u	1
Data streams in UEs	$Q_{u,c}$	1
Number of external interferers	L_c, $L_{c'}$	0
Signal to noise ratio	SNR	20 dB
Image rejection ratio	IRR	20 dB

subsection, we assume that each RX antenna is connected to a separate RX branch. Moreover, we assume that the UEs are simple single-antenna devices, i.e., $M_u = 1$, and consequently set also the number of transmitted data streams in each UE to $Q_{u,c} = 1$. This way the network is considered to support also low-cost and simple UEs which are, e.g., a crucial element in the increasingly popular internet of things (IoT) concept. We also fix IRR $= 20$ dB since the transceivers in massive MIMO systems, especially in the BS side, are considered to be implemented with low-cost components which, in turn, are prone to severe impairments [32], [50], [51]. In addition, we assume no external interference, i.e., $L = 0$, since the massive MIMO concept is often considered to be adopted at centimeter or millimeter wave frequencies where the interference even from closely located devices may be low due to high propagation losses. Finally, there has been some speculation that, in order to achieve a very simple system, massive MIMO could be adopted without frequency multiplexing through the OFDMA principle, thus resulting in a plain OFDM based scheme where simultaneous UE multiplexing is carried out only spatially. Therefore, in the following, we set $u = v$ and $U = V$, i.e., the same set of UEs use both subcarriers c and c'. All parameters for the massive MIMO scenario are summarized in Table IV.

Massive MIMO systems require extreme simplicity not only in the hardware but also in the associated signal processing [32]. Consequently, we adopt maximum ratio combining (MRC), which is known of its low computational burden and straightforward implementation, as a benchmark against the per-subcarrier Wiener and augmented Wiener approaches. In general, the classical MRC weights for a single UE are of the form $\mathbf{W}_{u,c}^{\text{MRC}} = \mathbf{H}_{u,c}$ [52]. However, under RF impairments, the effective channel includes also the influence of imperfect electronics in the TX and RX and consequently, stemming from our earlier modeling, the MRC weights under I/Q imbalances become equal to

$$\mathbf{W}_{u,c}^{\text{MRC}} = \widetilde{\mathbf{\Psi}}_{u,c}. \tag{26}$$

Here, MRC is, indeed, assumed to be aware of the user-specific effective propagation channel $\widetilde{\mathbf{\Psi}}_{u,c}$ incorporating partially the I/Q imbalance response as given in (5). This assumption is justified since in practice the channel estimation is really done for the effective spatial channel matrix and thus it does include also the effects of non-ideal transceivers. It is worth noting that the MRC detector of UE u can utilize neither the channel information of the other UEs nor of the possible external interferers.

In the numerical evaluations, we focus now on the influence of I/Q imbalances while varying the number of RX antennas and the number of UEs. Fig. 12 illustrates the SINR of the MRC, Wiener and augmented Wiener approaches as a function of the number of RX antennas. At first, we notice that all methods have a slope equal to $10\log_{10}(N)$ under perfect I/Q matching, i.e., without I/Q imbalance. What is interesting, however, is that MRC has some 25 dB worse SINR than the other methods. This is caused by the fact that MRC cannot structurally suppress any interference including, in this case, also the inter-user interference from the other spatially multiplexed UEs. This also means that, under the considered scenario, MRC requires roughly 300 times more RX antennas than Wiener and the augmented Wiener in order to provide an equal SINR performance, which is practically not feasible. Under I/Q imbalances, the SINR performance is even more interesting. The SINR of MRC does not anymore follow the slope of $10\log_{10}(N)$. In fact, it saturates to 20 dB *even when the number of RX antennas approaches infinity*. This is explained by the following fact. As visible in (26), the MRC weights are matched to the effective channel $\widetilde{\mathbf{\Psi}}_{u,c}$ which, in turn, is dominated by the term $\mathbf{K}_{\mathrm{Rx1},c}\mathbf{H}_{u,c}K_{\mathrm{Tx1},u,c}$, as given in (5). However, when interpreting the received signal (4) from the OFDM perspective, the inter-carrier interference from the same UE propagates through $\widetilde{\mathbf{\Omega}}_{u,c}$ which includes a term $\mathbf{K}_{\mathrm{Rx1},c}\mathbf{H}_{u,c}K_{\mathrm{Tx2},u,c}$, see again (5). Thus, the only difference lies in the different TX I/Q imbalance scaling factors. Based on this, we conclude that *the SINR of MRC under TX+RX I/Q imbalances is limited to* $10\log_{10}(|K_{\mathrm{Tx1},u,c}|^2/|K_{\mathrm{Tx2},u,c}|^2)$ *which is exactly the same as the TX IRR*. In contrast, the per-subcarrier Wiener has 3–6 dB loss in the SINR compared to the no I/Q imbalance case. This is caused purely by the leakage of the UE signals from the image sucarrier since there are no external interference sources involved now. It is, however, important to note that the Wiener method still provides the same slope in the SINR and thus its performance is not restricted to any fixed upper bound. The augmented Wiener under TX+RX I/Q imbalance has, again, an equal performance to a system with no I/Q imbalance and hence it outperforms the per-subcarrier methods clearly. For any given SINR target, by using the augmented Wiener processing, one can thus lower the number of deployed antennas or the transceiver I/Q matching specifications, or both.

Next, the SINR as a function of the number of UEs is depicted in Fig. 13. As expected, the increasing number of spatially multiplexed UEs decreases the SINR in all cases. Naturally, this stems from the increased inter-user interference as well as from the limited degrees of freedom in the RX processing. Also now, MRC has the worst SINR performance and this time there are no big differences between the I/Q imbalance scenarios. It is noticeable that the SINR of MRC may be, in practice, too low for many communications applications especially when the ratio between the number of RX antennas and UEs, i.e. N/U, decreases. On the contrary, the per-subcarrier Wiener has much better SINR than MRC. However, it cannot structurally suppress the inter-carrier and inter-user interference and thus suffers heavily from I/Q imbalance. Therefore, the augmented subcarrier processing

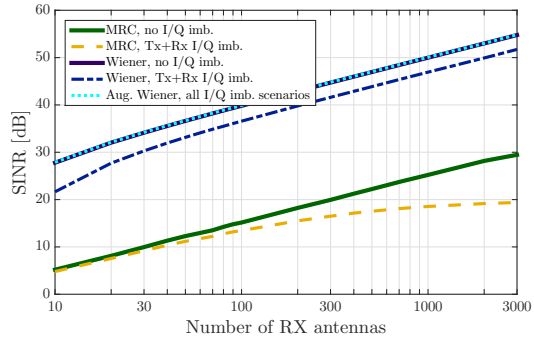

Fig. 12: Average SINR as a function of the number of RX antennas N for massive MIMO scenario. Note the logarithmic x-axis. Basic simulation parameters are given in Table IV.

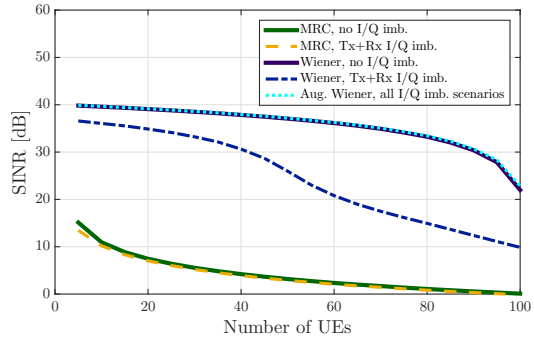

Fig. 13: Average SINR as a function of the number of UEs U for massive MIMO scenario. Basic simulation parameters are given in Table IV.

turns out to have, once more, the best SINR performance among the considered processing methods. Naturally, this performance improvement comes at a cost of more complex combining process but may still provide the best cost/quality ratio even in massive MIMO systems. Furthermore, we want to emphasize that, as discussed in Section III.D, the overall complexity of the whole digital signal processing chain is not necessarily increased dramatically when changing the per-subcarrier processing to the augmented one.

V. Conclusion

Radio transceiver I/Q imbalances in MIMO communications with OFDM waveforms have been widely studied in the existing literature. This paper, however, extended the system approach to multiuser OFDMA-based MIMO uplink where multiple UEs are active simultaneously at each subcarrier and in addition to that frequency division multiplexing is deployed. We also included the effects of possible external interference in the modeling and analysis and thus provided valuable insight for the future heterogeneous network designs where system coexistence and interference suppression are key issues. It was explicitly shown that I/Q imbalances of UE transmitters and BS receiver distort the signal properties and cause inter-

carrier and inter-user interference originating from the image subcarrier. This phenomenon turns out to be especially harmful when the external interference at the image subcarrier is strong. Furthermore, I/Q imbalance complicates separating the spatially multiplexed UEs at a given considered subcarrier.

The provided extensive SINR analysis, as a function of multiple system parameters, shows that the performance of the conventional per-subcarrier processing is heavily limited under I/Q imbalances and external interference. Stemming from that, an augmented spatial combiner was formulated, combining the signals jointly between image subcarriers and across all RX antennas. The proposed augmented subcarrier processing mitigates the effects of the transceiver I/Q imbalances efficiently and indeed provides combiner output SINRs practically identical to a reference system with I/Q imbalance free transceivers. Note that the augmented processing is implemented completely by digital signal processing in the BS RX. Thus the number of costly RF chains and demanding FFT processing blocks are equal to those of the conventional per-subcarrier processing and, in fact, we showed that the increase in the computational complexity can be only a few tens of percents when utilizing the augmented processing instead of the conventional one. Moreover, the augmented processing integrates the data stream separation, interference suppression, noise suppression and I/Q imbalance mitigation all into a single processing stage, thus avoiding separate transceiver calibration. The augmented approach was shown to operate very effectively and reliably also in massive MIMO framework whereas the per-subcarrier based processing approaches suffer from limited performance, in spite of the huge number of RX antennas. Overall the results demonstrate that reliable and high-performance spatial processing characteristics can be obtained by the proposed augmented combiner principle, in spite of challenging levels of the external interference, transceiver I/Q imbalances and high number of spatially multiplexed users, in the considered OFDMA MU-MIMO systems.

APPENDIX A

The power terms in (14) can be expressed easily, since the covariance matrix $\widetilde{\mathbf{R}}_{\text{TxRxi},c}$ in (11) is a sum of multiple independent terms. We only need to define two stream selection matrices: $\mathbf{\Gamma}_{q,u,c} = \text{diag}(\mathbf{e}_q) \in \mathbb{R}^{Q_{u,c}\times Q_{u,c}}$ and $\mathbf{\Delta}_{q,u,c} = \mathbf{I} - \mathbf{\Gamma}_{q,u,c} \in \mathbb{R}^{Q_{u,c}\times Q_{u,c}}$ which refer to data stream q of user u at subcarrier c, and to the interfering other streams of the same UE, respectively. Then the power terms in (14) are given with the help of (11) and the stream selection matrices by

$$\widetilde{P}_{x,q,u,c} = \sigma^2_{\text{x},u,c}\widetilde{\mathbf{w}}^{\text{H}}_{q,u,c}\widetilde{\mathbf{\Xi}}_{u,c}\mathbf{G}_{u,c}\mathbf{\Gamma}_{q,u,c}\mathbf{G}^{\text{H}}_{u,c}\widetilde{\mathbf{\Xi}}^{\text{H}}_{u,c}\widetilde{\mathbf{w}}_{q,u,c} \quad (27)$$

$$\widetilde{P}_{\text{ISI},q,u,c} = \sigma^2_{\text{x},u,c}\widetilde{\mathbf{w}}^{\text{H}}_{q,u,c}\widetilde{\mathbf{\Xi}}_{u,c}\mathbf{G}_{u,c}\mathbf{\Delta}_{q,u,c}\mathbf{G}^{\text{H}}_{u,c}\widetilde{\mathbf{\Xi}}^{\text{H}}_{u,c}\widetilde{\mathbf{w}}_{q,u,c} \quad (28)$$

$$\widetilde{P}_{\text{IUI},u,c} = \sum_{i=1,i\neq u}^{U} \sigma^2_{\text{x},i,c}\widetilde{\mathbf{w}}^{\text{H}}_{q,u,c}\widetilde{\mathbf{\Xi}}_{i,c}\mathbf{G}_{i,c}\mathbf{G}^{\text{H}}_{i,c}\widetilde{\mathbf{\Xi}}^{\text{H}}_{i,c}\widetilde{\mathbf{w}}_{q,u,c} \quad (29)$$

$$\widetilde{P}_{\text{IUI},c'} = \sum_{v=1}^{V} \sigma^2_{\text{x},v,c'}\widetilde{\mathbf{w}}^{\text{H}}_{q,u,c}\widetilde{\mathbf{\Phi}}_{v,c}\mathbf{G}^{*}_{v,c'}\mathbf{G}^{\text{T}}_{v,c'}\widetilde{\mathbf{\Phi}}^{\text{H}}_{v,c}\widetilde{\mathbf{w}}_{q,u,c} \quad (30)$$

$$\widetilde{P}_{\text{z},c} = \widetilde{\mathbf{w}}^{\text{H}}_{q,u,c}\widetilde{\mathbf{K}}_{\text{RxA},c}\mathbf{R}_{\text{z},c}\widetilde{\mathbf{K}}^{\text{H}}_{\text{RxA},c}\widetilde{\mathbf{w}}_{q,u,c} \quad (31)$$

$$\widetilde{P}_{\text{z},c'} = \widetilde{\mathbf{w}}^{\text{H}}_{q,u,c}\widetilde{\mathbf{K}}_{\text{RxB},c}\mathbf{R}^{*}_{\text{z},c'}\widetilde{\mathbf{K}}^{\text{H}}_{\text{RxB},c}\widetilde{\mathbf{w}}_{q,u,c}. \quad (32)$$

Note that $\sigma^2_{\text{x},u,c}$ denotes the power of a single data stream of UE u and thus the total power of the data streams of UE u at subcarrier c is equal to $Q_{u,c}\sigma^2_{\text{x},u,c}$.

REFERENCES

[1] A. Hakkarainen, J. Werner, K. R. Dandekar, and M. Valkama, "Precoded massive MU-MIMO uplink transmission under transceiver I/Q imbalance," in *Proc. IEEE GLOBECOM Workshops*, Dec. 2014, pp. 405–411.

[2] A. Hakkarainen, J. Werner, M. Renfors, K. R. Dandekar, and M. Valkama, "Transceiver I/Q imbalance and widely-linear spatial processing in large antenna systems," in *Proc. Int. Symp. on Wireless Commun. Syst. (ISWCS)*, Aug. 2015, pp. 651–655.

[3] S. Mirabbasi and K. Martin, "Classical and modern receiver architectures," *IEEE Commun. Mag.*, vol. 38, no. 11, pp. 132–139, Nov. 2000.

[4] T. Schenk, *RF Imperfections in High-rate Wireless Systems: Impact and Digital Compensation*, 1st ed. Springer, 2008.

[5] A. Tarighat, R. Bagheri, and A. Sayed, "Compensation schemes and performance analysis of IQ imbalances in OFDM receivers," *IEEE Trans. Signal Process.*, vol. 53, no. 8, pp. 3257–3268, Aug. 2005.

[6] A. Tarighat and A. Sayed, "Joint compensation of transmitter and receiver impairments in OFDM systems," *IEEE Trans. Wireless Commun.*, vol. 6, no. 1, pp. 240–247, Jan. 2007.

[7] Ö. Özdemir, R. Hamila, and N. Al-Dhahir, "Exact SINR analysis of OFDM systems under joint Tx/RX I/Q imbalance," in *Proc. IEEE PIMRC*, 2013, pp. 646–650.

[8] ——, "Exact average OFDM subcarrier SINR analysis under joint transmit-receive I/Q imbalance," *IEEE Trans. Veh. Technol.*, vol. 63, no. 8, pp. 4125–4130, Oct. 2014.

[9] S. Krone and G. Fettweis, "On the Capacity of OFDM Systems with Receiver I/Q Imbalance," in *Proc. IEEE ICC*, May 2008, pp. 1317–1321.

[10] B. Narasimhan, D. Wang, S. Narayanan, H. Minn, and N. Al-Dhahir, "Digital compensation of frequency-dependent joint Tx/Rx I/Q imbalance in OFDM systems under high mobility," *IEEE J. Sel. Topics Signal Process.*, vol. 3, no. 3, pp. 405–417, jun 2009.

[11] B. Maham, O. Tirkkonen, and A. Hjorungnes, "Impact of transceiver I/Q imbalance on transmit diversity of beamforming OFDM systems," *IEEE Trans. Commun.*, vol. 60, no. 3, pp. 643–648, Mar. 2012.

[12] Ö. Özdemir, R. Hamila, and N. Al-Dhahir, "SINR analysis for beamforming OFDM systems under joint transmit-receive I/Q imbalance," in *Proc. IEEE PIMRC*, 2012, pp. 1896–1901.

[13] A. Tarighat and A. Sayed, "MIMO OFDM receivers for systems with IQ imbalances," *IEEE Trans. Signal Process.*, vol. 53, no. 9, pp. 3583–3596, Sep. 2005.

[14] T. C. W. Schenk, P. F. M. Smulders, and E. Fledderus, "Estimation and compensation of frequency selective TX/RX IQ imbalance in MIMO OFDM systems," in *Proc. IEEE ICC*, 2006, pp. 251–256.

[15] T. C. W. Schenk, E. Fledderus, and P. F. M. Smulders, "Performance impact of IQ mismatch in direct-conversion MIMO OFDM transceivers," in *Proc. IEEE RWS*, 2007, pp. 329–332.

[16] Ö. Özdemir, R. Hamila, and N. Al-Dhahir, "I/Q imbalance in multiple beamforming OFDM transceivers: SINR analysis and digital baseband compensation," *IEEE Trans. Commun.*, vol. 61, no. 5, pp. 1914–1925, May 2013.

[17] J. Qi and S. Aissa, "Compensation for HPA nonlinearity and I/Q imbalance in MIMO beamforming systems," in *Proc. IEEE WiMob*, 2010, pp. 78–82.

[18] D. Tandur and M. Moonen, "Joint adaptive compensation of transmitter and receiver IQ imbalance under carrier frequency offset in OFDM-based systems," *IEEE Trans. Signal Process.*, vol. 55, no. 11, pp. 5246–5252, Nov. 2007.

[19] J. Tubbax, B. Come, L. Van der Perre, S. Donnay, M. Engels, H. De Man, and M. Moonen, "Compensation of IQ imbalance and phase noise in OFDM systems," *IEEE Trans. Wireless Commun.*, vol. 4, no. 3, pp. 872–877, May 2005.

[20] Q. Zou, A. Tarighat, and A. Sayed, "Joint compensation of IQ imbalance and phase noise in OFDM wireless systems," *IEEE Trans. Commun.*, vol. 57, no. 2, pp. 404–414, Feb. 2009.

[21] A. Ishaque, P. Sakulkar, and G. Ascheid, "Capacity analysis of uplink multi-user SC-FDMA system with frequency-dependent I/Q imbalance," in *Proc. Allerton*, Oct. 2013, pp. 1067–1074.

[22] Y. Yoshida, K. Hayashi, H. Sakai, and W. Bocquet, "Analysis and Compensation of Transmitter IQ Imbalances in OFDMA and SC-FDMA Systems," *IEEE Trans. Signal Process.*, vol. 57, no. 8, pp. 3119–3129, Aug. 2009.

[23] B. Picinbono and P. Chevalier, "Widely linear estimation with complex data," *IEEE Trans. Signal Process.*, vol. 43, no. 8, pp. 2030–2033, Aug. 1995.

[24] P. Schreier and L. Scharf, "Second-order analysis of improper complex random vectors and processes," *IEEE Trans. Signal Process.*, vol. 51, no. 3, pp. 714–725, Mar. 2003.

[25] T. Adali, P. Schreier, and L. Scharf, "Complex-valued signal processing: The proper way to deal with impropriety," *IEEE Trans. Signal Process.*, vol. 59, no. 11, pp. 5101–5125, Nov. 2011.

[26] M. Valkama, M. Renfors, and V. Koivunen, "Blind signal estimation in conjugate signal models with application to I/Q imbalance compensation," *IEEE Signal Process. Lett.*, vol. 12, no. 11, pp. 733–736, Nov. 2005.

[27] L. Anttila, M. Valkama, and M. Renfors, "Circularity-based I/Q imbalance compensation in wideband direct-conversion receivers," *IEEE Trans. Veh. Technol.*, vol. 57, no. 4, pp. 2099 –2113, Jul. 2008.

[28] D. Gesbert, M. Kountouris, R. Heath, C.-B. Chae, and T. Salzer, "Shifting the MIMO paradigm," *IEEE Signal Process. Mag.*, vol. 24, no. 5, pp. 36–46, Sep. 2007.

[29] A. Gomaa and N. Al-Dhahir, "Multi-user SC-FDMA systems under IQ imbalance: EVM and subcarrier mapping impact," in *Proc. IEEE GLOBECOM*, Dec. 2011, pp. 1–5.

[30] A. Hakkarainen, J. Werner, K. Dandekar, and M. Valkama, "Interference suppression with antenna arrays in OFDM systems under transceiver I/Q imbalance," in *Proc. CROWNCOM*, Jun. 2014, pp. 278–284.

[31] J. Hoydis, S. ten Brink, and M. Debbah, "Massive MIMO in the UL/DL of cellular networks: How many antennas do we need?" *IEEE J. Sel. Areas Commun.*, vol. 31, no. 2, pp. 160–171, Feb. 2013.

[32] E. Larsson, O. Edfors, F. Tufvesson, and T. Marzetta, "Massive MIMO for next generation wireless systems," *IEEE Commun. Mag.*, vol. 52, no. 2, pp. 186–195, Feb. 2014.

[33] L. Lu, G. Li, A. Swindlehurst, A. Ashikhmin, and R. Zhang, "An overview of massive MIMO: Benefits and challenges," *IEEE J. Sel. Topics Signal Process.*, vol. 8, no. 5, Oct. 2014.

[34] *IEEE Standard for WirelessMAN-Advanced Air Interface for Broadband Wireless Access Systems*, IEEE Standards Association Standard 802.16.1-2012, sep 2012. [Online]. Available: http://standards.ieee.org/getieee802/download/802.16.1-2012.pdf

[35] Institute of Electrical and Electronics Engineers, Inc. (IEEE). (2014) Status of IEEE 802.11 HEW study group. [Online]. Available: http://www.ieee802.org/11/Reports/hew_update.htm

[36] IEEE Standards Association. (2014) IEEE 802.11 documents. [Online]. Available: https://mentor.ieee.org/802.11/documents

[37] E. Björnson, M. Matthaiou, and M. Debbah, "Massive MIMO systems with hardware-constrained base stations," in *Proc. IEEE ICASSP*, May 2014, pp. 3142–3146.

[38] E. Björnson, E. G. Larsson, and M. Debbah, "Massive MIMO for maximal spectral efficiency: How many users and pilots should be allocated?" *IEEE Trans. Wireless Commun.*, 2015. [Online]. Available: http://arxiv.org/abs/1412.7102

[39] L. Anttila, M. Valkama, and M. Renfors, "Frequency-selective I/Q mismatch calibration of wideband direct-conversion transmitters," *IEEE Trans. Circuits Syst. II, Exp. Briefs*, vol. 55, no. 4, pp. 359 –363, Apr. 2008.

[40] F.-L. Luo, *Digital Front-End in Wireless Communications and Broadcasting: Circuits and Signal Processing*. Cambridge University Press, Sep. 2011.

[41] J. Litva, *Digital Beamforming in Wireless Communications*. Artech House Publishers, Aug. 1996.

[42] A. Gomaa and N. Al-Dhahir, "Phase Noise in Asynchronous SC-FDMA Systems: Performance Analysis and Data-Aided Compensation," *IEEE Trans. Veh. Technol.*, vol. 63, no. 6, pp. 2642–2652, Jul. 2014.

[43] H. L. V. Trees, *Detection, Estimation, and Modulation Theory, Optimum Array Processing*. John Wiley & Sons, Apr. 2004.

[44] *Evolved Universal Terrestrial Radio Access (E-UTRA); User Equipment (UE) radio transmission and reception*. The 3rd Generation Partnership Project (3GPP) Tech. Spec. V11.8.0, Release 11, TS36.101, Mar. 2014.

[45] *Evolved Universal Terrestrial Radio Access (E-UTRA); User Equipment (UE) conformance specification; Radio transmission and reception*. The 3rd Generation Partnership Project (3GPP) Tech. Spec. V11.2.0, Release 11, TS36.521.-1, Sep. 2013.

[46] B. Widrow et al., "Adaptive antenna systems," *Proc. IEEE*, vol. 55, no. 12, pp. 2143–2159, Dec. 1967.

[47] S. Johnson and M. Frigo, "A modified split-radix FFT with fewer arithmetic operations," *IEEE Trans. Signal Process.*, vol. 55, no. 1, pp. 111–119, Jan. 2007.

[48] S. Haykin, *Adaptive Filter Theory*, 4th ed. Prentice Hall, 2002.

[49] A. Hakkarainen, J. Werner, K. R. Dandekar, and M. Valkama, "Widely-linear beamforming and RF impairment suppression in massive antenna arrays," *J. Commun. and Netw.*, vol. 15, no. 4, pp. 383–397, Aug. 2013.

[50] E. Björnson, M. Matthaiou, and M. Debbah, "Circuit-aware design of energy-efficient massive MIMO systems," in *Proc. ISCCSP*, May 2014. [Online]. Available: http://arxiv.org/abs/1403.4851

[51] E. Björnson, J. Hoydis, M. Kountouris, and M. Debbah, "Massive MIMO systems with non-ideal hardware: Energy efficiency, estimation, and capacity limits," *IEEE Trans. Inf. Theory*, vol. 60, no. 11, pp. 7112–7139, Nov. 2014.

[52] H. Q. Ngo, E. Larsson, and T. Marzetta, "Energy and spectral efficiency of very large multiuser MIMO systems," *IEEE Trans. Commun.*, vol. 61, no. 4, pp. 1436–1449, Apr. 2013.

Aki Hakkarainen (S'14) was born in Joensuu, Finland, in 1982. He received the M.Sc. (with honors) in communication electronics from Tampere University of Technology (TUT), Finland, in 2007. From 2007 to 2009, he was working as a RF design engineer with Nokia, Salo. From 2009 to 2011, he was working as a Radio system specialist with Elisa, Tampere. Currently he is working towards the Ph.D. degree at the Department of Electronics and Communications Engineering, TUT. His research interests include digital signal processing methods for flexible radio transceivers with a focus on RF impairment mitigation, and directional antennas in 5G networks with an emphasis on radio localization aspects.

Janis Werner was born in Berlin, Germany, in 1986. He received the Dipl. Ing. degree in electrical engineering from Dresden University of Technology (TUD), Germany in 2011 and his Ph.D. degree from Tampere University of Technology (TUT), Finland in 2015. His main research interests are localization with an emphasis on directional antenna-based systems as well as the utilization and further processing of location information in future generation mobile networks.

Kapil R. Dandekar (S'95–M'01–SM'07) received the B.S. degree in electrical engineering from the University of Virginia in 1997. He received the M.S. and Ph.D. degrees in Electrical and Computer Engineering from the University of Texas at Austin in 1998 and 2001, respectively. In 1992, he worked at the U.S. Naval Observatory and from 1993-1997, he worked at the U.S. Naval Research Laboratory.

In 2001, Dandekar joined the Electrical and Computer Engineering Department at Drexel University in Philadelphia, Pennsylvania. He is currently a Professor in Electrical and Computer Engineering at Drexel University; the Director of the Drexel Wireless Systems Laboratory (DWSL); Associate Dean for Research and Graduate Studies in the Drexel University College of Engineering. DWSL has been supported by the U.S. National Science Foundation, Army CERDEC, National Security Agency, Office of Naval Research, and private industry. Dandekars current research interests and publications involve wireless, ultrasonic, and optical communications, reconfigurable antennas, and smart textiles. Intellectual property from DWSL has been licensed by external companies for commercialization. Dandekar is also a past member of the IEEE Educational Activities Board and co-founder of the EPICS-in-IEEE program.

Mikko Valkama was born in Pirkkala, Finland, on November 27, 1975. He received the M.Sc. and Ph.D. Degrees (both with honors) in electrical engineering (EE) from Tampere University of Technology (TUT), Finland, in 2000 and 2001, respectively. In 2002, he received the Best Ph.D. Thesis -award by the Finnish Academy of Science and Letters for his dissertation entitled ”Advanced I/Q signal processing for wideband receivers: Models and algorithms”. In 2003, he was working as a visiting researcher with the Communications Systems and Signal Processing Institute at SDSU, San Diego, CA. Currently, he is a Full Professor and Department Vice-Head at the Department of Electronics and Communications Engineering at TUT, Finland. His general research interests include communications signal processing, estimation and detection techniques, signal processing algorithms for software defined flexible radios, cognitive radio, full-duplex radio, radio localization, 5G mobile cellular radio, digital transmission techniques such as different variants of multicarrier modulation methods and OFDM, and radio resource management for ad-hoc and mobile networks.

Tampereen teknillinen yliopisto
PL 527
33101 Tampere

Tampere University of Technology
P.O.B. 527
FI-33101 Tampere, Finland

ISBN 978-952-15-3871-1
ISSN 1459-2045